DISS. ETH NO. 23574

SHAPE UNCERTAINTY QUANTIFICATION FOR SCATTERING TRANSMISSION PROBLEMS

A thesis submitted to attain the degree of
DOCTOR OF SCIENCES of ETH ZURICH
(Dr. sc. ETH Zurich)

presented by

LAURA SCARABOSIO

M. sc. Mathematical Modelling in Engineering
at Politecnico di Torino

born January 05, 1988
citizen of Italy

accepted on the recommendation of
Prof. Dr. Ralf Hiptmair, ETH Zurich, examiner
Prof. Dr. Helmut Harbrecht, Universität Basel, co-examiner
Prof. Dr. Christoph Schwab, ETH Zurich, co-examiner

2016

Scarabosio, Laura
Shape Uncertainty Quantification for Scattering Transmission Problems
Diss. ETH Zurich No. 23574
DOI: 10.3929/ethz-a-010703504
ISBN: 978-3-906327-51-8

Acknowledgements

My first thanks go to Prof. Ralf Hiptmair, for giving me the chance to pursue my Ph.D. at the ETH Zürich, and for the nice advisor-doctoral student relationship he established. This work would have not been as it is without the co-advising of Prof. Christoph Schwab. I learned a lot from him and from Ralf, in terms of both mathematical knowledge and scientific approach. I hope to be able, in the future, to take their teaching to heart. I would like to express my gratitude to Dr. Claudia Schillings, for guiding me in my first steps with sparse grids and providing me with her implementation of the adaptive Smolyak algorithm, and to Robert Gantner, for his super efficient and user-friendly implementation of the high-order quasi-Monte Carlo code I used for the reference solutions, and for his very useful programming hints. I would also like to thank Prof. Harbrecht, for revising this thesis.

A special 'Grazie' goes to my family, for always being there for me, and to Alessandro, for always being by my side and supporting me in the most difficult moments. My life in Zürich would have been much more boring and depressing without Cecilia, Pegah, Sahar and Alberto, whom I thank for their precious, not only scientific, support. Also, I enjoyed a lot talking, having fun, exchanging opinions with all my colleagues of SAM; we also suffered together, but then the humor and kindness of them made hard times lighter. I thank my non-SAM friends too, for all the nice moments we shared.

Finally, I would like to mention the important technical support of ISG, in particular of Michele Marcionelli, that helped me a lot handling the installation of NGSolve, and the administrative support of the SAM and D-MATH secretaries.

This work was supported by the ETH CHIRP1 Grant CH1-02 11-1.

Abstract

We address shape uncertainty quantification for two-dimensional Helmholtz transmission problems, where the shape of the scatterer is the only source of uncertainty. As quantities of interest, we target the solutions to the underlying partial differential equations and linear output functionals of them. However, the techniques and theory presented in this work can be easily generalized to any elliptic problem on a stochastic domain. In the framework of the so-called deterministic approach, we provide a high-dimensional parametrization for the interface. Each domain configuration is mapped to a nominal configuration, obtaining a problem on a fixed domain with stochastic coefficients. To compute surrogate models and statistics of quantities of interest, that is to perform interpolation and quadrature with respect to the parameter, we use sparse stochastic collocation. In particular, we apply an adaptive, anisotropic Smolyak algorithm, which allows to attain high convergence rates that are independent of the number of dimensions activated in the parameter space, thus breaking the so-called 'curse of dimensionality'. To ensure validity of the convergence theorems for sparse interpolation and quadrature, we need to show analytic dependence of the solution with respect to the high-dimensional parameter. When proving this, special attention is needed when, as in our case, the high-dimensional parametrization is associated with the geometry. Once the smooth dependence of the solution on the parameter has been assessed, we prove convergence estimates for the full sparse tensor discretization, namely when the discretization in the parameter space is coupled to a space discretization for each parameter realization. The theory for this is first presented in a general setting that goes beyond the application to partial differential equations on random domain configurations. Then, the convergence estimates obtained are applied to our framework of Helmholtz transmission problems mapped back to a nominal configuration. To this aim, we develop a regularity theory with respect to the spatial variable, with norm bounds that are independent of the parametric dimension, and this enables us to state convergence rates for the finite element discretization which are independent of the parameter realization and dimension. Several numerical experiments confirm the theoretical results and the effectivity of the adaptive Smolyak algorithm. Lastly, we present cases, peculiar to interface problems, where high-order quadrature methods fail to converge. Namely, we show that, for point evaluations on the physical domain, the smooth dependence of the solution on the high-dimensional parameter breaks down if the point might be crossed by the interface for some parameter realizations. In this case, alternative solutions to classical high-order methods need to be found.

Prefazione

Questo lavoro è rivolto alla quantificazione dell'incertezza nella forma nel caso di problemi di trasmissione per l'equazione di Helmholtz in due dimensioni, in cui assumiamo che la sagoma dell'oggetto attraversato dalle onde sia l'unica fonte di incertezza. Come quantità d'interesse, consideriamo le soluzioni delle equazioni differenziali alle derivate parziali associate al fenomeno di trasmissione, o suoi funzionali lineari di output. È importante però osservare che le tecniche e la teoria presentati in questa tesi possono essere facilmente generalizzati a qualunque problema ellittico posto su un dominio stocastico. Nell'ambito del cosiddetto approccio deterministico, formuliamo una parametrizzazione dell'interfaccia in cui il parametro ha valori in uno spazio alto-dimensionale. Ogni configurazione del dominio viene mappata su una cosiddetta configurazione nominale, ottenendo così un problema posto su una configurazione fissa con coefficienti stocastici. Per calcolare modelli surrogati o statistiche della quantità d'interesse, ossia per effettuare interpolazione e quadratura nello spazio dei parametri, ricorriamo al metodo di collocazione stocastica. In particolare, utilizziamo un algoritmo di Smolyak adattativo e anisotropico, che ci permette di ottenere ordini di convergenza elevati che sono indipendenti dal numero di dimensioni attivate. Per assicurare la validità dei teoremi di convergenza per interpolazione e quadratura sparse, occorre dimostrare l'analiticità della soluzione rispetto al parametro alto-dimensionale. Nel provare ciò, è necessario prestare particolare attenzione nel caso in cui, come nella nostra applicazione, la parametrizzazione è associata alla geometria. Una volta stabilita la regolarità della soluzione rispetto al parametro, dimostriamo stime di convergenza per la discretizzazione completa, vale a dire quando la discretizzazione nello spazio dei parametri è associata ad una discretizzazione spaziale per ogni realizzazione del parametro. La teoria viene dapprima presentata in un contesto generale, che va oltre l'applicazione ad equazioni differenziali alle derivate parziali su domini stocastici. Dopodiché, applichiamo le stime di convergenza ottenute ai problemi di trasmissione per l'equazione di Helmholtz posti sulla configurazione nominale. A tal scopo, sviluppiamo una teoria di regolarità rispetto alla variabile spaziale, con maggioranti delle norme che sono indipendenti dalla dimensione dello spazio dei parametri, di modo di ottenere tassi di convergenza per la discretizzazione agli elementi finiti che sono indipendenti dalla realizzazione del parametro. A supporto dei risultati teorici, riportiamo numerosi esperimenti numerici, che mostrano anche l'efficacia dell'algoritmo di Smolyak adattativo. Infine presentiamo casi, strettamente collegati al fatto di considerare problemi di interfaccia, in cui i metodi di quadratura di ordine elevato non forniscono la convergenza desiderata. Più precisamente, mostriamo come, se si considera come quantità di interesse il valore della soluzione in un punto nella configurazione fisica, la regolarità rispetto al parametro alto-dimensionale viene a mancare se questo punto può essere attraversato dall'interfaccia per alcune realizzazioni del parametro. In tal caso, è necessario ricorrere a soluzioni alternative ai classici metodi di ordine elevato.

Introduction

Consider a light beam illuminating a metallic particle. How the light is reflected and absorbed by the particle depends, among other factors, on the shape of the particle itself. More generally, we can say that the answer of a physical system upon excitation depends on the shape of the domain or, for interface problems, on the shape of the interface.

In nano-optics applications, electromagnetic waves are used to excite nano-sized, usually metallic, scatterers, whose shape is uncertain due to imperfections in the manufacturing process. Our goal is to study numerical methods that allow to *quantify* how such shape variations affect the optical response of the nano-particle. We refer to the quantity for which we want to study the effects of shape variations as *quantity of interest* (Q.o.I.). This will be the solution to a partial differential equation (PDE), as for the electric or magnetic field, or a linear output functional of it, for instance the intensity of the energy flux reflected in a particular direction.

By quantifying we mean two things: computing a surrogate model for the Q.o.I. or approximating statistical moments (mean, variance, etc.) of it. In engineering terms, a surrogate model, also referred to as metamodel or emulator, is a model that is computationally much cheaper to evaluate than the Q.o.I. but that still mimics its essential features. In our case, the surrogate model will be the interpolant of the Q.o.I. over the possible realizations. Statistical moments are instead defined as integrals over the probability space, which means that approximating them boils down to performing quadrature in the probability space.

State of the art in shape uncertainty quantification

Shape uncertainty quantification is a field that has seen a considerable development in the last ten-fifteen years. One of the main difficulties associated with the treatment of stochastic domains or interfaces is the *nonlinear* relationship between the uncertain input (the domain) and the uncertain output (the solution to a PDE or output functionals of it). The approaches proposed in literature can be divided into four main categories: perturbation methods, level-set methods, fictitious domain approach and mapping approaches. In the following, we present the main features of each of them. Since they have many aspects in common, we present the fictitious domain approach together with the level-set techniques.

Perturbation methods

These methods hold for the case of small shape perturbations.

The largest class of the approaches proposed consists in using shape calculus techniques [DZ11, Ch. 9 and 10] to approximate the Q.o.I. on the randomly perturbed shape with a Taylor expansion centered at the unperturbed domain, leading to a linearization of the problem. This allows to establish deterministic relationships between moments of the random domain and moments of the Q.o.I., reason why these methods are called *distribution free*. The approach was first proposed in [HSS08], which addresses the estimation of the mean and of the two-point correlation of the solution to an elliptic equation from the mean and two-point correlation of the domain perturbation field. There, the resulting equations are recasted as boundary integral equations, and the tensor equation for the two-point correlation is solved efficiently with a sparse tensor product Galerkin

scheme based on wavelets. The work in [HL13] addresses, with the same method, computation of moments of solutions to stochastic interface problems, and, as alternative to sparse tensor product schemes, proposes a low rank approximation based on the pivoted Cholesky decomposition to solve the tensor equation for the two-point correlation. The above techniques have been extended in [Har10] for the computation of moments of output functionals. The perturbation approach based on shape calculus has been inserted in [CS13] in a more abstract framework for uncertainty quantification of nonlinear operator equations. There, the method used in the previous works for computing the first two moments has been generalized to the computation of any moment; also, the paper presents explicit bounds on the range of perturbations for which the approach is applicable, and shows an application to a nonstationary diffusion problem on a random domain.

A different approach, still based on perturbation techniques, is the one developed in [Hon05] in the framework of elastostatic or elastodynamic problems on random domains, where the Taylor series expansion for the random fluctuations of the geometry leads to a Taylor expansion for the boundary element matrices arising from the underlying system of PDEs.

Level-set methods and fictitious domain approach

These two methods are based on embedding the random domain in a larger, deterministic domain containing all possible realizations.

The level-set approach has been developed in [NSM07] and [NCSM08]. The key idea is to represent the random boundary of the domain as the zero level-set of a function. The function used is usually the signed distance function, so that the random domain is identified by the negative set and the exterior, nonphysical domain as the positive set. The main advantage of this method is that it can handle complex geometries and topologies.

The fictitious domain approach is described in [CK07]. The variational formulation for the PDE considered is posed on the larger, fictitious domain in which the random domain is embedded. The boundary conditions are enforced via a Lagrange multiplier acting on the random boundary, turning the solution of the variational formulation to the solution of a saddle point problem. The advantage of this method is that it avoids complete reassembling, at each domain realization, of the matrices associated with the spatial discretization of the problem.

Due to the embedding in a larger domain, both methods recast a problem on a random domain as a random interface problem. The presence of the interface introduces a nonsmoothness with respect to the parameters which describe the random domain fluctuations. For this reason, in [CK12] the convergence analysis for high-order methods treating the uncertainty holds only on subdomains not intersecting the random boundary. In [NCSM08], the loss of regularity is compensated by constructing, for each domain realization and for each element in the space discretization, an ad hoc quadrature rule to compute the necessary integrals in the probability space.

Mapping approaches

The original mapping approach has been introduced in [TX06, XT06]. The idea is to use a realization-dependent coordinate transformation to map each domain realization to a fixed, reference configuration, also called nominal configuration. The variational formulation of the PDE on the random domain can then be posed on the reference domain, reducing the problem to a PDE on a fixed domain with stochastic coefficients and stochastic right-hand side. The random boundary is mapped back to a reference boundary, and the map is extended to the whole domain either using a harmonic extension [XT06], or constructing an analytic map [TX06]. It is shown in [MNK11] that the mapping approach on the continuous level, subject to a finite element discretization, is mathematically equivalent to a discrete mapping where, given a mesh, the connectivity is fixed and the node coordinates are changed according to the realization.

We mention the papers [MCMM10, MCM11a, MCM11b] for application of the mapping technique to electromagnetic problems.

The mapping approach is the most common tool used for the mathematical analysis of PDEs on random domains. The paper [CCNT16] shows the regularity properties of the solution to the PDE with respect to the parameters describing the uncertainty in order to prove convergence for the algorithm performing the quadrature in the probability space. The paper [HPS16] also shows similar regularity results and proposes to use parametric finite elements for the space discretization.

The mapping approach is also the method adapted in this thesis to deal with the stochastic interface. Thus, further details about this technique will be provided in Section 3.1.

Outline

Most of the content of this thesis is based on [HSSS].

In Chapter 1 we introduce the two *model problems* addressed in this work, which are both interface problems where the shape of the interface is the only source of uncertainty.

In Chapter 2, we address the modeling of the random interface. For this, we follow the so-called *parametric approach*, developed by Ghanem and Spanos [GS03] from the pioneering ideas of Wiener [Wie38]. As it is commonly done to model the stochastic diffusion coefficient in the scalar diffusion model (see [CDS10, CDS11, SG11], just to mention some), we introduce a probabilistic description of the interface $\Gamma = \Gamma(\omega)$, so that it will then depend on $\omega \in \Omega$ indirectly through a deterministic, high-dimensional parameter representing the stochasticity.

In Chapter 3 we cast the variational formulation for the interface problems in a form that is easier to treat from the theoretical and algorithmic point of view. Namely, in Section 3.1 we apply the *mapping approach* [TX06, XT06] to obtain a variational formulation on a domain with fixed, parameter-independent interface, whose well-posedness is addressed in Section 3.2.

Chapter 4 treats the *discretization* with respect to the *parameter space*. For the computation of the interpolant and integrals of the Q.o.I., we use stochastic collocation [BNT10, XH05], preferring it to the stochastic Galerkin approach (see [SG11] for a comprehensive review) because of its nonintrusive nature and thus more immediate applicability for nonlinear dependence of the Q.o.I. on the parameter. To overcome the so-called *curse of dimensionality* due to the high dimension of the parameter space, we use the sparse adaptive Smolyak algorithm for stochastic quadrature and interpolation described in [SS13] and pioneered in the earlier work [GG03]. In the same chapter (Section 4.3) we also discuss the fulfillment, in our framework, of the key assumption of all convergence theorems, that is the holomorphy of the Q.o.I. with respect to an extension of the high-dimensional parameter to the complex plane. Our approach and results are different from the regularity analysis in [HPS16], because what is discussed there is the regularity with respect to the *real-valued* parameter (and not its complex extension). The difference with [CCNT16] relies instead mostly in the methodology used, which in our case relies more on properties of holomorphic functions rather than direct computation, making the procedure more easily extendable to other domain mappings or PDEs.

In Chapter 5 we prove the *convergence results* for the Q.o.I. when discretization with respect to both the parameter and the space variable on the nominal configuration is considered. Since these estimates hold in general when sparse stochastic collocation or quadrature are combined with space discretization and not only for PDEs on stochastic domains, we present them in an abstract setting.

In Chapter 6 we apply the results of the previous chapter to our setting of the interface problem on the nominal domain. For the space discretization, we use finite elements. We point out that a boundary element formulation (as used, for instance, in [HSS08]) is not applicable in the context of the mapping approach, due to variable coefficients in the resulting variational formulation. To establish the convergence results regarding the space discretization, we present the *regularity analysis* with respect to the space variable.

Chapter 7 is dedicated to the *numerical results* for the two model problems.

Chapter 8 addresses the difficulties that arise when computing moments of the solution in the *physical space*, where the interface is different for each realization. We emphasize that this task is different from performing quadrature on the nominal domain, as addressed instead in the previous chapters and in [HPS16] and [MCM11a]. The difficulties that we encounter are due to the discontinuity of the material properties across the interface. Similar problems have been faced in [MNT13] in the framework of the second-order wave equation with discontinuous random velocity, and are the same reason why realization-dependent, ad hoc quadrature rules are needed in level-set approaches.

Contents

Notation

$\boldsymbol{n}$ unit normal vector, oriented outward.

$A^\top$ transpose of matrix A.

$C^k(D)$ k-times continuously differentiable functions on D.

$C^k_{per}([0,2\pi))$ k-times continuously differentiable, periodic functions on $[0,2\pi)$.

DF Jacobian matrix of map F.

DtN Dirichlet-to-Neumann map.

$H^k(D)$ Sobolev space of k-times weakly differentiable functions on D.

I_Λ sparse interpolation operator on set Λ.

$L^p(D)$ Lebesgue pth power integrable functions on D.

$L^p_{per}([0,2\pi))$ Lebesgue pth power integrable, periodic functions on $[0,2\pi)$.

Q_Λ sparse quadrature operator on set Λ.

X^* space of bounded linear functionals on a Banach space X (dual space of X).

$\boldsymbol{x}$ coordinates on the physical configuration.

Δ^I difference interpolation operator.

Δ^Q difference quadrature operator.

Im imaginary part (of complex-valued quantity).

Ω set of elementary events.

Re real part (of complex-valued quantity).

$\mathbb{N}_0$ natural numbers, including 0.

$\mathbb{N}$ natural numbers, excluding 0.

$\mathbb{P}$ probability measure.

$\mathbb{R}_+$ positive real numbers, excluding 0.

$\mathbb{R}_{0,+}$ positive real numbers, including 0.

$\mathbb{R}$ real numbers.

$\ell^p(\mathbb{N})$ space of p-summable sequences.

$\hat{\boldsymbol{x}}$ coordinates on the nominal configuration .

$\|\cdot\|_2$ Euclidean vector norm in $\mathbb{R}^n$.

$\|\cdot\|_{C^k(D_1)\cup C^k(D_2)}$ broken C^k-norm: $\|\cdot\|_{C^k(D_1)} + \|\cdot\|_{C^k(D_2)}$.

$\|\cdot\|_{H^k(D_1)\cup H^k(D_2)}$ broken Sobolev norm: $\sqrt{\|\cdot\|^2_{H^k(D_1)} + \|\cdot\|^2_{H^k(D_2)}}$.

$\|\cdot\|_\infty$ maximum vector norm in $\mathbb{R}^n$.

$\|\cdot\|$ Euclidean vector norm in $\mathbb{R}^2$.

$\mathcal{F}$ set of finitely supported multiindices.

$\mathcal{I}(g)$ exact integral of g.

$\mathcal{N}(\Lambda)$ set of neighbors of a set Λ of multiindices.

$\mathcal{P}_J$ parameter space with finite dimension.

$\mathcal{P}$ parameter space with infinite dimension.

$\mathcal{U}([a,b])$ uniformly distributed random variable on $[a,b]$.

$\otimes, \bigotimes$ tensor product.

$\sharp S$ cardinality of set S.

Cov_X covariance operator of random variable X.

cov_X covariance kernel of random variable X.

i.i.d. independent, identically distributed.

1. Model problems

We consider time-harmonic solutions to Maxwell's equations, and study the propagation of waves in a cylinder of infinite length. Introducing the orthogonal system of coordinates (x_1, x_2, x_3), with the x_3-axis coinciding with the axis of the cylinder, we denote by $\mathbf{E} = (E_{x_1}, E_{x_2}, E_{x_3})$ the electric field and by $\mathbf{H} = (H_{x_1}, H_{x_2}, H_{x_3})$ the magnetic field. We assume that $\mathbf{E} = \mathbf{E}(x_1, x_2)$ and $\mathbf{H} = \mathbf{H}(x_1, x_2)$. Considering a direction of propagation for the waves that lies in the (x_1, x_2)-plane, we are interested in the transverse electric (TE) and transverse magnetic (TM) modes. In the former, the electric field is assumed to be perpendicular (transversal) to the direction of propagation, leading to $E_{x_1} = E_{x_2} = H_{x_3} = 0$ and $E_{x_3}, H_{x_1}, H_{x_2} \neq 0$. In the latter, we assume the magnetic field to be perpendicular to the direction of propagation, and we have $H_{x_1} = H_{x_2} = E_{x_3} = 0$ and $H_{x_3}, E_{x_1}, E_{x_2} \neq 0$. In both cases, TE and TM, the out-of-plane component solves a two-dimensional Helmholtz equation.

In this work, we consider the *Helmholtz transmission problem* with an incoming plane wave for the two geometries depicted in Figure 1.0.1, referred to as particle in free space and particle on substrate, respectively. In the second case, we suppose that the substrate is non-penetrable and of infinite extension, and that the bottom part of the particle adheres perfectly to it. We consider materials which are isotropic and non-magnetic. Moreover, we assume that the shape of the scatterer is the only source of uncertainty in our system, so that the material parameters are supposed to be known exactly.

To model the random shape variations, we introduce a probability space $(\Omega, \mathcal{A}, \mathbb{P})$, where Ω is the set of elementary events, $\mathcal{A}$ is a σ-algebra on the power set $\mathscr{P}(\Omega)$ and $\mathbb{P}$ is a probability measure on $(\Omega, \mathcal{A})$. For every $\omega \in \Omega$, we formally define $\Gamma(\omega)$ to be the boundary of the scatterer, $D_1(\omega)$ the exterior, unbounded domain, and $D_2(\omega)$ the domain occupied by the scatterer; for the substrate case, $D_1(\omega)$ is divided into the free space and the substrate parts, i.e., $D_1(\omega) = D_{1,fs}(\omega) \cup D_{1,sub}$. We assume that $D_1(\omega) \cup \Gamma(\omega) \cup D_2(\omega) = \mathbb{R}^2$ for every $\omega \in \Omega$. Let $\Gamma_T(\omega)$ denote the union of all interfaces in the system. For the particle in free space, $\Gamma_T(\omega) = \Gamma(\omega)$. For the particle on substrate, $\Gamma_T(\omega) = \Gamma(\omega) \cup \Gamma_{sub}$, where Γ_{sub} is the interface between the substrate and the free space.

The transmission problem for the Helmholtz equation reads:

$$\begin{cases} -\nabla \cdot (\alpha(\Gamma(\omega), \boldsymbol{x})\nabla u) - \kappa^2(\Gamma(\omega), \boldsymbol{x})u = 0 \quad \text{in } \mathbb{R}^2, & \text{(1.0.1a)} \\ [\![u]\!]_{\Gamma_T(\omega)} = 0, \ \left[\!\left[\alpha(\Gamma(\omega), \boldsymbol{x})\nabla u \cdot \boldsymbol{n}\right]\!\right]_{\Gamma_T(\omega)} = 0, & \text{(1.0.1b)} \\ + \text{ radiation condition at infinity}, & \text{(1.0.1c)} \\ \text{for every } \omega \in \Omega, \end{cases}$$

with uniformly positive, real-valued, piecewise-constant coefficients in each subdomain, namely

$$\alpha(\Gamma(\omega), \boldsymbol{x}) = \begin{cases} 1 & \text{if } \boldsymbol{x} \in D_1(\omega), \\ \alpha_2 & \text{if } \boldsymbol{x} \in D_2(\omega), \end{cases} \qquad \kappa^2(\Gamma(\omega), \boldsymbol{x}) = \begin{cases} \kappa_1^2 & \text{if } \boldsymbol{x} \in D_1(\omega), \\ \alpha_2\,\kappa_2^2 & \text{if } \boldsymbol{x} \in D_2(\omega), \end{cases} \tag{1.0.2}$$

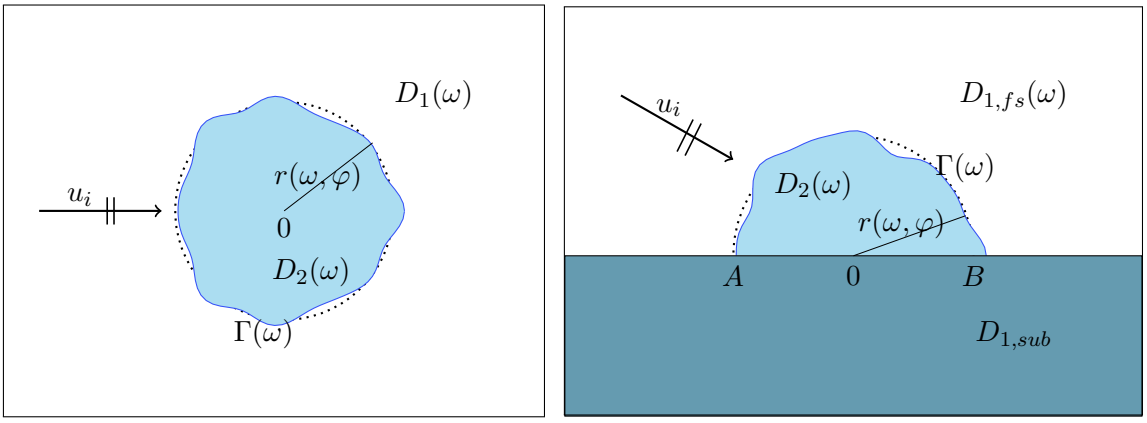

(a) Particle in free space.

(b) Particle on substrate.

Figure 1.0.1: Geometries considered in this work.

in the free space case, and

$$\alpha(\Gamma(\omega),\boldsymbol{x}) = \begin{cases} 1 & \text{if } \boldsymbol{x} \in D_{1,fs}(\omega), \\ \alpha_{sub} & \text{if } \boldsymbol{x} \in D_{1,sub}, \\ \alpha_2 & \text{if } \boldsymbol{x} \in D_2(\omega), \end{cases} \qquad \kappa^2(\Gamma(\omega),\boldsymbol{x}) = \begin{cases} \kappa_1^2 & \text{if } \boldsymbol{x} \in D_{1,fs}(\omega), \\ \alpha_{sub}\,\kappa_{sub}^2 & \text{if } \boldsymbol{x} \in D_{1,sub}, \\ \alpha_2\,\kappa_2^2 & \text{if } \boldsymbol{x} \in D_2(\omega), \end{cases} \tag{1.0.3}$$

in the substrate case. The vector $\boldsymbol{n}$ in (1.0.1b) is the exterior unit normal to $\Gamma(\omega)$ and, in the substrate case, to the substrate.

In the TE mode, the solution u corresponds to the nonzero component E_{x_3} of the total electric field (incoming plus scattered field), and the coefficients are given by $\alpha_2 = \frac{\mu_2}{\mu_1}$ and $\alpha_{sub} = \frac{\mu_{sub}}{\mu_1}$, where μ_1, μ_2 and μ_{sub} are the magnetic permeabilities in free space, in the scatterer and in the substrate, respectively. Since we consider non-magnetic materials, in the TE case $\alpha_2 = \alpha_{sub} = 1$. In the TM mode, u is the nonzero component H_{x_3} of the total magnetic field, and $\alpha_2 = \frac{\varepsilon_2}{\varepsilon_1}$ and $\alpha_{sub} = \frac{\varepsilon_{sub}}{\varepsilon_1}$, with ε_1, ε_2 and ε_{sub} the electric permittivities of free space, scatterer and substrate, respectively; in general, $\alpha_2, \alpha_{sub} \neq 1$.

The constants κ_1, κ_2 and κ_{sub} denote the wavenumbers in the corresponding domains.

The transmission conditions (1.0.1b) impose the continuity of the tangential components of $\mathbf{E}$ and $\mathbf{H}$ across the interfaces. More precisely, in the TE mode the continuity of the Dirichlet trace refers to the continuity of the tangential components of $\mathbf{E}$, and the continuity of the Neumann trace refers to the continuity of the tangential components of $\mathbf{H}$. Conversely, in the TM case the continuity of the Dirichlet trace expresses the continuity of the tangential components of $\mathbf{H}$ and the continuity of the Neumann traces expresses the continuity of the tangential components of $\mathbf{E}$. We refer to [Mai07, Sect. 2.1] for details about the physical interpretation of (1.0.1a)-(1.0.1b).

The radiation condition expresses the fact that the scattered wave must be an *outgoing* wave decaying to 0 at infinity. In the free space case, it is given by the so-called Sommerfeld radiation condition

$$\lim_{|\boldsymbol{x}|\to\infty} \sqrt{|\boldsymbol{x}|}\left(\frac{\partial}{\partial\,|\boldsymbol{x}|} - i\kappa_1\right)(u(\omega) - u_i)(\boldsymbol{x}) = 0, \tag{1.0.4}$$

whilst in the substrate case it is more involved and we refer to [JHN12] for details. Here $u_i(\boldsymbol{x}) = e^{i\kappa_1 \boldsymbol{d}\cdot\boldsymbol{x}}$ denotes an incoming plane wave, with $\boldsymbol{d}$ a unit vector indicating the direction of propagation.

We work in the *large wavelength regime*, which excludes the presence of resonant geometric structures; thus, the results of this work are not restricted to the Helmholtz equation, but also hold for any elliptic equation.

Although we treat two-dimensional domains, the results and methodology presented in this work hold for the three-dimensional Helmholtz equation too, when the Fourier harmonics used to model the shape variations (see Chapter 2) are replaced by spherical harmonics. The physical interpretation, though, would be different, because in three dimensions the Helmholtz equation describes the propagation of pressure waves instead of electromagnetic waves.

2. Interface parametrization

In the first section, we give a probabilistic model for the interface Γ. Using the probabilistic characterization, in the second section we convert the stochastic problem to a deterministic problem on a high-dimensional parameter domain. This approach is particularly relevant in the perspective of a discretization, since we will see that it is easier to discretize the space where the deterministic parameter lives rather than the probability space Ω.

2.1. Probabilistic modeling of the interface

For presenting the key ingredients of our approach, here we focus on the particle in free space. For the extension to the particle on substrate we refer to subsection 3.1.2. In order to have a simple representation of the interface, we require:

Assumption 2.1.1. For every $\omega \in \Omega$, the domain of the scatterer, $D_2(\omega)$, is star-shaped with respect to the origin, and the interface $\Gamma(\omega)$ is of class C^1.

In this way, $D_2(\omega)$ can be fully described by a stochastic, angle-dependent radius $r = r(\omega, \varphi) \in C^k_{per}([0, 2\pi))$ representing the interface $\Gamma = \Gamma(\omega)$, for every $\omega \in \Omega$ and some $k \geq 1$. The techniques we are going to present can be extended to the case of an interface that is only piecewise of class C^k $(k \geq 1)$, but for ease of treatment do not consider this case.

As it is commonly done in the framework of partial differential equations with stochastic diffusion coefficient (see e.g. [CDS10, CDS11, SG11]), we expand the uncertain radius as:

$$r(\omega, \varphi) = r_0(\varphi) + \sum_{j=1}^{J} c_j Y_{2j-1}(\omega) \cos(j\varphi) + s_j Y_{2j}(\omega) \sin(j\varphi), \ \varphi \in [0, 2\pi), \ J \in \mathbb{N}, \omega \in \Omega. \quad (2.1.1)$$

In this formal expression, $r_0 = r_0(\varphi) \in C^k_{per}([0, 2\pi))$, $k \geq 1$, is referred to as the nominal shape. For the following analysis, r_0 can be whatever deterministic quantity related to the radius, but since in the Fourier expansion we do not include the constant term, we consider r_0 to be an approximate parametrization of the mean shape. The truncation of the expansion in (2.1.1) is commonly referred to in the literature [BNT10] as *finite noise assumption*. However, since we want a method which is robust with respect to the number of dimensions, hereinafter, in particular in Chapter 6, we will ensure that all the estimates obtained hold *uniformly* in the truncation parameter $J \in \mathbb{N}$.

The random variables $\{Y_l\}_{l=1}^{2J}$ are assumed to satisfy the following conditions:

Assumption 2.1.2. $\{Y_l\}_{l=1}^{2J}$ are i.i.d., with $Y_l \sim \mathcal{U}([-1, 1])$ for every $1 \leq l \leq 2J$ and every $J \in \mathbb{N}$.

In particular $\{Y_l\}_{l=1}^{2J}$ have compact image, as $|Y_l| \leq 1$ for every l. Therefore, the only way to have a J-independent bound on the radius expansion (2.1.1) and a decay of its Fourier coefficients is to impose some constraints on the real coefficient sequences.

To ensure, for every $\omega \in \Omega$, boundedness and positivity at each angle φ for the stochastic radius r, we require that $r = r(\omega, \varphi)$ varies inside the range $[\frac{r_0(\varphi)}{2}, \frac{3r_0(\varphi)}{2}]$:

Assumption 2.1.3. The coefficient sequences $\mathcal{C} := (c_j)_{j\geq 1}$ and $\mathcal{S} := (s_j)_{j\geq 1}$ in (2.1.1) satisfy

$$\sum_{j\geq 1}(|c_j| + |s_j|) \leq \frac{r_0^-}{2},$$

with $r_0^- = \inf_{\varphi\in[0,2\pi)} r_0(\varphi) > 0$.

We require that the Fourier coefficients have a 'sufficiently fast' polynomial decay, in the sense made precise below. This can be ensured by either of the two following assumptions:

Assumption 2.1.4.A. The sequences $\mathcal{C} := (c_j)_{j\geq 1}$ and $\mathcal{S} := (s_j)_{j\geq 1}$ have a monotonically decreasing majorant which belongs to $\ell^p(\mathbb{N})$ with $0 < p < \frac{1}{2}$, and the sequences $(j|c_j|^p)_{j\geq 1}$ and $(j|s_j|^p)_{j\geq 1}$ have a monotonically decreasing majorant.

Assumption 2.1.4.B. For every $\omega \in \Omega$, the radius $r(\omega, \varphi)$ as given in (2.1.1) belongs to $C^k_{per}([0, 2\pi))$, for an integer $k \geq 3$, with an ω-independent norm bound.

Assumption 2.1.4.B might be easier to check in applications, when some a priori information about the smoothness of the particle boundary is available.

Actually, we have that:

Proposition 2.1.5. *If Assumption 2.1.4.B holds, then also Assumption 2.1.4.A does.*

Proof. From Lemma C.0.6, we have that, for every $p > \frac{1}{k}$, the sequences $(|c_j Y_{2j-1}(\omega)|)_{j\geq 1}$ and $(|s_j Y_{2j}(\omega)|)_{j\geq 1}$ have a monotonically decreasing majorant in $\ell^p(\mathbb{N})$, *for every* $\omega \in \Omega$. Then, in particular, the sequences $\mathcal{C}$ and $\mathcal{S}$ have a monotonically decreasing majorant in $\ell^p(\mathbb{N})$. Since we have an ω-uniform bound on $\|r(\omega, \cdot)\|_{C^k_{per}([0,2\pi))}$, the proof of Lemma C.0.6 shows that the majorant too is independent of ω. Finally, the fact that $k \geq 3$ allows us to choose $0 < p < \frac{1}{2}$.

We remark that the fact that $p > \frac{1}{k}$ also insures the monotonicity of the sequences $(j|c_j|^p)_{j\geq 1}$ and $(j|s_j|^p)_{j\geq 1}$. □

Conversely, Assumption 2.1.4.A implies Assumption 2.1.4.B, with a smoothness parameter $k = k(p)$, but only if p is small enough:

Lemma 2.1.6. *If the coefficient sequences $\mathcal{C}$, $\mathcal{S}$ satisfy Assumption 2.1.4.A, then, for every $\omega \in \Omega$, the radius $r = r(\omega, \varphi)$ given by* (2.1.1) *satisfies*

$$\|r(\omega)\|_{C^k_{per}([0,2\pi))} \leq C(\mathcal{C}, \mathcal{S}), \tag{2.1.2}$$

under the assumption that the nominal radius r_0 belongs to $C^k_{per}([0, 2\pi))$ too. The constant C depends on the regularity parameter k and on the sequences $\mathcal{C} = (c_j)_{j\geq 1}$ and $\mathcal{S} = (s_j)_{j\geq 1}$, but not on the truncation parameter $J \in \mathbb{N}$ and on $\omega \in \Omega$. The regularity parameter k is given by:

$$k = \begin{cases} \left\lfloor \frac{1}{p} - 1 \right\rfloor & \text{if } \frac{1}{p} - 1 \text{ is not an integer,} \\ \frac{1}{p} - 2 & \text{otherwise.} \end{cases} \tag{2.1.3}$$

In particular, if $0 < p < \frac{1}{4}$, then Assumption 2.1.4.A implies Assumption 2.1.4.B.

Proof. See Lemma C.0.5. □

According to the aforementioned results, we can say that Assumption 2.1.4.A is more general than Assumption 2.1.4.B.

Remark 2.1.7. Equation (2.1.1) can be rewritten as

$$r(\omega,\varphi) = r_0(\varphi) + \sum_{l=1}^{L} \beta_l Y_l(\omega)\psi_l(\varphi), \quad \varphi \in [0,2\pi), L \in \mathbb{N}, \omega \in \Omega, \tag{2.1.4}$$

with $\psi_l = \cos(\frac{l+1}{2}\varphi)$ and $\beta_l = c_{\frac{l+1}{2}}$ if l is odd, $\psi_l = \sin(\frac{l}{2}\varphi)$ and $\beta_l = s_{\frac{l}{2}}$ if l is even. The truncation L is given by $L = 2J$, with J as in (2.1.1).

In general, any basis $(\psi_l)_{l\geq 1}$ of $L^2_{per}([0,2\pi))$ could be considered, provided that $\psi_l \in C^1_{per}([0,2\pi))$ for each $l \geq 1$. Nevertheless, the choice of the Fourier basis is particularly relevant in view of possible applications.

More precisely, in applications the probabilistic model for $r = r(\omega,\varphi)$ will not be imposed theoretically as we did in Assumption 2.1.2, but extrapolated from measurement data. A possible procedure is to estimate the symmetric covariance kernel $\mathrm{cov}_r = \mathrm{cov}_r(\varphi,\varphi')$ of the distribution of r and use the Karhunen-Loève expansion for (2.1.1). In this case, $(\psi_l)_{l\geq 1}$ are the eigenfunctions of the covariance kernel and $(\beta_l)_{l\geq 1}$ the square roots of the corresponding eigenvalues.

Now, it is reasonable to assume the covariance kernel to be rotationally invariant, i.e.

$$\mathrm{cov}_r(\varphi,\varphi') = \mathrm{cov}_r(\varphi-\varphi'), \quad \text{for every } \varphi,\, \varphi' \in [0,2\pi). \tag{2.1.5}$$

In this case, it is easy to see that, if r_0 is a circle, then the eigenfunctions of the covariance kernel are the elements of the Fourier basis of $L^2_{per}([0,2\pi))$.

Remark 2.1.8. In Assumption 2.1.4.A we have imposed some decay on the coefficient sequences $\mathcal{C}$ and $\mathcal{S}$ in order to have some decay in the Fourier coefficients in (2.1.1). Together with the truncation up to the Jth term, this means that, although this hypothesis may be fulfilled by stochastic radii that do not satisfy Assumption 2.1.4.B, some $L^2_{per}([0,2\pi))$ functions are anyway excluded from our treatment. However, it is legitimate to think that we discard only very irregular functions, which would not be realistic realizations of a particle boundary.

2.2. Parametric formulation

In view of a discretization, it is not suitable to have quantities expressed in terms of $\omega \in \Omega$, because we do not know how to discretize a probability space. The probabilistic model (2.1.1) introduced in the previous section allows us to circumvent this issue, moving from the probability space to the tensor product of the image spaces of Ω under the random variables Y_l, $1 \leq l \leq 2J$.

We recall, via application to our case, the standard parametrization procedure followed in stochastic Galerkin and stochastic collocation frameworks; we refer to [SG11] for an exhaustive survey of the topic.

From Assumption 2.1.2, we know that for each random variable $Y_l : \Omega \to \mathcal{P}_l$, $1 \leq l \leq 2J$, with $\mathcal{P}_l = [-1,1]$ endowed with the Borel σ-algebra Σ_l, the distribution of Y_l is the uniform distribution. Then the sequence $(Y_l)_{l=1}^{2J}$ defines a map

$$\boldsymbol{Y} : \Omega \to \mathcal{P}_J := \bigotimes_{l=1}^{2J} \mathcal{P}_l = [-1,1]^{2J}, \quad \omega \mapsto (Y_l(\omega))_{l=1}^{2J}, \tag{2.2.1}$$

measurable with respect to the product σ-algebra $\Sigma := \bigotimes_{l=1}^{2J} \Sigma_l$ on $\mathcal{P}_J$. The image space $\mathcal{P}_J$ is commonly referred to as the *parameter space*. The random variables Y_l being independent, the probability measure of $\boldsymbol{Y}$ is the product probability measure

$$\mu := \bigotimes_{l=1}^{2J} \mu_l, \tag{2.2.2}$$

where μ_l is the probability measure of Y_l, $1 \leq l \leq 2J$.

Now, we denote by $\boldsymbol{y} = (y_l)_{l=1}^{2J} \in \mathcal{P}_J$ one realization of the random variable $\boldsymbol{Y}$, so that we can rewrite (2.1.1) as

$$r(\boldsymbol{y}, \varphi) = r_0(\varphi) + \sum_{j=1}^{J} c_j y_{2j-1} \cos(j\varphi) + s_j y_{2j} \sin(j\varphi), \quad \boldsymbol{y} = (y_j)_{j=1}^{2J} \in \mathcal{P}_J,\ \varphi \in [0, 2\pi). \tag{2.2.3}$$

This means that, exploiting some a priori assumptions on the distribution of the stochastic quantity (Assumption 2.1.2), we have moved from a description of the radius defined on the probability space to a description through a deterministic parameter $\boldsymbol{y}$ taking values in $\mathcal{P}_J$, measurable with respect to the product image measure induced by $\boldsymbol{Y}$.

3. Problem formulation on a fixed domain

After the interface parametrization, the model problem (1.0.1) is posed over a domain with parameter-dependent, deterministic interface $\Gamma = \Gamma(\boldsymbol{y})$, different for each realization $\boldsymbol{y} \in \mathcal{P}_J$. This is not easy to handle from both the theoretical and the implementation side. To remedy this, in the following we consider a bijective, $\boldsymbol{y}$-dependent diffeomorphism to map each physical, $\boldsymbol{y}$-dependent geometry to a fixed geometry, that is, a configuration where the the interface $\hat{\Gamma}$ is the same for all realizations.

In the first section we introduce the so-called *mapping approach* introduced by Xiu and Tartakovski in [TX06] and [XT06], and then we apply it to our model problems. In the second section, we address the well-posedness of the resulting variational formulation on the nominal configuration.

3.1. The mapping approach

3.1.1. General description

To overcome the unboundedness of the domain, we consider, in the domain with interface $\Gamma(\boldsymbol{y})$, a circle ∂K_R of arbitrary radius R containing, for every $J \in \mathbb{N}$ and every $\boldsymbol{y} \in \mathcal{P}_J$, the scatterer $D_2(\boldsymbol{y})$ in its interior. We assume ∂K_R to be *fixed for all realizations* $\boldsymbol{y} \in \mathcal{P}_J$, $J \in \mathbb{N}$, and we denote by K_R the region enclosed inside ∂K_R, no matter which realization $\Gamma(\boldsymbol{y})$ of the interface is considered.

Remark 3.1.1. In general, the boundary ∂K_R of the domain does not need to be a circle and the analysis would not change if it is not.

Following the approach also adopted, for instance, in [XT06], [CCS15], [HPS16] and [CCNT16], we consider a *nominal configuration* of the domain K_R, where the interface $\hat{\Gamma}$ is *fixed* (i.e. independent of the truncation J and of the realization $\boldsymbol{y}$), and a bijective, parameter-dependent mapping

$$\begin{aligned} \Phi(\boldsymbol{y}): \quad K_R &\longrightarrow K_R \\ (\hat{x}_1, \hat{x}_2) &\mapsto (x_1, x_2) \end{aligned} \tag{3.1.1}$$

from the nominal configuration to the configuration with interface $\Gamma(\boldsymbol{y})$.

A possible choice for $\hat{\Gamma}$ is the interface associated with the nominal radius r_0, or, in other words, to the case when $\boldsymbol{y} = \boldsymbol{0}$. In the following, we denote by $\hat{D}_2$ the scatterer region when the interface is $\hat{\Gamma}$, and by $\hat{D}_1 := \mathbb{R}^2 \setminus \hat{D}_2$. In order to preserve the well-posedness of the problem as it will be discussed in the next section, we formulate some assumptions on Φ:

Assumption 3.1.2. For every $J \in \mathbb{N}$, every $\boldsymbol{y} \in \mathcal{P}_J$ and an integer $k \geq 1$, the mapping $\Phi(\boldsymbol{y}) : K_R \to K_R$ fulfills the following properties:

(i) $\Phi(\boldsymbol{y})$ is a C^k-orientation preserving diffeomorphism in each of the two subdomains $\hat{D}_1 \cap K_R$ and $\hat{D}_2$, with uniformly bounded norms, i.e.:

$$\|\Phi(\boldsymbol{y})\|_{C^k_{\mathrm{pw}}(\overline{K_R})} \leq C_1, \quad \|\Phi^{-1}(\boldsymbol{y})\|_{C^k_{\mathrm{pw}_{\boldsymbol{y}}}(\overline{K_R})} \leq C_2, \quad \text{for all } J \in \mathbb{N} \text{ and all } \boldsymbol{y} \in \mathcal{P}_J,$$

where C_1 and C_2 are independent of the truncation parameter $J \in \mathbb{N}$ and of $\boldsymbol{y} \in \mathcal{P}_J$, and $\|\cdot\|_{C^k_{\mathrm{pw}}(\overline{K_R})} := \|\cdot\|_{C^k(\overline{\hat{D}_1 \cap K_R}) \cup C^k(\overline{\hat{D}_2})} = \|\cdot\|_{C^k(\overline{\hat{D}_1 \cap K_R})} + \|\cdot\|_{C^k(\overline{\hat{D}_2})}$ (similarly in $\|\cdot\|_{C^k_{\mathrm{pw}_{\boldsymbol{y}}}(\overline{K_R})}$ the discontinuities are allowed across $\Gamma(\boldsymbol{y})$).

(ii) $\Phi(\boldsymbol{y})$ is the identity on ∂K_R:

$$\Phi(\boldsymbol{y}, \hat{\boldsymbol{x}}) = \hat{\boldsymbol{x}}, \text{ for all } \hat{\boldsymbol{x}} \in \partial K_R \text{ and all } J \in \mathbb{N}, \boldsymbol{y} \in \mathcal{P}_J.$$

(iii) Let $\sigma_1 = \sigma_1(\boldsymbol{y}, \boldsymbol{x})$, $\sigma_2 = \sigma_2(\boldsymbol{y}, \boldsymbol{x})$ be the singular values of $D\Phi^{-1}(\boldsymbol{y})$, the Jacobian matrix of $\Phi^{-1}(\boldsymbol{y})$. We require that there exist constants $\sigma_{\min}, \sigma_{\max} > 0$ independent of the truncation parameter $J \in \mathbb{N}$ and of $\boldsymbol{y} \in \mathcal{P}_J$ such that

$$\sigma_{\min} \leq \|\sigma_1(\boldsymbol{y}, \cdot)\|_{C^0_{\mathrm{pw}_{\boldsymbol{y}}}(\overline{K_R})}, \|\sigma_2(\boldsymbol{y}, \cdot)\|_{C^0_{\mathrm{pw}_{\boldsymbol{y}}}(\overline{K_R})} \leq \sigma_{\max}, \quad \text{for all } J \in \mathbb{N}, \boldsymbol{y} \in \mathcal{P}_J$$

(or, equivalently, analogous bounds hold for the singular values of $D\Phi(\boldsymbol{y})$).

The part *(ii)* of this assumption is not necessary but it simplifies both the theoretical analysis and the implementation. It implies in particular that the exterior boundary ∂K_R is fixed for every $J \in \mathbb{N}$ and every $\boldsymbol{y} \in \mathcal{P}_J$.

3.1.2. Geometries

The cases considered are sketched in Figure 1.0.1. For them, we describe both the domain parametrization and the mapping from the nominal configuration.

Particle in free space

We choose $r_0(\varphi)$ as the boundary of the scatterer in the nominal configuration, and map it to the boundary of the actual scatterer. The movement of the interface is propagated in the regions inside and outside the scatterer using a mollifier:

$$\boldsymbol{x}(\boldsymbol{y}) = \Phi(\boldsymbol{y}, \hat{\boldsymbol{x}}) = \hat{\boldsymbol{x}} + \chi(\hat{\boldsymbol{x}}) \left(r(\boldsymbol{y}, \hat{\varphi}_{\hat{\boldsymbol{x}}}) - r_0(\hat{\varphi}_{\hat{\boldsymbol{x}}})\right) \frac{\hat{\boldsymbol{x}}}{\|\hat{\boldsymbol{x}}\|}, \tag{3.1.2}$$

with $\hat{\varphi}_{\hat{\boldsymbol{x}}} := \arg(\hat{\boldsymbol{x}}) = \arg(\boldsymbol{x}) = \varphi$. The mollifier $\chi : K_R \to \mathbb{R}_{0,+} := \mathbb{R}_+ \cup \{0\}$ satisfies the following conditions:

- $\chi(\hat{\boldsymbol{x}}) = \chi(\|\hat{\boldsymbol{x}}\|, r_0)$, that is, χ acts on the radial component of $\hat{\boldsymbol{x}} \in K_R$, and its dependence on the angle $\hat{\varphi}_{\hat{\boldsymbol{x}}}$ is only due to the fact that it depends on $r_0 = r_0(\hat{\varphi}_{\hat{\boldsymbol{x}}})$, $\hat{\varphi}_{\hat{\boldsymbol{x}}} \in [0, 2\pi)$;
- $0 \leq \chi(\hat{\boldsymbol{x}}) \leq 1$, $\hat{\boldsymbol{x}} \in K_R$, with $\chi(\hat{\boldsymbol{x}}) = 0$ for $\|\hat{\boldsymbol{x}}\| \leq \frac{r_0^-}{4}$ (r_0^- being the quantity defined in Assumption 2.1.3) and for $\|\hat{\boldsymbol{x}}\| \geq \tilde{R}$ ($\tilde{R} \in \mathbb{R}$, $\sup_{\varphi \in [0,2\pi)} r_0(\varphi) + \frac{r_0^-}{2} < \tilde{R} \leq R$), and with $\chi(\hat{\boldsymbol{x}}) = 1$ for $\|\hat{\boldsymbol{x}}\| = r_0(\hat{\varphi}_{\hat{\boldsymbol{x}}})$;
- χ is globally continuous, and it is strictly increasing for $\frac{r_0^-}{4} \leq \|\hat{\boldsymbol{x}}\| \leq r_0(\hat{\varphi}_{\hat{\boldsymbol{x}}})$ and strictly decreasing for $r_0(\hat{\varphi}_{\hat{\boldsymbol{x}}}) \leq \|\hat{\boldsymbol{x}}\| \leq \tilde{R}$.

The map is illustrated in Figure 3.1.1. We also require:

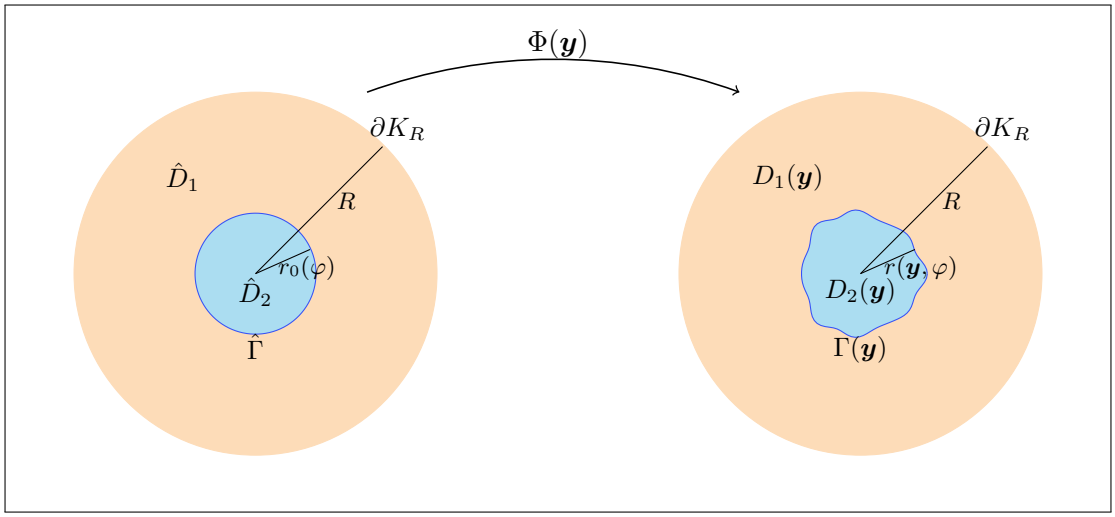

Figure 3.1.1: Mapping for the case of particle in free space.

Assumption 3.1.3. The mollifier χ in (3.1.2) has in $\hat{D}_2$ and in $\hat{D}_1 \cap K_R$ at least the same smoothness as the nominal radius r_0 has in $[0, 2\pi)$. Furthermore, $\max\left\{\|\chi\|_{C^1(\hat{D}_2)}, \|\chi\|_{C^1(\hat{D}_1 \cap K_R)}\right\} \leq C_\chi$, where $C_\chi \in \mathbb{R}$ is such that $0 < C_\chi < \frac{1}{\sqrt{2}\left(\frac{\bar{r_0}}{2} + c_\chi\right)}$ for some $c_\chi > 0$.

Lemma 3.1.4. *Let Assumptions 2.1.3 and 2.1.4.A be satisfied, and let the nominal radius r_0 belong to $C^k_{per}([0, 2\pi))$, with k as in (2.1.3). If we choose χ according to Assumption 3.1.3, then the mapping Φ given by (3.1.2) satisfies Assumption 3.1.2, with k the smoothness parameter of the radius r.*

Proof. The statement is quite clear from (3.1.2), since there we can see that $\Phi(\boldsymbol{y})$ consists just of scalings by $r(\boldsymbol{y})$ and r_0. However, we postpone the technical proof to the Appendix, Section E. □

For the implementation, it is not easy to find a mollifier for the mapping (3.1.2) that fulfills Assumption 3.1.3 and such that Φ and its inverse have a close form. What can be done instead is to relax Assumption 3.1.3. Namely, in (3.1.2) we use the following:

$$\chi(\hat{\boldsymbol{x}}) = \begin{cases} 0 & \text{if } \|\hat{\boldsymbol{x}}\| \leq \frac{\bar{r_0}}{4}, \\ \frac{\|\hat{\boldsymbol{x}}\| - \frac{\bar{r_0}}{4}}{r_0(\hat{\varphi}_{\hat{\boldsymbol{x}}}) - \frac{\bar{r_0}}{4}} & \text{if } \frac{\bar{r_0}}{4} < \|\hat{\boldsymbol{x}}\| \leq r_0(\hat{\varphi}_{\hat{\boldsymbol{x}}}), \\ \frac{R - \|\hat{\boldsymbol{x}}\|}{R - r_0(\hat{\varphi}_{\hat{\boldsymbol{x}}})} & \text{if } r_0(\hat{\varphi}_{\hat{\boldsymbol{x}}}) \leq \|\hat{\boldsymbol{x}}\| \leq R. \end{cases} \tag{3.1.3}$$

It is clear that this mollifier does not fulfill Assumption 3.1.3, because the mapping Φ is not a C^k-diffeomorphism in $\hat{D}_2$. However, denoting $\hat{D}_2^{in} := \left\{\hat{\boldsymbol{x}} \in \hat{D}_2 : \|\hat{\boldsymbol{x}}\| < \frac{\bar{r_0}}{4}\right\}$, we have that Φ is a C^k-diffeomorphism piecewise, in $\hat{D}_2^{in}$ and $\hat{D}_2 \setminus \hat{D}_2^{in}$, with k the smoothness parameter of the radius r. With such a property, we will see in the following chapters that, using some caution, the theory would still work (see Remark 6.1.10).

The multiplication by a mollifier is not the only way of propagating the movement of the interface. Among the valid alternatives we mention, for instance, the use of a harmonic extension [XT06, LTZ01] or of level set methods [OF01, AJT02] (see Conclusions).

Particle on substrate

We assume that the endpoints of the boundary can move horizontally, and denote the position of the left point by $\boldsymbol{x}^A$ and of the right one by $\boldsymbol{x}^B$.

To model the variation of the positions of $\boldsymbol{x}^A$ and $\boldsymbol{x}^B$, we associate to each of these points a uniform random variable, i.e.:

$$\begin{array}{lll} \boldsymbol{x}^A(\omega) = & -r_0 - r_0\beta_1 Y_A(\omega) & = -r_A(\omega), \quad \omega \in \Omega, \\ \boldsymbol{x}^B(\omega) = & r_0 + r_0\beta_2 Y_B(\omega) & = r_B(\omega), \quad \omega \in \Omega, \end{array} \tag{3.1.4}$$

where:

- Y_A, $Y_B \sim \mathcal{U}([-1,1])$;
- r_0 is the nominal radius, assumed to be angle-independent (although an angle-dependent radius is possible and the procedure would not change);
- $-\frac{1}{2} < \beta_1,\, \beta_2 < \frac{1}{2}$.

In the parametric formulation, $\boldsymbol{x}^A = \boldsymbol{x}^A(y_A)$ and $\boldsymbol{x}^B = \boldsymbol{x}^B(y_B)$, with $y_A, y_B \in [-1,1]$.

Since we assume that the substrate is non-penetrable and that the bottom part of the particle adheres perfectly to it, there cannot be random boundary perturbations in the normal direction at the interface between the particle and the substrate. For the interface between the particle and the free space, instead, we consider an angle-dependent radius $\tilde{r} = \tilde{r}(y_A, y_B, \varphi)$, which can be regarded as the mean radius once the boundary points $\boldsymbol{x}^A$ and $\boldsymbol{x}^B$ have been fixed:

$$\tilde{r}(y_A, y_B, \varphi) = r_A(y_A) + \frac{r_B(y_B) - r_A(y_A)}{\pi}\varphi, \quad \varphi \in [0,\pi], \tag{3.1.5}$$

where we use the convention that $\varphi = 0$ at $\boldsymbol{x}^A$ and $\varphi = \pi$ at $\boldsymbol{x}^B$. The radius $\tilde{r}(\boldsymbol{y}, \varphi)$ plays the same role as $r_0(\varphi)$ in (2.2.3). We model the shape variations adding random sinusoidal perturbations to $\tilde{r}(\varphi)$ in the radial direction:

$$r(\boldsymbol{y}, \varphi) = \tilde{r}(y_A, y_B, \varphi) + \sum_{j=1}^{J} s_j \sin(j\varphi) y_j, \quad \varphi \in [0,\pi], \tag{3.1.6}$$

where $\{y_j\}_{j=1}^J$ are, as before, the images of uniformly distributed random variables. Now we have $\boldsymbol{y} = (y_A, y_B, y_1, ..., y_J) \in [-1,1]^{J+2}$. In (3.1.6) just sines and no cosines are present because the boundary points are fixed.

In order to bound the radius (3.1.6) from above and from below, a *sufficient* condition is that $\sum_{j=1}^J |s_j| < \frac{1}{2}\min\{r_A, r_B\}$, i.e., introducing the adimensional coefficients $\tilde{s}_j := \frac{|s_j|}{r_0}$ for $j = 1, \ldots, J$:

$$\sum_{j=1}^{J} |\tilde{s}_j| = \sum_{j=1}^{J} \frac{|s_j|}{r_0} < \min\{1-\beta_1, 1-\beta_2\}. \tag{3.1.7}$$

In particular, since the perturbations are in the radial direction, the particle can never penetrate into the substrate, and ensuring a lower bound for the radius r is sufficient to avoid self-intersection of the boundary.

Considering (3.1.4), (3.1.5) and (3.1.6) together, we finally have:

$$\begin{aligned} & r(\boldsymbol{y}, \varphi) = r_0 + r_0\beta_1 y_A\left(1 - \frac{\varphi}{\pi}\right) + r_0\beta_2 y_B \frac{\varphi}{\pi} + \sum_{j=1}^{J} r_0 \tilde{s}_j \sin(j\varphi) y_j, \\ & \varphi \in [0,\pi],\ \boldsymbol{y} = (y_A, y_B, y_1, \ldots, y_J) \in [-1,1]^{J+2},\ J \in \mathbb{N}. \end{aligned} \tag{3.1.8}$$

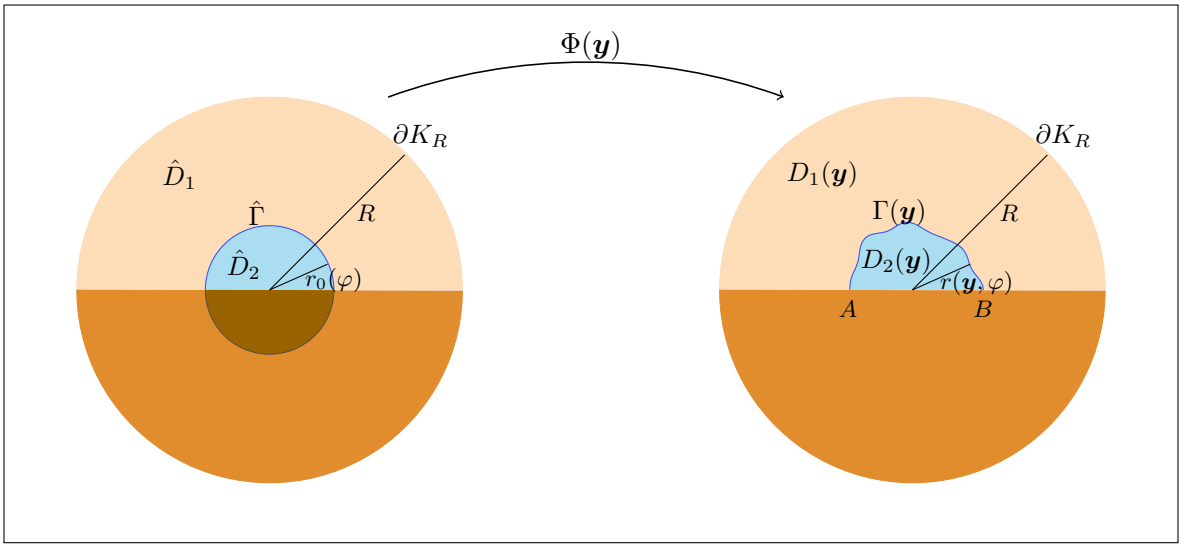

Figure 3.1.2: Mapping for the case of half-circular particle on substrate.

Remark 3.1.5. Adding the random perturbations in radial direction, the sinusoids in (3.1.8) are skewed with respect to $\tilde{r} = \tilde{r}(y_A, y_B, \varphi)$, and one may wonder if we still model all possible shapes. This can be achieved if we allow the random variables $\{Y_j\}_{j=1}^J$ to be still independent but not identically distributed (as long as they have compact image).

The map $\Phi(\boldsymbol{y})$ from the nominal configuration is shown in Figure 3.1.2 and it is built in the following way:

- the two points on the substrate surface with radius $-r_0$ and r_0 are mapped to $\boldsymbol{x}^A$ and $\boldsymbol{x}^B$, respectively;
- we consider a spiral section with radius $\tilde{r}(\boldsymbol{y}, \varphi)$, $\varphi \in [0, \pi)$, as defined in (3.1.5), and map it to the scatterer boundary (light blue areas in Figure 3.1.2);
- in order to have a mapping which is continuous across the substrate surface, on the nominal configuration we consider $\tilde{r}(\boldsymbol{y}, \varphi)$ mirrored with respect to the horizontal plane, i.e. $\tilde{r}(\boldsymbol{y}, \varphi)$ for $\varphi \in [\pi, 2\pi)$ (darker orange area in Figure 3.1.2), and map it to the scatterer boundary mirrored with respect to the substrate surface;
- as in the previous example, a circle sufficiently far from the scatterer playing the role of ∂K_R, and thus fixed for all parameter realizations, is considered.

More precisely, in the end $\Phi = \Phi(\boldsymbol{y})$ is the same as in (3.1.2) with $r_0(\varphi)$ replaced by $\tilde{r}(\boldsymbol{y}, \varphi)$:

$$\boldsymbol{x}(\boldsymbol{y}) = \Phi(\boldsymbol{y}, \hat{\boldsymbol{x}}) = \hat{\boldsymbol{x}} + \chi(\hat{\boldsymbol{x}}) \left(r(\boldsymbol{y}, \hat{\varphi}_{\hat{\boldsymbol{x}}}) - \tilde{r}(\boldsymbol{y}, \hat{\varphi}_{\hat{\boldsymbol{x}}}) \right) \frac{\hat{\boldsymbol{x}}}{\|\hat{\boldsymbol{x}}\|}, \tag{3.1.9}$$

where χ is a mollifier satisfying similar properties as the ones in the free space case and fulfilling Assumption 3.1.3 with $C_\chi < \frac{1}{\frac{3}{\sqrt{2}}\left(\frac{\bar{r_0}}{2} + c_\chi\right)}$ for some $c_\chi > 0$.

Therefore, in an analogous manner as we will do in Section 6 for the mapping (3.1.2), it can be shown that this map satisfies Assumption 3.1.2 too.

Alternatively, one can relax the assumptions on the mollifier and define it in a similar way as in (3.1.3).

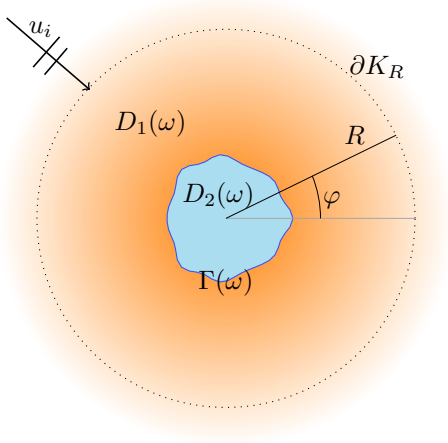

Figure 3.2.1: Domain considered in (3.2.1).

3.2. Variational formulation on the nominal configuration

The analysis developed in this section refers only to the particle in free space case, although it could be extended to the particle on substrate case. In the first subsection we derive the variational formulation for the model problem (1.0.1), while in the second subsection we address its well-posedness (in Hadamard's sense).

3.2.1. Variational formulation

We consider again the space K_R enclosed inside a circle of radius $R > 0$, the latter *fixed for all realizations* $\omega \in \Omega$ and containing the scatterer in its interior (see Figure 3.2.1). Then, using the Dirichlet-to-Neumann map (DtN, see [Néd01, Sect. 2.6.3]) for the exterior of K_R, we can state the variational formulation for (1.0.1) on the *bounded* domain K_R. Denoting $V := H^1(K_R)$, we have:

$$\begin{aligned}
&\text{Find } u(\omega) \in V : \\
&\int_{K_R} \alpha(\omega, \boldsymbol{x})\, \nabla u(\omega) \cdot \nabla v - \kappa^2(\omega, \boldsymbol{x})\, u(\omega) v \, d\boldsymbol{x} \\
&- \int_{\partial K_R} \left(DtN(u(\omega) - u_i) + \frac{\partial u_i}{\partial \boldsymbol{n}_R} \right) v \, dS = 0, \quad \text{for all } v \in V \text{ and every } \omega \in \Omega,
\end{aligned} \tag{3.2.1}$$

where $\boldsymbol{n}_R$ is the outer normal to ∂K_R.

Reordering the terms, this results in:

$$\begin{aligned}
&\text{Find } u(\omega) \in V : \\
&a_\omega(u(\omega), v) := \int_{K_R} \alpha(\omega, \boldsymbol{x})\, \nabla u(\omega) \cdot \nabla v - \kappa^2(\omega, \boldsymbol{x})\, u(\omega) v \, d\boldsymbol{x} - \int_{\partial K_R} DtN(u(\omega)) v \, dS \\
&= \int_{\partial K_R} \left(-DtN(u_i) + \frac{\partial u_i}{\partial \boldsymbol{n}_R} \right) v \, dS, \quad \text{for all } v \in V \text{ and every } \omega \in \Omega.
\end{aligned} \tag{3.2.2}$$

Using the parametric description of the uncertain interface developed in Chapter 2, we can replace

$\Gamma(\omega)$, $\omega \in \Omega$, by $\Gamma(\boldsymbol{y})$, $\boldsymbol{y} \in \mathcal{P}_J$, and the variational formulation (3.2.2) reads:

$$\begin{aligned}
&\text{Find } u(\boldsymbol{y}) \in V : \\
&a_y(u(\boldsymbol{y}), v) := \int_{K_R} \alpha(\boldsymbol{y}, \boldsymbol{x})\, \nabla u(\boldsymbol{y}) \cdot \nabla v - \kappa^2(\boldsymbol{y}, \boldsymbol{x})\, u(\boldsymbol{y}) v \, d\boldsymbol{x} - \int_{\partial K_R} DtN(u(\boldsymbol{y}))v \, dS \\
&= \int_{\partial K_R} \left(-DtN(u_i) + \frac{\partial u_i}{\partial \boldsymbol{n}_R} \right) v \, dS, \quad \text{for all } v \in V \text{ and all } \boldsymbol{y} \in \mathcal{P}_J.
\end{aligned} \tag{3.2.3}$$

Finally, we can use the inverse of the diffeomorphism $\Phi(\boldsymbol{y})$, $\boldsymbol{y} \in \mathcal{P}_J$, $J \in \mathbb{N}$, introduced in Section 3.1, to map the physical configuration with interface $\Gamma(\boldsymbol{y})$ to the nominal configuration. In this way we obtain the following parametric, variational formulation on the *fixed*, deterministic configuration with interface $\hat{\Gamma}$:

$$\begin{aligned}
&\text{Find } \hat{u}(\boldsymbol{y}) \in \hat{V} : \\
&\hat{a}_y(\hat{u}(\boldsymbol{y}), \hat{v}) := \int_{K_R} \hat{\alpha}(\boldsymbol{y}, \hat{\boldsymbol{x}})\, \hat{\nabla} \hat{u}(\boldsymbol{y}) \cdot \hat{\nabla} \hat{v} \, d\hat{\boldsymbol{x}} - \hat{\kappa}^2(\boldsymbol{y}, \hat{\boldsymbol{x}})\, \hat{u}(\boldsymbol{y}) \hat{v} \, d\hat{\boldsymbol{x}} - \int_{\partial K_R} DtN(\hat{u}(\boldsymbol{y}))\hat{v} \, dS \\
&= \int_{\partial K_R} \left(-DtN(u_i) + \frac{\partial u_i}{\partial \boldsymbol{n}_R} \right) \hat{v} \, dS, \quad \text{for all } \hat{v} \in \hat{V} \text{ and all } \boldsymbol{y} \in \mathcal{P}_J,
\end{aligned} \tag{3.2.4}$$

where $\hat{V} = H^1(K_R) = V$ and

$$\begin{aligned}
\hat{\alpha}(\boldsymbol{y}, \hat{\boldsymbol{x}}) &= D\Phi(\boldsymbol{y})^{-1} D\Phi(\boldsymbol{y})^{-\top} \det D\Phi(\boldsymbol{y}) \alpha(\boldsymbol{y}, \Phi^{-1}(\boldsymbol{y})(\boldsymbol{x})), \\
\hat{\kappa}^2(\boldsymbol{y}, \hat{\boldsymbol{x}}) &= \det D\Phi(\boldsymbol{y}) \kappa^2(\boldsymbol{y}, \Phi^{-1}(\boldsymbol{y})(\boldsymbol{x}))
\end{aligned} \tag{3.2.5}$$

(with $D\Phi(\boldsymbol{y})$ the Jacobian matrix of $\Phi(\boldsymbol{y})$). In (3.2.4), $\hat{\nabla}$ denotes the gradient with respect to $\hat{\boldsymbol{x}} \in K_R$, the coordinates in the nominal configuration.

Remark 3.2.1. Formulas (3.2.5) explain why we have to require $k \geq 1$ in Assumption 3.1.2 and either $p < \frac{1}{2}$ in Assumption 2.1.4.A, or $k \geq 3$ in Assumption 2.1.4.B (since in general $D\Phi$ and its inverse will depend on $\dfrac{\partial r}{\partial \varphi}$).

We are now in a position to give a rigorous definition for the solution to (3.2.3) (or equivalently for the solution to (3.2.2)):

Definition 3.2.2. The function $u(\boldsymbol{y})$, $\boldsymbol{y} \in \mathcal{P}_J$, $J \in \mathbb{N}$, is a solution to (3.2.3) if and only if its pullback $(\Phi^*(\boldsymbol{y})u(\boldsymbol{y}))(\hat{\boldsymbol{x}}) := u(\Phi(\boldsymbol{y}, \hat{\boldsymbol{x}})) \in H^1(K_R)$ is a solution to (3.2.4).

3.2.2. Well-posedness of the model problem

The boundedness of K_R allows us to apply the Fredholm Alternative [McL00, Thm. 2.27] to prove existence of the solution to (3.2.4), while uniqueness is ensured by the sign properties of the DtN map.

Theorem 3.2.3. *The solution to the variational formulation* (3.2.2) *exists and is unique, for every $\omega \in \Omega$. Equivalently, if Assumption 3.1.2 is fulfilled, then* (3.2.4) *admits a unique solution, for every $J \in \mathbb{N}$ and every $\boldsymbol{y} \in \mathcal{P}_J$.*

Proof. We denote

$$a^p_\omega(u, v) := \int_{K_R} \alpha(\omega, \boldsymbol{x})\, \nabla u(\omega) \cdot \nabla v \, d\boldsymbol{x} - \int_{\partial K_R} DtN(u(\omega))v \, dS.$$

If we show that the bilinear form $a^p_\omega(u,v)$ is coercive, then the associated operator $\mathcal{A}^p_\omega$ defined as $(A^p_\omega u, v) := a^p_\omega(u,v)$ is Fredholm with index 0 [McL00, Lemma 2.32].

The operator $\mathcal{B}_\omega : H^1(K_R) \to H^{-1}(K_R)$ associated with $\int_{K_R} \kappa^2(\omega,\boldsymbol{x})u(\omega)v\,d\boldsymbol{x}$ is given by $\mathcal{B}_\omega = \kappa^2(\omega,\boldsymbol{x})I$, with $I : H^1(K_R) \to H^{-1}(K_R)$ the identity operator. Since K_R is bounded, $I : H^1(K_R) \to H^{-1}(K_R)$ and thus $\mathcal{B}_\omega$ are compact thanks to Rellich's embedding theorem [McL00, Thm. 3.27].

Therefore, if $a^p_\omega(u,v)$ is coercive, then the operator $\mathcal{A}^p_\omega + \mathcal{B}_\omega$ is Fredholm with index 0 [McL00, Thm. 2.33], and we can apply the Fredholm Alternative [McL00, Thm. 2.27] to get existence of the solution and uniqueness if the associated homogeneous problem

$$a_\omega(u(\omega), v) = 0, \quad \text{for all } v \in V, \tag{3.2.6}$$

admits only the trivial solution.

For the coercivity of $a^p_\omega(\cdot,\cdot)$ it holds that, for every $w \in H^1(K_R)$:

$$\begin{aligned} \operatorname{Re} a^p_\omega(w,w) &\geq \min\{1,\alpha_2\}\,|w|^2_{H^1(K_R)} - \operatorname{Re}\langle DtN w, w\rangle_{L^2(\partial K_R)} \\ &\geq \min\{1,\alpha_2\}\,|w|^2_{H^1(K_R)} + \|w\|^2_{L^2(\partial K_R)} \\ &\geq \min\{1,\alpha_2\}\,\frac{C(R)}{C(R)+1}\,\|w\|^2_{H^1(K_R)}\,. \end{aligned} \tag{3.2.7}$$

The first inequality is obtained exploiting the sign conditions of the DtN map [Néd01, Thm. 2.6.4], the second one is a Poincaré-Friedrichs-type inequality

$$|w|^2_{H^1(K_R)} + \|w\|^2_{L^2(\partial K_R)} \geq C(R)\,\|w\|^2_{L^2(K_R)}\,, \quad \text{for every } w \in H^1(K_R), \tag{3.2.8}$$

where the constant $C > 0$ depends on the radius R of K_R. This latter inequality can be proved in the same way as the classical Poincaré-Friedrichs inequality. Equation 3.2.7 implies that the Fredholm Alternative holds, and we have existence of the solution.

For uniqueness, let us consider the homogeneous problem (3.2.6). It is sufficient to show that

$$a_\omega(u,u) = 0 \iff u \equiv 0.$$

If $a_\omega(u,u) = 0$, it means in particular that

$$\operatorname{Im} a_\omega(u,u) = \operatorname{Im} \int_{\partial K_R} DtN(u(\omega))u\,dS = 0.$$

For the sign properties of the DtN map [Néd01, Thm. 2.6.1 and Thm. 2.6.4],

$$\operatorname{Im}\langle DtN u, u\rangle_{L^2(\partial K_R)} = 0 \iff u \equiv 0 \text{ on } \partial K_R,$$

while the linearity of the DtN map implies that also $\dfrac{\partial u}{\partial \boldsymbol{n}_R} = 0$ on ∂K_R and thus $u \equiv 0$ for $|\boldsymbol{x}| \geq R$.

Consider now a ball B_r with center on ∂K_R and radius $r < \operatorname{dist}(\partial K_R, D_2)$. In B_r, the solution u satisfies the homogeneous equation $-\Delta u - \kappa^2(\omega,\boldsymbol{x})u = 0$ and thus $u|_{B_r} \in H^2(B_r)$. Also, from the previous considerations we know that there exists a ball $B_{r'} \subset B_r \setminus K_R$, with $r' < r$, such that $u|_{B_{r'}} \equiv 0$. Then, the unique continuation principle [CK12, Thm. 8.6] implies that $u \equiv 0$ in the whole B_r. Iterating this argument and using the compactness of K_R, we obtain that $u \equiv 0$ in K_R.

After substitution of $\omega \in \Omega$ with $\boldsymbol{y} \in \mathcal{P}_J$, we obtain that also the solution to (3.2.4) exists and is unique thanks to the bijectivity of the maps $\Phi(\boldsymbol{y})$, $\boldsymbol{y} \in \mathcal{P}_J$, $J \in \mathbb{N}$ (and Definition 3.2.2). □

To have well-posedness of the problem, we still have to prove that the solution to (3.2.4) depends continuously on the data, which in our case consist of the incoming wave u_i. Thus, we would desire to have a bound on the $H^1(K_R)$-norm of $\hat{u}$ by some norm of u_i. This stability property will be needed later for convergence purposes. More precisely, for reasons that will become clearer in Chapter 4, we need a bound for the solution on the nominal configuration which is uniform over all the realizations, i.e. independent of the truncation parameter $J \in \mathbb{N}$ and of $\boldsymbol{y} \in \mathcal{P}_J$.

Unfortunately, a $\boldsymbol{y}$-uniform stability result cannot be achieved in general for the Helmholtz equation. The reason being that, without any limitation on the wavenumber and for a generic star-shaped scatterer, it can happen that a small wavenumber excites resonances at the boundary of the object, with an uncontrollable increase of the amplitude of the field u in that region.

Therefore, in order to get a J- and $\boldsymbol{y}$-uniform stability estimate, we formulate the following hypothesis, which consists in requiring the wavelength to be large compared to the diameter of the scatterer (this is fulfilled, for example, in nano-optics applications).

Assumption 3.2.4 (Large wavelength assumption)**.** The wavenumbers in (1.0.2) satisfy the condition:

$$\kappa_1^2, \kappa_2^2 \leq \tau\, C(R), \quad \text{for some } 0 < \tau < \min\{1, \alpha_2\},$$

with $C(R)$ as in (3.2.8):

$$C(R) = \inf_{w \in H^1(K_R)} \frac{|w|^2_{H^1(K_R)} + \|w\|^2_{L^2(\partial K_R)}}{\|w\|^2_{L^2(K_R)}}. \tag{3.2.9}$$

To obtain a J- and $\boldsymbol{y}$- uniform bound on the solution, we prove coercivity of the bilinear form $\hat{a}_y(\cdot,\cdot)$, with a coercivity constant uniform in $J \in \mathbb{N}$ and in $\boldsymbol{y} \in \mathcal{P}_J$. This is assessed in the following lemma, which, together with its corollary, show that, if the domain mapping satisfies Assumption 3.1.2, then Assumption 3.2.4 ensures uniform stability for (3.2.4) under some constraints on the constant τ:

Lemma 3.2.5. *Let Assumption 3.1.2 be satisfied. There exists a constant $0 < T < 1$ independent of $J \in \mathbb{N}$ and $\boldsymbol{y} \in \mathcal{P}_J$ such that, if Assumption 3.2.4 holds with $\tau < T$, then the bilinear form $\hat{a}_y(\cdot,\cdot)$ in* (3.2.4) *is coercive, with coercivity constant γ independent of $J \in \mathbb{N}$ and $\boldsymbol{y} \in \mathcal{P}_J$.*

Proof. Thanks to Assumption 3.1.2, we have that there exist $\sigma_{\min}, \sigma_{\max} > 0$ such that, for every $J \in \mathbb{N}$ and every $\boldsymbol{y} \in \mathcal{P}_J$:

$$\sigma^2_{\min} \|\boldsymbol{\xi}\|^2_{\mathbb{C}^2} \leq \|D\Phi^{-\top}(\boldsymbol{y}, \hat{\boldsymbol{x}})\boldsymbol{\xi}\|^2_{\mathbb{C}^2}, \tag{3.2.10}$$

$$\frac{1}{\sigma^2_{\max}} \leq \det D\Phi(\boldsymbol{y}, \hat{\boldsymbol{x}}) \leq \frac{1}{\sigma^2_{\min}}, \tag{3.2.11}$$

for every $\boldsymbol{\xi} \in \mathbb{C}^2$, $\hat{\boldsymbol{x}} \in K_R$. Then, for every $J \in \mathbb{N}$, $\boldsymbol{y} \in \mathcal{P}_J$ and every $\hat{w} \in H^1(K_R)$, we have:

$$\begin{aligned}
\operatorname{Re} \hat{a}_y(\hat{w}, \hat{w}) &\geq \min\{1, \alpha_2\} |D\Phi^{-\top}(\boldsymbol{y})\hat{\nabla}\hat{w}(\det D\Phi(\boldsymbol{y}))^{\frac{1}{2}}|^2_{H^1(K_R)} \\
&\quad - \max\left\{\kappa_1^2, \alpha_2\kappa_2^2\right\} \left\|\hat{w}(\det D\Phi(\boldsymbol{y}))^{\frac{1}{2}}\right\|^2_{L^2(K_R)} - \operatorname{Re}\langle DtN(\hat{w}), \hat{w}\rangle_{L^2(\partial K_R)} \\
&\geq \min\{1, \alpha_2\} \frac{\sigma^2_{\min}}{\sigma^2_{\max}} |\hat{w}|^2_{H^1(K_R)} - \max\left\{\kappa_1^2, \alpha_2\kappa_2^2\right\} \frac{1}{\sigma^2_{\min}} \|\hat{w}\|^2_{L^2(K_R)} + \|\hat{w}\|^2_{L^2(\partial K_R)} \\
&\geq \left(\min\{1, \alpha_2\} \frac{\sigma^2_{\min}}{\sigma^2_{\max}} - \max\{1, \alpha_2\} \frac{\tau}{\sigma^2_{\min}}\right) |\hat{w}|^2_{H^1(K_R)} \\
&\quad + \left(1 - \max\{1, \alpha_2\} \frac{\tau}{\sigma^2_{\min}}\right) \|\hat{w}\|^2_{L^2(\partial K_R)}.
\end{aligned}$$

In the second inequality we have used equations (3.2.10)-(3.2.11) and the sign conditions of the DtN map [Néd01, Thm. 2.6.4].

Now, if we choose τ in Assumption 3.2.4 such that

$$\tau < T := \frac{\sigma_{\min}^4 \min\{1, \alpha_2\}}{\sigma_{\max}^2 \max\{1, \alpha_2\}},$$

we have that

$$C_1 := \min\{1, \alpha_2\} \frac{\sigma_{\min}^2}{\sigma_{\max}^2} - \max\{1, \alpha_2\} \frac{\tau}{\sigma_{\min}^2} > 0, \qquad C_2 := 1 - \max\{1, \alpha_2\} \frac{\tau}{\sigma_{\min}^2} > 0.$$

Using a Poincaré-Friedrichs-type inequality on K_R as in (3.2.8), we finally obtain

$$\operatorname{Re} \hat{a}_y(\hat{w}, \hat{w}) \geq \min\{C_1, C_2\} \frac{C(R)}{C(R)+1} \|\hat{w}\|_{H^1(K_R)}^2,$$

for every $J \in \mathbb{N}$, every $\boldsymbol{y} \in \mathcal{P}_J$ and every $\hat{w} \in H^1(K_R)$. This means that the bilinear form $\hat{a}_y(\cdot, \cdot)$ is coercive with coercivity constant

$$\gamma := \min\{C_1, C_2\} \frac{C(R)}{C(R)+1},$$

independent of $J \in \mathbb{N}$ and of $\boldsymbol{y} \in \mathcal{P}_J$. □

Corollary 3.2.6. *Let Assumptions 3.1.2 and 3.2.4 with $\tau \leq T$ from Lemma 3.2.5 be satisfied. Then there exist positive constants B_1, B_2 independent of $J \in \mathbb{N}$ and of $\boldsymbol{y} \in \mathcal{P}_J$ (but which do depend on $\alpha_2, \sigma_{min}, \sigma_{max}, \kappa_1, \kappa_2$ and R) such that, for every $J \in \mathbb{N}$ and every $\boldsymbol{y} \in \mathcal{P}_J$:*

$$\|\hat{u}(\boldsymbol{y})\|_{H^1(K_R)} \leq B_1 \|u_i\|_{H^{\frac{1}{2}}(\partial K_R)} + B_2 \left\| \frac{\partial u_i}{\partial \boldsymbol{n}_R} \right\|_{H^{-\frac{1}{2}}(\partial K_R)}. \tag{3.2.12}$$

The bound is uniform over the realizations once we use the analytic expression for $\dfrac{\partial u_i}{\partial \boldsymbol{n}_i}$, i.e. $\dfrac{\partial u_i}{\partial \boldsymbol{n}_R} = \kappa_1 \boldsymbol{d} \cdot \boldsymbol{n}_R e^{i\kappa_1 \boldsymbol{d} \cdot \boldsymbol{x}}$ for the incoming wave.

Proof. Lemma 3.2.5 ensures that the parameter-dependent bilinear form $\hat{a}_y(\cdot, \cdot)$ is uniformly coercive, with coercivity constant γ independent of $J \in \mathbb{N}$ and $\boldsymbol{y} \in \mathcal{P}_J$. Moreover, the right-hand side in (3.2.4) is continuous with respect to the H^1-norm:

$$\begin{aligned}
\left| \int_{\partial K_R} \left(-DtN(u_i) + \frac{\partial u_i}{\partial \boldsymbol{n}_R} \right) v \, dS \right| &\leq \left(\|DtN(u_i)\|_{H^{-\frac{1}{2}}(\partial K_R)} + \left\| \frac{\partial u_i}{\partial \boldsymbol{n}_R} \right\|_{H^{-\frac{1}{2}}(\partial K_R)} \right) \|v\|_{H^{\frac{1}{2}}(\partial K_R)} \\
&\leq \left(\|DtN(u_i)\|_{H^{-\frac{1}{2}}(\partial K_R)} + \left\| \frac{\partial u_i}{\partial \boldsymbol{n}_R} \right\|_{H^{-\frac{1}{2}}(\partial K_R)} \right) C(\partial K_R) \|v\|_{H^1(K_R)} \\
&\leq \left(\tilde{C}(R) \|u_i\|_{H^{\frac{1}{2}}(\partial K_R)} + \left\| \frac{\partial u_i}{\partial \boldsymbol{n}_R} \right\|_{H^{-\frac{1}{2}}(\partial K_R)} \right) C(\partial K_R) \|v\|_{H^1(K_R)},
\end{aligned}$$

where we have used the continuity of the trace operator on ∂K_R, with continuity constant $C(\partial K_R)$, and the continuity of the DtN operator [Néd01, Thm. 2.6.4], with continuity constant $\tilde{C}(R)$. We highlight that the constant $\tilde{C}$ depends only on the radius R. Also the constant $C(\partial K_R)$ is independent of $J \in \mathbb{N}$ and of $\boldsymbol{y} \in \mathcal{P}_j$.

Together with the coercivity of the bilinear form, this allows to apply the Lax-Milgram lemma and obtain (3.2.12) with $B_1 := \frac{\tilde{C}(R) C(\partial K_R)}{\gamma}$ and $B_2 := \frac{C(\partial K_R)}{\gamma}$. □

Remark 3.2.7. In order to have a stability estimate for the solution on the *physical* configuration K_R for a realization $\boldsymbol{y} \in \mathcal{P}_J$, we can consider the nominal radius r_0 to be the actual radius of that realization, and as mapping $\Phi(\boldsymbol{y})$ the identity map. In this case, we would have $\sigma_{\min} = \sigma_{\max} = 1$. The coercivity constant would then be $\gamma = (\min\{1, \alpha_2\} - \max\{1, \alpha_2\}\,\tau)\frac{C(R)}{C(R)+1}$, and we would need the restriction $\tau < T = \frac{\min\{1,\alpha_2\}}{\max\{1,\alpha_2\}}$ in Assumption 3.1.2.

Remark 3.2.8. In the variational formulation that we have considered, the right-hand side involves only integration over the fixed outer boundary, and thus also after the change of coordinates it does not depend on $\boldsymbol{y}$. In general, for a right-hand side involving volume integrals, we stress that after the coordinate transformation it would depend on the parameter $\boldsymbol{y}$ also in the case that in the original formulation it was deterministic. In this latter case, in order to have a J- and $\boldsymbol{y}$-independent bound as in equation (3.2.12), one needs to provide also a J- and $\boldsymbol{y}$-independent bound for the right-hand side, which is guaranteed by Assumption 3.1.2.

The variational form (3.2.4) is now ready to be discretized. Notice that in this case *two* discretizations are needed: the discretization with respect to $\boldsymbol{y}$ and the discretization with respect to $\hat{\boldsymbol{x}}$. The former will be considered in Chapter 4, while for the latter we will rely on a standard finite element discretization, for which we will provide more details in Chapter 6.

4. Stochastic collocation

In this chapter we address the parameter space discretization of (3.2.4) through stochastic collocation. In the first section we recall the main features of this method and in particular of sparse interpolation and quadrature. In the second section, we describe the sparse adaptive Smolyak algorithm used in our numerical experiments to select the collocation points. In the third and last section, we show that the hypotheses for the convergence theorems for the sparse interpolation and quadrature hold for the Helmholtz transmission problem.

In the first two sections, we present the results in the general case that the parameter space is $\mathcal{P} := [-1,1]^d$ with d large and possibly infinite (in the latter case we write $[-1,1]^\infty = \bigotimes_{j\geq 1}[-1,1]$ for the set of infinite sequences where every term is in $[-1,1]$). Considering $d = \infty$, we ensure that our convergence results are independent of the dimension of the parameter space.

4.1. High-dimensional sparse polynomial interpolation and quadrature

Let $g = g(\boldsymbol{y})$ be the Q.o.I., for instance the solution to a parametric differential equation, taking values, for each *fixed* value of the parameter $\boldsymbol{y}$, in a separable Banach space X. For example, if g is the the solution $\hat{u}$ to (3.2.4), then $X = V = H^1(K_R)$. We consider the map $\mathcal{P} \to X$ such that $\boldsymbol{y} \mapsto g(\boldsymbol{y})$, and call it the *solution map*.

The sparse polynomial interpolation and quadrature fit into the framework of high-order polynomial approximation methods, and in particular of stochastic collocation.

High-order polynomial approximation methods in uncertainty quantification are the extension of high-order polynomial approximation in the one-dimensional case, in order to approximate maps $\mathcal{P} \to X$, where $\mathcal{P}$ is high, and possibly infinite, dimensional. To this aim, let us introduce the set

$$\mathcal{F} = \left\{ \nu \in \mathbb{N}_0^{\mathbb{N}} : \sharp \operatorname{supp} \nu < \infty \right\}, \tag{4.1.1}$$

with $\mathbb{N}_0 = \mathbb{N} \cup \{0\}$ and the support of a multi-index defined as $\operatorname{supp} \nu = \{j \in \mathbb{N} : \nu_j \neq 0\}$.

The idea is to approximate the Q.o.I. by

$$g_\Lambda(\boldsymbol{y}) = \sum_{\nu \in \Lambda} g_\nu \boldsymbol{y}^\nu, \quad g_\nu \in X, \tag{4.1.2}$$

where $\boldsymbol{y}^\nu = \prod_{j\geq 1} y_j^{\nu_j}$, $j \geq 1$, and $\Lambda \subset \mathcal{F}$ a *finite* subset of $\mathcal{F}$. The approximate quantity g_Λ belongs then to the finite dimensional space

$$X_\Lambda = \operatorname{span} \left\{ \sum_{\nu \in \Lambda} v_\nu \boldsymbol{y}^\nu : v_\nu \in X, \nu \in \Lambda \right\}.$$

In the stochastic collocation framework, the polynomial approximation relies on the computation of samples of the solution $g(\boldsymbol{y}_i)$ at some points $\boldsymbol{y}_i$, $i = 1 \ldots, \ldots k$, $k \in \mathbb{N}$, referred to as *collocation points*. We direct to [BNT10] and [XH05] for an exhaustive survey of this method. In

the following, we focus on *sparse* polynomial approximation, following the lines of [CCS14] for interpolation and of [SS13] for quadrature.

In order to consider sparse approximation operators, we require Λ to be a downward closed index set :

Definition 4.1.1. (Definition 1.1 in [CCS14]) A subset $\Lambda \subset \mathcal{F}$ of finite cardinality N is a downward closed index set[1] if

$$\nu \in \Lambda \text{ and } \mu \leq \nu \ \Rightarrow \mu \in \Lambda, \tag{4.1.3}$$

where $\mu \leq \nu$ means that $\mu_j \leq \nu_j$ for all j.

Equivalently (Definition 3.1 in [SS13]), $\Lambda \subset \mathcal{F}$ is downward closed if $0_{\mathcal{F}} = (0, 0, \ldots) \in \Lambda$ and if, for every $\nu \in \Lambda$, $\nu \neq 0_{\mathcal{F}}$, it holds that $\nu - e_j \in \Lambda$ for all $j \in \operatorname{supp} \nu$, where $e_j \in \{0,1\}^{\mathbb{N}}$ denotes the index vector with 1 in position $j \in \mathbb{N}$ and 0 in all other positions $i \in \mathbb{N} \setminus \{j\}$.

We define the following relations:

- $\mu \neq \nu$ if there exists a $j \in \mathbb{N}$ such that $\mu_j \neq \nu_j$,
- $\mu < \nu$ if $\mu \leq \nu$ but $\mu \neq \nu$,
- $\mu \not\leq \nu$ if there exists a $j \in \mathbb{N}$ for which $\mu_j > \nu_j$.

We say that an index $\nu \in \Lambda$ is *maximal* if and only if there is no $\mu \in \Lambda$ such that $\nu < \mu$. Any finite index set Λ contains at least one maximal element. For a downward closed set Λ:

$$\nu \in \Lambda \text{ is maximal } \ \Leftrightarrow \ \Lambda \setminus \{\nu\} \text{ is downward closed.} \tag{4.1.4}$$

Therefore, if $(\Lambda_n)_{n\geq 1}$ is a nested sequence of downward closed sets with $\sharp \Lambda_n = n$, there exists a unique sequence of indices $(\nu^n)_{n\geq 1} \in \mathcal{F}^{\mathbb{N}}$, with $\nu^1 = 0_{\mathcal{F}}$, such that, for all $n \geq 1$,

$$\Lambda_n = \left\{\nu^1, \ldots, \nu^n\right\}, \quad \nu^n \text{ maximal in } \Lambda_n.$$

Univariate operators and tensorization

Let $(\zeta_j^k)_{j=0}^{n_k}$ be a sequence of distinct points in $\mathcal{P}_l = [-1, 1]$ (for a generic integer $l \geq 1$) and I_k, $k \in \mathbb{N}_0$, the univariate polynomial interpolation operator associated with these points, defined as

$$I_k g_l = \sum_{i=0}^{n_k} g_l(\zeta_i^k) l_i^{n_k}, \tag{4.1.5}$$

where (considering $l \in \mathbb{N}$ a fixed number) g_l is a real- or complex-valued function defined on $\mathcal{P}_l$, and $l_i^{n_k}(y) = \prod_{\substack{j=0 \\ j\neq i}}^{n_k} \frac{y-\zeta_j^k}{\zeta_i^k - \zeta_j^k}$ is the Lagrange polynomial associated with the nodes $(\zeta_j^k)_{j=0}^{n_k}$. We require that $n_0 = 0$.

We introduce the univariate interpolation difference operators

$$\Delta_k^I = I_k - I_{k-1}, \quad k \geq 0, \tag{4.1.6}$$

where we set $I_{-1} = 0$, so that $\Delta_0^I g_l = g_l(\zeta_0^0)$. Therefore, (4.1.5) can be rewritten as

$$I_k g_l = \sum_{j=0}^{n_k} \Delta_j^I g_l. \tag{4.1.7}$$

[1] Also referred to in the literature as *lower index set* or *monotone index set*.

We remark that any univariate family of interpolation points can be used for the above construction, in particular the sequences do not need to be nested.

To extend these concepts to the multi-dimensional case, we proceed as follows. To any multi-index $\nu \in \mathcal{F}$, we can associate the set of multivariate points

$$\boldsymbol{\zeta}_\nu = \bigotimes_{j\geq 1} (\zeta_i^{\nu_j})_{i=0}^{n_{\nu_j}} \in \mathcal{P}, \tag{4.1.8}$$

and the tensorized multivariate operators

$$I_\nu = \bigotimes_{j\geq 1} I_{\nu_j} \quad \text{and} \quad \Delta_\nu^I = \bigotimes_{j\geq 1} \Delta_{\nu_j}^I. \tag{4.1.9}$$

The above tensorization can be defined inductively:

- if $\nu = 0_\mathcal{F}$, then $I_\nu g = \Delta_\nu^I g = g(\boldsymbol{\zeta}_{0_\mathcal{F}})$;
- if $\nu \neq 0_\mathcal{F}$, then

$$I_\nu g = I_{\nu_1}(t \mapsto I_{\tilde{\nu}} g_t) \quad \text{and} \quad \Delta_\nu^I g = \Delta_{\nu_1}^I (t \mapsto \Delta_{\tilde{\nu}}^I g_t), \tag{4.1.10}$$

  where $\tilde{\nu} = (\nu_2, \nu_3, \ldots)$ and $g_t(\hat{\boldsymbol{y}}) = g(t, \hat{\boldsymbol{y}})$, with $\hat{\boldsymbol{y}} = (y_2, y_3, \ldots) \in \bigotimes_{l\geq 2} \mathcal{P}_l$.

The definition of univariate quadrature operators and their tensorization follows the same lines. Let $(Q_k)_{k\geq 0}$ denote a sequence of univariate quadrature formulas associated with the quadrature points $(\zeta_j^k)_{j=0}^{n_k}$ in $\mathcal{P}_l = [-1, 1]$ and with the weights $(w_j^k)_{j=0}^{n_k}$. The univariate quadrature operators associated with the sequence $(\zeta_j^k)_{j=0}^{n_k}$ are defined as

$$Q_k g_l = \sum_{i=0}^{n_k} w_i^{n_k} \cdot g_l(\zeta_i^k), \tag{4.1.11}$$

where g_l is defined as before.

Let $\mathcal{I}(\cdot)$ be the exact integration operator. We state the following assumption on the quadrature operators:

Assumption 4.1.2. For each $k \in \mathbb{N}_0$, the univariate quadrature formula Q_k associated with the quadrature points $(\zeta_j^k)_{j=0}^{n_k}$ satisfies:

(i) Q_k is of order k, i.e. $(\mathcal{I} - Q_k)(p_k) = 0$ for all $p_k \in \mathbb{P}_k$, with $\mathbb{P}_k$ the set of polynomials up to the kth degree;

(ii) one of the two following condition holds:

  (a) $w_j^k > 0$ for each $0 \leq j \leq n_k$;

  (b) the Lebesgue constants λ_k of I_k, $k \geq 0$, satisfy $\lambda_k \leq C(k+1)^\theta$, for some $\theta \geq 1$ and a constant $C \in \mathbb{R}_+$ (independent of k).

The univariate quadrature difference operators are defined as

$$\Delta_k^Q = Q_k - Q_{k-1}, \quad k \geq 0, \tag{4.1.12}$$

with again the convention that $Q_{-1} = 0$; moreover, we require $\zeta_0^0 = 0$, $w_0^0 = 1$ and $n_0 = 0$, so that $Q_0 g_l = g_l(0)$. Then, (4.1.11) can be rewritten as

$$Q_k g_l = \sum_{j=0}^{n_k} \Delta_j^Q g_l, \tag{4.1.13}$$

with again no need for the sequences of quadrature points to be nested.

The corresponding multivariate operators are defined, for a generic multi-index $\nu \in \mathcal{F}$, as

$$Q_\nu = \bigotimes_{j\geq 1} Q_{\nu_j} \quad \text{and} \quad \Delta_\nu^Q = \bigotimes_{j\geq 1} \Delta_{\nu_j}^Q, \tag{4.1.14}$$

with associated sets of multivariate points $\boldsymbol{\zeta}_\nu$ as in (4.1.8). The tensorization can be defined inductively as for the interpolation operators.

Sparse interpolation and quadrature operators

For any downward closed set $\Lambda \subset \mathcal{F}$, the sparse interpolation operator is defined as

$$I_\Lambda = \sum_{\nu\in\Lambda} \Delta_\nu^I, \tag{4.1.15}$$

with Δ_ν^I the multivariate difference operators defined in (4.1.10). We denote by

$$\mathcal{G}_\Lambda = \{\boldsymbol{\zeta}_\nu : \nu \in \Lambda\} \tag{4.1.16}$$

the grid associated with (4.1.15).

Similarly, the sparse quadrature operator is

$$Q_\Lambda = \sum_{\nu\in\Lambda} \Delta_\nu^Q, \tag{4.1.17}$$

with Δ_ν^Q the multivariate difference operators defined in (4.1.14).

We stress that the downward closedness of the set Λ is essential for the previous definitions.

Let us denote $\mathbb{P}_\Lambda := \operatorname{span}\{\boldsymbol{y}^\nu, \nu \in \Lambda\}$. The following results ensure that the sparse interpolation and quadrature operators are well defined.

Theorem 4.1.3. *(Theorem 2.1 in [CCS14]) For any downward closed index set $\Lambda \subset \mathcal{F}$, the grid $\mathcal{G}_\Lambda$ is unisolvent for $\mathbb{P}_\Lambda$ and for any function defined on $\mathcal{P} = [-1,1]^\infty$. $I_\Lambda g$ is the unique element in $\mathbb{P}_\Lambda$ which agrees with g on $\mathcal{G}_\Lambda$, i.e.:*

$$I_\Lambda g(\boldsymbol{\zeta}_\nu) = g(\boldsymbol{\zeta}_\nu), \quad \textit{for all } \nu \in \Lambda, \ \textit{ all } g \textit{ continuous on } \mathcal{P}.$$

Theorem 4.1.4. *(Theorem 4.2 in [SS13]) For any downward closed index set $\Lambda \subset \mathcal{F}$, the sparse quadrature operator Q_Λ is exact for any polynomial $g \in \mathbb{P}_\Lambda$, i.e.:*

$$Q_\Lambda g = \mathcal{I}(g), \quad \textit{for all } g \in \mathbb{P}_\Lambda,$$

where $\mathcal{I}$ denotes the exact integral.

For the proofs we refer to [CCS14] and [SS13], respectively.

We have presented definitions and results for sparse interpolation and quadrature in the case that $X = \mathbb{R}$ or $X = \mathbb{C}$, but they can be extended in a straightforward way to the case that X is a separable Banach space, and we refer to [CCS14] and [SS13] for details.

Best N-term convergence rates for sparse interpolation and quadrature

For $s > 1$, we define the Bernstein ellipse in the complex plane as $\mathcal{E}_s := \left\{ \frac{w+w^{-1}}{2} : 1 \leq |w| \leq s \right\}$. Given a sequence $\boldsymbol{\rho} = (\rho_l)_{l \geq 1}$, $\mathcal{E}_{\boldsymbol{\rho}} := \bigotimes_{l \geq 1} \mathcal{E}_{\rho_l}$ denotes the tensorized polyellipse [CCS15].

For the convergence results for the sparse interpolation and quadrature operators to hold, we need that the function that we want to interpolate or integrate fulfills some regularity properties [CCS15, SS13, SS14]:

$(\boldsymbol{b}, p, \varepsilon)$-holomorphy assumption
Let $g : \mathcal{P} \to X$ denote a bounded, continuous function of countably many variables $y_1, y_2, ...$, defined on $\mathcal{P} = [-1, 1]^\infty$ and taking values in a separable Banach space X. We require that:
(i) Given a positive sequence $\boldsymbol{b} = (b_l)_{l \geq 1} \in \ell^p(\mathbb{N})$ for some $0 < p < 1$, there exists a real number $0 < \varepsilon < 1$ such that, for every $(\boldsymbol{b}, \varepsilon)$-admissible sequence of poly-radii, i.e. for every sequence $\boldsymbol{\rho} = (\rho_l)_{l \geq 1}$ such that $\rho_l > 1$, for every $l \geq 1$, and

$$\sum_{l \geq 1} (\rho_l - 1) b_l \leq \varepsilon, \tag{4.1.18}$$

the solution map $\boldsymbol{y} \mapsto g(\boldsymbol{y})$ admits a holomorphic extension to a set of the form $\mathcal{O}_{\boldsymbol{\rho}} := \bigotimes_{l \geq 1} \mathcal{O}_{\rho_l}$, with $\mathcal{O}_{\rho_l} \subset \mathbb{C}$ an open set containing $\mathcal{E}_{\rho_l}$, $l \geq 1$.
(ii) *g satisfies an a priori estimate (uniform upper bound)*

$$\sup_{\boldsymbol{z} \in \mathcal{E}_{\boldsymbol{\rho}}} \|g(\boldsymbol{z})\|_X \leq B(\varepsilon), \tag{4.1.19}$$

for a constant $B = B(\varepsilon)$ independent of $\boldsymbol{\rho}$ and of the dimension of the parameter space.

Lemma 4.4 in [CCS15] ensures that, for $s > 1$, the open set $\mathcal{O}_s := \{z \in \mathbb{C} : \operatorname{dist}(z, [-1, 1]) < s - 1\}$ is an open neighborhood of $\mathcal{E}_s$. Then, it is sufficient to verify the $(\boldsymbol{b}, p, \varepsilon)$-holomorphy assumption on sets of the form

$$\mathcal{O}_{\boldsymbol{\rho}} = \bigotimes_{l \geq 1} \mathcal{O}_{\rho_l}, \quad \text{with } \mathcal{O}_{\rho_l} = \{z \in \mathbb{C} : \operatorname{dist}(z, [-1, 1]) < \rho_l - 1\}, \ l \geq 1. \tag{4.1.20}$$

Given $g : \mathcal{P} \to X$, we can expand it in terms of Legendre polynomials:

$$g(\boldsymbol{y}) = \sum_{\nu \in \mathcal{F}} g_\nu P_\nu(\boldsymbol{y}), \tag{4.1.21}$$

where $P_\nu = \prod_{l \geq 1} P_{\nu_l}$, $\nu \in \mathcal{F}$, are the multivariate Legendre polynomials, normalized according to $\|P_{\nu_l}\|_{L^\infty([-1,1],\mathbb{R})} = 1$ for every $l \geq 1$, and $(g_\nu)_{\nu \in \mathcal{F}}$ are the Legendre coefficients of g. It holds

$$g_\nu = \prod_{l \geq 1} (2\nu_l + 1) \int_{\mathcal{P}} g(\boldsymbol{y}) P_\nu(\boldsymbol{y}) \, \mathrm{d}\mu(\boldsymbol{y}). \tag{4.1.22}$$

If g fulfills the $(\boldsymbol{b}, p, \varepsilon)$-holomorphy assumption, then, using Cauchy's integral formula, one can express the values of g inside the integral in (4.1.22) as integrals in $\mathcal{E}_{\boldsymbol{\rho}}$. Owing to the uniform

bound (4.1.19) and properties of the Legendre polynomials, one obtains [CCS15, Proof of Thm. 2.2]

$$\|g_\nu\|_X \leq B(\varepsilon) \prod_{l\geq 1:\nu_l\neq 0} (2\nu_l+1)\frac{\pi\rho_l}{2(\rho_l-1)}\rho_l^{-\nu_l}, \tag{4.1.23}$$

with the convention that the empty product equals one for $\nu = 0_{\mathcal{F}}$, and with $B(\varepsilon)$ the constant in (4.1.19). For each index ν, we can choose the polyradii $(\rho_l)_{l\geq 1}$ such that ρ_l is inversely proportional to b_l, $l \geq 1$, the entries of the sequence $\boldsymbol{b}$ [CCS15, Proof of Thm. 2.2]. The idea is that the faster the coefficients b_l, $l \geq 1$, decay, the faster the polyradii ρ_l, $l \geq 1$, increase when going to higher dimensions, and the faster the coefficients $(\|g_\nu\|_X)_{\nu\in\mathcal{F}}$ decrease. In the end, we obtain that $(\|g_\nu\|_X)_{\nu\in\mathcal{F}} \in \ell^p(\mathcal{F})$ with p the same sparsity parameter as for the sequence $\boldsymbol{b}$. Since $p < 1$, the Legendre series (4.1.21) converges absolutely and thus unconditionally. We refer to [CCS15, Proof of Thm. 2.2] for the details about the ℓ^p-summability of the Legendre coefficients.

Now, the sparse interpolation and the sparse quadrature operators satisfy the estimates (see [CCS14, Lemma 4.2] and [SS13, Lemma 4.5], respectively)

$$\|g - I_\Lambda g\|_{L^\infty(\mathcal{P},X)} \leq 2\sum_{\nu\notin\Lambda} p_\nu\|P_\nu\|_X\,, \quad \|\mathcal{I}(g) - Q_\Lambda g\|_X \leq 2\sum_{\nu\notin\Lambda} p_\nu\|P_\nu\|_X,$$

with $p_\nu = \prod_{l\geq 1}(1+\nu_l)^b$, $b \geq 1$ for the interpolation case and $b = 2$ for the quadrature case.

Exploiting the bound (4.1.23) on the Legendre coefficients, one can show that, in both cases, $(p_\nu\|P_\nu\|)_{\nu\in\mathcal{F}} \in \ell^p(\mathcal{F})$ (cf. [CCS14, Thm. 4.3] and [SS13, Thm. 4.6]). Then, Stechkin's Lemma (see e.g. [CDS11, Sect. 3.3]) ensures the existence of a sequence of sets Λ_N, with $\sharp\Lambda_N = N$, for which the convergence results hold, and in [CCS14, Sect. 4.2] it is shown that the sets Λ_N can always be chosen to be downward closed and nested.

This leads to:

Theorem 4.1.5. *(Theorem 4.4 in [CCS14]) Let the $(\boldsymbol{b}, p, \varepsilon)$-holomorphy assumption be satisfied. If the univariate sequence $(\zeta_j^k)_{j=0}^{n_k}$ is chosen so that its Lebesgue constant λ_k satisfies $\lambda_k \leq C(k+1)^\theta$ for some $\theta \geq 1$ and a constant $C \in \mathbb{R}_+$ (independent of k), then there exists a sequence $(\Lambda_N)_{N\geq 1}$ of downward closed sets $\Lambda_N \subset \mathcal{F}$ such that $\sharp\Lambda_N = N$ and*

$$\|g - I_\Lambda g\|_{L^\infty(\mathcal{P},X)} \leq CN^{-s}, \quad s = \frac{1}{p} - 1. \tag{4.1.24}$$

Theorem 4.1.6. *(Lemma 4.10 in [SS13]) Let the $(\boldsymbol{b}, p, \varepsilon)$-holomorphy assumption and Assumption 4.1.2 be satisfied. Then there exists a sequence $(\Lambda_N)_{N\geq 1}$ of downward closed sets $\Lambda_N \subset \mathcal{F}$ such that $\sharp\Lambda_N \leq N$ and*

$$\|\mathcal{I}(g) - Q_\Lambda g\|_X \leq CN^{-s}, \quad s = \frac{1}{p} - 1. \tag{4.1.25}$$

Remark 4.1.7. These two results show convergence rates which depend only on p, referred to as the 'sparsity class of the unknown', while they do not depend on the number of dimensions activated. This means that it is possible to break the curse of dimensionality by algorithms which adaptively construct downward closed index sets for the sparse interpolation and quadrature operators.

The above theorems do not provide indications for the construction of the sets $(\Lambda_N)_{N\geq 1}$. In the next section, we describe an adaptive algorithm which will be seen in practice to achieve this.

4.2. The sparse adaptive Smolyak algorithm

We present here the main features of the algorithm for sparse interpolation and quadrature that has been used in our numerical experiments. Our survey is based on [SS13] and for a complete treatment we refer to that paper itself.

For sake of exposition, let us focus on the quadrature case. The difference operators are the ones defined in (4.1.14). The idea is to identify the index set Λ_N of the N indices in $\mathcal{F}$ giving the highest contribution to the approximations (4.1.15) or (4.1.17), or, in other words, the N indices with largest

$$\|\Delta_\nu^Q(g)\|_X = \Big\| \bigotimes_{j\geq 1} \Delta_{\nu_j}^Q(g) \Big\|_X, \quad \nu \in \mathcal{F},$$

so that the approximation error is minimized.

However, the index set Λ_N built in this way would be nested but not downward closed; even worse, each time we want to add an index to Λ_N, the cardinality of the set of candidate indices would grow exponentially with the number of dimensions activated, and it would be infinite in the case of countably many parameters. To overcome this, one considers a local subset, referred to as the *reduced set of neighbors* of a given finite set $\Lambda \subset \mathcal{F}$, specifically [GG03]:

$$\mathcal{N}(\Lambda) = \{\nu \notin \Lambda : \nu - e_j \in \Lambda, \text{ for all } j \in \text{ supp}\nu \text{ and } \nu_j = 0, \text{ all } j > j(\Lambda) + 1\}, \tag{4.2.1}$$

for any downward closed index set Λ, where $j(\Lambda) = \max\{j : \nu_j > 0 \text{ for some } \nu \in \Lambda\}$. Using this set of neighbors, at each iteration at most one dimension can be activated.

The algorithm constructs then an anisotropic downward closed index set Λ comprising those indices in $\mathcal{N}(\Lambda)$ which are expected to contribute most to the approximation (see [SS13] for details):

Algorithm 1 Sparse adaptive Smolyak algorithm.

1: **function** ASG
2: Set $\Lambda_1 = \{0_\mathcal{F}\}, k = 1$ and compute $\Delta_0^Q(g)$.
3: Determine the reduced set of neighbors $\mathcal{N}(\Lambda_1)$.
4: Compute $\Delta_\nu^Q(g)$, for all $\nu \in \mathcal{N}(\Lambda_1)$.
5: **while** $\sum_{\nu\in\mathcal{N}(\Lambda_k)} \|\Delta_\nu^Q(g)\|_X > tol$ **do**
6: Set $\Lambda_{k+1} = \Lambda_k \cup \left\{\mu \in \mathcal{N}(\Lambda_k) : \|\Delta_\mu^Q(g)\|_X \geq \vartheta \max_{\nu\in\mathcal{N}_\Lambda} \|\Delta_\nu^Q(g)\|_X\right\}$.
7: Determine the reduced set of neighbors $\mathcal{N}(\Lambda_{k+1})$.
8: Compute $\Delta_\nu^Q(g)$, for all $\nu \in \mathcal{N}(\Lambda_{k+1})$.
9: Set $k = k + 1$.
10: **end while**
11: **end function**

In line 6, $\vartheta \in [0, 1]$ is a parameter chosen at the beginning of the algorithm, and determining how many indices in the reduced set of neighbors are included in the set Λ at each iteration. For $\vartheta = 1$, we have $\Lambda_{k+1} = \Lambda_k \cup \{\bar\nu\}$ with $\bar\nu = \text{argmax}_{\nu\in\mathcal{N}_\Lambda} \|\Delta_\nu^Q(g)\|_X$.

For the interpolation, the difference operators are the ones defined in (4.1.10). For each $\nu \in \mathcal{F}$, $\|\Delta_\nu^Q(g)\|_X$ is replaced by $\|\Delta_\nu^I(g)\|_{L^\infty(\mathcal{P},X)}$, and the condition $\sum_{\nu\in\mathcal{N}(\Lambda_k)} \|\Delta_\nu^Q(g)\|_X > tol$ at line 5 of Algorithm 1 is substituted by the criterion $\max_{\nu\in\mathcal{N}(\Lambda_k)} \|\Delta_\nu^I(g)\|_X > tol$.

We remark that there is no guarantee and it has not been proved that the downward closed index sets obtained with this algorithm are the ones for which the estimates in Theorems 4.1.5 and

4.1.6 hold, and there are test cases where no convergence was observed (see [CCS14]). However, in [SS13] several numerical examples are shown where the convergence rates of Theorems 4.1.5 and 4.1.6 are achieved.

4.3. Analyticity and uniform boundedness of solutions to elliptic PDEs

We now return to our model problem as stated in (3.2.4). We show that the solution to (3.2.4) satisfies the $(\boldsymbol{b}, p, \varepsilon)$-holomorphy assumption, so that the convergence results stated in Theorem 4.1.5 and Theorem 4.1.6 hold.

To this aim, we replace the definition of $(\boldsymbol{b}, \varepsilon)$-admissible sequence of polyradii by the following:

Definition 4.3.1. A sequence $\boldsymbol{\rho} = (\rho_l)_{l\geq 1}$ of polyradii, with $\rho_l > 1$ for every $l \geq 1$, is said to be $(\boldsymbol{b}, \varepsilon)^*$-admissible if it is $(\boldsymbol{b}, \varepsilon)$-admissible for a sequence $\boldsymbol{b}$ that has a *monotonic* majorant in $\ell^p(\mathcal{F})$ for $0 < p < \frac{1}{2}$ and is such that $(lb_l^p)_{l\geq 1}$ has a monotonic majorant, and if (4.1.18) is replaced by

$$\sum_{l\geq 1}(\rho_l - 1)lb_l \leq \varepsilon. \tag{4.3.1}$$

We use the term $(\boldsymbol{b}, p, \varepsilon)^*$-holomorphy assumption to denote the $(\boldsymbol{b}, p, \varepsilon)$-holomorphy assumption when $(\boldsymbol{b}, \varepsilon)$-admissible sequences are replaced by $(\boldsymbol{b}, \varepsilon)^*$-admissible sequences.

Proposition 4.3.2. *Let the $(\boldsymbol{b}, p, \varepsilon)$-assumption be replaced by the $(\boldsymbol{b}, p, \varepsilon)^*$-assumption. Then the algebraic convergence of the sparse interpolation and quadrature operators, prescribed by Theorems 4.1.5 and 4.1.6 respectively, still holds with rate of convergence $s = \frac{1}{p} - 2$.*

Proof. Since the sequence $\boldsymbol{b}$ has a monotonic majorant in $\ell^p(\mathcal{F})$ and the sequence $(lb_l^p)_{l\geq 1}$ has a monotonic majorant, then Lemma C.0.7 in the Appendix ensures that the sequence $(lb_l)_{l\geq 1}$ belongs to $\ell^q(\mathcal{F})$ with $q = \frac{p}{1-p}$. Applying Theorems 4.1.5 and 4.1.6 using the $(\boldsymbol{b}, p, \varepsilon)$-assumption for the sequence $\tilde{\boldsymbol{b}} = (lb_l)_{l\geq 1}$, we obtain the claim. □

Remark 4.3.3. The condition expressed by the inequality in (4.3.1), differently from the condition $\boldsymbol{b} \in \ell^p(\mathbb{N})$, entails an implicit ordering of the dimensions of the parameter space with respect to decreasing significance. However, thanks to Assumption 2.1.4.A, the bound ε in (4.3.1) does not depend on the sequence $\boldsymbol{b}$ itself but on its (monotonically decreasing) majorant.

Remark 4.3.4. Condition (4.3.1) implies in particular condition (4.1.18) for the same sequence $\boldsymbol{b}$.

Our plan is to show that the $(\boldsymbol{b}, p, \varepsilon)^*$-holomorphy assumption is fulfilled for our model problem.

As it is done in [CCS15, Sect. 5.3], we choose the sequence $\boldsymbol{b}$ as

$$b_l = \|\beta_l\psi_l\|_{C^0_{per}([0,2\pi))} + \left\|\beta_l\psi_l'\right\|_{C^0_{per}([0,2\pi))} = |\beta_l| + l|\beta_l|, \quad l \geq 1, \tag{4.3.2}$$

with β_l and ψ_l as in Remark 2.1.7, $l \geq 1$.

Notice that, thanks to Assumption 2.1.4.A on the sequence $(\beta_l)_{l\geq 1}$ (i.e. existence of a monotonic majorant belonging to $\ell^p(\mathbb{N})$ with $p < \frac{1}{2}$), there exist sequences of polyradii that are $(\boldsymbol{b}, \varepsilon)^*$-admissible.

Let us first look at the uniform bound (4.1.19).

We point out that Assumption 3.1.2 is not sufficient by itself to ensure well-posedness of the problem with a parameter-independent upper bound on the solution for $\boldsymbol{z} \in \mathcal{O}_{\boldsymbol{\rho}}$, with $\boldsymbol{\rho}$ a $(\boldsymbol{b},\varepsilon)^*$-admissible sequence. Instead, we have to impose a slightly stronger requirement:

Assumption 4.3.5. (i) The domain mapping $\Phi = \Phi(\boldsymbol{y})$, its Jacobian $D\Phi(\boldsymbol{y})$ and its Jacobian inverse $D\Phi^{-1}(\boldsymbol{y})$, $\boldsymbol{y} \in \mathcal{P}_J$, $J \in \mathbb{N}$, admit a holomorphic extension to the subsets $\mathcal{O}_{\boldsymbol{\rho}} \subset \mathbb{C}^{\mathbb{N}}$ as defined in (4.1.20), for any $(\boldsymbol{b},\varepsilon)^*$-admissible sequence $\boldsymbol{\rho}$ of polyradii.
(ii) For every $\boldsymbol{z} \in \mathcal{O}_{\boldsymbol{\rho}}$, $\Phi = \Phi(\boldsymbol{z})$ fulfills Assumption 3.1.2, with bounds possibly depending on ε. For Assumption 3.1.2(i), the requirement on the diffeomorphism to be orientation-preserving is replaced by: there exists a real constant $\sigma = \sigma(\varepsilon) > 0$, independent of $\boldsymbol{z} \in \mathcal{O}_{\boldsymbol{\rho}}$, such that

$$\operatorname{Re}\det D\Phi(\boldsymbol{z}) > \sigma(\varepsilon), \qquad \text{for every } \boldsymbol{z} \in \mathcal{O}_{\boldsymbol{\rho}}. \tag{4.3.3}$$

Since in general the domain mapping Φ will depend on $r = r(\boldsymbol{z})$, $\boldsymbol{z} \in \mathcal{O}_{\boldsymbol{\rho}}$, in order to have Assumption 4.3.5 fulfilled we can expect that we need to ensure $\boldsymbol{z}$-uniform bounds and holomorphy of the radius and its derivative with respect to $\varphi \in [0, 2\pi)$. We are going to show that $\boldsymbol{z}$-uniform bounds hold for $\operatorname{Re} r(\boldsymbol{z})$, $|r(\boldsymbol{z})|$ and $\left|\dfrac{\partial r}{\partial \varphi}(\boldsymbol{z})\right|$, and that such bounds are sufficient for the mapping (3.1.2) to satisfy Assumption 4.3.5.

Assumption 2.1.3 ensures that there exist $0 < r^-, r^+ < \infty$ such that

$$r^- \le r(\boldsymbol{y},\varphi) \le r^+, \qquad \text{for a.e. } \varphi \in [0,2\pi), \text{ all } J \in \mathbb{N}, \text{ and all } \boldsymbol{y} \in \mathcal{P}_J \tag{4.3.4}$$

(more precisely, in our case $r^- = \frac{r_0^-}{2}$, $r^+ = r_0^+ + \frac{r_0^-}{2}$, with $r_0^+ = \sup_{\varphi\in[0,2\pi)} r_0(\varphi)$ and r_0^- as in Assumption 2.1.3). Moreover, Assumption 2.1.4.A guarantees that there exists a J- and $\boldsymbol{y}$-independent constant $0 < C_r < \infty$ such that

$$\left\|\frac{\partial r}{\partial \varphi}(\boldsymbol{y})\right\|_{C^0_{per}([0,2\pi))} \le \left\|\frac{\partial r_0}{\partial \varphi}\right\|_{C^0_{per}([0,2\pi))} + C_r, \qquad \text{for all } J \in \mathbb{N} \text{ and all } \boldsymbol{y} \in \mathcal{P}_J. \tag{4.3.5}$$

Then, we can prove the following:

Lemma 4.3.6. *Let $\boldsymbol{b}$ be as in (4.3.2) and $0 < \varepsilon \le \frac{r^-}{2}$, with r^- as in (4.3.4). Then, for every $(\boldsymbol{b},\varepsilon)^*$-admissible sequence $\boldsymbol{\rho}$ and every $\boldsymbol{z} \in \mathcal{O}_{\boldsymbol{\rho}}$, with $\mathcal{O}_{\boldsymbol{\rho}}$ as in (4.1.20), we have the $\boldsymbol{z}$-independent bounds*

$$\frac{r^-}{2} \le \operatorname{Re} r(\boldsymbol{z},\varphi), \qquad \varphi \in [0,2\pi), \tag{4.3.6}$$

$$\frac{r^-}{2} \le |r(\boldsymbol{z},\varphi)| \le r^+ + \varepsilon, \qquad \varphi \in [0,2\pi), \tag{4.3.7}$$

$$\left|\frac{\partial r}{\partial \varphi}(\boldsymbol{z},\varphi)\right| \le \left\|\frac{\partial r_0}{\partial \varphi}\right\|_{C^0_{per}([0,2\pi))} + C_r + \varepsilon, \qquad \varphi \in [0,2\pi), \tag{4.3.8}$$

with r^- and r^+ as in (4.3.4), and C_r as in (4.3.5).

In particular, the mapping Φ defined in (3.1.2) fulfills Assumption 4.3.5 (ii) if the mollifier fulfills Assumption 3.1.3 and $0 < \varepsilon < \min\left\{c_\chi, \frac{r^-}{2}\right\}$.

Proof. From (2.2.3), we have that:

$$r(\boldsymbol{z},\varphi) = r(\boldsymbol{y},\varphi) + \sum_{j=1}^{J} c_j(z_{2j-1} - y_{2j-1})\cos(j\varphi) + s_j(z_{2j} - y_{2j})\sin(j\varphi).$$

Since $\boldsymbol{z} \in \mathcal{O}_{\boldsymbol{\rho}}$, for every $J \in \mathbb{N}$ there exists $\boldsymbol{y} \in \mathcal{P}_J$ such that, for every $1 \leq l \leq L = 2J$, $|z_l - y_l| < \rho_l - 1$; moreover, being $\boldsymbol{\rho}$ $(\boldsymbol{b}, \varepsilon)^*$-admissible, it is in particular $(\boldsymbol{b}, \varepsilon)$-admissible, which, together with (4.3.4), implies that

$$|r(\boldsymbol{z}, \varphi)| \leq r^+ + \varepsilon, \quad \text{for every } \varphi \in [0, 2\pi).$$

Analogously, taking into account that $0 < \varepsilon \leq \frac{r^-}{2}$, we get

$$|r(\boldsymbol{z}, \varphi)| \geq \operatorname{Re} r(\boldsymbol{z}, \varphi) \geq r^- - \varepsilon \geq \frac{r^-}{2}, \quad \text{for every } \varphi \in [0, 2\pi). \tag{4.3.9}$$

Finally, using (4.3.5) and (4.3.1), for every $J \in \mathbb{N}$ and $\boldsymbol{y} \in \mathcal{P}_J$ such that, for every $1 \leq l \leq L$, $|z_l - y_l| < \rho_l - 1$:

$$\begin{aligned}
\Big|\frac{\partial r}{\partial \varphi}(\boldsymbol{z}, \varphi)\Big| &= \Big|\frac{\partial r}{\partial \varphi}(\boldsymbol{y}, \varphi) + \sum_{j=1}^{J} c_j j (z_{2j-1} - y_{2j-1}) \cos(j\varphi) + s_j j (z_{2j} - y_{2j}) \sin(j\varphi)\Big| \\
&\leq \Big\|\frac{\partial r}{\partial \varphi}(\boldsymbol{y})\Big\|_{C^0_{per}([0,2\pi))} + \varepsilon \\
&\leq \Big\|\frac{\partial r_0}{\partial \varphi}\Big\|_{C^0_{per}([0,2\pi))} + C_r + \varepsilon, \quad \text{for every } \varphi \in [0, 2\pi).
\end{aligned}$$

We remark that all the bounds are independent of the truncation parameter $J \in \mathbb{N}$.

Proceeding as in the proof to show that $\Phi = \Phi(\boldsymbol{y})$ given by (3.1.2), $\boldsymbol{y} \in \mathcal{P}_J$, fulfills Assumption 3.1.2 (see Appendix, Section E), it is easy to see that the bounds proved in this lemma guarantee that this map fulfills Assumption 4.3.5 for $\boldsymbol{z} \in \mathcal{O}_{\boldsymbol{\rho}}$. □

The same argument used in the proofs of Lemma 3.2.5 and Corollary 3.2.6 leads to:

Proposition 4.3.7. *Let the sequence $\boldsymbol{b}$ be as in (4.3.2) and $0 < \varepsilon \leq \frac{r^-}{2}$, with r^- as in (4.3.4).*

If the mapping Φ satisfies Assumption 4.3.5, then part (ii) of the $(\boldsymbol{b}, p, \varepsilon)^*$-holomorphy assumption is fulfilled, i.e. there exist constants $B_1 = B_1(\varepsilon)$ and $B_2 = B_2(\varepsilon)$ such that

$$\sup_{\boldsymbol{z} \in \mathcal{O}_{\boldsymbol{\rho}}} \|\hat{u}(\boldsymbol{z})\|_{H^1(K_R)} \leq B_1(\varepsilon) \|u_i\|_{H^1(\partial K_R)} + B_2(\varepsilon) \left\|\frac{\partial u_i}{\partial \boldsymbol{n}_R}\right\|_{L^2(\partial K_R)}, \tag{4.3.10}$$

for every $\mathcal{O}_{\boldsymbol{\rho}}$ as in (4.1.20), with $\boldsymbol{\rho}$ any sequence of $(\boldsymbol{b}, \varepsilon)^*$-admissible polyradii. The constants B_1 and B_2 are independent of $J \in \mathbb{N}$ and $\boldsymbol{\rho}$.

In particular, the bound (4.3.10) holds for the mapping Φ given in (3.1.2) if the mollifier fulfills Assumption 3.1.3 and $0 < \varepsilon < \min\left\{c_\chi, \frac{r^-}{2}\right\}$.

To prove that part (i) of the $(\boldsymbol{b}, p, \varepsilon)^*$-holomorphy assumption holds, we need to show that, for $0 < \varepsilon \leq \frac{r^-}{2}$ and any sequence $\boldsymbol{\rho}$ of $(\boldsymbol{b}, \varepsilon)^*$-admissible poly-radii, the solution $\hat{u}$ to (3.2.4) admits a holomorphic extension to the sets $\mathcal{O}_{\boldsymbol{\rho}}$ defined in (4.1.20). The proof is rather general and actually it applies, with minor modifications, to any elliptic PDE as long as the parameter-dependent configuration can be mapped to a reference configuration through a mapping satisfying Assumption 4.3.5 and depending smoothly (in a sense to be specified later, see Remark 4.3.10) on the stochastic quantity $r = r(\boldsymbol{y})$.

Namely, we first show the existence of a holomorphic extension for the parameter-dependent radius (2.2.3) and its φ-derivative. From this, analyticity of the map $\Phi(\boldsymbol{y})$ and then of the solution to the PDE on the nominal configuration follow. The arguments used to establish the forthcoming results are a particular case of the theory elaborated in [CCS15] and follow some of the techniques presented in [CDS11], where analyticity of the solution to the diffusion equation with stochastic diffusion coefficient is proved.

Lemma 4.3.8. *For every $\boldsymbol{z} \in \mathcal{O}_{\boldsymbol{\rho}}$, with $\mathcal{O}_{\boldsymbol{\rho}}$ as in* (4.1.20) *and $\boldsymbol{\rho}$ any $(\boldsymbol{b}, \varepsilon)^*$-admissible sequence, the maps $\boldsymbol{z} \mapsto r(\boldsymbol{z}) \in C^1_{per}([0, 2\pi))$ and $\boldsymbol{z} \mapsto \dfrac{\partial r}{\partial \varphi}(\boldsymbol{z}) \in C^0_{per}([0, 2\pi))$, with $r = r(\boldsymbol{z}, \cdot)$ given by* (2.2.3)*, are holomorphic.*

Proof. We prove the statement just for the map $\boldsymbol{z} \mapsto r(\boldsymbol{z})$, $\boldsymbol{z} \in \mathcal{O}_{\boldsymbol{\rho}}$, since the argument for the map $\boldsymbol{z} \mapsto \dfrac{\partial r}{\partial \varphi}(\boldsymbol{z})$, $\boldsymbol{z} \in \mathcal{O}_{\boldsymbol{\rho}}$, is analogous.

Thanks to Hartogs' theorem on separate analyticity (see e.g. [Kra82, Sect. 2.4]), it is sufficient to show that $r(\boldsymbol{z})$ is holomorphic with respect to each of the variables z_l separately, for every $l \geq 1$. In other words, we just have to show that, for any $l \geq 1$, the function

$$z_l \mapsto r^l(z_l) := r(\bar{z}_1, \ldots, \bar{z}_{l-1}, z_l, \bar{z}_{l+1}, \ldots),$$

with $z_1 = \bar{z}_1, \ldots, z_{l-1} = \bar{z}_{l-1}, z_{l+1} = \bar{z}_{l+1}, \ldots$ fixed, is holomorphic.

Let us first consider the case when $\boldsymbol{z} \in \mathcal{O}_{\boldsymbol{\rho}}$ with $\bar{z}_1 = \ldots = \bar{z}_{l-1} = \bar{z}_{l+1} = \ldots = 0$. For this, we can write:

$$r(\boldsymbol{z}, \varphi) = r^l(z_l, \varphi) := r_0(\varphi) + \beta_l z_l \psi_l(\varphi), \tag{4.3.11}$$

with β_l and $\psi_l(\varphi)$ as in Remark 2.1.7. For $\delta \in \mathbb{C} \setminus \{0\}$, we have:

$$r^l(z_l + \delta, \cdot) - r^l(z_l, \cdot) = \delta \beta_l \psi_l.$$

Thus, for any δ with $|\delta|$ small, the difference quotient belongs to $C^1_{per}([0, 2\pi))$:

$$\frac{\left\| r^l(z_l + \delta, \cdot) - r^l(z_l, \cdot) \right\|_{C^1_{per}([0,2\pi))}}{|\delta|} = |\beta_l| \, \|\psi_l\|_{C^1_{per}([0,2\pi))} < \infty.$$

The existence of the limit as $|\delta|$ tends to zero implies that $z_l \mapsto r^l(z_l)$ is complex differentiable with

$$\frac{\partial r}{\partial z_l}(\boldsymbol{z}) = \frac{dr^l}{dz_l}(z_l) = \beta_l \psi_l, \quad z_l \in \mathcal{O}_{\rho_l}, z_j = 0, \text{ for } j \neq l,$$

and thus $z_l \mapsto r_l(z_l)$ is holomorphic.

In the general case that $\bar{z}_1, \ldots, \bar{z}_{l-1}, \bar{z}_{l+1}, \ldots \neq 0$, since these values, although nonzero, are considered to be fixed, we can write

$$r(\boldsymbol{z}, \varphi) = r^l(z_l, \varphi) = r_0(\varphi) + \sum_{\substack{j \geq 1 \\ j \neq l}} \bar{z}_j \beta_j \psi_j(\varphi) + z_l \beta_l \psi_l(\varphi) = \tilde{r}_0(\varphi) + z_l \beta_l \psi_l(\varphi),$$

with $\tilde{r}_0(\varphi) = r_0(\varphi) + \sum_{\substack{j \geq 1 \\ j \neq l}} \bar{z}_j \beta_j \psi_j(\varphi)$; then we can start from (4.3.11) with $\tilde{r}_0$ instead of r_0, proceed as before and thus show that $z_l \mapsto r_l(z_l)$ is holomorphic in $\mathcal{O}_{\boldsymbol{\rho}}$. □

For ease of treatment, we now state the analyticity of the mapping Φ for the special case described in (3.1.2), but, as it will be specified in Remark 4.3.10, the following result holds for a wide class of mappings.

Let $\mathrm{Diff}^k_{+,\mathrm{pw}}(K_R, K_R)$ be the space of diffeomorphisms which are of order C^k in each of the two subdomains $\overline{\hat{D}_1 \cap K_R}$ and $\overline{\hat{D}_2}$, and with determinant with positive real part. Since algebraic sum, multiplication and, when not zero, division by holomorphic functions is still holomorphic, it follows immediately from Lemma 4.3.8 that:

Lemma 4.3.9. *Let us consider the map Φ defined in* (3.1.2) *with mollifier fulfilling Assumption 3.1.3. Then the mappings $\boldsymbol{z} \mapsto \Phi(\boldsymbol{z}, \cdot) \in \mathit{Diff}^1_{+,pw}(K_R, K_R)$, $\boldsymbol{z} \mapsto D\Phi^{-1}(\boldsymbol{z}, \cdot) \in C^0_{pw}(\overline{K_R})$ and $\boldsymbol{z} \mapsto \det D\Phi(\boldsymbol{z}, \cdot) \in C^0_{pw}(\overline{K_R})$ are holomorphic in $\mathcal{O}_{\boldsymbol{\rho}}$, with $\mathcal{O}_{\boldsymbol{\rho}}$ as defined in* (4.1.20) *for any $(\boldsymbol{b}, \varepsilon)^*$-admissible sequence $\boldsymbol{\rho}$ and $0 < \varepsilon < \min\left\{c_\chi, \frac{r^-}{2}\right\}$.*

Together with Lemma 4.3.6, this implies that the mapping defined in (3.1.2) *(with Assumption 3.1.3 on the mollifier) satisfies Assumption 4.3.5.*

Proof. Thanks to Assumption 2.1.3 and the restrictions on the mollifier χ, proceeding as in Section E in the Appendix (as in formula (E.0.3)), we note that $\det D\Phi(\boldsymbol{z})$, which appears as denominator in $D\Phi^{-1}(\boldsymbol{z})$ (see (E.0.2)), is never zero. Using the result of Lemma 4.3.6, the statement follows. □

Remark 4.3.10. It is clear that our framework and in particular Lemma 4.3.9 fit not only the specific map Φ given in (3.1.2), but any map involving composition of r with holomorphic maps, as well as linear combinations, multiplications and divisions (when never zero), as long as Assumption 4.3.5 is satisfied.

For the same reasons as for the previous lemma, we also have:

Lemma 4.3.11. *Let Assumption 4.3.5 be fulfilled. Then the coefficients $\hat{\alpha}(\boldsymbol{y})$, $\hat{\kappa}^2(\boldsymbol{y})$ as defined in* (3.2.5) *are holomorphic when considered as maps from $\boldsymbol{z} \in \mathcal{O}_{\boldsymbol{\rho}}$ to $C^0_{pw}(\overline{K_R})$.*

We have proved that all the coefficients in (3.2.4) admit a holomorphic extension to $\mathcal{O}_{\boldsymbol{\rho}}$. From this, we want to prove that the map $\boldsymbol{z} \mapsto \hat{u}(\boldsymbol{z})$ too has a holomorphic extension to $\mathcal{O}_{\boldsymbol{\rho}}$.

This result follows direcly from [CCS15, Thm. 2.2 and Thm. 4.1], stating that, if the bilinear form and the linear form in the PDE fulfill the $(\boldsymbol{b}, p, \varepsilon)$-assumption in $\mathcal{O}_{\boldsymbol{\rho}}$, and if the coercivity constant of the bilinear form and the continuity constants of the bilinear and linear forms are uniform with respect to $\boldsymbol{z} \in \mathcal{O}_{\boldsymbol{\rho}}$, then the map $\boldsymbol{z} \mapsto \hat{u}(\boldsymbol{z})$ too has a holomorphic extension to $\mathcal{O}_{\boldsymbol{\rho}}$.

However, here we present how one can show holomorphy of the solution $\hat{u}(\boldsymbol{z})$ by direct application to our model problem. For this, we proceed as in [CDS11].

We first need the following technical result:

Lemma 4.3.12. *Let $\boldsymbol{z}_1, \boldsymbol{z}_2 \in \mathcal{O}_{\boldsymbol{\rho}}$, with $\mathcal{O}_{\boldsymbol{\rho}} \subset \mathbb{C}^{\mathbb{N}}$ defined as in* (4.1.20) *and $\boldsymbol{\rho}$ a $(\boldsymbol{b}, \varepsilon)^*$-admissible sequence.*

Let $\hat{u}_1$ and $\hat{u}_2$ be two solutions to (3.2.4)*, with coefficients $\hat{\alpha}_1(\boldsymbol{x}) := \hat{\alpha}(\boldsymbol{z}_1, \boldsymbol{x})$, $\hat{\kappa}^2_1(\boldsymbol{x}) := \hat{\kappa}^2(\boldsymbol{z}_1, \boldsymbol{x})$ and $\hat{\alpha}_2(\boldsymbol{x}) := \hat{\alpha}(\boldsymbol{z}_2, \boldsymbol{x})$, $\hat{\kappa}^2_2(\boldsymbol{x}) := \hat{\kappa}^2(\boldsymbol{z}_2, \boldsymbol{x})$ respectively, and with the same incoming wave u_i. Also, let Assumption 4.3.5 be satisfied.*

Then, if Assumption 3.2.4 holds with $\tau < T$ and T as in Lemma 3.2.5, then the difference between the two solutions satisfies

$$\|\hat{u}_1 - \hat{u}_2\|_{H^1(K_R)} \leq C \left(\|\hat{\alpha}_1 - \hat{\alpha}_2\|_{C^0_{pw}(\overline{K}_R)} + \|\hat{\kappa}^2_1 - \hat{\kappa}^2_2\|_{C^0_{pw}(\overline{K_R})} \right), \tag{4.3.12}$$

for a constant $C > 0$ independent of $\boldsymbol{z} \in \mathcal{O}_{\boldsymbol{\rho}}$.

Proof. Taking the difference of the two variational formulations for $\hat{u}_1$ and $\hat{u}_2$, we obtain:

$$\int_{K_R} \hat{\alpha}_1 \hat{\nabla}(\hat{u}_1 - \hat{u}_2) \cdot \hat{\nabla}\hat{v} - \hat{\kappa}_1^2(\hat{u}_1 - \hat{u}_2)\hat{v}\, d\hat{\boldsymbol{x}} - \int_{\partial K_R} DtN(\hat{u}_1 - \hat{u}_2)\hat{v}\, dS$$
$$= \int_{K_R} (\hat{\alpha}_2 - \hat{\alpha}_1)\, \hat{\nabla}\hat{u}_2 \cdot \hat{\nabla}\hat{v} - (\hat{\kappa}_2^2 - \hat{\kappa}_1^2)\hat{u}_2\hat{v}\, d\hat{\boldsymbol{x}}, \quad \text{for all } v \in H^1(K_R).$$

Assumption 4.3.5 and Lemma 3.2.5 ensure coercivity of the bilinear form on the left-hand side, with a coercivity constant γ independent of $\boldsymbol{z} \in \mathcal{O}_{\boldsymbol{\rho}}$.

To get (4.3.12), we need a $\boldsymbol{z}$-independent bound on the norm of the linear form on the right-hand side:

$$\begin{aligned}
|L(\hat{v})| &= \left| \int_{K_R} (\hat{\alpha}_2 - \hat{\alpha}_1)\, \hat{\nabla}\hat{u}_2 \cdot \hat{\nabla}\hat{v} - (\hat{\kappa}_2^2 - \hat{\kappa}_1^2)\hat{u}_2\hat{v}\, d\hat{\boldsymbol{x}} \right| \\
&\leq \left(\|\hat{\alpha}_1 - \hat{\alpha}_2\|_{C^0_{\mathrm{pw}}(\overline{K_R})} + \|\hat{\kappa}_1^2 - \hat{\kappa}_2^2\|_{C^0_{\mathrm{pw}}(\overline{K_R})} \right) \|\hat{u}_2\|_{H^1(K_R)} \|\hat{v}\|_{H^1(K_R)} \\
&\leq \tilde{C}(\varepsilon) \left(\|\hat{\alpha}_1 - \hat{\alpha}_2\|_{C^0_{\mathrm{pw}}(\overline{K_R})} + \|\hat{\kappa}_1^2 - \hat{\kappa}_2^2\|_{C^0_{\mathrm{pw}}(\overline{K_R})} \right) \|\hat{v}\|_{H^1(K_R)},
\end{aligned}$$

with $\tilde{C}(\varepsilon) = B_1(\varepsilon)\, \|u_i\|_{H^1(\partial K_R)} + B_2(\varepsilon) \left\| \dfrac{\partial u_i}{\partial \boldsymbol{n}_R} \right\|_{L^2(\partial K_R)}$ the uniform bound on the H^1-norm of $\hat{u}_2$ from Proposition 4.3.7.

The estimate (4.3.12), with $C = \frac{\tilde{C}}{\gamma}$, follows then from the Lax-Milgram lemma. □

To prove the analyticity of the solution to (3.2.4), we follow the lines of Lemma 2.2 in [CDS11].

Lemma 4.3.13. *Let Assumptions 3.2.4 and 4.3.5 hold, the former with $\tau < T$ and T as in Lemma 3.2.5. Then, if $\hat{u}$ is a solution to (3.2.4), the solution map $\boldsymbol{z} \mapsto \hat{u}(\boldsymbol{z}) \in V = H^1(K_R)$, admits a holomorphic extension to any open set $\mathcal{O}_{\boldsymbol{\rho}} \subset \mathbb{C}^{\mathbb{N}}$ as defined in (4.1.20), with $\boldsymbol{\rho}$ a $(\boldsymbol{b}, \varepsilon)^*$-admissible sequence.*

For each variable z_l, $l \geq 1$, the complex derivative $(\partial_{z_l}\hat{u})(\boldsymbol{z}) \in V$ is the weak solution to the variational problem:

$$\begin{aligned}
&\text{Find } (\partial_{z_l}\hat{u})(\boldsymbol{z}) \in V : \\
&\int_{K_R} \left(\hat{\alpha}(\boldsymbol{z}, \hat{\boldsymbol{x}}) \hat{\nabla} \partial_{z_l}\hat{u}(\boldsymbol{z}, \hat{\boldsymbol{x}}) \cdot \hat{\nabla}\hat{v}(\hat{\boldsymbol{x}}) - \hat{\kappa}^2(\boldsymbol{z}, \hat{\boldsymbol{x}}) \partial_{z_l}\hat{u}(\boldsymbol{z}, \hat{\boldsymbol{x}}) \hat{v}(\hat{\boldsymbol{x}}) \right) d\hat{\boldsymbol{x}} \\
&- \int_{\partial K_R} DtN(\partial_{z_l}\hat{u}(\boldsymbol{z}, \hat{\boldsymbol{x}}))\hat{v}(\hat{\boldsymbol{x}})\, dS = L_0(\boldsymbol{z}, \hat{v}), \quad \text{for all } \hat{v} \in V \text{ and all } \boldsymbol{z} \in \mathcal{O}_{\boldsymbol{\rho}}.
\end{aligned} \tag{4.3.13}$$

The right-hand side L_0 is given by

$$L_0(\boldsymbol{z}, \hat{v}) = \int_{K_R} -\frac{\partial \hat{\alpha}}{\partial z_l}(\boldsymbol{z}, \hat{\boldsymbol{x}}) \hat{\nabla}\hat{u}(\boldsymbol{z}, \hat{\boldsymbol{x}}) \cdot \hat{\nabla}\hat{v}(\hat{\boldsymbol{x}})\, d\hat{\boldsymbol{x}} + \frac{\partial \hat{\kappa}^2}{\partial z_l}(\boldsymbol{z}, \hat{\boldsymbol{x}}) \hat{u}(\boldsymbol{z}, \hat{\boldsymbol{x}}) \hat{v}(\hat{\boldsymbol{x}})\, d\hat{\boldsymbol{x}}.$$

In particular, this result holds if Assumption 3.2.4 if fulfilled (with $\tau < T$) and the domain mapping is the one defined in (3.1.2) with the mollifier fulfilling Assumption 3.1.3.

Proof. We observe that, due to Hartogs' theorem, it is sufficient to prove separate analyticity.

Let then $\boldsymbol{e}_l$ denote the Kronecker sequence, i.e. $(e_l)_m = \delta_{lm}$. For $\delta \in \mathbb{C} \setminus \{0\}$, we consider the difference quotient

$$\hat{w}_\delta(\boldsymbol{z}) = \frac{\hat{u}(\boldsymbol{z} + \delta \boldsymbol{e}_l) - \hat{u}(\boldsymbol{z})}{\delta}.$$

Thanks to Assumption 4.3.5, for $|\delta|$ sufficiently small, $\hat{u}(\boldsymbol{z}+\delta\boldsymbol{e}_l)$ and thus $\hat{w}_\delta$ are well defined as elements of $H^1(K_R)$. In particular, for the mapping defined in (3.1.2): if $|\delta|\,|\beta_l|\,\|\psi_l\|_{C^0_{per}([0,2\pi))} = |\delta|\,|\beta_l| \leq \frac{\varepsilon}{2}$ and $|\delta| l\,|\beta_l|\,\|\psi_l\|_{C^0_{per}([0,2\pi))} = |\delta| l\,|\beta_l| \leq \frac{\varepsilon}{2}$, then

$$\begin{aligned} \frac{r^-}{4} \leq \operatorname{Re} r(\boldsymbol{z}+\delta\boldsymbol{e}_l) \leq |r(\boldsymbol{z}+\delta\boldsymbol{e}_l)| \leq r^+ + \frac{3\varepsilon}{2} \\ \Big\| \frac{\partial r}{\partial \varphi}(\boldsymbol{z}+\delta\boldsymbol{e}_l) \Big\|_{C^0_{per}([0,2\pi))} \leq \Big\| \frac{\partial r_0}{\partial \varphi} \Big\|_{C^0_{per}([0,2\pi))} + C_r + \frac{3\varepsilon}{2}, \end{aligned}$$

with C_r as in (4.3.5) (where we have used that $0 < \varepsilon \leq \frac{r^-}{2}$).

For $|\delta|$ sufficiently small, subtracting (3.2.4) for $\hat{u}(\boldsymbol{z}+\delta\boldsymbol{e}_i)$ and (3.2.4) for $\hat{u}(\boldsymbol{z})$, we obtain:

$$\begin{aligned} 0 &= \int_{K_R} \Big(\hat{\alpha}(\boldsymbol{z}+\delta\boldsymbol{e}_i,\hat{\boldsymbol{x}}) \hat{\nabla}\hat{u}(\boldsymbol{z}+\delta\boldsymbol{e}_i,\hat{\boldsymbol{x}}) \cdot \hat{\nabla}\hat{v}(\hat{\boldsymbol{x}}) - \hat{\kappa}^2(\boldsymbol{z}+\delta\boldsymbol{e}_i,\hat{\boldsymbol{x}}) \hat{u}(\boldsymbol{z}+\delta\boldsymbol{e}_i,\hat{\boldsymbol{x}}) \hat{v}(\hat{\boldsymbol{x}}) \Big)\, d\hat{\boldsymbol{x}} \\ &- \int_{K_R} \Big(\hat{\alpha}(\boldsymbol{z},\hat{\boldsymbol{x}}) \hat{\nabla}\hat{u}(\boldsymbol{z},\hat{\boldsymbol{x}}) \cdot \hat{\nabla}\hat{v}(\hat{\boldsymbol{x}}) - \hat{\kappa}^2(\boldsymbol{z},\hat{\boldsymbol{x}}) \hat{u}(\boldsymbol{z},\hat{\boldsymbol{x}}) \hat{v}(\hat{\boldsymbol{x}}) \Big)\, d\hat{\boldsymbol{x}} \\ &- \int_{\partial K_R} DtN(\hat{u}(\boldsymbol{z}+\delta\boldsymbol{e}_i,\hat{\boldsymbol{x}}) - \hat{u}(\boldsymbol{z},\hat{\boldsymbol{x}})) \hat{v}(\hat{\boldsymbol{x}})\, dS \\ &= \delta \int_{K_R} \Big(\hat{\alpha}(\boldsymbol{z},\hat{\boldsymbol{x}}) \hat{\nabla}\hat{w}_\delta(\boldsymbol{z},\hat{\boldsymbol{x}}) \cdot \hat{\nabla}\hat{v}(\hat{\boldsymbol{x}}) - \hat{\kappa}^2(\boldsymbol{z},\hat{\boldsymbol{x}}) \hat{w}_\delta(\boldsymbol{z},\hat{\boldsymbol{x}}) \hat{v}(\hat{\boldsymbol{x}}) \Big)\, d\hat{\boldsymbol{x}} \\ &+ \int_{K_R} \big(\hat{\alpha}(\boldsymbol{z}+\delta\boldsymbol{e}_i,\hat{\boldsymbol{x}}) - \hat{\alpha}(\boldsymbol{z},\hat{\boldsymbol{x}}) \big)\, \hat{\nabla}\hat{u}(\boldsymbol{z}+\delta\boldsymbol{e}_i,\hat{\boldsymbol{x}}) \cdot \hat{\nabla}\hat{v}(\hat{\boldsymbol{x}})\, d\hat{\boldsymbol{x}} \\ &- \int_{K_R} \big(\hat{\kappa}^2(\boldsymbol{z}+\delta\boldsymbol{e}_i,\hat{\boldsymbol{x}}) - \hat{\kappa}^2(\boldsymbol{z},\hat{\boldsymbol{x}}) \big)\, \hat{u}(\boldsymbol{z}+\delta\boldsymbol{e}_i,\hat{\boldsymbol{x}}) \hat{v}(\hat{\boldsymbol{x}})\, d\hat{\boldsymbol{x}} - \delta \int_{\partial K_R} DtN(\hat{w}_\delta(\boldsymbol{z},\hat{\boldsymbol{x}})) \hat{v}(\hat{\boldsymbol{x}})\, dS. \end{aligned}$$

Thus, $\hat{w}_\delta$ satisfies the following variational formulation:

$$\begin{aligned} &\text{Find } \hat{w}_\delta(\boldsymbol{z}) \in V : \\ &\int_{K_R} \Big(\hat{\alpha}(\boldsymbol{z},\hat{\boldsymbol{x}}) \hat{\nabla}\hat{w}_\delta(\boldsymbol{z},\hat{\boldsymbol{x}}) \cdot \hat{\nabla}\hat{v}(\hat{\boldsymbol{x}}) - \hat{\kappa}^2(\boldsymbol{z},\hat{\boldsymbol{x}}) \hat{w}_\delta(\boldsymbol{z},\hat{\boldsymbol{x}}) \hat{v}(\hat{\boldsymbol{x}}) \Big)\, d\hat{\boldsymbol{x}} \\ &- \int_{\partial K_R} DtN(\hat{w}_\delta(\boldsymbol{z},\hat{\boldsymbol{x}})) \hat{v}(\hat{\boldsymbol{x}})\, dS = L_\delta(\boldsymbol{z},\hat{v}), \qquad \text{for all } \hat{v} \in V \text{ and all } \boldsymbol{z} \in \mathcal{O}_{\boldsymbol{\rho}}; \end{aligned} \tag{4.3.14}$$

the right-hand side is defined as

$$\begin{aligned} L_\delta(\boldsymbol{z},\hat{v}) = &- \int_{K_R} \frac{\hat{\alpha}(\boldsymbol{z}+\delta\boldsymbol{e}_l,\hat{\boldsymbol{x}}) - \hat{\alpha}(\boldsymbol{z},\hat{\boldsymbol{x}})}{\delta} \hat{\nabla}\hat{u}(\boldsymbol{z}+\delta\boldsymbol{e}_l,\hat{\boldsymbol{x}}) \cdot \hat{\nabla}\hat{v}(\hat{\boldsymbol{x}})\, d\hat{\boldsymbol{x}} \\ &+ \int_{K_R} \frac{\hat{\kappa}^2(\boldsymbol{z}+\delta\boldsymbol{e}_l,\hat{\boldsymbol{x}}) - \hat{\kappa}^2(\boldsymbol{z},\hat{\boldsymbol{x}})}{\delta} \hat{u}(\boldsymbol{z}+\delta\boldsymbol{e}_l,\hat{\boldsymbol{x}}) \hat{v}(\hat{\boldsymbol{x}})\, d\hat{\boldsymbol{x}}. \end{aligned}$$

For every δ with $|\delta|$ sufficiently small, existence and uniqueness of the solution $\hat{w}_\delta(\boldsymbol{z})$ to (4.3.14) follow from either applying the Fredholm Alternative and the sign properties of the DtN map as we did for Theorem 3.2.3, or exploiting the coercivity of the bilinear form (ensured by Assumption 3.2.4, with the restrictions on τ, and Assumption 4.3.5) to apply the Lax-Milgram lemma.

As $|\delta|$ tends to zero, for each $\hat{v} \in V$ and every $\boldsymbol{z} \in \mathcal{O}_{\boldsymbol{\rho}}$ fixed, the right-hand side $L_\delta(\boldsymbol{z},\hat{v})$ tends to

$$L_0(\boldsymbol{z},\hat{v}) := \int_{K_R} -\frac{\partial \hat{\alpha}}{\partial z_l}(\boldsymbol{z},\hat{\boldsymbol{x}}) \hat{\nabla}\hat{u}(\boldsymbol{z},\hat{\boldsymbol{x}}) \cdot \hat{\nabla}\hat{v}(\hat{\boldsymbol{x}})\, d\hat{\boldsymbol{x}} + \frac{\partial \hat{\kappa}^2}{\partial z_l}(\boldsymbol{z},\hat{\boldsymbol{x}}) \hat{u}(\boldsymbol{z},\hat{\boldsymbol{x}}) \hat{v}(\hat{\boldsymbol{x}})\, d\hat{\boldsymbol{x}}.$$

Indeed, subtracting L_δ and L_0 and denoting $\hat{\alpha}_\delta(\boldsymbol{z}) := \frac{\hat{\alpha}(\boldsymbol{z}+\delta\boldsymbol{e}_l)-\hat{\alpha}(\boldsymbol{z})}{\delta}$ we have, for the first summand:

$$\begin{aligned}
&\Big| \int_{K_R} \hat{\alpha}_\delta(\boldsymbol{z}) \hat{\nabla}\hat{u}(\boldsymbol{z}+\delta\boldsymbol{e}_l,\hat{\boldsymbol{x}}) \cdot \hat{\nabla}\hat{v}(\hat{\boldsymbol{x}}) - \frac{\partial\hat{\alpha}}{\partial z_l}(\boldsymbol{z}) \hat{\nabla}\hat{u}(\boldsymbol{z},\hat{\boldsymbol{x}}) \cdot \hat{\nabla}\hat{v}(\hat{\boldsymbol{x}})\, d\hat{\boldsymbol{x}} \Big| \\
&\leq \Big| \int_{K_R} \left(\hat{\alpha}_\delta - \frac{\partial\hat{\alpha}}{\partial z_l} \right) \hat{\nabla}\hat{u}(\boldsymbol{z}+\delta\boldsymbol{e}_l,\hat{\boldsymbol{x}}) \cdot \hat{\nabla}\hat{v}(\hat{\boldsymbol{x}})\, d\boldsymbol{x} \Big| \\
&+ \Big| \int_{K_R} \frac{\partial\hat{\alpha}}{\partial z_l} \left(\hat{\nabla}\hat{u}(\boldsymbol{z}+\delta\boldsymbol{e}_l,\hat{\boldsymbol{x}}) - \hat{\nabla}\hat{u}(\boldsymbol{z},\hat{\boldsymbol{x}}) \right) \cdot \hat{\nabla}\hat{v}(\hat{\boldsymbol{x}})\, d\hat{\boldsymbol{x}} \Big| \\
&\leq \left\| \hat{\alpha}_\delta(\boldsymbol{z}) - \frac{\partial\hat{\alpha}}{\partial z_l}(\boldsymbol{z}) \right\|_{C^0_{\mathrm{pw}}(\overline{K_R})} |\hat{u}(\boldsymbol{z}+\delta\boldsymbol{e}_i)|_{H^1(K_R)}\, |\hat{v}|_{H^1(K_R)} \\
&+ \left\| \frac{\partial\hat{\alpha}}{\partial z_l}(\boldsymbol{z}) \right\|_{C^0_{\mathrm{pw}}(\overline{K_R})} |\hat{u}(\boldsymbol{z}+\delta\boldsymbol{e}_i) - \hat{u}(\boldsymbol{z})|_{H^1(K_R)}\, |\hat{v}|_{H^1(K_R)}\,.
\end{aligned}$$

Since $\boldsymbol{z} \mapsto \hat{\alpha}(\boldsymbol{z})$ is holomorphic and C^0_{pw}-valued, there exist constants $C_1^{\boldsymbol{z}}, C_2^{\boldsymbol{z}} < \infty$, possibly depending on $\boldsymbol{z} \in \mathcal{O}_{\boldsymbol{\rho}}$ but not on δ, such that

$$\begin{aligned}
\left\| \hat{\alpha}_\delta(\boldsymbol{z}) - \frac{\partial\hat{\alpha}}{\partial z_l}(\boldsymbol{z}) \right\|_{C^0_{\mathrm{pw}}(\overline{K_R})} &\leq C_1^{\boldsymbol{z}}|\delta|, \\
\left\| \frac{\partial\hat{\alpha}}{\partial z_l}(\boldsymbol{z}) \right\|_{C^0_{\mathrm{pw}}(\overline{K_R})} &= C_2^{\boldsymbol{z}}.
\end{aligned}$$

The uniform bound given by Proposition 4.3.7 ensures that there exists $C_3 < \infty$, independent of $\boldsymbol{z} \in \mathcal{O}_{\boldsymbol{\rho}}$ and of δ, such that $|\hat{u}(\boldsymbol{z}+\delta\boldsymbol{e}_i)|_{H^1(K_R)} \leq C_3$ for every $\delta \in \mathbb{C}$ with $|\delta|$ sufficiently small. Lemma 4.3.12 together with the analyticity of $\boldsymbol{z} \mapsto \hat{\alpha}(\boldsymbol{z})$ and $\boldsymbol{z} \mapsto \hat{\kappa}^2(\boldsymbol{z})$, ensure the existence of a constant $C_4^{\boldsymbol{z}} < \infty$, independent of δ (but that might depend on $\boldsymbol{z} \in \mathcal{O}_{\boldsymbol{\rho}}$), such that

$$|\hat{u}(\boldsymbol{z}+\delta\boldsymbol{e}_i) - \hat{u}(\boldsymbol{z})|_{H^1(K_R)} \leq C_4^{\boldsymbol{z}}|\delta| \left(\left\| \frac{\partial\hat{\alpha}}{\partial z_l}(\boldsymbol{z}) \right\|_{C^0_{\mathrm{pw}}(\overline{K_R})} + \left\| \frac{\partial\hat{\kappa}^2}{\partial z_l}(\boldsymbol{z}) \right\|_{C^0_{\mathrm{pw}}(\overline{K_R})} \right),$$

for $|\delta| \to 0$. Together, these bounds imply that there exists a constant $C_5^{\boldsymbol{z}} < \infty$, possibly depending on $\boldsymbol{z} \in \mathcal{O}_{\boldsymbol{\rho}}$ but independent of δ, such that

$$\Big| \int_{K_R} \hat{\alpha}_\delta(\boldsymbol{z}) \hat{\nabla}\hat{u}(\boldsymbol{z}+\delta\boldsymbol{e}_l,\hat{\boldsymbol{x}}) \cdot \hat{\nabla}\hat{v}(\hat{\boldsymbol{x}}) - \frac{\partial\hat{\alpha}}{\partial z_l}(\boldsymbol{z}) \hat{\nabla}\hat{u}(\boldsymbol{z},\hat{\boldsymbol{x}}) \cdot \hat{\nabla}\hat{v}(\hat{\boldsymbol{x}})\, d\hat{\boldsymbol{x}} \Big| \leq C_5^{\boldsymbol{z}}|\delta|,$$

for $|\delta| \to 0$. Applying the same technique to the second summand of $L_\delta - L_0$, we finally get that, as $|\delta| \to 0$, $L_\delta \to L_0$ in the dual space V^*.

Thus, the complex derivative $(\partial_{z_l}\hat{u})(\boldsymbol{z})$, if it exists, is the unique solution to

$$\begin{aligned}
&\text{Find } (\partial_{z_l}\hat{u})(\boldsymbol{z}) \in V : \\
&\int_{K_R} \left(\hat{\alpha}(\boldsymbol{z},\hat{\boldsymbol{x}}) \hat{\nabla}\partial_{z_l}\hat{u}(\boldsymbol{z},\hat{\boldsymbol{x}}) \cdot \hat{\nabla}\hat{v}(\hat{\boldsymbol{x}}) - \hat{\kappa}^2(\boldsymbol{z},\hat{\boldsymbol{x}}) \partial_{z_l}\hat{u}(\boldsymbol{z},\hat{\boldsymbol{x}}) \hat{v}(\hat{\boldsymbol{x}}) \right) d\hat{\boldsymbol{x}} \\
&- \int_{\partial K_R} DtN(\partial_{z_l}\hat{u}(\boldsymbol{z},\hat{\boldsymbol{x}}))\hat{v}(\hat{\boldsymbol{x}})\, dS = L_0(\boldsymbol{z},\hat{v}), \quad \text{for all } \hat{v} \in V \text{ and all } \boldsymbol{z} \in \mathcal{O}_{\boldsymbol{\rho}}. \qquad (4.3.15)
\end{aligned}$$

For every $\boldsymbol{z} \in \mathcal{O}_{\boldsymbol{\rho}}$, Assumption 4.3.5 guarantees coercivity and continuity of the bilinear form in (4.3.15); together with the continuity of $L_0(\boldsymbol{z})$ on V, this implies that the variational problem above is well-posed for every $\boldsymbol{z} \in \mathcal{O}_{\boldsymbol{\rho}}$. Thus, for every $\boldsymbol{z} \in \mathcal{O}_{\boldsymbol{\rho}}$, the complex derivative $(\partial_{z_l}\hat{u})(\boldsymbol{z})$ exists and is given by the solution to (4.3.15). □

Summarizing the results obtained in this section:

Theorem 4.3.14. *Let Assumptions 2.1.2, 2.1.3, 2.1.4.A or 2.1.4.B, and 3.2.4 be satisfied. Then the $(\boldsymbol{b}, p, \varepsilon)^*$-holomorphy assumption is fulfilled for the domain mapping* (3.1.2)*, with the same restrictions on the mollifier as in Lemma 4.3.9, and the results of Theorems 4.1.5 and 4.1.6 hold with convergence rate $s = \frac{1}{p} - 2$.*

For a generic domain mapping, the $(\boldsymbol{b}, p, \varepsilon)^*$-holomorphy assumption is satisfied and the algebraic convergence prescribed by Theorems 4.1.5 and 4.1.6 is achieved with $s = \frac{1}{p} - 2$ if the map fulfills Assumption 4.3.5.

Remark 4.3.15. It is clear from our treatment that the above result can be easily extended when for the mapping (3.1.2) we use the mollifier (3.1.3).

5. Sparse tensor discretization: abstract setting

The convergence results of Theorems 4.1.5 and 4.1.6 assume that the Q.o.I. g can be computed exactly at the interpolation/quadrature points. Often in applications, though, for each realization $\boldsymbol{y}$ just a discrete approximation to g can be calculated.

This chapter is devoted to the convergence analysis for the full sparse tensor discretization, i.e. for the interpolant or the mean of the Q.o.I. obtained with a sparse interpolation/quadrature algorithm in the case that each realization is subject to a space discretization error.

We develop the analysis in a general setting, that goes beyond the application presented in this work. In the next chapter, we will see how the results obtained apply for the Helmholtz transmission problem.

We state the convergence results in two cases: first, assuming that the space discretization used is the same for every interpolation/quadrature point, second, in the case of nested sequences of interpolation/quadrature points, allowing the space discretization to be different for every realization.

5.1. Abstract problem setting

Let X, Y be reflexive, separable Banach spaces over $\mathbb{C}$. Let $(u, v) \mapsto B(\boldsymbol{y}, u, v)$ and $v \mapsto L(\boldsymbol{y}, v)$ denote the parameter-dependent sesquilinear and antilinear forms on $X \times Y$ and on Y, respectively. We consider the parametric PDE in the general variational form:

$$\text{Find } u \in X: \quad B(\boldsymbol{y}, u, v) = L(\boldsymbol{y}, v), \quad \text{for every } v \in Y, \boldsymbol{y} \in \mathcal{P}_J, J \in \mathbb{N}. \tag{5.1.1}$$

We assume that the sesquilinear and antilinear forms fulfill the $(\boldsymbol{b}, p, \varepsilon)$-holomorphy assumption [CCS15]. Then Theorem 4.1 in [CCS15] guarantees that the map $\boldsymbol{y} \mapsto u(\boldsymbol{y})$ from the parameter space to X, with $u(\boldsymbol{y})$ the solution to (5.1.1), fulfills the $(\boldsymbol{b}, p, \varepsilon)$-holomorphy assumption with the same p, ε and sequence $\boldsymbol{b}$ as the sesquilinear and antilinear forms.

Introducing the families of finite dimensional subspaces $X_{l,h} \subset X$ and $Y_{l,h} \subset Y$, $l \in \mathbb{N}$ and $h \in \mathbb{R}_+$, the discrete variational formulation of (5.1.1) for every $l \in \mathbb{N}$ reads:

$$\text{Find } u_{l,h} \in X_{l,h}: \quad B(\boldsymbol{y}, u_{l,h}, v_{l,h}) = L(\boldsymbol{y}, v_{l,h}), \quad \text{for every } v_{l,h} \in Y_{l,h}, \boldsymbol{y} \in \mathcal{P}_J, J \in \mathbb{N}. \tag{5.1.2}$$

We assume the existence of a convergence estimate of the form:

$$\inf_{v_{l,h} \in X_{l,h}} \|w - v_{l,h}\|_X \leq C_l h^{t_l} \|w\|_W \quad \text{as } h \to 0, \tag{5.1.3}$$

for any $w \in W$ and some $t_l \in \mathbb{R}_+$, and for every $l \in \mathbb{N}$. For every $l \in \mathbb{N}$, C_l is a positive constant, independent of h and of the truncation parameter J (but possibly dependent of l).

For instance, we can think about l as the polynomial degree in a finite element discretization, and h as the meshwidth.

5.2. Holomorphy of the discrete solution

Since we apply sparse interpolation and quadrature to the discrete solution, we have to show its holomorphy.

Lemma 5.2.1. *Let $(X_{l,h})_{l\geq 1,h>0}$ be a family of finite dimensional subspaces of X, and, for every $l \in \mathbb{N}$ and $h \in \mathbb{R}_+$, let $u_{l,h} \in X_{l,h}$ be the discrete solution to (5.1.1). Then, for every $l \in \mathbb{N}$ and every $h \in \mathbb{R}_+$, the mapping $\boldsymbol{y} \to u_{l,h}(\boldsymbol{y}) \in X$ fulfills the $(\boldsymbol{b}, p, \varepsilon)$-holomorphy assumption with the same sequence $\boldsymbol{b}$, the same p and the same ε with which the sesquilinear form and the antilinear form fulfill the $(\boldsymbol{b}, p, \varepsilon)$-holomorphy assumption.*

Proof. The proof is the same as in the continuous case [CCS15, Thm. 4.1], replacing the variational formulation (5.1.1) with the corresponding discrete variational formulation. □

Remark 5.2.2. The assumption that $X_{l,h} \subset X$ and $Y_{l,h} \subset Y$ can be dropped if we require that the sesquilinear and antilinear form fulfill the $(\boldsymbol{b}, p, \varepsilon)$-assumption on the discrete spaces, with domain of holomorphy and inf-sup and continuity constants independent of h.

5.3. Convergence estimate for fixed finite element discretization

In this case, we fix $l \in \mathbb{N}$, consider the family $(X_{l,h})_{h>0}$ with l fixed, and denote by $t := t_l$ the convergence rate in (5.1.3). We indicate by $I_\Lambda u_h$ and $Q_\Lambda u_h$ the quantities obtained applying, respectively, sparse interpolation and quadrature to the discrete solution $u_h \subset X_{l,h}$ to (5.1.2).

The estimate follows by a simple application of the triangle inequality:

Theorem 5.3.1. *Assume that the sesquilinear and antilinear forms in (5.1.1) fulfill the $(\boldsymbol{b}, p, \varepsilon)$-holomorphy assumption. Assume that (5.1.3) holds and that, for every $J \in \mathbb{N}$ and every $\boldsymbol{y} \in \mathcal{P}_J$, $\|u(\boldsymbol{y})\|_W$ is uniformly bounded.*

For the interpolation, we assume that the Lebesgue constant λ_m associated with the univariate sequence of interpolation points $(\zeta_i^m)_{i=0}^{n_m}$ satisfies $\lambda_m \leq C(m+1)^\theta$ for some $\theta \geq 1$ and a constant $C \in \mathbb{R}_+$ (independent of m). For quadrature, assume that the univariate quadrature operators fulfill Assumption 4.1.2.

Consider that the same space discretization is used at all parameter realizations $\boldsymbol{y}_\nu$, $\nu \in \Lambda$.

Then there exists a downward closed set Λ of cardinality at most N such that

$$\|u - I_\Lambda u_h\|_{L^\infty(\mathcal{P}_J, X)} \leq Ch^t + C_1 N^{-s}, \quad s = \frac{1}{p} - 1, \tag{5.3.1}$$

$$\|\mathcal{I}(u) - Q_\Lambda u_h\|_X \leq Ch^t + C_2 N^{-s}, \quad s = \frac{1}{p} - 1. \tag{5.3.2}$$

with $s, C, C_1, C_2 > 0$ independent of N, h, of the truncation parameter $J \in \mathbb{N}$ and of $\boldsymbol{y} \in \mathcal{P}_J$.

Proof. For each $\boldsymbol{y} \in \mathcal{P}_J$, we can write

$$\|u(\boldsymbol{y}) - I_\Lambda u_h(\boldsymbol{y})\|_X \leq \|u(\boldsymbol{y}) - u_h(\boldsymbol{y})\|_X + \|u_h(\boldsymbol{y}) - I_\Lambda u_h(\boldsymbol{y})\|_X. \tag{5.3.3}$$

We highlight that when doing this splitting we exploit the fact that the same finite element space is used for all interpolation/quadrature points, so that we can define $u_h(\boldsymbol{y})$ for all $\boldsymbol{y} \in \mathcal{P}_J$.

The first term is bounded by (5.1.3). The bound for the second term in (5.3.3) follows directly from Lemma 5.2.1 and Theorem 4.1.5.

For the quadrature case, we have that

$$\|\mathcal{I}(u(\boldsymbol{y})) - Q_\Lambda u_h(\boldsymbol{y})\|_X \leq \|\mathcal{I}(u(\boldsymbol{y}) - u_h(\boldsymbol{y}))\|_X + \|\mathcal{I}(u_h(\boldsymbol{y})) - Q_\Lambda u_h(\boldsymbol{y})\|_X;$$

once we observe, for the first term, that $\|\mathcal{I}\|_{\mathcal{L}(L^\infty(\mathcal{P}_J,X))} = 1$ for every $J \in \mathbb{N}$, the result follows as in the interpolation case using Theorem 4.1.6 to bound the second term. □

5.4. Convergence estimate for parameter-adaptive discretization

The idea is to distinguish the contribution of the space discretization for each difference operator Δ_ν^I or Δ_ν^Q as defined in (4.1.5)-(4.1.10) for the interpolation case and in (4.1.11)-(4.1.14) for the quadrature case. In particular, we associate a family $(X_{l,h})_{h>0}$ to each interpolation/quadrature point. The approach is similar to the one followed in [SG11] for the Legendre coefficients.

In the following, we denote by $\boldsymbol{H}_m(\boldsymbol{y})$ the multivariate hierarchical polynomial associated with the node $\boldsymbol{y}_m$ in the case of nested sequences of interpolation points (see [CCS14] for details). Also, $\{\boldsymbol{y}_m \in \Delta_\nu^I\}$ indicates the set of new interpolation points (or quadrature points using Δ_ν^Q) introduced by the difference operator Δ_ν^I (resp. Δ_ν^Q), ω_m denotes the quadrature weight associated with $\boldsymbol{y}_m$ and $\mathbb{L}_{\mathcal{R}_\nu}$ is the Lebesgue constant of the interpolation operator $I_{\mathcal{R}_\nu}$ on $\mathcal{R}_\nu := \{\mu \in \mathcal{F} : \mu < \nu\}$.

The quantities $I_\Lambda u_{h,\Lambda}$ and $Q_\Lambda u_{h,\Lambda}$ denote the solutions obtained respectively from sparse interpolation and quadrature of the discrete solution $u_{h,\Lambda}$ to (5.1.2).

Theorem 5.4.1. *Assume that the sesquilinear and antilinear forms in* (5.1.1) *fulfill the* $(\boldsymbol{b}, p, \varepsilon)$*-holomorphy assumption. Assume that* (5.1.3) *holds and that, for every* $J \in \mathbb{N}$ *and every* $\boldsymbol{y} \in \mathcal{P}_J$, $\|u(\boldsymbol{y})\|_W$ *is uniformly bounded.*

For the interpolation, we ask that the Lebesgue constant λ_m *associated with the univariate sequence of interpolation points* $(\zeta_i^m)_{i=0}^{n_m}$ *satisfies* $\lambda_m \leq C(m+1)^\theta$ *for some* $\theta \geq 1$ *and a constant* $C \in \mathbb{R}_+$ *(independent of* m*). For quadrature, assume that the univariate quadrature operators fulfill Assumption 4.1.2. Let* X_{h_m,l_m} *be the finite dimensional discretization space associated with* $\boldsymbol{y}_m$*.*

There exists a downward closed set Λ *of cardinality at most* N *such that*

$$\|u - I_\Lambda u_{h,\Lambda}\|_{L^\infty(\mathcal{P}_J,X)} \leq \sum_{\nu\in\Lambda} \|\Delta_\nu^I(u - u_{h,\Lambda})\|_{L^\infty(\mathcal{P}_J,X)} + C_1 N^{-s}, \quad s = \frac{1}{p} - 1, \tag{5.4.1}$$

$$\|\mathcal{I}(u) - Q_\Lambda u_{h,\Lambda}\|_X \leq \sum_{\nu\in\Lambda} \|\Delta_\nu^Q(u - u_{h,\Lambda})\|_X + C_2 N^{-s}, \quad s = \frac{1}{p} - 1, \tag{5.4.2}$$

with $s, C_1, C_2 > 0$ *independent of* N*, of* h_m *for every* m*, of* $J \in \mathbb{N}$ *and of* $\boldsymbol{y} \in \mathcal{P}_J$*.*

If the sequences $(\zeta_i)_{i\geq 0}$ *of interpolation/quadrature points are nested, then the addends in the sum on the right-hand side satisfy, for the interpolation and quadrature case respectively:*

$$\|\Delta_\nu^I(u - u_{h,\Lambda})\|_{L^\infty(\mathcal{P}_J,X)} \leq (1 + \mathbb{L}_{\mathcal{R}_\nu}) \sum_{\boldsymbol{y}_m\in\Delta_\nu^I} C_{l_m} \|\boldsymbol{H}_m(\cdot)\|_{L^\infty(\mathcal{P}_J,\mathbb{R})} h_m^{t_{l_m}} \|u(\boldsymbol{y}_m)\|_W, \tag{5.4.3}$$

$$\|\Delta_\nu^Q(u - u_{h,\Lambda})\|_X \leq \sum_{\boldsymbol{y}_m\in\Delta_\nu^Q} C_{l_m} |\omega_m| h_m^{t_{l_m}} \|u(\boldsymbol{y}_m)\|_W, \tag{5.4.4}$$

with, for every $m \in \mathbb{N}$, C_{l_m} *independent of* N*, of* h_m *for every* m*, of* $J \in \mathbb{N}$ *and of* $\boldsymbol{y} \in \mathcal{P}_J$*. The Lebesgue constant* $\mathbb{L}_{\mathcal{R}_\nu}$ *is bounded by*

$$\mathbb{L}_{\mathcal{R}_\nu} \leq (\sharp\mathcal{R}_\nu)^{\theta+1}. \tag{5.4.5}$$

We have $\|\boldsymbol{H}_m(\cdot)\|_{L^\infty(\mathcal{P}_J,\mathbb{R})} \geq 1$ for every sequence of interpolation points and $\|\boldsymbol{H}_m(\cdot)\|_{L^\infty(\mathcal{P}_J,\mathbb{R})} = 1$ for every $m \in \mathbb{N}$ in the case of Leja points on the real interval $[-1,1]$ (see e.g. [Chk13] for their definition).

Proof. We first consider the interpolation case. Simply applying the triangle inequality we obtain:

$$\begin{aligned}\|u - I_\Lambda u_{h,\Lambda}\|_{L^\infty(\mathcal{P}_J,X)} &\leq \|u - I_\Lambda u\|_{L^\infty(\mathcal{P}_J,X)} + \|I_\Lambda u - I_\Lambda u_{h,\Lambda}\|_{L^\infty(\mathcal{P}_J,X)} \\ &\leq \|u - I_\Lambda u\|_{L^\infty(\mathcal{P}_J,X)} + \sum_{\nu\in\Lambda} \|\Delta_\nu^I u - \Delta_\nu^I u_{h,\Lambda}\|_{L^\infty(\mathcal{P}_J,X)}.\end{aligned}$$

Thanks to Lemma 5.2.1, Theorem 4.1.5 holds and thus we get (5.4.1).

If the sequence of interpolation points is nested, then, according to [CCS14, Formula (2.25)], one can write, for a generic element $g \in L^\infty(\mathcal{P}_J, X)$,

$$\Delta_\nu^I g(\boldsymbol{y}) = \sum_{\boldsymbol{y}_m \in \Delta_\nu^I} \left(g(\boldsymbol{y}_m) - I_{\mathcal{R}_\nu} g(\boldsymbol{y}_m)\right) \boldsymbol{H}_m(\boldsymbol{y}),$$

with $I_{\mathcal{R}_\nu}$ the interpolation operator on $\mathcal{R}_\nu$. Thus, for each $\nu \in \Lambda$:

$$\begin{aligned}&\|\Delta_\nu^I u - \Delta_\nu^I u_{h,\Lambda}\|_{L^\infty(\mathcal{P}_J,X)} \\ &\leq \sum_{\boldsymbol{y}_m \in \Delta_\nu^I} \|u(\boldsymbol{y}_m) - u_{h,\Lambda}(\boldsymbol{y}_m) - I_{\mathcal{R}_\nu}(u(\boldsymbol{y}_m) - u_{h,\Lambda}(\boldsymbol{y}_m))\|_X \|\boldsymbol{H}_m(\cdot)\|_{L^\infty(\mathcal{P}_J,\mathbb{R})} \\ &\leq \sum_{\boldsymbol{y}_m \in \Delta_\nu^I} (1 + \mathbb{L}_{\mathcal{R}_\nu}) \|u(\boldsymbol{y}_m) - u_{h,\Lambda}(\boldsymbol{y}_m)\|_X \|\boldsymbol{H}_m(\cdot)\|_{L^\infty(\mathcal{P}_J,\mathbb{R})} \\ &\leq (1 + \mathbb{L}_{\mathcal{R}_\nu}) \sum_{\boldsymbol{y}_m \in \Delta_\nu^I} C_{l_m} h_m^{t_{l_m}} \|u(\boldsymbol{y}_m)\|_W \|\boldsymbol{H}_m(\cdot)\|_{L^\infty(\mathcal{P}_J,\mathbb{R})}.\end{aligned}$$

Under the hypothesis on the Lebesgue constants for the univariate operators, we have $\mathbb{L}_{\mathcal{R}_\nu} \leq (\sharp\mathcal{R}_\nu)^{\theta+1}$, and thus $\mathbb{L}_{\mathcal{R}_\nu}$ grows with $\sharp\mathcal{R}_\nu$. We have obtained (6.2.5), with $\|\boldsymbol{H}_m(\cdot)\|_{L^\infty(\mathcal{P}_J)} \geq 1$ in general and $\|\boldsymbol{H}_m(\cdot)\|_{L^\infty(\mathcal{P}_J)} = 1$ for every l in the case of Leja points [CCS14].

The result for the quadrature operators follows the same lines. The difference is, of course, in the definition of the difference operators for nested sequences. In this case, for a continuous $g \in L^2(\mathcal{P}_J, X)$:

$$\Delta_\nu^Q g = \sum_{\boldsymbol{y}_m \in \Delta_\nu^Q} \omega_m g(\boldsymbol{y}_m),$$

and thus

$$\|\Delta_\nu^Q u - \Delta_\nu^Q u_{h,\Lambda}\|_X \leq \sum_{\boldsymbol{y}_m \in \Delta_\nu^Q} C_{l_m} |\omega_m| h_m^{t_{l_m}} \|u(\boldsymbol{y}_m)\|_W.$$

□

The above theorem can be considered as a starting point for an adaptive strategy, where one tries to minimize the total number of degrees of freedom used overall in the space discretizations in such a way that the total error induced by them is of the same order as the Smolyak algorithm error ($\sim N^{-s}$). Differently from [CDS11], when using the adaptive Smolyak algorithm described in Section 4.2, we do not know the index set apriori; thus, the adaptive strategy cannot be based on the solution of an optimization problem as in [CDS11], but rather on an online choice of the finite element space each time the algorithm selects an interpolation/quadrature point.

Remark 5.4.2. We have deduced the convergence results for the full solution without proving that the solution $u(\boldsymbol{y})$ to (5.1.1) admits a holomorphic extension to the complex plane as map from $\mathcal{P}$ to W, as it is done instead in [CDS11]. In [CDS11] such a holomorphic extension was needed because the space discretization was applied to the Taylor coefficients of the solution. In our case, when we apply the convergence results of Theorems 4.1.5 and 4.1.6, we always consider u as map from $\mathcal{P}$ to X, and the convergence results for the space discretization are applied on realizations of u for values of the *real* parameter $\boldsymbol{y}$. Thus, what we need only is a J- and $\boldsymbol{y}$-independent bound on $\|u(\boldsymbol{y})\|_W$ for every realization of the real-valued parameter $\boldsymbol{y}$.

We also highlight that, if we needed to show holomorphy of u as a W-valued map, then it might happen that the radii of the polyellipses where u can be extended would decay much slower than the polyradii for which u can be extended as a X-valued map, and this would significantly deteriorate the convergence rate for sparse interpolation and quadrature. For instance, in the application considered in this work, the expansion of the radius in terms of sinusouids would imply an increase of the p in the $(\boldsymbol{b}, p, \varepsilon)$-holomorphy assumption each time we differentiate to consider higher space regularity for the solution $\hat{u}$.

5.5. Convergence of linear output functionals

Let $F = F(\boldsymbol{y})$, $\boldsymbol{y} \in \mathcal{P}_J$, $J \in \mathbb{N}$, be a linear output functional on X. If $F(u)$ depended only on the solution u to (5.1.1), then, thanks to the linearity, the holomorphy of F would follow immediately from the holomorphy of u. However, since in general F is parameter-dependent by itself, we require that:

Assumption 5.5.1. The linear output functional $F = F(\boldsymbol{y}, u)$ admits an analytic extension to the complex plane, with the same domain of analyticity as the solution u to (5.1.1).

We also assume that F fulfills a convergence estimate of the form

$$|F(\boldsymbol{y}, w) - F(\boldsymbol{y}, w_{l,h})| \leq C_l^F h^{t_l^F} \inf_{v_{l,h} \in X_{l,h}} \|w - v_{l,h}\|_X \quad \text{as } h \to 0, \tag{5.5.1}$$

for some $t_l^F \in \mathbb{R}_{0,+}$ for every $l \in \mathbb{N}$. For every $l \in \mathbb{N}$, C_l^F is a positive constant independent of h, of $J \in \mathbb{N}$ and of $\boldsymbol{y} \in \mathcal{P}_J$ (but possibly dependent of l).

Let us denote $F_h := F(u_h)$ and $F_{l,h} := F(u_{l,h})$, where u_h and $u_{l,h}$ correspond to the solution to (5.1.2) in the case of fixed and parameter-dependent space discretization, respectively. Then we have the two following results:

Theorem 5.5.2. *Let F fulfill Assumption 5.5.1 and let u be the solution to* (5.1.1)*. Let the assumptions of Theorem 5.3.1 be satisfied. Consider that the same space discretization is used at all parameter realizations $\boldsymbol{y}_\nu$, $\nu \in \Lambda$.*

Then there exists a downward closed set Λ of cardinality at most N such that the following estimates hold:

$$\|F - I_\Lambda F_h\|_{L^\infty(\mathcal{P}_J, X)} \leq C h^{t^F + t} + C_1 N^{-s}, \quad s = \frac{1}{p} - 1, \tag{5.5.2}$$

$$\|\mathcal{I}(F) - Q_\Lambda F_h\|_X \leq C h^{t^F + t} + C_2 N^{-s}, \quad s = \frac{1}{p} - 1, \tag{5.5.3}$$

with $s, C, C_1, C_2 > 0$ independent of N, h, of $J \in \mathbb{N}$ and of $\boldsymbol{y} \in \mathcal{P}_J$.

Theorem 5.5.3. *Let F fulfill Assumption 5.5.1 and let u be the solution to* (5.1.1)*. Let the assumptions of Theorem 5.4.1 be satisfied.*

Then there exists a downward closed set Λ of cardinality at most N such that

$$\|F - I_\Lambda F_{h,\Lambda}\|_{L^\infty(\mathcal{P}_J,X)} \leq \sum_{\nu\in\Lambda} \|\Delta_\nu^I(F - F_{h,\Lambda})\|_{L^\infty(\mathcal{P}_J,X)} + C_1 N^{-s}, \quad s = \frac{1}{p} - 1, \tag{5.5.4}$$

$$\|\mathcal{I}(F) - Q_\Lambda F_{h,\Lambda}\|_X \leq \sum_{\nu\in\Lambda} \|\Delta_\nu^Q(F - F_{h,\Lambda})\|_X + C_2 N^{-s}, \quad s = \frac{1}{p} - 1, \tag{5.5.5}$$

with $s, C_1, C_2 > 0$ independent of N, of h_m for every m, of $J \in \mathbb{N}$ and of $\boldsymbol{y} \in \mathcal{P}_J$.

If the sequences $(\zeta_i)_{i\geq 0}$ of interpolation/quadrature points are nested, then the addends in the sum on the right-hand side satisfy, for the interpolation and quadrature case respectively:

$$\|\Delta_\nu^I(F - F_{h,\Lambda})\|_{L^\infty(\mathcal{P}_J,X)} \leq (1 + \mathbb{L}_{\mathcal{R}_\nu}) \sum_{\boldsymbol{y}_m\in\Delta_\nu^I} C_{l_m} \|\boldsymbol{H}_m(\cdot)\|_{L^\infty(\mathcal{P}_J\mathbb{R})} h_m^{t_{l_m}^F + t_{l_m}} \|u(\boldsymbol{y}_m)\|_W, \tag{5.5.6}$$

$$\|\Delta_\nu^Q(F - F_{h,\Lambda})\|_X \leq \sum_{\boldsymbol{y}_m\in\Delta_\nu^Q} C_{l_m} |\omega_m| h_m^{t_{l_m}^F + t_{l_m}} \|u(\boldsymbol{y}_m)\|_W, \tag{5.5.7}$$

with, for every $m \in \mathbb{N}$, $C_{l_m} > 0$ independent of N, of h_m for every m, of $J \in \mathbb{N}$ and of $\boldsymbol{y} \in \mathcal{P}_J$, and the Lebesgue constant $\mathbb{L}_{\mathcal{R}_\nu}$ bounded as in (5.4.5)*, i.e. $\mathbb{L}_{\mathcal{R}_\nu} \leq (\sharp\mathcal{R}_\nu)^{\theta+1}$.*

The proofs of these theorems are analogous to the proofs of Theorems 5.3.1 and 5.4.1.

6. Spatial regularity and sparse tensor discretization for the Helmholtz problem

In the first section, we establish the relationship between the order of summability p of the coefficient sequences $\mathcal{C} = (c_j)_{j\geq 1}$, $\mathcal{S} = (s_j)_{j\geq 1}$ in (2.2.3) and the regularity of the solution to (3.2.4) for a single parameter realization. This information is then used in the second and third sections to obtain the convergence results for the fully discrete solution and linear output functionals as particular cases of the results of Chapter 5.

The whole analysis is carried out for the particle in free space case only.

6.1. Spatial regularity of the parametric solution

In Lemma 2.1.6 we have shown how the summability of the coefficient sequences $\mathcal{C} = (c_j)_{j\geq 1}$ and $\mathcal{S} = (s_j)_{j\geq 1}$ relates to the smoothness of the radius $r = r(\boldsymbol{y}, \varphi)$ given by (2.2.3), for every $J \in \mathbb{N}$ and every $\boldsymbol{y} \in \mathcal{P}_J$.

Furthermore, in Lemma 3.1.4, we have seen that the smoothness of the radius turns into smoothness of the mapping (3.1.2) for the particle in free space case.

Starting from these results, in this section we state how the summability of the coefficient sequences $\mathcal{C} = (c_j)_{j\geq 1}$ and $\mathcal{S} = (s_j)_{j\geq 1}$ turns in the end into smoothness of the solution to (3.2.4) for every parameter realization.

One may wonder why, since we have the finite dimensional noise assumption, we do not consider bounds in C^∞ spaces. The point is that such bounds would blow up to infinity as $J \to \infty$. In view of the convergence estimates, instead, we need norm bounds which are independent of the truncation parameter $J \in \mathbb{N}$ in the radius expansion.

The theorem implying smoothness of the solution to a PDE from the smoothness of the coefficients requires the latter to have essentially bounded derivatives. It turns out that the proper spaces in which to state regularity are the Sobolev spaces $W^{k,\infty}$ of functions with essentially bounded weak derivatives up to the kth-order. However, not to distinguish between weak and strong measurability of the coefficient maps $\omega \mapsto \hat{\alpha}(\omega)$, $\omega \mapsto \hat{\kappa}(\omega)$, and, thus, of the solution map $\omega \mapsto \hat{u}(\omega)$, we prefer to work in separable Banach spaces. For this reason, we state the regularity results in the spaces of piecewise-C^k functions with k finite.

From Lemma 2.1.6 and Lemma 3.1.4 it follows immediately:

Lemma 6.1.1. *Let Assumption 2.1.4.A hold and let the map $\Phi : \mathcal{P}_J \times K_R \to \mathcal{P}_J \times K_R$ satisfy Assumption 3.1.2.*

Then, for every $r(\boldsymbol{y})$ given by (2.2.3) and every $\boldsymbol{y} \in \mathcal{P}_J$, $J \in \mathbb{N}$, the coefficients $\hat{\alpha}$ and $\hat{\kappa}^2$ in (3.2.4) satisfy

$$\|\hat{\alpha}(\boldsymbol{y})\|_{C^{k-1}_{pw}(\overline{K_R})} \leq C_1(\mathcal{C}, \mathcal{S}), \quad \|\hat{\kappa}^2(\boldsymbol{y})\|_{C^{k-1}_{pw}(\overline{K_R})} \leq C_2(\mathcal{C}, \mathcal{S}),$$

with $\|\cdot\|_{C^{k-1}_{pw}(\overline{K_R})} = \|\cdot\|_{C^{k-1}(\overline{\hat{D}_1 \cap K_R}) \cup C^{k-1}(\overline{\hat{D}_2})}$, under the additional hypothesis (not needed if Assumption 2.1.4.B holds) that the nominal radius r_0 belongs to $C^k_{per}([0, 2\pi))$. The constants C_1 and

C_2 depend on the regularity parameter k and on the coefficient sequences $\mathcal{C} = (c_j)_{j\geq 1}$, $\mathcal{S} = (s_j)_{j\geq 1}$, but they are independent of the truncation parameter $J \in \mathbb{N}$ and of $\boldsymbol{y} \in \mathcal{P}_J$. The regularity parameter k is the same as in Lemma 2.1.6:

$$k = \begin{cases} \left\lfloor \frac{1}{p} - 1 \right\rfloor & \text{if } \frac{1}{p} - 1 \text{ is not an integer,} \\ \frac{1}{p} - 2 & \text{otherwise.} \end{cases}$$

Corollary 6.1.2. *Under Assumption 2.1.4.A, the result of Lemma 6.1.1 holds for the mapping 3.1.2 if the mollifier fulfills Assumption 3.1.3.*

We are now ready to state the result on the smoothness of the solution to (3.2.4). For this, we proceed in three steps: local interior regularity, local regularity at the interface $\hat{\Gamma}$ and at the boundary ∂K_R, and global regularity. We prove these regularity estimates in a more general framework, of which problem (3.2.4) is a particular case.

Consider the problem:

$$\begin{cases} \mathcal{L}(\boldsymbol{y})\hat{u}(\boldsymbol{y}) = \hat{f}(\boldsymbol{y}) & \text{in } \hat{D}_1 \cup \hat{D}_2, \quad (6.1.1a) \\ [\![\hat{u}(\boldsymbol{y})]\!]_{\hat{\Gamma}} = \hat{h}_1(\boldsymbol{y}),\ [\![\mathcal{B}_{\hat{\boldsymbol{n}}}\hat{u}(\boldsymbol{y})]\!]_{\hat{\Gamma}} = \hat{h}_2(\boldsymbol{y}), & \quad (6.1.1b) \\ \text{for every } \boldsymbol{y} \in \mathcal{P}_J \text{ and every } J \in \mathbb{N}, \end{cases}$$

to be considered in the weak sense, with $\hat{u} \in H^1(K_R \cap \hat{D}_1) \cup H^1(\hat{D}_2)$. The latter space is equipped with the norm $\|\cdot\|_{H^k(K_R\cap\hat{D}_1)\cup H^k(\hat{D}_2)} := \sqrt{\|\cdot\|^2_{H^k(K_R\cap\hat{D}_1)} + \|\cdot\|^2_{H^k(\hat{D}_2)}}$ for $k = 1$. The differential operator is given by

$$\mathcal{L}(\boldsymbol{y})\hat{u}(\boldsymbol{y}) = \hat{\nabla} \cdot (\hat{a}(\boldsymbol{y}, \hat{\boldsymbol{x}})\hat{\nabla}\hat{u}(\boldsymbol{y}) + \hat{b}(\boldsymbol{y}, \hat{\boldsymbol{x}})\hat{u}(\boldsymbol{y})) + \hat{c}(\boldsymbol{y}, \hat{\boldsymbol{x}}) \cdot \hat{\nabla}\hat{u}(\boldsymbol{y}) + \hat{d}(\boldsymbol{y}, \hat{\boldsymbol{x}})\hat{u}(\boldsymbol{y}), \tag{6.1.2}$$

with complex-valued, measurable coefficients $\hat{a} = (\hat{a}_{ij})$, $\hat{b} = (\hat{b}_i)$, $\hat{c} = (\hat{c}_i)$ and $\hat{d}$ $(i, j = 1, 2)$, and $\mathcal{B}_{\hat{\boldsymbol{n}}} = \hat{a}(\boldsymbol{y})\dfrac{\partial}{\partial \hat{\boldsymbol{n}}}$ ($\hat{\boldsymbol{n}}$ outer normal to $\hat{\Gamma}$).

We assume $\mathcal{L}$ to be *strongly elliptic* (as defined in [McL00, p. 122]), i.e.:

$$\mathrm{Re} \sum_{i=1}^{2}\sum_{j=1}^{2} \overline{\hat{a}_{ij}(\boldsymbol{y}, \hat{\boldsymbol{x}})\xi_j}\xi_i \geq a_-(\boldsymbol{y}) \left|\boldsymbol{\xi}\right|^2, \quad \text{for all } \hat{\boldsymbol{x}} \in K_R,\ J \in \mathbb{N},\ \boldsymbol{y} \in \mathcal{P}_J \text{ and } \boldsymbol{\xi} \in \mathbb{C}^2, \tag{6.1.3}$$

and we call $a_-(\boldsymbol{y})$ the *ellipticity constant* of $\mathcal{L}$.

If in (6.1.1) and (6.1.2) we set $\hat{a}(\boldsymbol{y}, \hat{\boldsymbol{x}}) = \hat{\alpha}(\boldsymbol{y}, \hat{x})$, $\hat{d}(\boldsymbol{y}, \hat{\boldsymbol{x}}) = \hat{\kappa}^2(\boldsymbol{y}, \hat{x})$ and $\hat{b} = \hat{c} \equiv \mathbf{0}$, $\hat{f} \equiv 0$, $\hat{h}_1 = \hat{h}_2 \equiv 0$, and add the radiation condition at infinity, we retrieve (1.0.1).

We highlight that the following proofs are developed for a two-dimensional domain, but, as it will become clear, they can be generalized to any dimension.

Throughout this subsection we adopt the notation $\hat{\partial}_j := \dfrac{\hat{\partial}}{\hat{\partial}\hat{x}_j}$, $j = 1, 2$.

The local interior regularity is a consequence of Theorem 8.10 in [GT01].

Theorem 6.1.3. *Let $\hat{u}(\boldsymbol{y}) \in H^1(K_R)$ be a weak solution to (6.1.1) in K_R, and $k \in \mathbb{N}$, $k \geq 2$. We assume that:*

- *$\mathcal{L}(\boldsymbol{y})$ is strictly elliptic in K_R, with a lower bound a_- on the ellipticity constant independent of the truncation parameter $J \in \mathbb{N}$ and of $\boldsymbol{y} \in \mathcal{P}_J$;*

- *the coefficients in* (6.1.2) *satisfy*

$$\begin{aligned} \sup_{\boldsymbol{y}\in\mathcal{P}_J, J\in\mathbb{N}} \|\hat{a}(\boldsymbol{y})\|_{C^{k-1}_{pw}(\overline{K_R})} \leq C_a, \quad \sup_{\boldsymbol{y}\in\mathcal{P}_J, J\in\mathbb{N}} \|\hat{b}(\boldsymbol{y})\|_{C^{k-1}_{pw}(\overline{K_R})} \leq C_b, \\ \sup_{\boldsymbol{y}\in\mathcal{P}_J, J\in\mathbb{N}} \|\hat{c}(\boldsymbol{y})\|_{C^{k-2}_{pw}(\overline{K_R})} \leq C_c, \quad \sup_{\boldsymbol{y}\in\mathcal{P}_J, J\in\mathbb{N}} \|\hat{d}(\boldsymbol{y})\|_{C^{k-2}_{pw}(\overline{K_R})} \leq C_d, \end{aligned} \tag{6.1.4}$$

  with $C^{k-1}_{pw}(\overline{K_R}) = C^{k-1}\left(\overline{K_R \cap \hat{D}_1}\right) \cup C^{k-1}\left(\overline{\hat{D}_2}\right)$ *and* $C^{k-2}_{pw}(\overline{K_R})$ *defined analogously;*

- *the right-hand side satisfies*

$$\sup_{\boldsymbol{y}\in\mathcal{P}_J, J\in\mathbb{N}} \|\hat{f}(\boldsymbol{y})\|_{H^{k-2}(K_R\cap\hat{D}_1)\cup H^{k-2}(\hat{D}_2)} \leq C_f. \tag{6.1.5}$$

The constants C_a, C_b, C_c, C_d *and* C_f *might depend on the regularity parameter* k*.*

Then, for every subdomain $\hat{D}' \subset K_R \cap \hat{D}_1$ *or* $\hat{D}' \subset \hat{D}_2$*, we have* $\hat{u}(\boldsymbol{y}) \in H^k(\hat{D}')$ *for every* $J \in \mathbb{N}$ *and every* $\boldsymbol{y} \in \mathcal{P}_J$*, and*

$$\|\hat{u}(\boldsymbol{y})\|_{H^k(\hat{D}')} \leq C\left(\|\hat{u}(\boldsymbol{y})\|_{H^1(K_R)} + C_f\right), \tag{6.1.6}$$

for $C = C(a_-, \mathcal{K}, d', k, |\hat{D}_1 \cap K_R|, |\hat{D}_2|)$*, where* $\mathcal{K} = \max\{C_a, C_b, C_c, C_d\}$*,* $|\hat{D}_1 \cap K_R|$ *and* $|\hat{D}_2|$ *denote the sizes of the two subdomains, and* $d' = \min\left\{\operatorname{dist}(\hat{D}', \partial K_R), \operatorname{dist}(\hat{D}', \hat{\Gamma})\right\}$*.*

Proof. Along the lines of the proofs of Theorems 8.8 and 8.10 in [GT01].

We consider the interior regularity inside $\hat{D}_2$. The argument for the regularity inside $\hat{D}_1 \cap K_R$ is the same.

We start proving the result for the case $k = 2$.

From (6.1.1a) we have that, for every $J \in \mathbb{N}$ and every $\boldsymbol{y} \in \mathcal{P}_J$,

$$\int_{\hat{D}_2} \hat{a}(\boldsymbol{y})\hat{\nabla}\hat{u}(\boldsymbol{y}) \cdot \hat{\nabla}\hat{v}\,\mathrm{d}\hat{\boldsymbol{x}} = \int_{\hat{D}_2} \hat{g}(\boldsymbol{y})\hat{v}\,\mathrm{d}\hat{\boldsymbol{x}}, \quad \text{for all } \hat{v} \in C^1_0(\hat{D}_2), \tag{6.1.7}$$

with $\hat{g}(\boldsymbol{y}) \in L^2(\hat{D}_2)$ given by

$$\hat{g}(\boldsymbol{y}) := (\hat{b}(\boldsymbol{y}) + \hat{c}(\boldsymbol{y})) \cdot \hat{\nabla}\hat{u}(\boldsymbol{y}) + (\hat{\nabla} \cdot \hat{b}(\boldsymbol{y}) + \hat{d}(\boldsymbol{y}))\hat{u}(\boldsymbol{y}) - \hat{f}(\boldsymbol{y}). \tag{6.1.8}$$

We now replace $\hat{v}$ by its difference quotient

$$\nabla_j^{-h}\hat{v} := \frac{\hat{v}(\boldsymbol{x} - h\boldsymbol{e}_j) - \hat{v}(\boldsymbol{x})}{-h},$$

for $j = 1, 2$ (with $(\boldsymbol{e}_j)_i = \delta_{ij}$), and choosing $h \in \mathbb{R}$ such that $|2h| < \operatorname{dist}(\operatorname{supp}\hat{v}, \hat{\Gamma})$. Then, adding and subtracting $\frac{1}{h}\int_{\hat{D}_2} \hat{a}(\boldsymbol{y}, \hat{\boldsymbol{x}} + h\boldsymbol{e}_j)\hat{\nabla}\hat{u}(\boldsymbol{y}, \hat{\boldsymbol{x}}+h\boldsymbol{e}_j) \cdot \hat{\nabla}\hat{v}(\hat{\boldsymbol{x}})\,\mathrm{d}\hat{\boldsymbol{x}}$, we obtain:

$$\int_{\hat{D}_2} \nabla_j^h(\hat{a}(\boldsymbol{y})\hat{\nabla}\hat{u}(\boldsymbol{y})) \cdot \hat{\nabla}\hat{v}\,\mathrm{d}\hat{\boldsymbol{x}} = -\int_{\hat{D}_2} \hat{a}(\boldsymbol{y})\hat{\nabla}\hat{u}(\boldsymbol{y}) \cdot \hat{\nabla}(\nabla_j^{-h}\hat{v})\,\mathrm{d}\hat{\boldsymbol{x}} = -\int_{\hat{D}_2} \hat{g}(\boldsymbol{y})\nabla_j^{-h}\hat{v}\,\mathrm{d}\hat{\boldsymbol{x}}.$$

Using the chain rule on $\nabla_j^h(\hat{a}(\boldsymbol{y})\hat{\nabla}\hat{u}(\boldsymbol{y}))$, we get

$$\int_{\hat{D}_2} \hat{a}(\hat{\boldsymbol{x}} + h\boldsymbol{e}_j, \boldsymbol{y})\hat{\nabla}(\nabla_j^h\hat{u}(\boldsymbol{y})) \cdot \hat{\nabla}\hat{v}\,\mathrm{d}\hat{\boldsymbol{x}} = -\int_{\hat{D}_2} \left(\overline{g}(\boldsymbol{y}) \cdot \hat{\nabla}\hat{v} + \hat{g}(\boldsymbol{y})\nabla_j^{-h}\hat{v}\right)\mathrm{d}\hat{\boldsymbol{x}},$$

with $\overline{g}(\boldsymbol{y}) := \nabla_j^h\hat{a}(\boldsymbol{y})\hat{\nabla}\hat{u}(\boldsymbol{y})$. Now, Lemma 7.23 in [GT01] ensures that, for every $\hat{D}' \subset\subset \hat{D}_2$ satisfying $h < \operatorname{dist}(\hat{D}', \hat{\Gamma})$ (where $\subset\subset$ denotes compact inclusion), $\|\nabla_j^h\hat{v}\|_{L^2(\hat{D}')} \leq \|\hat{\partial}_j\hat{v}\|_{L^2(\hat{D}_2)}$.

Applying the Cauchy-Schwarz inequality and this latter bound on the difference quotient, we obtain

$$\Big| \int_{\hat{D}_2} \hat{a}(\hat{\boldsymbol{x}} + h\boldsymbol{e}_j, \boldsymbol{y}) \hat{\nabla}(\nabla_j^h \hat{u}(\boldsymbol{y})) \cdot \hat{\nabla}\hat{v} \, \mathrm{d}\hat{\boldsymbol{x}} \Big| \leq \left(\|\overline{g}(\boldsymbol{y})\|_{L^2(\hat{D}_2)} + \|\hat{g}(\boldsymbol{y})\|_{L^2(\hat{D}_2)} \right) |\hat{v}|_{H^1(\hat{D}_2)}. \tag{6.1.9}$$

Thanks to the hypothesis of J- and $\boldsymbol{y}$-uniform bounds on the coefficients (and with again the help of Lemma 7.23 in [GT01] adapted to the L^∞-norm for the term involving the coefficient $\hat{a}$), we can get the following bounds on $\overline{g}(\boldsymbol{y})$ and $\hat{g}(\boldsymbol{y})$:

$$\|\overline{g}(\boldsymbol{y})\|_{L^2(\hat{D}_2)} \leq |\hat{D}_2| C_a \|\hat{u}(\boldsymbol{y})\|_{H^1(\hat{D}_2)}, \tag{6.1.10}$$

$$\|\hat{g}(\boldsymbol{y})\|_{L^2(\hat{D}_2)} \leq |\hat{D}_2| (C_b + C_c + C_d) \|\hat{u}(\boldsymbol{y})\|_{H^1(\hat{D}_2)} + C_f, \tag{6.1.11}$$

with the J- and $\boldsymbol{y}$-independent constants C_a, C_b, C_c, C_d and C_f defined in (6.1.4) and (6.1.5), for $k = 2$. Thus, (6.1.9) becomes:

$$\Big| \int_{\hat{D}_2} \hat{a}(\hat{\boldsymbol{x}} + h\boldsymbol{e}_j, \boldsymbol{y}) \hat{\nabla}(\nabla_j^h \hat{u}(\boldsymbol{y})) \cdot \hat{\nabla}\hat{v} \, \mathrm{d}\hat{\boldsymbol{x}} \Big| \leq \left(|\hat{D}_2| \mathcal{K} \|\hat{u}(\boldsymbol{y})\|_{H^1(\hat{D}_2)} + C_f \right) |\hat{v}|_{H^1(\hat{D}_2)},$$

with $\mathcal{K}$ as defined in the theorem statement.

In order to get the local estimate, we consider a cut-off function $\eta \in C_0^1(\hat{D}_2)$, $0 \leq \eta \leq 1$, and take as test function $\hat{v}(\boldsymbol{y}) = \eta^2 \nabla_j^h \hat{u}(\boldsymbol{y})$. Then, using the J- and $\boldsymbol{y}$-uniform ellipticity assumption and the Cauchy-Schwarz inequality, we obtain:

$$\begin{aligned}
&a_- \int_{\hat{D}_2} |\eta \hat{\nabla}(\nabla_j^h \hat{u}(\boldsymbol{y}))|^2 \, \mathrm{d}\hat{\boldsymbol{x}} \\
&\leq \int_{\hat{D}_2} \eta^2 \hat{a}(\hat{\boldsymbol{x}} + h\boldsymbol{e}_j, \boldsymbol{y}) \hat{\nabla}(\nabla_j^h \hat{u}(\boldsymbol{y})) \cdot \hat{\nabla}(\nabla_j^h \hat{u}(\boldsymbol{y})) \, \mathrm{d}\hat{\boldsymbol{x}} \\
&= \int_{\hat{D}_2} \hat{a}(\hat{\boldsymbol{x}} + h\boldsymbol{e}_j, \boldsymbol{y}) \hat{\nabla}(\nabla_j^h \hat{u}(\boldsymbol{y})) \cdot \left(\hat{\nabla}\hat{v}(\boldsymbol{y}) - 2\eta \nabla_j^h \hat{u}(\boldsymbol{y}) \hat{\nabla}\eta \right) \mathrm{d}\hat{\boldsymbol{x}} \\
&\leq \left(|\hat{D}_2| \mathcal{K} \|\hat{u}(\boldsymbol{y})\|_{H^1(\hat{D}_2)} + C_f \right) \left(\|\eta \hat{\nabla}(\nabla_j^h \hat{u}(\boldsymbol{y}))\|_{L^2(\hat{D}_2)} + 2\|\nabla_j^h \hat{u}(\boldsymbol{y}) \hat{\nabla}\eta\|_{L^2(\hat{D}_2)} \right) \\
&+ 2|\hat{D}_2| \mathcal{K} \|\eta \hat{\nabla}(\nabla_j^h \hat{u}(\boldsymbol{y}))\|_{L^2(\hat{D}_2)} \|\nabla_j^h \hat{u}(\boldsymbol{y}) \hat{\nabla}\eta\|_{L^2(\hat{D}_2)}.
\end{aligned} \tag{6.1.12}$$

We apply Young's inequality [GT01, Eqn. (7.6)] to both addends on the right-hand side, choosing the same $\varepsilon > 0$ for both of them. In this way, we get

$$\begin{aligned}
\left(a_- - \frac{3}{2}\varepsilon \right) \|\eta \hat{\nabla}(\nabla_j^h \hat{u}(\boldsymbol{y}))\|_{L^2(\hat{D}_2)}^2 \leq \Bigg(&\frac{1}{\sqrt{2\varepsilon}} \left(|\hat{D}_2| \mathcal{K} \|\hat{u}(\boldsymbol{y})\|_{H^1(\hat{D}_2)} + C_f + |\hat{D}_2| \mathcal{K} \|\nabla_j^h \hat{u}(\boldsymbol{y}) \hat{\nabla}\eta\|_{L^2(\hat{D}_2)} \right) \\
&+ 2\sqrt{\varepsilon} \|\nabla_j^h \hat{u}(\boldsymbol{y}) \hat{\nabla}\eta\|_{L^2(\hat{D}_2)} \Bigg)^2.
\end{aligned}$$

Thus we can choose $\varepsilon < \frac{2}{3} a_-$, independent of J and of $\boldsymbol{y} \in \mathcal{P}_J$ because a_- is, obtaining

$$\begin{aligned}
\|\eta \hat{\nabla}(\nabla_j^h \hat{u}(\boldsymbol{y}))\|_{L^2(\hat{D}_2)} &\leq C(a_-, \mathcal{K}, |\hat{D}_2|) \left(\|\hat{u}(\boldsymbol{y})\|_{H^1(\hat{D}_2)} + C_f + \|\nabla_j^h \hat{u}(\boldsymbol{y}) \hat{\nabla}\eta\|_{L^2(\hat{D}_2)} \right) \\
&\leq C(a_-, \mathcal{K}, |\hat{D}_2|)(1 + \|\hat{\nabla}\eta\|_{L^\infty(\hat{D}_2)}) \left(\|\hat{u}(\boldsymbol{y})\|_{H^1(\hat{D}_2)} + C_f \right),
\end{aligned} \tag{6.1.13}$$

where for the last inequality we have used again Lemma 7.23 in [GT01]. We now choose the cut-off function such that $\eta = 1$ on $\hat{D}' \subset \hat{D}_2$ and $\|\hat{\nabla}\eta\|_{L^\infty(\hat{D}_2)} \leq \frac{2}{d'}$, where $d' = \operatorname{dist}(\hat{\Gamma}, \hat{D}') > 0$. Applying Lemma 7.24 in [GT01], we conclude that $\hat{\nabla}\hat{u}(\boldsymbol{y}) \in H^1(\hat{D}')$, and thus $\hat{u}(\boldsymbol{y}) \in H^2(\hat{D}')$ for every $J \in \mathbb{N}$ and every $\boldsymbol{y} \in \mathcal{P}_J$, with

$$\|\hat{u}(\boldsymbol{y})\|_{H^2(\hat{D}')} \leq \bar{C}(a_-, \mathcal{K}, |\hat{D}_2|) \left(\|\hat{u}(\boldsymbol{y})\|_{H^1(\hat{D}_2)} + C_f \right).$$

Repeating the same argument for $\hat{D}' \subset \hat{D}_1 \cap K_R$, we obtain the desired result for $k = 2$.

If the bounds (6.1.4) hold for $k = 3$, then, replacing $\hat{v}$ by $\hat{\partial}_j \hat{v}$, $j = 1, 2$, in (6.1.7), integrating by parts and applying the product rule, we obtain

$$\int_{\hat{D}_2} \hat{a}(\boldsymbol{y}) \hat{\nabla} \hat{\partial}_j \hat{u}(\boldsymbol{y}) \cdot \hat{\nabla} \hat{v} \, \mathrm{d}\hat{\boldsymbol{x}} = \int_{\hat{D}_2} \hat{\partial}_j \tilde{g}(\boldsymbol{y}) \hat{v} \, \mathrm{d}\hat{\boldsymbol{x}}, \quad \text{for all } v \in C_0^1(\hat{D}_2),$$

with

$$\tilde{g}(\boldsymbol{y}) := \hat{g}(\boldsymbol{y}) + \hat{\nabla} \cdot (\hat{a}(\boldsymbol{y}) \hat{\nabla} \hat{u}(\boldsymbol{y})). \tag{6.1.14}$$

Since $\hat{u}(\boldsymbol{y}) \in H^2(\hat{D}_2)$, we have $\hat{\partial}_j \tilde{g} \in L^2(\hat{D}_2)$. Proceeding as we did in (6.1.10)-(6.1.11), using the bound we already have for the H^2-norm of $\hat{u}$ we can bound $\|\hat{\partial}_j \tilde{g}(\boldsymbol{y})\|_{L^2(\hat{D}_2)}$ in terms of the constants C_a, C_b, C_c, C_d, C_f (with $k = 3$) and $\|\hat{u}(\boldsymbol{y})\|_{H^1(\hat{D}_2)}$. Doing the same on $\hat{D}_1 \cap K_R$, we obtain (6.1.6) for $k = 3$.

By induction we get then (6.1.6) for a general $k \geq 2$. □

From this theorem, using the regularity results obtained so far in this section together with Lemma 3.2.5 and the bound (4.3.10), which followed from Corollary 3.2.6, we infer the interior regularity result for our problem:

Corollary 6.1.4. *Let Assumptions 2.1.3, 2.1.4.A and 3.1.2 hold and let the nominal radius r_0 belong to $C^k_{per}([0, 2\pi))$, with k as in Lemma 2.1.6. If $k \geq 2$, then, for any subdomain $\hat{D}' \subset K_R \cap \hat{D}_1$ or $\hat{D}' \subset \hat{D}_2$, the solution $\hat{u}(\boldsymbol{y})$ to (3.2.4) belongs to $H^k(\hat{D}')$ and satisfies (6.1.6).*

Here $C_a = \sup_{\boldsymbol{y} \in \mathcal{P}_J, J \in \mathbb{N}} \|\hat{\alpha}(\boldsymbol{y})\|_{C^{k-1}_{pw}(\overline{\hat{K}_R})}$, $C_b = C_c = 0$, $C_d = \sup_{\boldsymbol{y} \in \mathcal{P}_J, J \in \mathbb{N}} \|\hat{\kappa}^2(\boldsymbol{y})\|_{C^{k-2}_{pw}(\overline{\hat{K}_R})}$ and $C_f = 0$; the uniform ellipticity constant is given by $a_- = \min\{1, \alpha_2\} \frac{\sigma^2_{min}}{\sigma^2_{max}}$ (with σ_{min} and σ_{max} as in Assumption 3.1.2).

Furthermore, if Assumption 3.2.4 holds, then we have a J- and $\boldsymbol{y}$-independent bound:

$$\|\hat{u}(\boldsymbol{y})\|_{H^k(\hat{D}')} \leq \tilde{C} \left(\|u_i\|_{H^{\frac{1}{2}}(\partial K_R)} + \left\| \frac{\partial u_i}{\partial \boldsymbol{n}_R} \right\|_{H^{-\frac{1}{2}}(\partial K_R)} \right),$$

with $\tilde{C} = \tilde{C}(R, a_-, \gamma, \mathcal{K}, d', k, |\hat{D}_1 \cap K_R|, |\hat{D}_2|)$, and γ denotes the uniform coercivity constant as in Lemma 3.2.5, depending on the lower and upper singular value bounds $\sigma_{min}, \sigma_{max}$ for $D\Phi^{-1}(\boldsymbol{y})$ as from Assumption 3.1.2.

The local regularity at the interface $\hat{\Gamma}$ follows from Theorem 4.20 in [McL00].

Theorem 6.1.5. *Let $\hat{u}(\boldsymbol{y}) \in H^1(\hat{D}_1) \cup H^1(K_R \cap \hat{D}_2)$, let the jumps across $\hat{\Gamma}$ satisfy*

$$\sup_{\boldsymbol{y} \in \mathcal{P}_J, J \in \mathbb{N}} \|\hat{h}_1(\boldsymbol{y})\|_{H^{k-1/2}(\hat{\Gamma})} \leq C_{h_1}, \qquad \sup_{\boldsymbol{y} \in \mathcal{P}_J, J \in \mathbb{N}} \|\hat{h}_2(\boldsymbol{y})\|_{H^{k-3/2}(\hat{\Gamma})} \leq C_{h_2},$$

for $k \geq 2$, and let assumptions of Theorem 6.1.3 be fulfilled. Furthermore, suppose that $\hat{\Gamma}$ is $C^{k-1,1}$.

Then, for every subdomain $\hat{D}' \subset K_R$ intersecting $\hat{\Gamma}$, $\hat{u}(\boldsymbol{y}) \in H^k(\hat{D}' \cap \hat{D}_1) \cup H^k(\hat{D}' \cap \hat{D}_2)$, and

$$\|\hat{u}(\boldsymbol{y})\|_{H^k(\hat{D}' \cap \hat{D}_1) \cup H^k(\hat{D}' \cap \hat{D}_2)} \leq C(\|\hat{u}(\boldsymbol{y})\|_{H^1(K_R \cap \hat{D}_1) \cup H^1(\hat{D}_2)} + C_f + C_{h_1} + C_{h_2}), \tag{6.1.15}$$

for $C = C(a_-, \mathcal{K}, d', k, |K_R|)$, with $d' = \operatorname{dist}(\hat{D}', \partial K_R)$ and the other constants defined as in Theorem 6.1.3.

Proof. We follow the proof of Theorem 4.20 in [McL00].

Again, we first prove the result for $k = 2$.

Since $\hat{\Gamma}$ is of class $C^{k-1,1}$, we can assume $K_R \cap \hat{D}_1$ to be the half-space $\hat{x}_2 > 0$ after a local $C^{k-1,1}$ change of coordinates.

We start considering the case when $\hat{h}_1(\boldsymbol{y}) \equiv 0$ (for all $\boldsymbol{y} \in \mathcal{P}_J$ and all $J \in \mathbb{N}$), so that $\hat{u}(\boldsymbol{y}) \in H^1(K_R)$. Then, the variational formulation on K_R reads

$$\int_{K_R} \hat{a}(\boldsymbol{y})\hat{\nabla}\hat{u}(\boldsymbol{y}) \cdot \hat{\nabla}\hat{v}\,\mathrm{d}\hat{\boldsymbol{x}} = \int_{K_R} \hat{g}(\boldsymbol{y})\hat{v}\,\mathrm{d}\hat{\boldsymbol{x}} + \int_{\hat{\Gamma}} \hat{h}_2(\boldsymbol{y})\tau_{\hat{\Gamma}}\hat{v}\,\mathrm{d}S, \quad \text{for all } \hat{v} \in C_0^1(K_R), \tag{6.1.16}$$

with $\tau_{\hat{\Gamma}} : L^2(\hat{D}_2) \to H^{-1/2}(\hat{\Gamma})$ the trace operator and $\hat{g}(\boldsymbol{y}) \in L^2(K_R)$ given by

$$\hat{g}(\boldsymbol{y}) := (\hat{b}(\boldsymbol{y}) + \hat{c}(\boldsymbol{y})) \cdot \hat{\nabla}\hat{u}(\boldsymbol{y}) + (\hat{\nabla} \cdot \hat{b}(\boldsymbol{y}) + \hat{d}(\boldsymbol{y}))\hat{u}(\boldsymbol{y}) - \hat{f}(\boldsymbol{y}).$$

Thus, we are in the same framework as in the interior regularity case, with an additional boundary term.

Replacing again $\hat{v}$ by the difference quotient $\nabla_j^{-h}\hat{v}$, $j = 1, 2$, and proceeding as for (6.1.12), we obtain:

$$\begin{aligned}
&a_- \int_{K_R} |\eta\hat{\nabla}(\nabla_j^h \hat{u}(\boldsymbol{y}))|^2\,\mathrm{d}\hat{\boldsymbol{x}} \\
&\le \left(|K_R|\mathcal{K}\|\hat{u}(\boldsymbol{y})\|_{H^1(K_R)} + C_f\right)\left(\|\eta\hat{\nabla}(\nabla_j^h\hat{u}(\boldsymbol{y}))\|_{L^2(K_R)} + 2\|\nabla_j^h\hat{u}(\boldsymbol{y})\hat{\nabla}\eta\|_{L^2(K_R)}\right) \\
&+ 2|K_R|\mathcal{K}\|\eta\hat{\nabla}(\nabla_j^h\hat{u}(\boldsymbol{y}))\|_{L^2(K_R)}\|\nabla_j^h\hat{u}(\boldsymbol{y})\hat{\nabla}\eta\|_{L^2(K_R)} + |\langle\hat{h}_2(\boldsymbol{y}), \tau_{\hat{\Gamma}}\nabla_j^{-h}(\eta^2\nabla_j^h\hat{u}(\boldsymbol{y}))\rangle|,
\end{aligned}$$

where $\langle\cdot,\cdot\rangle$ in the last term denotes the duality pairing between $H^{-\frac{1}{2}}$ and $H^{\frac{1}{2}}$.

For the tangential difference quotients, i.e. for $j = 1$, $\nabla_j^h\hat{u}(\boldsymbol{y}) \in H^1(K_R)$ because $\hat{u}(\boldsymbol{y})$ does; hence, we can estimate the boundary term:

$$\begin{aligned}
|\langle\hat{h}_2(\boldsymbol{y}), \tau_{\hat{\Gamma}}\nabla_j^{-h}(\eta^2\nabla_j^h\hat{u}(\boldsymbol{y}))\rangle| &\le \|\hat{h}_2(\boldsymbol{y})\|_{H^{1/2}(\hat{\Gamma})}\|\tau_{\hat{\Gamma}}\nabla_j^{-h}(\eta^2\nabla_j^h\hat{u}(\boldsymbol{y}))\|_{H^{-1/2}(\hat{\Gamma})} \\
&\le C_\tau C_{h_2}\|\nabla_j^{-h}(\eta^2\nabla_j^h\hat{u}(\boldsymbol{y}))\|_{L^2(K_R)} \\
&\le C_\tau C_{h_2}\|\hat{\nabla}(\eta^2\nabla_j^h\hat{u}(\boldsymbol{y}))\|_{L^2(K_R)} \\
&\le C_\tau C_{h_2}\left(\|\eta\hat{\nabla}(\nabla_j^h\hat{u}(\boldsymbol{y}))\|_{L^2(K_R)} + 2\|\nabla_j^h\hat{u}(\boldsymbol{y})\hat{\nabla}\eta\|_{L^2(K_R)}\right),
\end{aligned}$$

where in the second step we have used the continuity of the trace operator with constant C_τ (independent of $J \in \mathbb{N}$ and $\boldsymbol{y} \in \mathcal{P}_J$) and the bound on $\hat{h}_2(\boldsymbol{y})$, and in the third step we have used Lemma 7.23 in [GT01] (with $p = 2$). Then, (6.1.16) becomes:

$$\begin{aligned}
&a_- \int_{K_R} |\eta\hat{\nabla}(\nabla_j^h \hat{u}(\boldsymbol{y}))|^2\,\mathrm{d}\hat{\boldsymbol{x}} \\
&\le \left(|K_R|\mathcal{K}\|\hat{u}(\boldsymbol{y})\|_{H^1(K_R)} + C_f + C_\tau C_{h_2}\right)\left(\|\eta\hat{\nabla}(\nabla_j^h\hat{u}(\boldsymbol{y}))\|_{L^2(K_R)} + 2\|\nabla_j^h\hat{u}(\boldsymbol{y})\hat{\nabla}\eta\|_{L^2(K_R)}\right) \\
&+ 2|K_R|\mathcal{K}\|\eta\hat{\nabla}(\nabla_j^h\hat{u}(\boldsymbol{y}))\|_{L^2(K_R)}\|\nabla_j^h\hat{u}(\boldsymbol{y})\hat{\nabla}\eta\|_{L^2(K_R)}.
\end{aligned}$$

Applying Young's inequality, with the same steps leading to (6.1.13), we obtain:

$$\|\eta\hat{\nabla}(\nabla_j^h\hat{u}(\boldsymbol{y}))\|_{L^2(K_R)} \le C(a_-, \mathcal{K}, |K_R|)(1 + \|\hat{\nabla}\eta\|_{L^\infty(K_R)})\left(\|\hat{u}(\boldsymbol{y})\|_{H^1(K_R)} + C_f + C_{h_2}\right).$$

Choosing the cut-off function η such that $\eta = 1$ on $\hat{D}'$ and $\|\hat{\nabla}\eta\|_{L^\infty(K_R)} \le \frac{2}{d'}$, where $d' = \mathrm{dist}(\hat{D}', \partial K_R)$, and applying Lemma 7.24 in [GT01], we obtain

$$\left\|\frac{\hat{\partial}}{\hat{\partial}\hat{x}_j}\hat{u}(\boldsymbol{y})\right\|_{H^1(\hat{D}')} \le \tilde{C}(a_-, \mathcal{K}, |K_R|)\left(\|\hat{u}(\boldsymbol{y})\|_{H^1(K_R)} + C_f + C_{h_2}\right).$$

For the normal derivative to $\hat{\Gamma}$, i.e. for $j = 2$, in general $\dfrac{\hat{\partial}}{\hat{\partial}\hat{x}_2}\hat{u}(\boldsymbol{y}) \notin H^1(K_R)$, because it is discontinuous across $\hat{\Gamma}$; thus, we cannot apply Lemma 7.23 in [GT01]. However, it holds:

$$-\hat{a}_{22}(\boldsymbol{y})\frac{\hat{\partial}^2}{\hat{\partial}\hat{x}_2^2}\hat{u}(\boldsymbol{y}) = \tilde{f}(\boldsymbol{y}) \quad \text{in } \hat{D}', \tag{6.1.17}$$

with $|\hat{a}_{22}(\boldsymbol{y})| \geq a_-$ and

$$\begin{aligned}\|\tilde{f}(\boldsymbol{y})\|_{L^2(\hat{D}'\cap\hat{D}_1)\cup L^2(\hat{D}'\cap\hat{D}_2)} &\leq C_f + C_a\|\hat{u}(\boldsymbol{y})\|_{H^1(\hat{D}')} + C_a\Big\|\frac{\hat{\partial}}{\hat{\partial}\hat{x}_1}\hat{u}(\boldsymbol{y})\Big\|_{H^1(\hat{D}')}\\ &\quad + C_c\|\hat{u}(\boldsymbol{y})\|_{H^1(\hat{D}')} + C_d\|\hat{u}(\boldsymbol{y})\|_{L^2(\hat{D}')}\\ &\leq C_f + \mathcal{K}\|\hat{u}(\boldsymbol{y})\|_{H^1(\hat{D}')} + C_a\Big\|\frac{\hat{\partial}}{\hat{\partial}\hat{x}_1}\hat{u}(\boldsymbol{y})\Big\|_{H^1(\hat{D}')}.\end{aligned}$$

Hence, $\hat{u}(\boldsymbol{y}) \in H^2(\hat{D}'\cap\hat{D}_1) \cup H^2(\hat{D}'\cap\hat{D}_2)$ with J- and $\boldsymbol{y}$-independent norm bound and (6.1.15) holds for $\hat{h}_1 \equiv 0$ and $k = 2$.

In the case of nonzero Dirichlet jump, i.e. when $\hat{h}_1(\boldsymbol{y}) \neq 0$, we consider an extension operator η_0 (see Lemma 3.36 in [McL00]) to construct $\hat{w}(\boldsymbol{y}) = \eta_0(\hat{h}_1(\boldsymbol{y})) \in H^2(K_R)$ satisfying

$$\tau_{\hat{\Gamma}}\hat{w}(\boldsymbol{y}) = \hat{h}_1(\boldsymbol{y}) \quad \text{and} \quad \|\mathcal{B}_{\hat{\boldsymbol{n}}}\hat{w}(\boldsymbol{y})\|_{H^{1/2}(\hat{\Gamma})} + \|\hat{w}(\boldsymbol{y})\|_{H^2(K_R)} \leq C(\eta_0)\|\hat{h}_1(\boldsymbol{y})\|_{H^{3/2}(\hat{\Gamma})},$$

where the constant $C(\eta_0)$ is independent of J and of $\boldsymbol{y} \in \mathcal{P}_J$. Consider now the function

$$\hat{u}_1(\boldsymbol{y}) = \begin{cases}\hat{u}(\boldsymbol{y}) & \text{on } K_R\cap\hat{D}_1,\\ \hat{u}(\boldsymbol{y}) + \hat{w}(\boldsymbol{y}) & \text{on } \hat{D}_2.\end{cases}$$

It holds

$$\mathcal{L}(\boldsymbol{y})\hat{u}_1(\boldsymbol{y}) = \begin{cases}\hat{f}(\boldsymbol{y}) & \text{on } K_R\cap\hat{D}_1,\\ \hat{f}(\boldsymbol{y}) + \mathcal{L}(\boldsymbol{y})\hat{w}(\boldsymbol{y}) & \text{on } \hat{D}_2,\end{cases}$$

with $[\![\hat{u}_1(\boldsymbol{y})]\!]_{\hat{\Gamma}} = 0$ and $[\![\mathcal{B}_{\hat{\boldsymbol{n}}}\hat{u}_1(\boldsymbol{y})]\!]_{\hat{\Gamma}} = \hat{h}_2(\boldsymbol{y}) - \mathcal{B}_{\hat{\boldsymbol{n}}}\hat{w}(\boldsymbol{y}) \in H^{1/2}(\hat{\Gamma})$. Then, the previous argument for zero Dirichlet jump applies, showing that $\hat{u}_1(\boldsymbol{y}) \in H^2(\hat{D}'\cap\hat{D}_1) \cup H^2(\hat{D}'\cap\hat{D}_2)$, with J- and $\boldsymbol{y}$-independent norm bound. Since $\hat{w}(\boldsymbol{y}) \in H^2(K_R)$, this implies that $\hat{u}(\boldsymbol{y}) \in H^2(\hat{D}'\cap\hat{D}_1) \cup H^2(\hat{D}'\cap\hat{D}_2)$ and

$$\begin{aligned}\|\hat{u}(\boldsymbol{y})\|_{H^2(\hat{D}'\cap\hat{D}_1)\cup H^2(\hat{D}'\cap\hat{D}_2)} &\leq \|\hat{u}_1(\boldsymbol{y})\|_{H^2(\hat{D}'\cap\hat{D}_1)\cup H^2(\hat{D}'\cap\hat{D}_2)} + \|\hat{w}(\boldsymbol{y})\|_{H^2(\hat{D}'\cap\hat{D}_2)}\\ &\leq C\Big(\|\hat{u}_1(\boldsymbol{y})\|_{H^1(K_R)} + \|\hat{h}_2(\boldsymbol{y}) - \mathcal{B}_{\hat{\boldsymbol{n}}}\hat{w}(\boldsymbol{y})\|_{H^{1/2}(\hat{\Gamma})}\\ &\quad + \|\hat{f}(\boldsymbol{y})\|_{L^2(\hat{D}'\cap\hat{D}_1)} + \|\hat{f}(\boldsymbol{y}) + \mathcal{L}(\boldsymbol{y})\hat{w}(\boldsymbol{y})\|_{L^2(\hat{D}'\cap\hat{D}_2)}\Big)\\ &\quad + \|\hat{w}(\boldsymbol{y})\|_{H^2(\hat{D}'\cap\hat{D}_2)},\end{aligned}$$

with $C = C(a_-, \mathcal{K}, |K_R|)$ independent of J and of $\boldsymbol{y} \in \mathcal{P}_J$. Furthermore, we have that

$$\begin{aligned}\|\hat{u}_1(\boldsymbol{y})\|_{H^1(K_R)} &\leq \|\hat{u}(\boldsymbol{y})\|_{H^1(K_R\cap\hat{D}_1)\cup H^1(K_R\cap\hat{D}_2)} + \|\hat{w}(\boldsymbol{y})\|_{H^1(K_R)}\\ &\leq \|\hat{u}(\boldsymbol{y})\|_{H^1(K_R\cap\hat{D}_1)\cup H^1(K_R\cap\hat{D}_2)} + C(\eta_0)C_{h_1},\\ \|\hat{h}_2(\boldsymbol{y}) - \mathcal{B}_{\hat{\boldsymbol{n}}}\hat{w}(\boldsymbol{y})\|_{H^{1/2}(\hat{\Gamma})} &\leq C_{h_2} + C(\eta_0)C_{h_1},\end{aligned}$$

and

$$\begin{aligned}&\|\hat{f}(\boldsymbol{y})\|_{L^2(\hat{D}'\cap\hat{D}_1)} + \|\hat{f}(\boldsymbol{y}) + \mathcal{L}(\boldsymbol{y})\hat{w}(\boldsymbol{y})\|_{L^2(\hat{D}'\cap\hat{D}_2)} + \|\hat{w}(\boldsymbol{y})\|_{H^2(\hat{D}'\cap\hat{D}_2)}\\ &\leq C_f + \|\mathcal{L}(\boldsymbol{y})\hat{w}(\boldsymbol{y})\|_{L^2(\hat{D}'\cap\hat{D}_2)} + \|\hat{w}(\boldsymbol{y})\|_{H^2(\hat{D}'\cap\hat{D}_2)}\\ &\leq C_f + (\mathcal{K}+1)\|\hat{w}(\boldsymbol{y})\|_{H^2(\hat{D}'\cap\hat{D}_2)}\\ &\leq C_f + (\mathcal{K}+1)C(\eta_0)C_{h_1}.\end{aligned}$$

Hence, the desired J- and $\boldsymbol{y}$-independent estimate for $k = 2$ holds also for the case of nonzero Dirichlet jump across $\hat{\Gamma}$.

For $k = 3$ and zero Dirichlet jump, we distinguish again between tangential and normal derivatives.

For the derivatives in direction tangential to $\hat{\Gamma}$ ($j = 1$), we can proceed as for the interior regularity, replacing $\hat{v}$ by $\hat{\partial}_j \hat{v}$, and obtaining, after integration by parts:

$$\int_{K_R} \hat{a}(\boldsymbol{y}) \hat{\nabla} \hat{\partial}_j \hat{u}(\boldsymbol{y}) \cdot \hat{\nabla} \hat{v} \, \mathrm{d}\hat{\boldsymbol{x}} = \int_{K_R} \hat{\partial}_j \tilde{g}(\boldsymbol{y}) \hat{v} \, \mathrm{d}\hat{\boldsymbol{x}} + \int_{\hat{\Gamma}} \hat{\partial}_j \hat{h}_2(\boldsymbol{y}) \tau_{\hat{\Gamma}} \hat{v} \, \mathrm{d}S, \quad \text{for all } \hat{v} \in C_0^1(K_R),$$

with $\tilde{g}$ as in (6.1.14). Then we are in the same framework as in (6.1.16) and we can repeat the argument.

For the normal derivative, differentiating (6.1.17) with respect to $\hat{x}_2$, we get:

$$-\hat{a}_{22}(\boldsymbol{y}) \frac{\hat{\partial}^3}{\hat{\partial} \hat{x}_2^3} \hat{u}(\boldsymbol{y}) = \tilde{f}_2(\boldsymbol{y}) \quad \text{in } \hat{D}',$$

with $\tilde{f}_2(\boldsymbol{y}) := \dfrac{\hat{\partial}}{\hat{\partial} \hat{x}_2} \tilde{f}(\boldsymbol{y}) + \dfrac{\hat{\partial} \hat{a}_{22}}{\hat{\partial} \hat{x}_2}(\boldsymbol{y}) \dfrac{\hat{\partial}^2}{\hat{\partial} \hat{x}_2^2} \hat{u}(\boldsymbol{y})$; then, we can repeat the same reasoning as for $k = 2$.

For nonzero Dirichlet jump across the interface, the result follows as for $k = 2$.

Iterating, (6.1.15) is proved for every $k \geq 2$. □

Applying the latter theorem to our case, we obtain:

Corollary 6.1.6. *Let Assumptions 2.1.3, 2.1.4.A and 3.1.2 hold and let the nominal radius r_0 belong to $C^k_{per}([0, 2\pi))$, with k as in Lemma 2.1.6. Moreover, let the interfaces $\hat{\Gamma}$ and ∂K_R be $C^{k-1,1}$. If k as in Lemma 2.1.6 is such that $k \geq 2$ (which automatically holds if Assumption 2.1.4.B is satisfied), then:*

- *for any subdomain $\hat{D}' \subsetneq K_R$ intersecting $\hat{\Gamma}$ (but not ∂K_R) we have that the solution $\hat{u}(\boldsymbol{y})$ to (3.2.4) satisfies (6.1.15) with $C_f = C_{h_1} = C_{h_2} = 0$ and C_a, C_b, C_c, C_d as in Corollary 6.1.4.*
- *for any open set $\hat{D}'$ intersecting ∂K_R (but not $\hat{\Gamma}$) we have that the solution $\hat{u}(\boldsymbol{y})$ to (3.2.4) satisfies*

$$\begin{aligned} \|\hat{u}(\boldsymbol{y})\|_{H^k(\hat{D}' \cap K_R) \cup H^k(\hat{D}' \setminus K_R)} &\leq C \left(\|\hat{u}(\boldsymbol{y})\|_{H^1(\hat{D}' \cap K_R)} + \|\hat{u}(\boldsymbol{y}) - u_i\|_{H^1(\hat{D}' \setminus K_R)} \right) \\ &\quad + C \left(\|u_i\|_{H^{k-\frac{1}{2}}(\partial K_R)} + \left\| \frac{\partial u_i}{\partial \boldsymbol{n}_R} \right\|_{H^{k-\frac{3}{2}}(\partial K_R)} \right), \end{aligned} \tag{6.1.18}$$

with $C = C(a_-, \mathcal{K}, d', k, |K_{R'}|)$ with $d' = \operatorname{dist}(\hat{D}', \partial K_{R'})$, with $K_{R'}$ a circle of radius $R' > R$ containing $\hat{D}'$ in its interior, and the other constants defined as in Theorem 6.1.3 (where C_a, C_b, C_c, C_d are as in Corollary 6.1.4).

Furthermore, if Assumption 3.2.4 holds in K_R and in $K_{R'}$, then in both cases we have bounds on the norms which are independent of the truncation parameter $J \in \mathbb{N}$ and of $\boldsymbol{y} \in \mathcal{P}_J$:

$$\|\hat{u}(\boldsymbol{y})\|_{H^k(\hat{D}' \cap \hat{D}_1)} + \|\hat{u}(\boldsymbol{y})\|_{H^k(\hat{D}' \cap \hat{D}_2)} \leq \tilde{C}_1 \left(\|u_i\|_{H^{\frac{1}{2}}(\partial K_R)} + \left\| \frac{\partial u_i}{\partial \boldsymbol{n}_R} \right\|_{H^{-\frac{1}{2}}(\partial K_R)} \right),$$

$$\|\hat{u}(\boldsymbol{y})\|_{H^k(\hat{D}' \cap K_R)} + \|\hat{u}(\boldsymbol{y}) - u_i\|_{H^k(\hat{D}' \setminus K_R)} \leq \tilde{C}_2 \left(\|u_i\|_{H^{k-\frac{1}{2}}(\partial K_R)} + \left\| \frac{\partial u_i}{\partial \boldsymbol{n}_R} \right\|_{H^{k-\frac{3}{2}}(\partial K_R)} \right),$$

where the constants $\tilde{C}_1$ and $\tilde{C}_2$ depend on the same parameters as C in (6.1.18) *and of B_1, B_2 in Corollary 3.2.6.*

Here, ∂K_R has been treated as an interface because Assumption 3.1.2 allows the mapping Φ and its inverse to be nonsmooth across ∂K_R (and thus also the coefficients $\hat{\alpha}$ and $\hat{\kappa}^2$ may be nonsmooth). Also, consistently with (3.2.4), we have considered the total field $\hat{u}$ inside K_R and the scattered field $\hat{u} - u_i$ outside, so that across ∂K_R we have applied (6.1.15) with $\hat{h}_1 = u_i$ and $\hat{h}_2 = \dfrac{\partial u_i}{\partial \boldsymbol{n}_R}$.

Considering Corollaries 6.1.4 and 6.1.6 together we get the following global result:

Theorem 6.1.7. *Let Assumptions 2.1.3 and 2.1.4.A hold and let the nominal radius r_0 belong to $C^k_{per}([0,2\pi))$, with k as in Lemma 2.1.6. Let the map Φ be given by* (3.1.2)*, where the mollifier fulfills Assumption 3.1.3. Moreover, let the interface $\hat{\Gamma}$ be $C^{k-1,1}$. If k as in Lemma 2.1.6 is such that $k \geq 2$ (which automatically holds if Assumption 2.1.4.B is satisfied), then $\hat{u}$ belongs to $H^k(K_R \cap \hat{D}_1) \cup H^k(\hat{D}_2)$ and*

$$\begin{aligned}\|\hat{u}(\boldsymbol{y})\|_{H^k(K_R\cap\hat{D}_1)} + \|\hat{u}(\boldsymbol{y})\|_{H^k(\hat{D}_2)} \leq\, & C\left(\|\hat{u}(\boldsymbol{y})\|_{H^1(K_R)} + \|\hat{u}(\boldsymbol{y}) - u_i\|_{H^1(K_{R'}\setminus K_R)}\right) \\ & + C\left(\|u_i\|_{H^{k-\frac{1}{2}}(\partial K_R)} + \left\|\frac{\partial u_i}{\partial \boldsymbol{n}_R}\right\|_{H^{k-\frac{3}{2}}(\partial K_R)}\right),\end{aligned}$$

with $K_{R'}$ a circle of radius $R' > R$ and $C = C(a_-, \mathcal{K}, k, |K_R|)$ independent of $J \in \mathbb{N}$ and of $\boldsymbol{y} \in \mathcal{P}_J$. In particular, if Assumption 3.2.4 holds, then we have a J- and $\boldsymbol{y}$-independent bound

$$\|\hat{u}(\boldsymbol{y})\|_{H^k(K_R\cap\hat{D}_1)} + \|\hat{u}(\boldsymbol{y})\|_{H^k(\hat{D}_2)} \leq \tilde{C}\left(\|u_i\|_{H^{k-\frac{1}{2}}(\partial K_R)} + \left\|\frac{\partial u_i}{\partial \boldsymbol{n}_R}\right\|_{H^{k-\frac{3}{2}}(\partial K_R)}\right), \tag{6.1.19}$$

with $\tilde{C} = \tilde{C}(a_-, \gamma, \mathcal{K}, k, |K_R|)$. Here, a_-, γ and $\mathcal{K}$ are defined as in Corollary 6.1.4.

Remark 6.1.8. As it is evident from (2.1.3), we have that $k \to \infty$ as $p \to 0$.

Remark 6.1.9. Theorem 6.1.7 holds not only for the map (3.1.2), but for any map satisfying Assumption 3.1.2.

Remark 6.1.10. In the case of the mapping (3.1.2) with the mollifier given by (3.1.3), we treat $\partial\hat{D}_2^{in}$ as an additional interface with homogeneous transmission conditions, across which the coefficients are discontinuous because of the jump of the Jacobian matrix. Proceeding as before, we obtain

$$\|\hat{u}(\boldsymbol{y})\|_{H^k(K_R\cap\hat{D}_1)} + \|\hat{u}(\boldsymbol{y})\|_{H^k(\hat{D}_2\setminus\hat{D}_2^{in})} + \|\hat{u}(\boldsymbol{y})\|_{H^k(\hat{D}_2^{in})} \leq \tilde{C}\left(\|u_i\|_{H^{k-\frac{1}{2}}(\partial K_R)} + \left\|\frac{\partial u_i}{\partial \boldsymbol{n}_R}\right\|_{H^{k-\frac{3}{2}}(\partial K_R)}\right), \tag{6.1.20}$$

with constants defined as in (6.1.19).

Remark 6.1.11. In the particle on substrate case, the smoothness analysis for the solution is more involved since the presence of corners (points A and B in Figure 1.0.1b) imposes limits on the smoothness of the solution.

6.2. Convergence of the sparse tensor discretization

We consider finite element discretizations with piecewise-polynomial, globally continuous ansatz functions on simplicial, quasi-uniform meshes on K_R. We assume that, at ∂K_R, the exact DtN map is available. In the framework of Chapter 5, we denote by $h \in \mathbb{R}_+$ the meshwidth, and by $l \in \mathbb{N}$ the maximum polynomial degree in the finite element space.

Throughout this section, we assume that, for every $h \in \mathbb{R}_+$ and every $l \in \mathbb{N}$, the finite element space $X_{h,l}$ provides a lth-order approximation for the interface $\hat{\Gamma}$ and the boundary ∂K_R. Then, standard finite element results (see e.g. [LMWZ10] and [BS08, Thm. (4.4.20)]) imply the estimate (5.1.3), with $W = H^k(K_R \cap \hat{D}_1) \cup H^k(\hat{D}_2)$ and $t_l = \min(k-1, l)$, $k \geq 1$. Thanks to Theorem 6.1.7, the W-norm of the solution is bounded uniformly on $J \in \mathbb{N}$ and $\boldsymbol{y} \in \mathcal{P}_J$.

Then convergence results for the fully discrete solution are just a particular case of Theorems 5.3.1 and 5.4.1, when replacing the $(\boldsymbol{b}, p, \varepsilon)$-holomorphy assumption with the $(\boldsymbol{b}, p, \varepsilon)^*$-holomorphy assumption.

The notation used is the same as in Chapter 5.

Corollary 6.2.1. *Let $\hat{u} \in H^k(K_R \cap \hat{D}_1) \cup H^k(\hat{D}_2)$ be the solution to (3.2.4), for some $k \geq 1$, with J- and $\boldsymbol{y}$-independent norm bound. Let Assumptions 3.2.4 and 4.3.5 be fulfilled. Assume that the sparse interpolation and quadrature operators fulfill the assumptions of Theorem 5.3.1.*

Consider that the same space discretization is used at all parameter realizations $\boldsymbol{y}_\nu$, $\nu \in \Lambda$.

Then there exists a downward closed set Λ of cardinality at most N such that

$$\|\hat{u} - I_\Lambda \hat{u}_h\|_{L^\infty(\mathcal{P}_J, V)} \leq C h^{\min(k-1,l)} + C_1 N^{-s}, \quad s = \frac{1}{p} - 2, \tag{6.2.1}$$

$$\|\mathcal{I}(\hat{u}) - Q_\Lambda \hat{u}_h\|_V \leq C h^{\min(k-1,l)} + C_2 N^{-s}, \quad s = \frac{1}{p} - 2, \tag{6.2.2}$$

with $k \geq 1$ and $s, C, C_1, C_2 > 0$ independent of N, h, of the truncation parameter $J \in \mathbb{N}$ and of $\boldsymbol{y} \in \mathcal{P}_J$.

Corollary 6.2.2. *Let $\hat{u} \in H^k(K_R \cap \hat{D}_1) \cup H^k(\hat{D}_2)$ be the solution to (3.2.4), for some $k \geq 1$, with J- and $\boldsymbol{y}$-independent norm bound. Let Assumptions 3.2.4 and 4.3.5 be fulfilled. Assume that the sparse interpolation and quadrature operators fulfill the assumptions of Theorem 5.3.1.*

Then there exists a downward closed set Λ of cardinality at most N such that

$$\|\hat{u} - I_\Lambda \hat{u}_{h,\Lambda}\|_{L^\infty(\mathcal{P}_J, V)} \leq \sum_{\nu \in \Lambda} \|\Delta_\nu^I(\hat{u} - \hat{u}_{h,\Lambda})\|_{L^\infty(\mathcal{P}_J, V)} + C_1 N^{-s}, \quad s = \frac{1}{p} - 2, \tag{6.2.3}$$

$$\|\mathcal{I}(\hat{u}) - Q_\Lambda \hat{u}_{h,\Lambda}\|_V \leq \sum_{\nu \in \Lambda} \|\Delta_\nu^Q(\hat{u} - \hat{u}_{h,\Lambda})\|_V + C_2 N^{-s}, \quad s = \frac{1}{p} - 2, \tag{6.2.4}$$

with $s, C_1, C_2 > 0$ independent of N, of h_m for every m, of $J \in \mathbb{N}$ and of $\boldsymbol{y} \in \mathcal{P}_J$.

If the sequences $(\zeta_i)_{i \geq 0}$ of interpolation/quadrature points are nested, then the addends in the sum on the right-hand side satisfy, for the interpolation and quadrature case respectively:

$$\|\Delta_\nu^I(\hat{u} - \hat{u}_{h,\Lambda})\|_{L^\infty(\mathcal{P}_J, V)} \leq (1 + \mathbb{L}_{\mathcal{R}_\nu}) \sum_{\boldsymbol{y}_m \in \Delta_\nu^I} C_{l_m} \|\boldsymbol{H}_m(\cdot)\|_{L^\infty(\mathcal{P}_J, \mathbb{R})} h_m^{\min(k-1,l_m)} \|\hat{u}(\boldsymbol{y}_m)\|_W, \tag{6.2.5}$$

$$\|\Delta_\nu^Q(\hat{u} - \hat{u}_{h,\Lambda})\|_V \leq \sum_{\boldsymbol{y}_m \in \Delta_\nu^Q} C_{l_m} |\omega_m| h_m^{\min(k-1,l_m)} \|\hat{u}(\boldsymbol{y}_m)\|_W, \tag{6.2.6}$$

with $W = H^k(K_R \cap \hat{D}_1) \cup H^k(\hat{D}_2)$ and with, for every $m \in \mathbb{N}$, C_{l_m} independent of N, of h_m for every m, of $J \in \mathbb{N}$ and of $\boldsymbol{y} \in \mathcal{P}_J$. The Lebesgue constant $\mathbb{L}_{\mathcal{R}_\nu}$ is bounded by $\mathbb{L}_{\mathcal{R}_\nu} \leq (\sharp \mathcal{R}_\nu)^{\theta+1}$.

Remark 6.2.3. In the particle in free space case, if we use the mollifier (3.1.3) and, for every interpolation/quadrature point $\boldsymbol{y}_m$, we use a l_mth-order boundary approximation for $\partial\hat{D}_2^{in}$, then we still have the estimates (6.2.1), (6.2.2) and(6.2.5),(6.2.6) .

We have seen in the previous section that the smoothness $s = \frac{1}{p} - 2$ in the parameter space and the spatial smoothness k of the exact solution are not independent, thanks to Theorem 6.1.7. This is formalized in the following important corollary, obtained by combining Theorem 6.1.7 with Corollary 6.2.1 or Corollary 6.2.2:

Corollary 6.2.4. *Let Assumptions 2.1.3 and 3.2.4 be fulfilled. Let* Φ *be given by* (3.1.2) *with a mollifier satisfying Assumption 3.1.3 or the mollifier* (3.1.3)*. Also, let the sparse interpolation and quadrature operators fulfill the assumptions of Theorems 5.3.1 and 5.4.1.*

If the coefficient sequences $\mathcal{C} = (c_j)_{j\geq 1}$, $\mathcal{S} = (s_j)_{j\geq 1}$ *satisfy Assumption 2.1.4.A and the nominal radius* r_0 *belongs to* $C^k_{per}([0, 2\pi))$*, with* k *as below, then the estimates* (6.2.1)-(6.2.2) *and* (6.2.5)-(6.2.6) *hold with*

$$k = \begin{cases} \left\lfloor \frac{1}{p} - 1 \right\rfloor & \text{if } \frac{1}{p} - 1 \text{ is not an integer,} \\ \frac{1}{p} - 2 & \text{otherwise.} \end{cases} \tag{6.2.7}$$

6.3. Convergence of linear output functionals

The finite elements spaces considered are the same as in the previous section. Let us denote by $\hat{F}$ a linear output functional defined on the nominal configuration. We have seen in Section 5.5 that $\hat{F}$ must satisfy Assumption 5.5.1 (holomorphic extension to polyellipses). In our framework, this requirement is fulfilled in particular when

$$\hat{F}(\boldsymbol{y}, \hat{u}) = \int_{\hat{A}} \mathcal{L}_1(\boldsymbol{y}, \hat{u}(\boldsymbol{y}))\, d\hat{\boldsymbol{x}}, \tag{6.3.1}$$

where $\hat{A} \subseteq K_R$ is a set of nonzero measure and $\mathcal{L}_1$ is a first-order linear differential operator of the form $\mathcal{L}_1(\boldsymbol{y}, v) = \hat{a}_1(\boldsymbol{y}, \hat{\boldsymbol{x}}) \cdot \hat{\nabla}\hat{v} + \hat{b}_1(\boldsymbol{y}, \hat{\boldsymbol{x}})\hat{v}$, with coefficients which are bounded and measurable with respect to $\hat{\boldsymbol{x}}$ and admit a holomorphic extension in the same domain of analyticity as $\hat{u}$.

We also require that $\hat{F}$ is stable in the following sense:

Assumption 6.3.1. The linear output functional $\hat{F}$ belongs to $(H^n(K_R))^*$ for an integer $n \leq 1$, i.e. there exists $C > 0$ such that

$$\left|\hat{F}(\boldsymbol{y}, \hat{v})\right| \leq C\|\hat{v}\|_{H^n(K_R)}, \quad \text{for all } \hat{v} \in H^n(K_R),$$

with C independent of the truncation parameter $J \in \mathbb{N}$ and of $\boldsymbol{y} \in \mathcal{P}_J$ (but possibly dependent on the radius R of K_R).

This assumption is fulfilled, at least for $n = 1$, by functionals of the form (6.3.1). If Assumption 6.3.1 is fulfilled for $n = 1$, then we have the estimate (5.5.1) with $t_l = 0$ for every l. If Assumption 6.3.1 is fulfilled for $n \leq 0$, then, using duality techniques, we can prove [BS08, Sect. 5.7] that (5.5.1) holds with $t_l = 1$ for every $l \in \mathbb{N}$.

Then applying Theorems 5.5.2 and 5.5.3 replacing the $(\boldsymbol{b}, p, \varepsilon)$-holomorphy assumption with the $(\boldsymbol{b}, p, \varepsilon)^*$-holomorphy assumption, and using the same notation as in Chapter 5, we obtain the convergence estimates:

Corollary 6.3.2. *Let $\hat{F}$ be a linear output functional defined on the nominal configuration and satisfying Assumption 5.5.1. Let the assumptions of Corollary 6.2.1 be satisfied.*

Then there exists a downward closed set Λ of cardinality at most N such that the following estimates hold:

$$\|\hat{F} - I_\Lambda \hat{F}_h\|_{L^\infty(\mathcal{P}_J,V)} \leq Ch^{t^F} + C_1 N^{-s}, \quad s = \frac{1}{p} - 2, \tag{6.3.2}$$

$$\|\mathcal{I}(\hat{F}) - Q_\Lambda \hat{F}_h\|_V \leq Ch^{t^F} + C_2 N^{-s}, \quad s = \frac{1}{p} - 2, \tag{6.3.3}$$

with $k \geq 1$ and $s, C, C_1, C_2 > 0$ independent of N, h, of $J \in \mathbb{N}$ and of $\boldsymbol{y} \in \mathcal{P}_J$.

If $\hat{F}$ fulfills Assumption 6.3.1, then $t^F = \min(k-1, l)+1$ for $n \leq 0$, $t^F = \min(k-1, l)$ for $n = 1$.

Corollary 6.3.3. *Let $\hat{F}$ be a linear output functional defined on the nominal configuration and satisfying Assumption 5.5.1. Let the assumptions of Corollary 6.2.2 be satisfied.*

Then there exists a downward closed set Λ of cardinality at most N such that

$$\|\hat{F} - I_\Lambda \hat{F}_{h,\Lambda}\|_{L^\infty(\mathcal{P}_J,V)} \leq \sum_{\nu \in \Lambda} \|\Delta_\nu^I(\hat{F} - \hat{F}_{h,\Lambda})\|_{L^\infty(\mathcal{P}_J,V)} + C_1 N^{-s}, \quad s = \frac{1}{p} - 2, \tag{6.3.4}$$

$$\|\mathcal{I}(\hat{F}) - Q_\Lambda \hat{F}_{h,\Lambda}\|_V \leq \sum_{\nu \in \Lambda} \|\Delta_\nu^Q(\hat{F} - \hat{F}_{h,\Lambda})\|_V + C_2 N^{-s}, \quad s = \frac{1}{p} - 2, \tag{6.3.5}$$

with $s, C_1, C_2 > 0$ independent of N, of h_m for every m, of $J \in \mathbb{N}$ and of $\boldsymbol{y} \in \mathcal{P}_J$.

If the sequences $(\zeta_i)_{i \geq 0}$ of interpolation/quadrature points are nested, then the addends in the sum on the right-hand side satisfy, for the interpolation and quadrature case respectively:

$$\|\Delta_\nu^I(F - \hat{F}_{h,\Lambda})\|_{L^\infty(\mathcal{P}_J,V)} \leq (1 + \mathbb{L}_{\mathcal{R}_\nu}) \sum_{\boldsymbol{y}_m \in \Delta_\nu^I} C_{l_m} \|\boldsymbol{H}_m(\cdot)\|_{L^\infty(\mathcal{P}_J,\mathbb{R})} h_m^{t_{l_m}^F} \|\hat{u}(\boldsymbol{y}_m)\|_W, \tag{6.3.6}$$

$$\|\Delta_\nu^Q(F - \hat{F}_{h,\Lambda})\|_V \leq \sum_{\boldsymbol{y}_m \in \Delta_\nu^Q} C_{l_m} |\omega_m| h_m^{t_{l_m}^F} \|\hat{u}(\boldsymbol{y}_m)\|_W, \tag{6.3.7}$$

with $W = H^k(K_R \cap \hat{D}_1) \cup H^k(\hat{D}_2)$ and with, for every $m \in \mathbb{N}$, $C_{l_m} > 0$ independent of N, of h_m for every m, of $J \in \mathbb{N}$ and of $\boldsymbol{y} \in \mathcal{P}_J$, and the Lebesgue constant $\mathbb{L}_{\mathcal{R}_\nu}$ bounded as in (5.4.5), i.e. $\mathbb{L}_{\mathcal{R}_\nu} \leq (\sharp \mathcal{R}_\nu)^{\theta+1}$.

If $\hat{F}$ fulfills Assumption 6.3.1, then $t_{l_m}^F = \min(k-1, l_m)+1$ for $n \leq 0$, $t_{l_m}^F = \min(k-1, l_m)$ for $n = 1$, $k \geq 1$.

As we have done in Corollary 6.2.4, also for linear output functionals it is possible to determine the regularity parameter k for the above theorems from the decay of the Fourier coefficients in the radius expansion.

7. Numerical experiments

The geometries are shown in Figure 1.0.1. In both cases, the scatterer has a nominal, angle-independent radius of size $r_0 = 10\text{nm}$. The wavenumber in free space is $\kappa_0 = \frac{2\pi f}{c_0}$, with $c_0 = 3 \cdot 10^8 \text{m/s}$ the light speed.

For each of the two model problems, we consider the interpolation and quadrature of the real part of the solution to (3.2.4) and of the modulus of the far field pattern. Given a radiating solution $u_s = u - u_i$ to the Helmholtz equation (where u denotes the total field and u_i the incoming wave), the far field pattern is a function defined on the unit circle S^1, describing the asymptotic behavior of $u_s(\boldsymbol{x})$ for $|\boldsymbol{x}| \to \infty$. The far field mapping $F : H^1_{\text{loc}}(\mathbb{R}^2) \to C^\infty(S^1)$ associates to a scattered wave u_s its far field pattern. We will provide the expression of the far field pattern for each of the model problems of Chapter 1 separately. Since, for every $\boldsymbol{\xi} \in S^1$, $F(\boldsymbol{\xi})$ is complex-valued, by modulus of the far field pattern we mean its absolute value $|F(\boldsymbol{\xi})|$, $\boldsymbol{\xi} \in S^1$.

In all experiments, we compute the solution for the TE mode, that is the solution u to (1.0.1) is the out-of-plane component of the electric field.

The interpolants and the means of the Q.o.I.s are computed using the sparse grid algorithm described in Section 4.2 (Algorithm 1) with $\vartheta = 1$. In the case of the particle in free space, when increasing the dimension of the parameter space in the adaptive strategy, we add two dimensions per step, because of the equal weights in front of the sinusoids and cosinusoids for each frequency in the Fourier expansion.

The V-norm considered at lines 5-6 of Algorithm 1 of Section 4.2 is the maximum norm $\|\cdot\|_\infty$ of the Q.o.I. considered as a vector in $\mathbb{R}^n$, $n \geq 1$. More precisely, when the Q.o.I. is the real part of the solution, or rather its finite element approximation, we consider the maximum norm of the coefficient vector of the finite element function. When the Q.o.I. is the modulus of the far field functional, we consider the maximum norm of the Fourier coefficients in the free space case, and the maximum norm of a set of point evaluations on the unit circle in the substrate case. Thus, if we denote by $\boldsymbol{g}$ the vector associated to the Q.o.I., when reporting the error estimated by the algorithm we refer to the quantity $\max_{\nu \in \mathcal{N}(\Lambda)} \|\Delta^I_\nu(\boldsymbol{g})\|_\infty$ in the interpolation case, and to the quantity $\sum_{\nu \in \mathcal{N}(\Lambda)} \|\Delta^Q_\nu(\boldsymbol{g})\|_\infty$ in the quadrature case. The reason why, in the error estimator, we have not considered the H^1-norm for the solution and the norm $\|\cdot\|_2$ (Euclidean norm) for far field evaluations is that we have preferred to use the implementation of Algorithm 1 as a black box, avoiding, for instance, the close interaction with the finite element solver that would have been needed to compute the H^1-norm. When comparing the error with respect to a reference solution, instead, we report the H^1-error norm and $\|\cdot\|_2$-error norm for the solution and the far field Fourier coefficients (or evaluations), respectively.

For each experiment, we compare two choices for the univariate sequence $(\zeta^k_i)_{i=0}^{n_k}$ of interpolation/quadrature points:

- Clenshaw-Curtis (CC):

$$\begin{aligned} &\zeta^k_0 = 0 \ \text{ if } n_k = 1, \\ &\zeta^k_i = -\cos\left(\frac{\pi i}{n_k - 1}\right), \ i = 0, \dots, n_k - 1, \ \text{ if } n_k > 1, \end{aligned}$$

with $n_0 = 1$ and $n_k = 2^k + 1$, for $k \geq 1$;

- $\mathfrak{R}$-Leja sequence (RL): projection on $[-1, 1]$ of a Leja sequence for the complex unit disk initiated at 1:

$$\begin{aligned}
&\zeta_0^k = 0, \zeta_1^k = 1, \zeta_2^k = -1, \quad \text{if } i = 0, 1, 2, \\
&\zeta_i^k = \mathfrak{R}(\hat{z}), \text{ with } \hat{z} = \text{argmax}_{|\zeta|=1} \prod_{l=1}^{i-1} |\zeta - \zeta_l^k|, \; i = 3, \ldots, n_k, \quad \text{if } i \text{ odd}, \\
&\zeta_i^k = -\zeta_{i-1}^k, \; i = 3, \ldots, n_k, \quad \text{if } i \text{ even},
\end{aligned}$$

with $n_k = 2k + 1$, for $k \geq 0$, see [CM12].

The Clenshaw-Curtis points satisfy Assumption 4.1.2 with part (a) in condition (ii), while the $\mathfrak{R}$-Leja points satisfy Assumption 4.1.2 with part (b) in (ii).

The finite element solutions are computed using the C++ NGSolve library[1], providing high-order elements for any shape; NGSolve has been linked to the MKL version of the PARDISO library[2] to compute the solution of the resulting algebraic system.

To truncate the domain and approximate the DtN map, we consider, in both cases, a circular Perfectly Matched Layer (PML, see [Ber94, CM98]) around the boundary ∂K_R; for every $\boldsymbol{y} \in \mathcal{P}_J$, the mapping $\Phi(\boldsymbol{y})$ is prolongated as the identity in the PML. In [LS98] it is shown that, if the fictitious absorption coefficient is properly chosen, then the PML can be used in the finite element framework to truncate the domain for Helmholtz equation in a almost reflectionless manner for all frequencies.

The remainder of this chapter is organized as follows: in Sections 7.1 and 7.2 we present the numerical experiments for the particle in free space and the particle on substrate, respectively, and in Section 7.3 we discuss these results.

7.1. Particle in free space

The incident wave u_i is coming from the left with an incidence angle 0 with respect to the horizontal axis ($\boldsymbol{d} = (1, 0)$), and frequency $f = 10^4$THz. The scatterer is a dielectric with relative permittivity $\varepsilon_2 = 2$ and the surrounding medium is air ($\varepsilon_1 = 1$), so that the wavenumbers are $\kappa_1 = \kappa_0$ and $\kappa_2 = \kappa_0\sqrt{\varepsilon_2}$, respectively.

7.1.1. Interpolation of the real part of the solution on the nominal configuration

We consider the performance of the algorithm for small and large shape variations. By small variations we mean variations of the order of around 2% with respect to the nominal radius r_0, while by large variations we mean variations of around 20% with respect to r_0.

[1] http://sourceforge.net/apps/mediawiki/ngsolve

[2] https://software.intel.com/en-us/intel-mkl. See also http://www.pardiso-project.org/ for other versions of the PARDISO solver.

Small variations

For this case we use the domain mapping

$$\boldsymbol{x}(\boldsymbol{y}) = \Phi(\boldsymbol{y}, \hat{\boldsymbol{x}}) = \begin{cases} \mathbf{0} & \text{if } \hat{\boldsymbol{x}} = \mathbf{0}, \\ \frac{\hat{\boldsymbol{x}}}{r_0(\varphi)} r(\boldsymbol{y}, \varphi) & \text{if } 0 < \|\hat{\boldsymbol{x}}\| < r_0(\varphi), \\ \frac{R - r(\boldsymbol{y},\varphi)}{R - r_0(\varphi)} \left(1 + \frac{R(r(\boldsymbol{y},\varphi) - r_0(\varphi))}{R - r(\boldsymbol{y},\varphi)} \frac{1}{\|\hat{\boldsymbol{x}}\|}\right) \hat{\boldsymbol{x}} & \text{if } r_0(\varphi) \le \|\hat{\boldsymbol{x}}\| < R, \\ \hat{\boldsymbol{x}} & \text{if } \|\hat{\boldsymbol{x}}\| = R. \end{cases} \tag{7.1.1}$$

This mapping does not fulfill Assumption 3.1.2 because of the singularity in the origin, but it is easy to check that it fulfills the $(\boldsymbol{b}, p, \varepsilon)^*$-holomorphy assumption. We highlight that the assumption that Φ is at least of class C^2 in each subdomain is relevant for the space regularity and convergence analysis developed in Chapter 6. For well-posedness of the variational formulation (3.2.4), we only need that the Jacobian of Φ and its inverse are almost everywhere bounded, for every parameter realization. Since the Jacobian of the mapping (7.1.1) is not continuous at the origin, we cannot expect a full convergence rate for the finite element discretization. However, the focus in our experiments is on the performance of the the sparse interpolation/quadrature algorithm, and what really matters is that the finite element discretization produces an error just low enough not to interfere with the performance of the algorithm, rather than the convergence order of the space discretization.

We consider the expansion of the stochastic radius (2.1.1) for three variations of the sparsity parameter: $s_j = c_j = \frac{0.01 r_0}{j^{\frac{1}{p}}}, j \ge 1$, for $\frac{1}{p} = 2, 3, 4$. For each value of p, we compare the cases $2J = 16$, $2J = 32$ and $2J = 64$, with $2J = d$ the dimension of the parameter space. The maximal shape variations with respect to r_0 are of the order of 2.3% for $\frac{1}{p} = 2$, 1.7% for $\frac{1}{p} = 3$ and 1.5% for $\frac{1}{p} = 4$ (for all the three truncations of the radius expansion).

To compute the finite element solution given a parameter realization, we have used globally continuous, piecewise 4th-order polynomial ansatz functions on an unstructured, quasi-uniform triangulation, leading to a total of 60705 degrees of freedom (including the PML). A 4th-order boundary approximation has been considered, so that the error introduced by the discretization of the boundaries is of the same order as the error due to the finite element discretization. The Smolyak interpolation has been applied to the part of the solution that is not inside the PML, corresponding to an array carrying 37563 degrees of freedom. The PML starts at radius $R = 100$nm and ends at radius $R' = 150$nm, with absorption coefficient (or damping parameter) $\alpha = 0.5$ [CM98].

We first consider the behavior of the interpolation error $\max_{\nu \in \mathcal{N}(\Lambda)} \|\Delta^I_\nu(\hat{\boldsymbol{\mu}}_h)\|_\infty$ *estimated* by Algorithm 1. In the error indicator, $\hat{\boldsymbol{\mu}}_h$ denotes the vector of coefficients of the solution with respect to the finite element basis functions, associated with Ndof = 37563 degrees of freedom. The increments $\|\Delta^I_\nu(\hat{\boldsymbol{\mu}}_h)\|_\infty$, $\nu \in \Lambda$, are the relative increments with respect to $\|\Delta^I_0(\hat{\boldsymbol{\mu}}_h)\|_\infty = \|\hat{\boldsymbol{\mu}}_h(\boldsymbol{y} = \mathbf{0})\|_\infty$.

Figure 7.1.1 shows the comparison of the *estimated errors* according to the different decays in the coefficient sequences, for each of the dimensions 16, 32 and 64 of the parameter space. Figure 7.1.2 shows instead, for each of the variations $\frac{1}{p} = 2, 3, 4$ of the sparsity parameter, the comparison of the performance of the algorithm for different dimensions of the parameter space.

Since the behavior of the error estimator is fairly oscillatory, in Figures 7.1.3 and 7.1.4 we present the analogous of Figures 7.1.1 and 7.1.2, respectively, when considering an error with respect to a reference solution instead of the error estimated by the algorithm. Namely, as measure of the error we have considered $\sup_{\boldsymbol{y} \in \mathcal{P}_J} \|\mathrm{Re}\, \hat{u}_h(\boldsymbol{y}) - I_\Lambda(\mathrm{Re}\, \hat{u}_h)(\boldsymbol{y})\|_{H^1(K_R)}$, where each realization

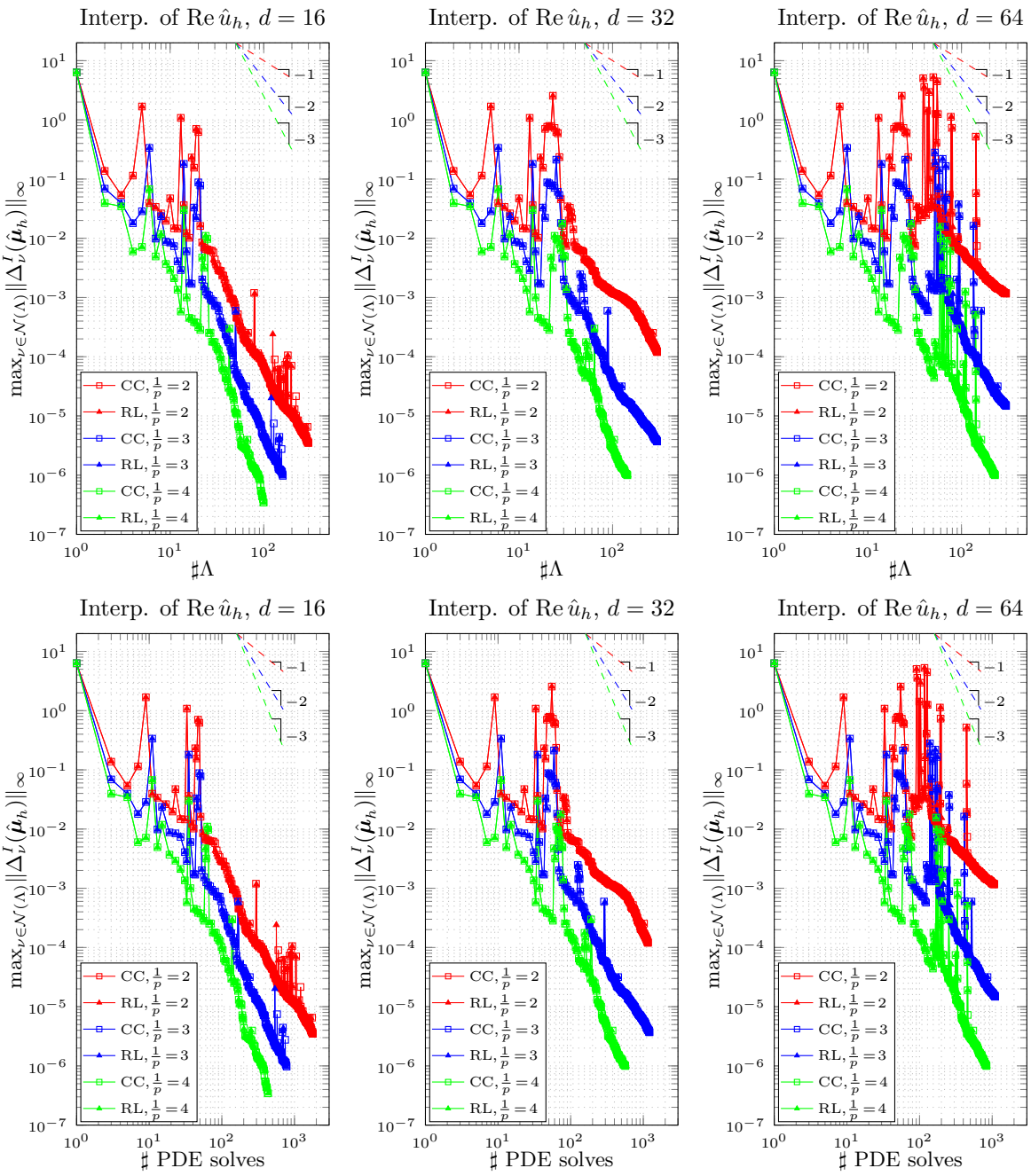

Figure 7.1.1: Comparison of the *estimated errors* for the interpolated solution with respect to the cardinality of the index set Λ (top) and to the number of PDE solves (bottom), using Clenshaw-Curtis and $\mathfrak{R}$-Leja points, for 16 (left), 32 (middle) and 64 (right) dimensions. The three dashed lines on the top of each plot correspond to the convergence rates of 1 (red), 2 (blue) and 3 (green). Maximal shape variations with respect to r_0 of about 2.3% for $\frac{1}{p} = 2$, 1.7% for $\frac{1}{p} = 3$ and 1.5% for $\frac{1}{p} = 4$. Domain mapping (7.1.1).

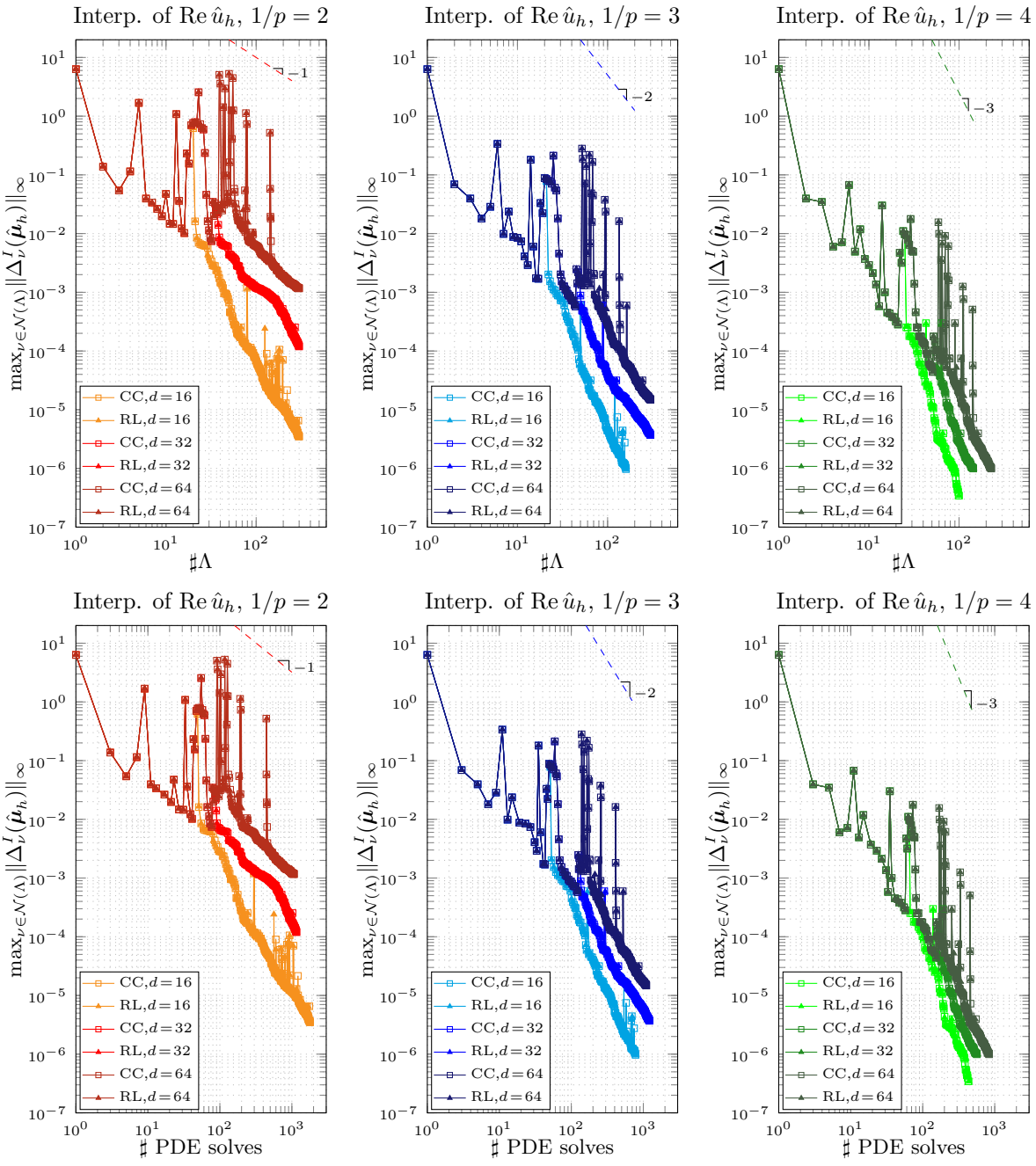

Figure 7.1.2: Comparison of the *estimated errors* for the interpolated solution with respect to the cardinality of the index set Λ (top) and to the number of PDE solves (bottom), using Clenshaw-Curtis and $\mathfrak{R}$-Leja points, for variations of the sparsity parameter $\frac{1}{p} = 2$ (left), 3 (middle) and 4 (right). Maximal shape variations with respect to r_0 of about 2.3% for $\frac{1}{p} = 2$, 1.7% for $\frac{1}{p} = 3$ and 1.5% for $\frac{1}{p} = 4$. Domain mapping (7.1.1).

$\operatorname{Re}\hat{u}_h(\boldsymbol{y})$ and the interpolated quantity $I_\Lambda(\operatorname{Re}\hat{u}_h)(\boldsymbol{y})$, $\boldsymbol{y}\in\mathcal{P}_J$, have been computed using the same finite element space as described above. To estimate the supremum norm, we have considered the maximum H^1-norm error among 2^{16} realizations of $\boldsymbol{y}\in\mathcal{P}_J$ corresponding to the quadrature points generated by the high-order quasi Monte-Carlo method described in [Gan16] and [GS16], using $C=0.1$ for the Walsh coefficient bound. The error has been computed every 10 iterations of the Smolyak algorithm, starting from the last one and going backward until the last iteration with number bigger or equal to 10.

Large variations

In this case, we consider the coefficient sequences $s_j=c_j=\frac{0.1r_0}{j^{\frac{1}{p}}}$, $j\geq 1$, for $\frac{1}{p}=2,3,4$ and $2J=16,32,64$. We use the domain mapping (3.1.2) with the mollifier (3.1.3). Resolving accurately the interface given by the inner circle of radius $\frac{r_0^-}{4}$, this map guarantees that we achieve full convergence rate for the finite element discretization. The PML starts at $R=80$nm and ends at $R'=110$nm, with absorption coefficient $\alpha=0.5$. We have used a 2nd-order finite element space with 2nd-order boundary approximation for the interfaces. The total number of degrees of freedom for the space discretization is 37309, of which 28415 are outside the PML. Again, as Q.o.I. we consider the real part of the solution that is not inside the PML.

In Figures 7.1.5 and 7.1.6 we show the behavior of the error comparing the different decays of the coefficient sequences and comparing the different parameter space dimensions, respectively. The error measured here is $\sup_{\boldsymbol{y}\in\mathcal{P}_J}\|\operatorname{Re}\hat{u}_h(\boldsymbol{y})-I_\Lambda(\operatorname{Re}\hat{u}_h)(\boldsymbol{y})\|_{H^1(K_R)}$, where each realization $\operatorname{Re}\hat{u}_h(\boldsymbol{y})$ and the interpolated quantity $I_\Lambda(\operatorname{Re}\hat{u}_h)(\boldsymbol{y})$, $\boldsymbol{y}\in\mathcal{P}_J$, have been computed on the same finite element space as described above. Again, to estimate the supremum norm, we have considered the maximum H^1-norm error among 2^{16} realizations of $\boldsymbol{y}\in\mathcal{P}_J$ corresponding to the quadrature points generated by the high-order quasi Monte-Carlo method described in [Gan16] and [GS16], using $C=0.1$ for the Walsh coefficient bound. The error has been computed every 10 iterations of the Smolyak algorithm, starting from the last one and going backward until the last iteration with number bigger or equal to 10.

7.1.2. Interpolation of the modulus of the far field pattern

The far field pattern is given by [MS98, Formulae (3) and (5)]

$$F(u_s)(\hat{\boldsymbol{\xi}})=C_F\int_\Sigma\left\{u_s(\boldsymbol{x})\frac{\partial G(\hat{\boldsymbol{\xi}},\boldsymbol{x})}{\partial\boldsymbol{n}(\boldsymbol{x})}-\frac{\partial u_s}{\partial\boldsymbol{n}}(\boldsymbol{x})G(\hat{\boldsymbol{\xi}},\boldsymbol{x})\right\}\mathrm{d}S(\boldsymbol{x}),\quad\hat{\boldsymbol{\xi}}\in S^1,\tag{7.1.2}$$

where Σ is a simple closed path around the scatterer and $\boldsymbol{n}$ its unit normal vector field pointing to the outer region. The function $G=G(\hat{\boldsymbol{\xi}},\boldsymbol{x})$ describes the behavior of the Green's function when the modulus of the second argument tends to infinity (we refer to [CK12, Sect. 2.2] for details). For a particle in free space, we have $G(\hat{\boldsymbol{\xi}},\boldsymbol{x})=\frac{1}{4\pi}e^{-i\kappa_1\hat{\boldsymbol{\xi}}\cdot\boldsymbol{x}}$ (with κ_1 the wavenumber in free space). In (7.1.2), C_F is a normalizing constant, that has been set to $C_F=\sqrt{\frac{2\pi}{\kappa_1}}e^{i\frac{\pi}{4}}$.

A simple application of Green's formula shows that the far field pattern is independent of the path Σ chosen to enclose the scatterer. Thus, we can consider two circles Σ_1 and Σ_2 around the particle, with Σ_1 contained in Σ_2, and the annulus A enclosed between them, and choose a cut-off function $\psi\in C^2(A)$ such that

$$\psi|_{\Sigma_2}=1,\quad\psi|_{\Sigma_1}=0,\quad\nabla\psi|_{\Sigma_1}=\nabla\psi|_{\Sigma_2}=\mathbf{0}.\tag{7.1.3}$$

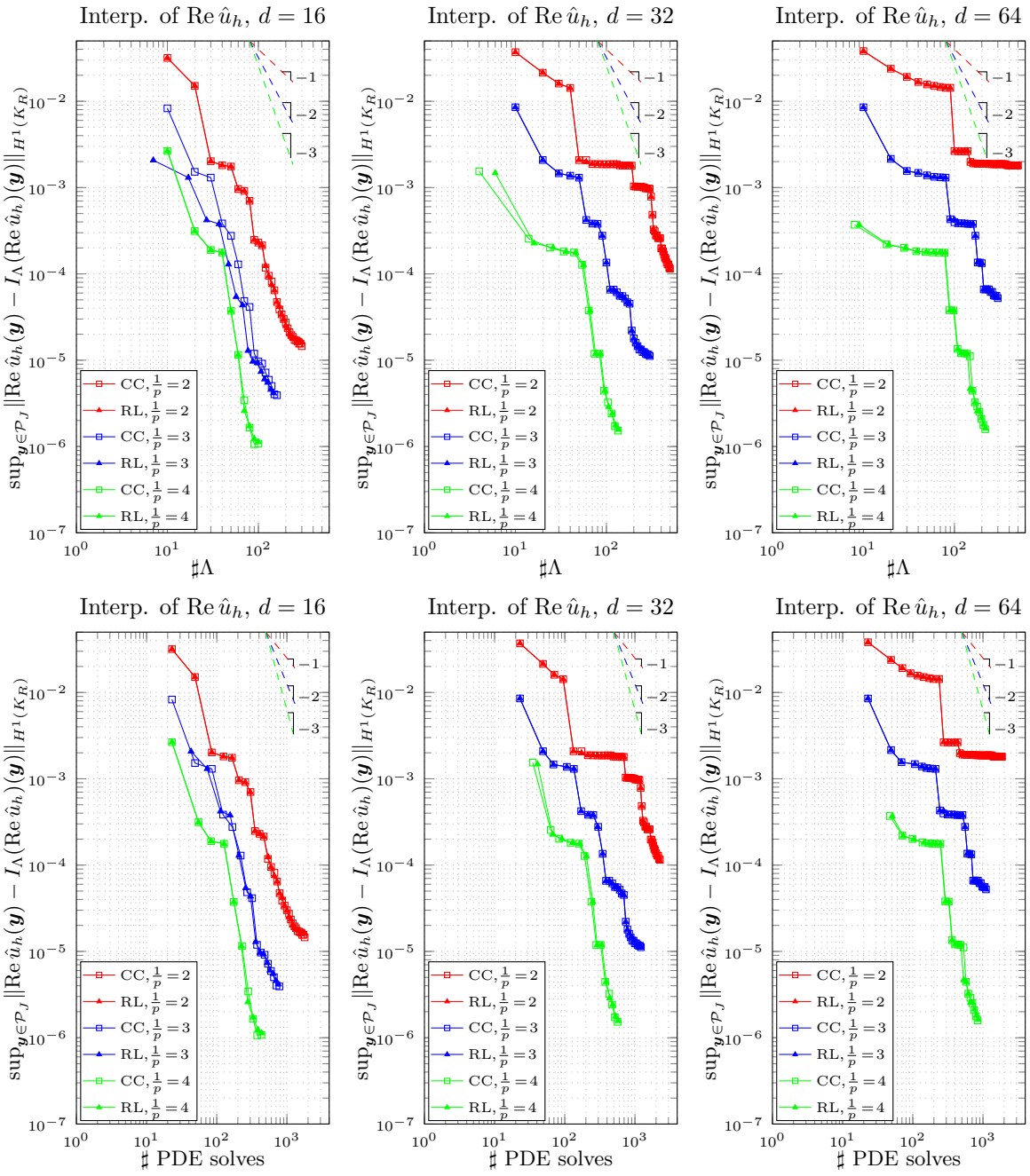

Figure 7.1.3: Comparison of the errors for the interpolated solution with respect to the cardinality of the index set Λ (top) and to the number of PDE solves (bottom), using Clenshaw-Curtis and $\mathfrak{R}$-Leja points, for 16 (left), 32 (middle) and 64 (right) dimensions. Maximal shape variations with respect to r_0 of about 2.3% for $\frac{1}{p} = 2$, 1.7% for $\frac{1}{p} = 3$ and 1.5% for $\frac{1}{p} = 4$. Domain mapping (7.1.1).

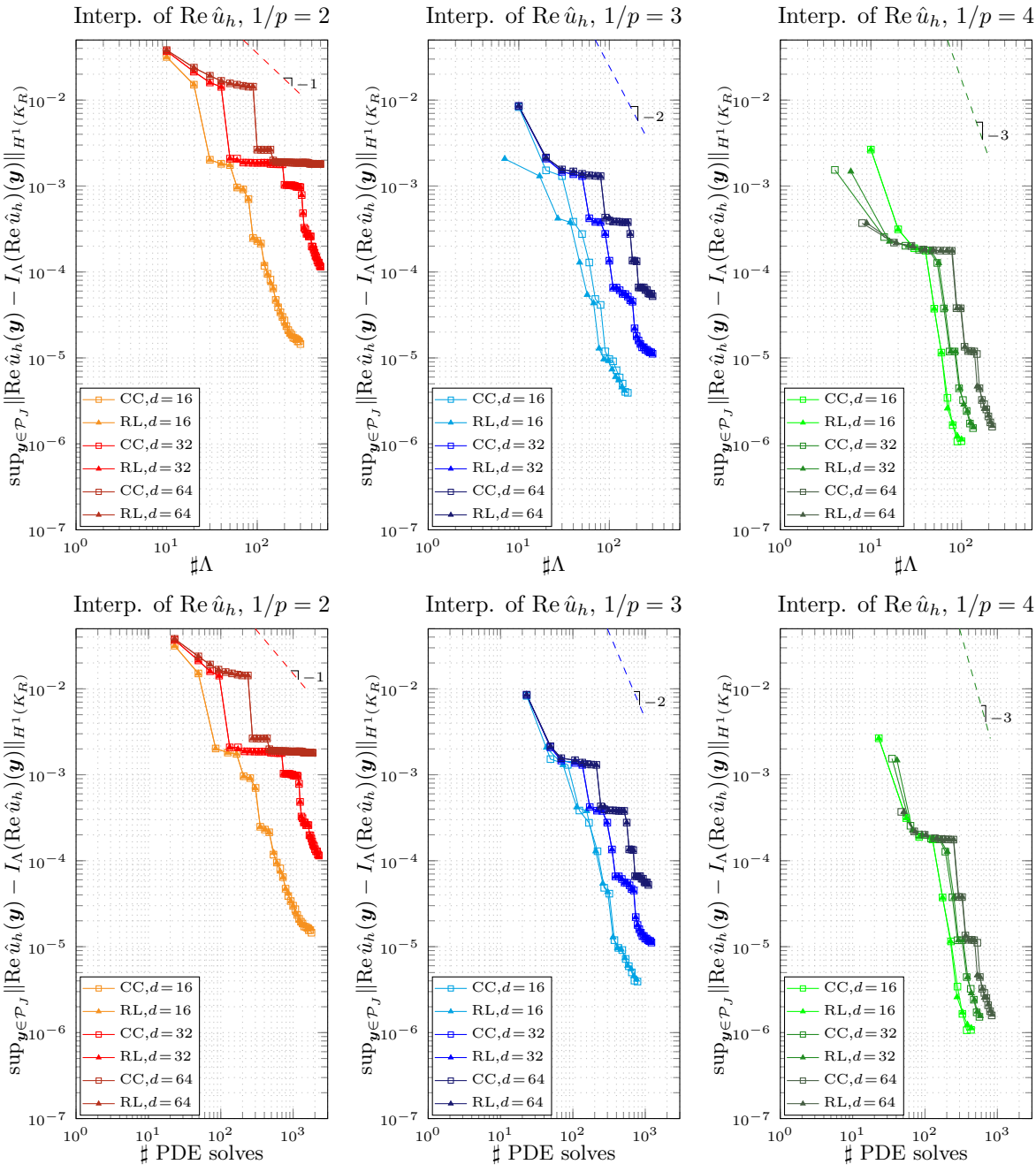

Figure 7.1.4: Comparison of the errors for the interpolated solution with respect to the cardinality of the index set Λ (top) and to the number of PDE solves (bottom), using Clenshaw-Curtis and $\mathfrak{R}$-Leja points, for variations of the sparsity parameter $\frac{1}{p} = 2$ (left), 3 (middle) and 4 (right). Maximal shape variations with respect to r_0 of about 2.3% for $\frac{1}{p} = 2$, 1.7% for $\frac{1}{p} = 3$ and 1.5% for $\frac{1}{p} = 4$. Domain mapping (7.1.1).

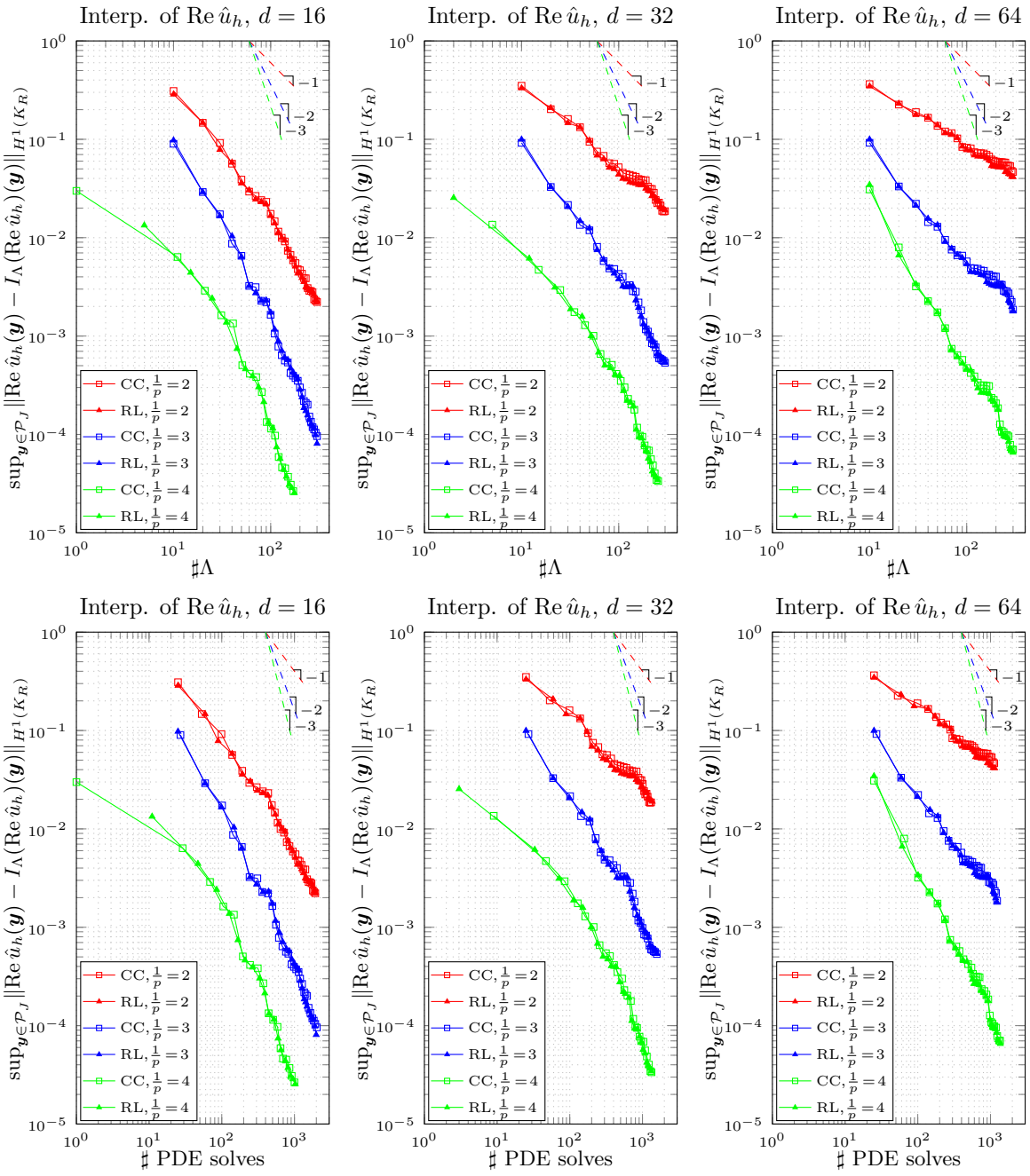

Figure 7.1.5: Comparison of the errors for the interpolated solution with respect to the cardinality of the index set Λ (top) and to the number of PDE solves (bottom), using Clenshaw-Curtis and $\mathfrak{R}$-Leja points, for 16 (left), 32 (middle) and 64 (right) dimensions. Maximal shape variations with respect to r_0 of about 22% for $\frac{1}{p} = 2$, 17% for $\frac{1}{p} = 3$ and 15% for $\frac{1}{p} = 4$. Domain mapping (3.1.2) with mollifier 3.1.3.

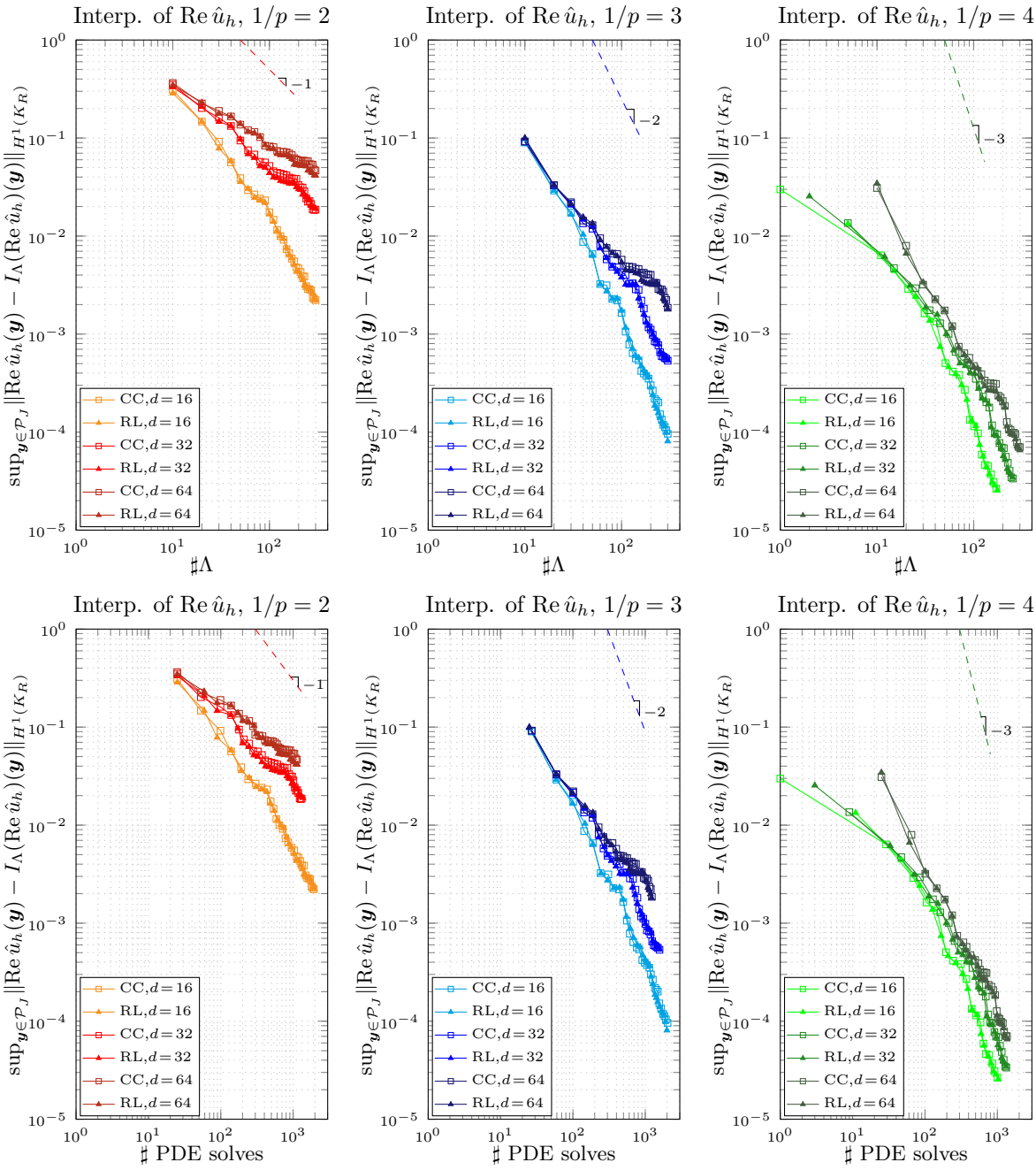

Figure 7.1.6: Comparison of the errors for the interpolated solution with respect to the cardinality of the index set Λ (top) and to the number of PDE solves (bottom), using Clenshaw-Curtis and $\mathfrak{R}$-Leja points, for variations of the sparsity parameter $\frac{1}{p} = 2$ (left), 3 (middle) and 4 (right). Maximal shape variations with respect to r_0 of about 22% for $\frac{1}{p} = 2$, 17% for $\frac{1}{p} = 3$ and 15% for $\frac{1}{p} = 4$. Domain mapping (3.1.2) with mollifier (3.1.3).

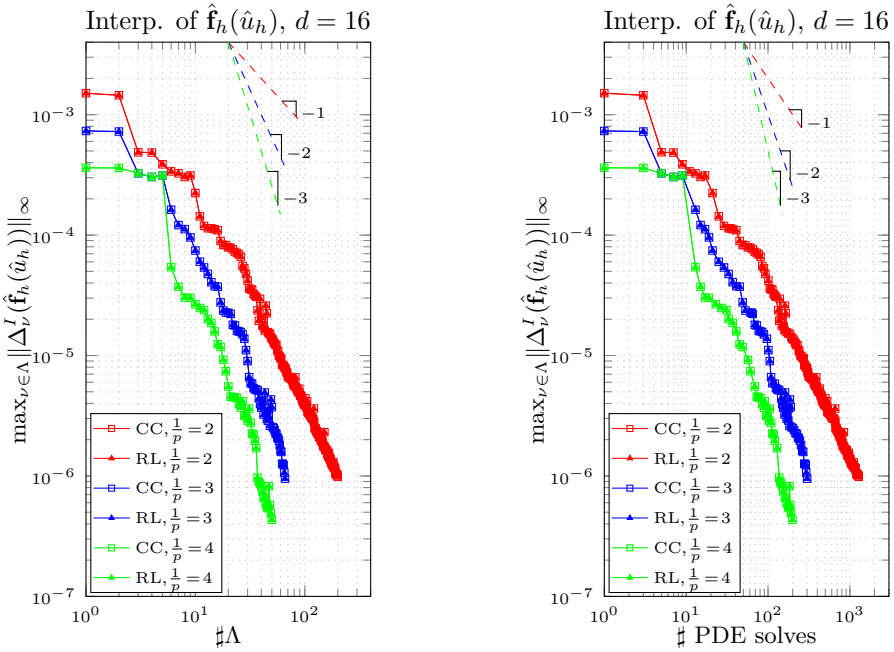

Figure 7.1.7: Comparison of the *estimated errors* for the interpolated far field Fourier coefficients with respect to the cardinality of the index set Λ (left) and the number of PDE solves (right), using Clenshaw-Curtis and $\mathfrak{R}$-Leja points, for 16 dimensions. The three dashed lines on the top of each plot correspond to the convergence rates of 1 (red), 2 (blue) and 3 (green). Maximal shape variations with respect to r_0 of 22% for $\frac{1}{p} = 2$, 17% for $\frac{1}{p} = 3$ and 15% for $\frac{1}{p} = 4$. Domain mapping (7.1.1).

Applying Green's formula, it is easy to see [HS] that (7.1.2) is equivalent to the modified far field mapping

$$F^*(u_s)(\hat{\boldsymbol{\xi}}) = C_F \int_A \nabla\psi(\boldsymbol{x}) \cdot \Big(u_s(\boldsymbol{x})\nabla G(\hat{\boldsymbol{\xi}},\boldsymbol{x}) - \nabla u_s(\boldsymbol{x}) G(\hat{\boldsymbol{\xi}},\boldsymbol{x})\Big)\,\mathrm{d}\boldsymbol{x}, \quad \hat{\boldsymbol{\xi}} \in S^1. \tag{7.1.4}$$

The advantage of formula (7.1.4) with respect to (7.1.2) is that, for fixed $\hat{\boldsymbol{\xi}} \in S^1$, $u_s \mapsto F^*(u_s)(\hat{\boldsymbol{\xi}})$ is a linear functional that is continuous on the energy space $H^1(A)$.

If we now apply the far field computation to the case when the scatterer has a stochastic boundary, we can fix an annular integration region $\hat{A}$ and a cut-off function $\hat{\psi}$ on the *nominal* domain $\hat{D}_1 \cap K_R$, and (7.1.4) reads:

$$\begin{aligned}\hat{F}^*(\hat{u}_s(\boldsymbol{y}))(\hat{\boldsymbol{\xi}}) = C_F \int_{\hat{A}} D\Phi(\boldsymbol{y})^{-\top}\hat{\nabla}\hat{\psi}(\hat{\boldsymbol{x}}) \cdot \hat{u}_s(\hat{\boldsymbol{x}}) D\Phi(\boldsymbol{y})^{-\top}\hat{\nabla}\hat{G}(\hat{\boldsymbol{\xi}},\hat{\boldsymbol{x}}) \det D\Phi(\boldsymbol{y})\,\mathrm{d}\hat{\boldsymbol{x}} + \\ - \int_{\hat{A}} D\Phi^{-\top}(\boldsymbol{y})\hat{\nabla}\hat{\psi} \cdot D\Phi(\boldsymbol{y})^{-\top}\hat{\nabla}\hat{u}_s(\hat{\boldsymbol{x}})\hat{G}(\hat{\boldsymbol{\xi}},\hat{\boldsymbol{x}}) \det D\Phi(\boldsymbol{y})\,\mathrm{d}\hat{\boldsymbol{x}}, \quad \hat{\boldsymbol{\xi}} \in S^1,\end{aligned} \tag{7.1.5}$$

where $\Phi(\boldsymbol{y})$ is the mapping from the nominal configuration, $\hat{u}_s(\boldsymbol{y},\hat{\boldsymbol{x}}) = \hat{u}(\boldsymbol{y},\hat{\boldsymbol{x}}) - u_i(\Phi(\boldsymbol{y},\hat{\boldsymbol{x}}))$ and $\hat{G}(\hat{\boldsymbol{\xi}},\hat{\boldsymbol{x}}) = G(\hat{\boldsymbol{\xi}},\Phi(\boldsymbol{y},\hat{\boldsymbol{x}}))$. For each $\hat{\boldsymbol{\xi}} \in S^1$, the functional $\hat{F}^*(\hat{\boldsymbol{\xi}})$ satisfies Assumption 5.5.1 because Φ and $\hat{u}_s$ are analytic, and thus Corollaries 6.3.2 and 6.3.3 hold. Moreover, if $\hat{\psi} \in C^2(\overline{\hat{A}})$ and if Φ fulfills Assumption 3.1.2 with $k \geq 2$, integration by parts shows that, for fixed $\hat{\boldsymbol{\xi}} \in S^1$, the functional $\hat{F}^*(\hat{\boldsymbol{\xi}})$ fulfills Assumption 6.3.1 with $n = 0$. In this case, for each realization $\boldsymbol{y}$, we can expect the gain in one order for the finite element convergence as explained in the second part of Corollaries 6.3.2 and 6.3.3.

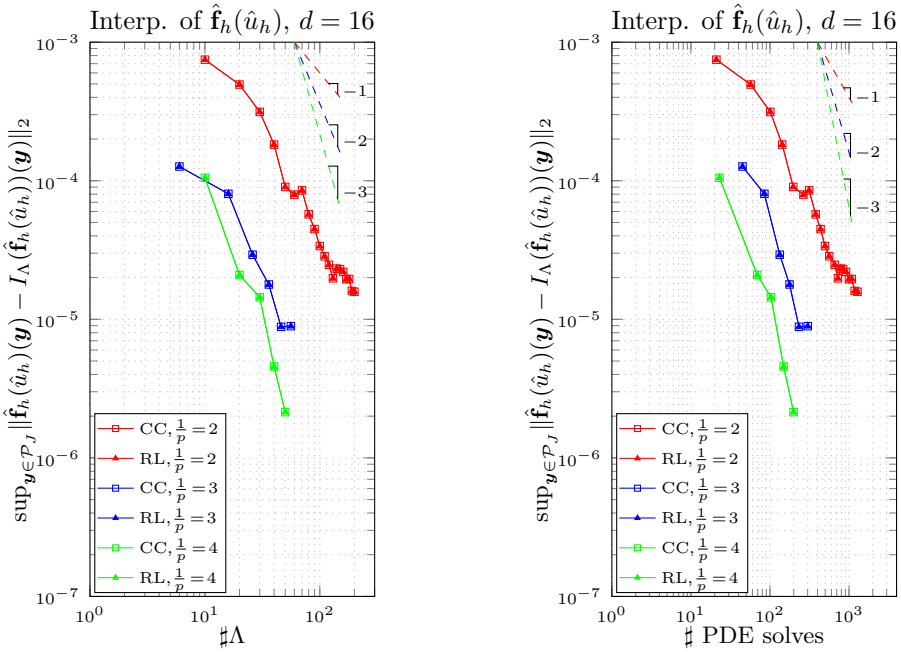

Figure 7.1.8: Comparison of the errors for the interpolated far field Fourier coefficients with respect to the cardinality of the index set Λ (left) and the number of PDE solves (right), using Clenshaw-Curtis and $\mathfrak{R}$-Leja points, for 16 dimensions. Maximal shape variations with respect to r_0 of 22% for $\frac{1}{p} = 2$, 17% for $\frac{1}{p} = 3$ and 15% for $\frac{1}{p} = 4$. Domain mapping (7.1.1).

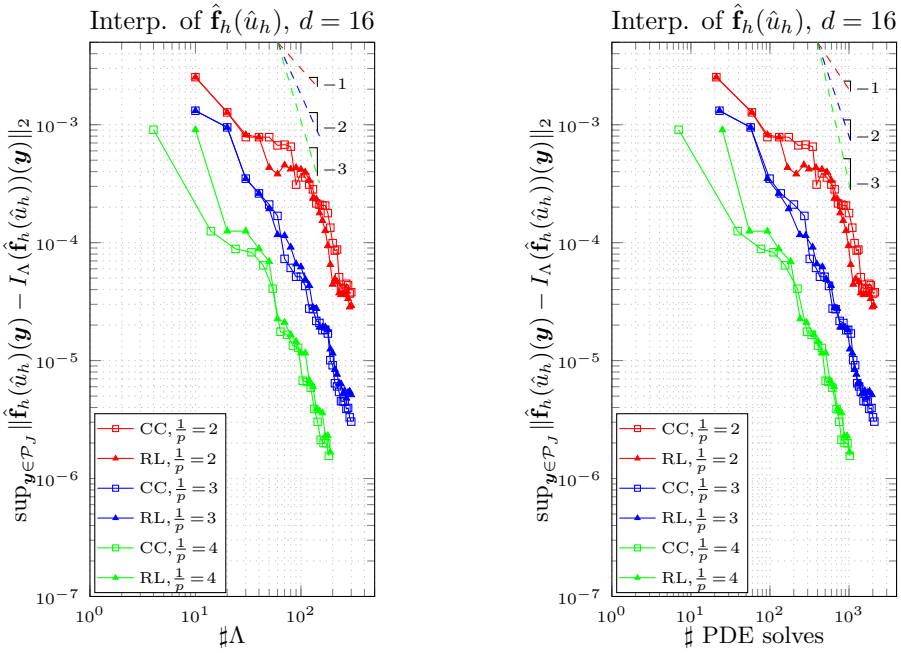

Figure 7.1.9: Comparison of the errors for the interpolated far field Fourier coefficients with respect to the cardinality of the index set Λ (left) and the number of PDE solves (right), using Clenshaw-Curtis and $\mathfrak{R}$-Leja points, for 16 dimensions. Maximal shape variations with respect to r_0 of 22% for $\frac{1}{p} = 2$, 17% for $\frac{1}{p} = 3$ and 15% for $\frac{1}{p} = 4$. Domain mapping (3.1.2) with mollifier (3.1.3).

In the simulations, for the interpolation of $\left|\hat{F}^*(\hat{u}_s(\boldsymbol{y}))\right| = \left|\hat{F}^*(\hat{u}_s(\boldsymbol{y}))(\hat{\boldsymbol{\xi}})\right|$, $\hat{\boldsymbol{\xi}} \in S^1$, we consider the first 11 coefficients in its real Fourier expansion with respect to the angle $\arg(\hat{\boldsymbol{\xi}}) \in [0, 2\pi)$.

Again, we compare three variations of the sparsity parameter: $s_j = c_j = \frac{0.1 r_0}{j^{\frac{1}{p}}}$, $j \geq 1$, for $\frac{1}{p} = 2, 3, 4$; they correpond to maximal shape variations of 22%, 17% and 15% with respect to r_0, respectively.

We have run the simulations using the domain mapping (7.1.1) and using the mapping (3.1.2) with the mollifier (3.1.3).

When using (7.1.1), the annulus $\hat{A}$ has been chosen with inner radius 20nm and outer radius 100nm, and the PML from $R = 100$nm to $R' = 150$nm, with absorption coefficient $\alpha = 0.5$. For each realization, we have considered a 3rd-order finite element space (with 3rd-order boundary approximation), carrying in total 403481 degrees of freedom, of which 37414 are inside the annulus $\hat{A}$. The results in the 16-dimensional case are shown in Figures 7.1.7 and 7.1.8. In 7.1.7, we report the error *estimated* by the algorithm, $\max_{\nu \in \mathcal{N}(\Lambda)} \|\Delta^I_\nu(\hat{\mathbf{f}}_h(\hat{u}_h))\|_\infty$, where $\hat{\mathbf{f}}_h(\hat{u}_h)$ denotes the vector of the approximated 11 Fourier coefficients, and the increments are this time the absolute error increments. Figure 7.1.8 shows instead the error $\sup_{\boldsymbol{y} \in \mathcal{P}_J} \|\hat{\mathbf{f}}_h(\hat{u}_h)(\boldsymbol{y}) - I_\Lambda(\hat{\mathbf{f}}_h(\hat{u}_h))(\boldsymbol{y})\|_2$ approximated by the maximum of the $\|\cdot\|_2$-norm error among 2^{16} realizations coinciding with the quadrature points of the algorithm presented in [Gan16] and [GS16], with again $C = 0.1$ as Walsh coefficient bound. The error has been computed every 10 iterations, with the same rule as in the interpolation of the solution, with $\hat{\mathbf{f}}_h(\hat{u}_h)(\boldsymbol{y})$ and $I_\Lambda(\hat{\mathbf{f}}_h(\hat{u}_h))(\boldsymbol{y})$ computed on the same finite element space.

When using the mapping (3.1.2) with the mollifier (3.1.3), the annulus $\hat{A}$ has inner circle with radius 40nm and outer circle with radius 70nm, and the PML starts at $R = 80$nm and ends at $R' = 110$nm, with absorption coefficient $\alpha = 0.5$. The spatial discretization consists of a 2nd-order finite element space with 2nd-order boundary approximation, with 33277 total degrees of freedom, 13719 of which in the annulus region. The error $\sup_{\boldsymbol{y} \in \mathcal{P}_J} \|\hat{\mathbf{f}}_h(\hat{u}_h)(\boldsymbol{y}) - I_\Lambda(\hat{\mathbf{f}}_h(\hat{u}_h))(\boldsymbol{y})\|_2$, computed with the same criterion as in Figure 7.1.8, is reported in Figure 7.1.9.

The computational cost required for the far field interpolation is very high, because, for each interpolation point, additionally to the whole solution, one has also to compute the integral (7.1.5) for many values of the variable $\hat{\boldsymbol{\xi}}$ (the same number as the Fourier coefficients when using the real-valued Fast Fourier Transform). Hence, this application highlights the importance of developing a parameter-adaptive strategy to use different finite element resolutions for different interpolation points.

7.1.3. Quadrature of the real part of the solution on the nominal configuration

In these experiments we consider the quadrature on the nominal space. As we did for the interpolation, we consider small and large shape variations.

Small variations

The setting is the same as in the interpolation case for small variations, that is same scaling of the coefficients ($s_j = c_j = \frac{0.01 r_0}{j^{\frac{1}{p}}}$, $j \geq 1$, for $\frac{1}{p} = 2, 3, 4$), same finite element space and domain mapping (7.1.1).

Figure 7.1.10 shows, for dimension $2J = 16, 32, 64$ of the parameter space, the comparison of the quadrature error $\sum_{\nu \in \mathcal{N}(\Lambda)} \|\Delta^Q_\nu(\hat{\boldsymbol{\mu}}_h)\|_\infty$ *estimated* by the Algorithm 1 for the different decays of the coefficient sequences (with $\hat{\boldsymbol{\mu}}_h$ the vector of coefficients of the solution with respect to the

finite element basis functions and Ndof=37563); the increments considered are the absolute error increments. Figure 7.1.11 shows, for each variation of the sparsity parameter, the comparison of the *estimated errors* for dimension 16, 32 and 64 of the parameter space.

Figures 7.1.12 and 7.1.13 show instead the behavior of the error $\|\mathcal{I}(\mathrm{Re}\,\hat{u}_h) - Q_\Lambda(\mathrm{Re}\,\hat{u}_h)\|_{H^1(K_R)}$, computed for every iteration. The reference solution used to estimate $\mathcal{I}(\mathrm{Re}\,\hat{u}_h)$ has been computed with the high-order quasi-Monte Carlo algorithm described in [Gan16] and [GS16], using 2^{18} quadrature points and $C = 0.1$ as bound on the Walsh coefficient. Each realization in the computation of the reference solution belongs to the same finite element space as the one used for the realizations of the Smolyak algorithm.

As an example, the estimated mean of the real part of the total field for $\frac{1}{p} = 3$, dimension 16 of the parameter space and Clenshaw-Curtis points is represented in the left plot in Figure 7.1.19; in this picture, the grey annulus coincides with the PML.

Large variations

The setting is the same as for the interpolation of the solution for large variations: same coefficient sequences, same finite element space and mapping (3.1.2) with mollifier (3.1.3).

Figures 7.1.14 and 7.1.15 present the behavior of the error $\|\mathcal{I}(\mathrm{Re}\,\hat{u}_h) - Q_\Lambda(\mathrm{Re}\,\hat{u}_h)\|_{H^1(K_R)}$, comparing the different coefficient decays and the different parameter space dimensions, respectively. The reference solution has been computed using the same finite element space and the high-order quasi-Monte Carlo algorithm described in [Gan16] and [GS16], with 2^{16} quadrature points and Walsh coefficient bound $C = 0.1$.

7.1.4. Quadrature of the modulus of the far field pattern

As we did for the interpolation, we consider the results using the two mappings (7.1.1) and (3.1.2) with (3.1.3). In both cases, the settings are the same as in the interpolation case, and we consider again the first 11 Fourier coefficients.

For the less smooth mapping (7.1.1), Figures 7.1.16 and 7.1.17 show, repectively, the error estimated by the algorithm and the error with respect to the reference solution. The error estimated by the algorithm is $\sum_{\nu\in\Lambda}\|\Delta_\nu^Q(\hat{\mathbf{f}}_h(\hat{u}_h))\|_\infty$, where absolute increments are considered. The error with respect to the reference solution instead, $\|\mathcal{I}(\hat{\mathbf{f}}_h(\hat{u}_h)) - Q_\Lambda(\hat{\mathbf{f}}_h(\hat{u}_h))\|_2$, has been obtained comparing the Smolyak solution with respect to the high-order quasi-Monte Carlo solution [Gan16, GS16], with 2^{16} quadrature points and bound $C = 0.1$ for the Walsh coefficient, with realizations computed on the same finite element space as the one used in the Smolyak algorithm; the error has been computed for each iteration of the adaptive algorithm.

For the mapping (3.1.2) with mollifier (3.1.3), we report in Figure 7.1.18 the error $\|\mathcal{I}(\hat{\mathbf{f}}_h(\hat{u}_h)) - Q_\Lambda(\hat{\mathbf{f}}_h(\hat{u}_h))\|_2$ computed with respect to the reference solution obtained using the same finite element space in the high-order quasi-Monte Carlo quadrature rule [Gan16, GS16] with 2^{16} points and $C = 0.1$ as Walsh coefficient bound.

The right plot in Figure 7.1.19 represents the modulus of the far field pattern computed from the estimated mean of the Fourier coefficients, for $\frac{1}{p} = 2, 3, 4$, using Clenshaw-Curtis points and the mapping (7.1.1). In the plot, we have denoted by 'nominal' the far field pattern that is obtained when the scatterer has the nominal radius r_0. We can see that the mean values for different values of $\frac{1}{p}$ and for the nominal case are nearly coinciding, as one may expect from the fact that the far field functional is not sensitive to small variations in the shape of the scatterer.

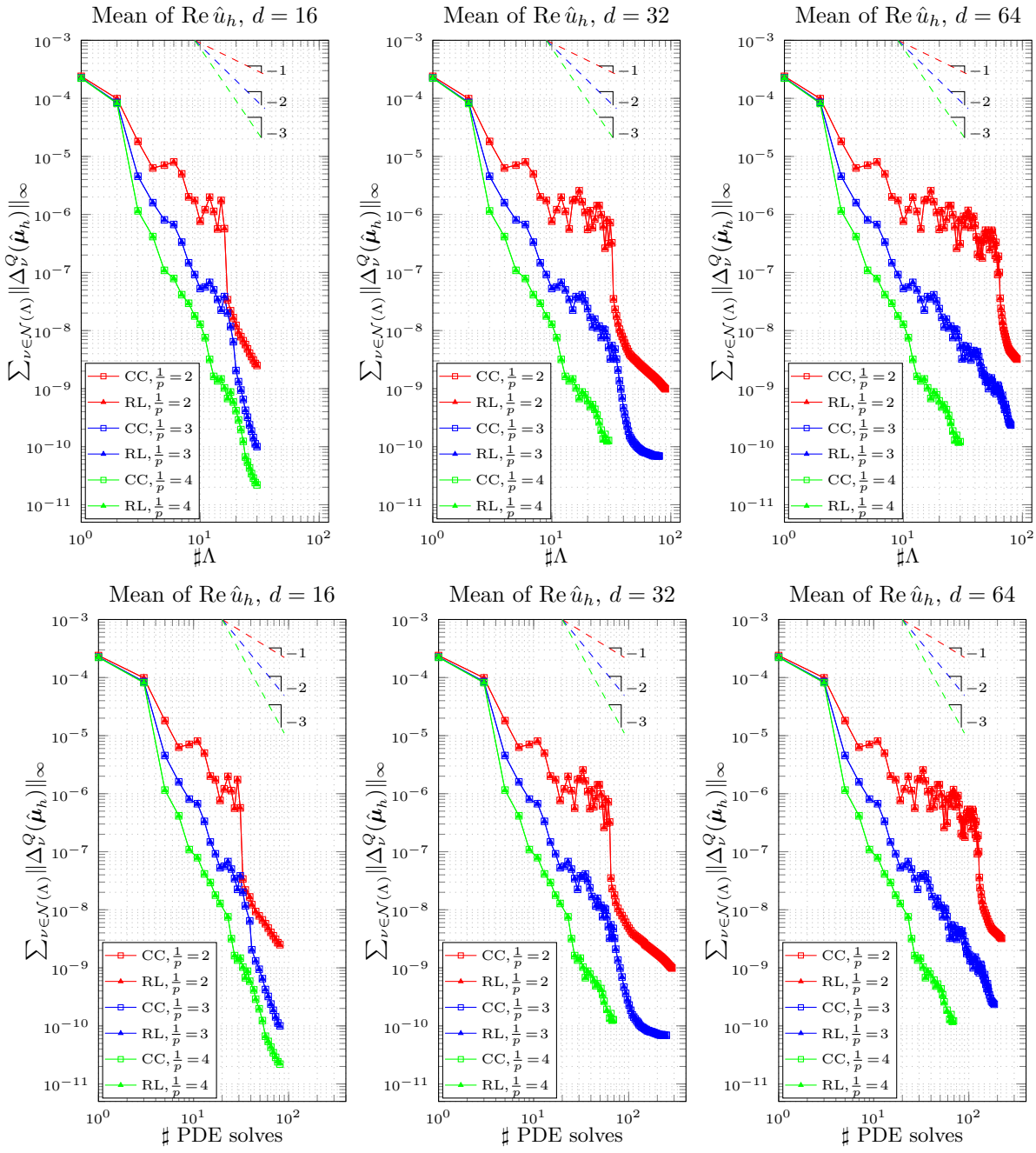

Figure 7.1.10: Comparison of the *estimated errors* for the quadrature of the solution with respect to the cardinality of the index set Λ (top) and to the number of PDE solves (bottom), using Clenshaw-Curtis and $\mathfrak{R}$-Leja points, for 16 (left), 32 (middle) and 64 (right) dimensions. The three dashed lines on the top of each plot correspond to the convergence rates of 1 (red), 2 (blue) and 3 (green). Maximal shape variations with respect to r_0 of about 2.3% for $\frac{1}{p} = 2$, 1.7% for $\frac{1}{p} = 3$ and 1.5% for $\frac{1}{p} = 4$. Domain mapping (7.1.1).

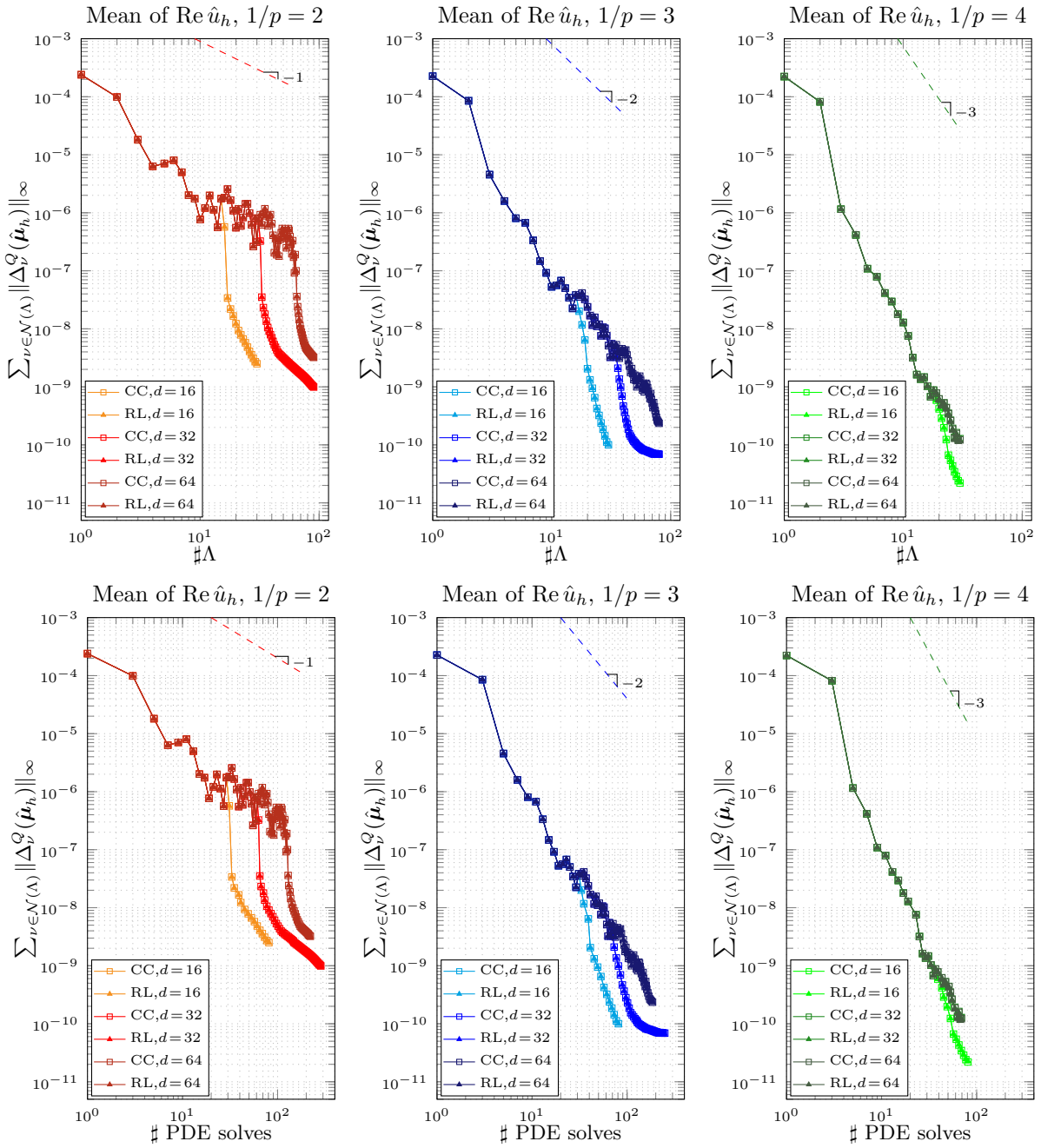

Figure 7.1.11: Comparison of the *estimated errors* for the quadrature of the solution with respect to the cardinality of the index set Λ (top) and to the number of PDE solves (bottom), using Clenshaw-Curtis and $\mathfrak{R}$-Leja points, for variations of the sparsity parameter $\frac{1}{p} = 2$ (left), 3 (middle) and 4 (right). Maximal shape variations with respect to r_0 of about 2.3% for $\frac{1}{p} = 2$, 1.7% for $\frac{1}{p} = 3$ and 1.5% for $\frac{1}{p} = 4$. Domain mapping (7.1.1).

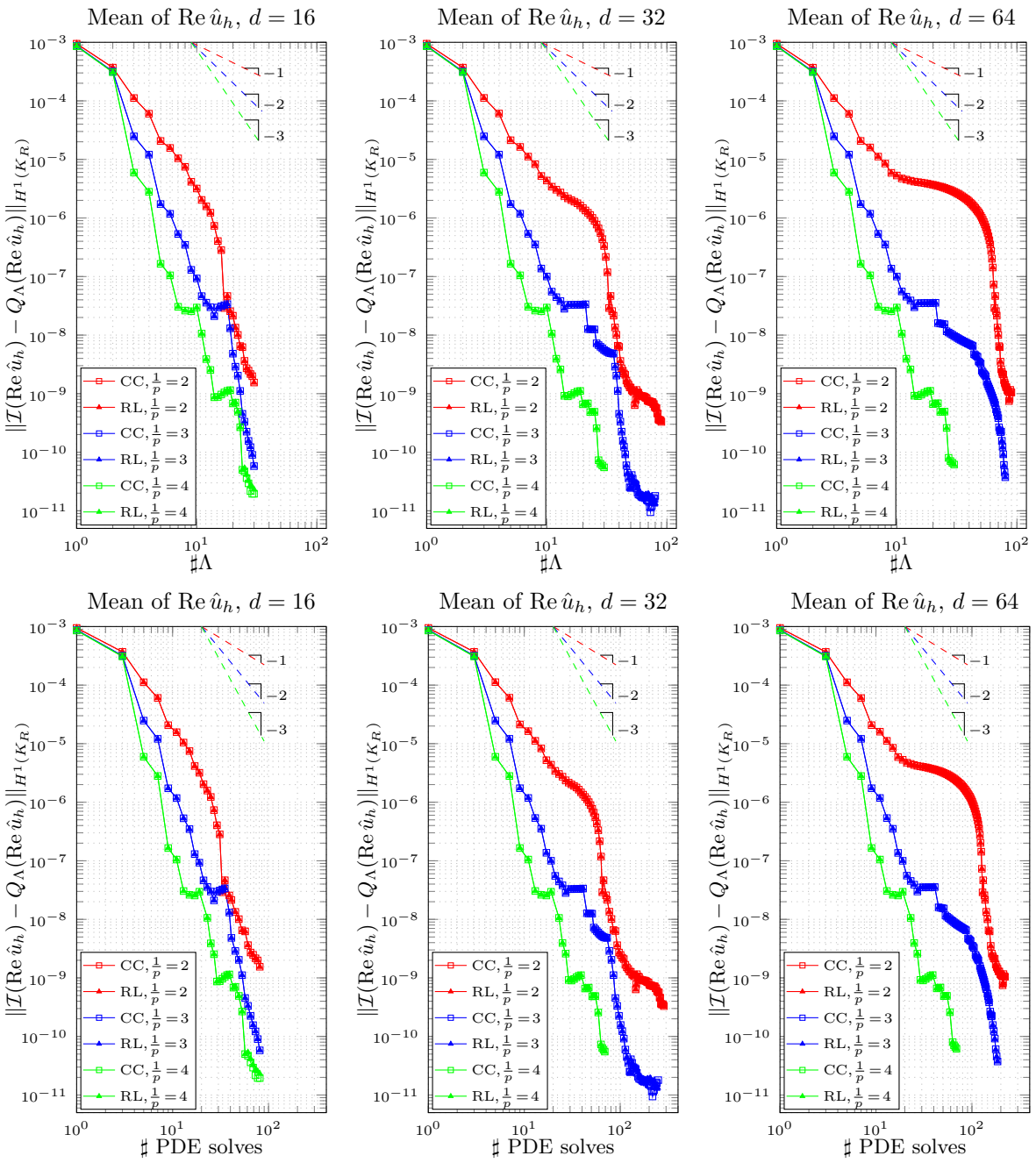

Figure 7.1.12: Comparison of the errors for the quadrature of the real part of the solution with respect to the cardinality of the index set Λ (top) and to the number of PDE solves (bottom), using Clenshaw-Curtis and $\mathfrak{R}$-Leja points, for 16 (left), 32 (middle) and 64 (right) dimensions. Maximal shape variations with respect to r_0 of about 2.3% for $\frac{1}{p} = 2$, 1.7% for $\frac{1}{p} = 3$ and 1.5% for $\frac{1}{p} = 4$. Domain mapping (7.1.1).

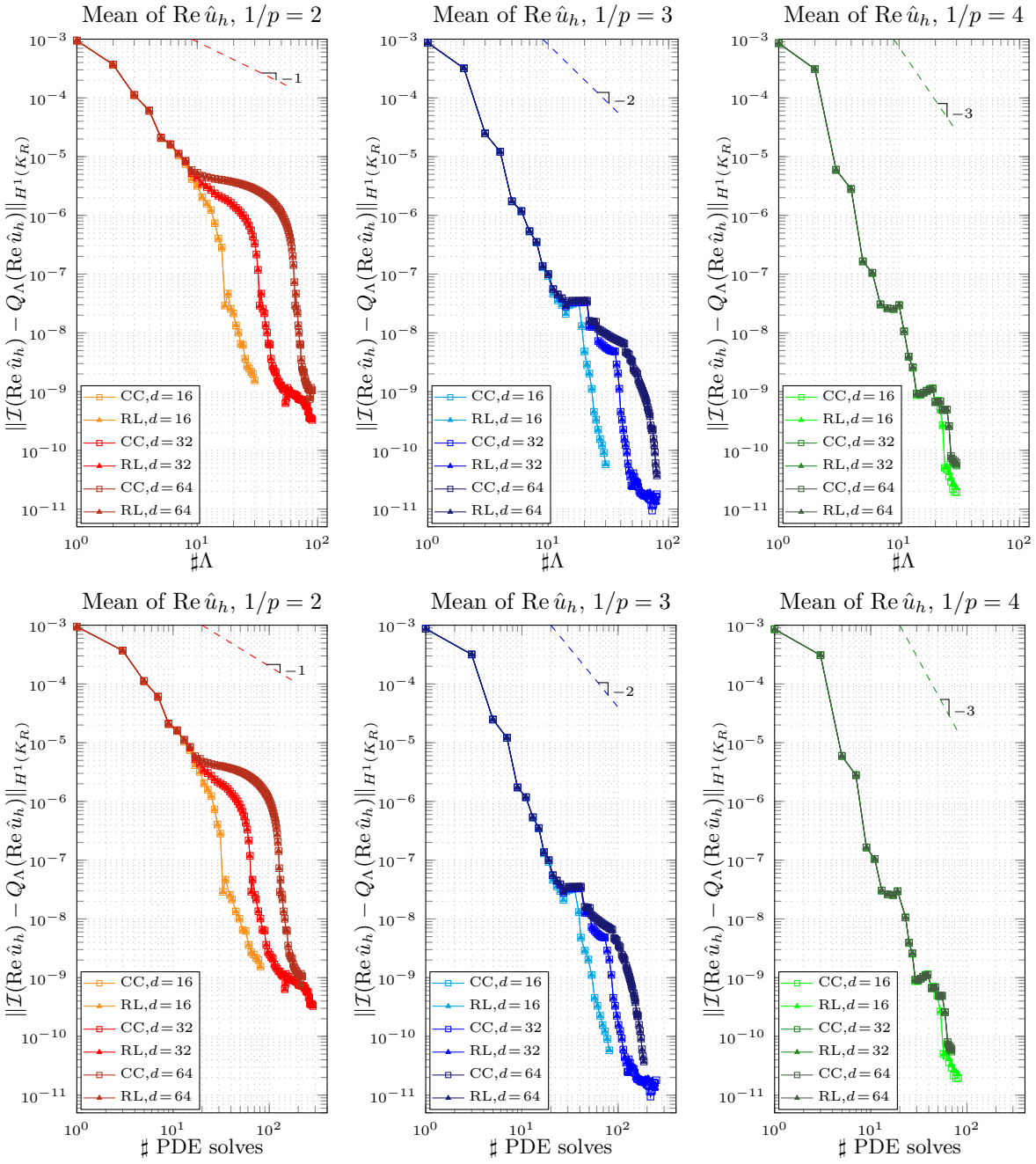

Figure 7.1.13: Comparison of the errors for the quadrature of the real part of the solution with respect to the cardinality of the index set Λ (top) and to the number of PDE solves (bottom), using Clenshaw-Curtis and $\mathfrak{R}$-Leja points, for variations of the sparsity parameter $\frac{1}{p} = 2$ (left), 3 (middle) and 4 (right). Maximal shape variations with respect to r_0 of about 2.3% for $\frac{1}{p} = 2$, 1.7% for $\frac{1}{p} = 3$ and 1.5% for $\frac{1}{p} = 4$. Domain mapping (7.1.1).

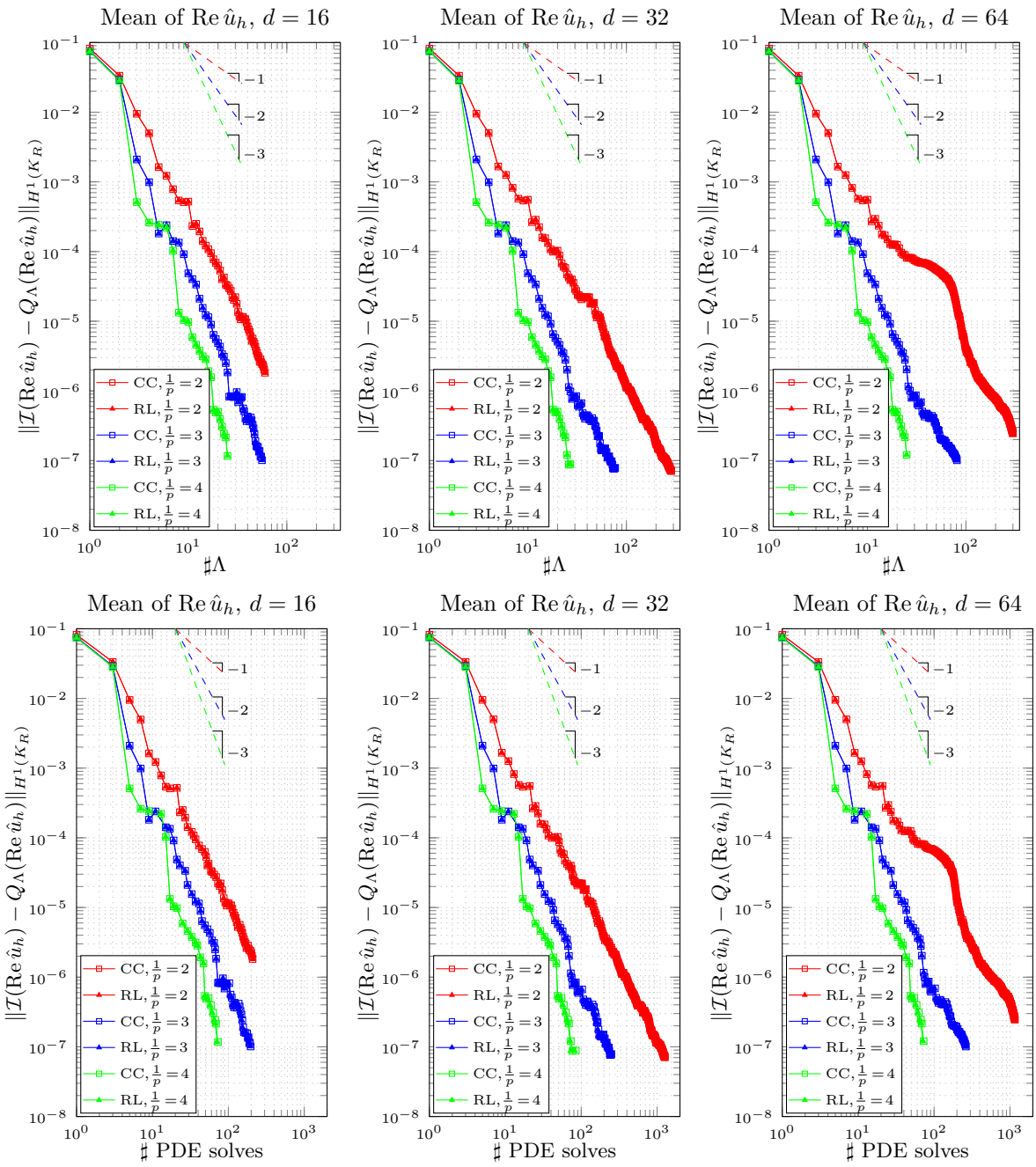

Figure 7.1.14: Comparison of the errors for the quadrature of the real part of the solution with respect to the cardinality of the index set Λ (top) and to the number of PDE solves (bottom), using Clenshaw-Curtis and $\mathfrak{R}$-Leja points, for 16 (left), 32 (middle) and 64 (right) dimensions. Maximal shape variations with respect to r_0 of about 22% for $\frac{1}{p} = 2$, 17% for $\frac{1}{p} = 3$ and 15% for $\frac{1}{p} = 4$. Domain mapping (3.1.2) with mollifier (3.1.3).

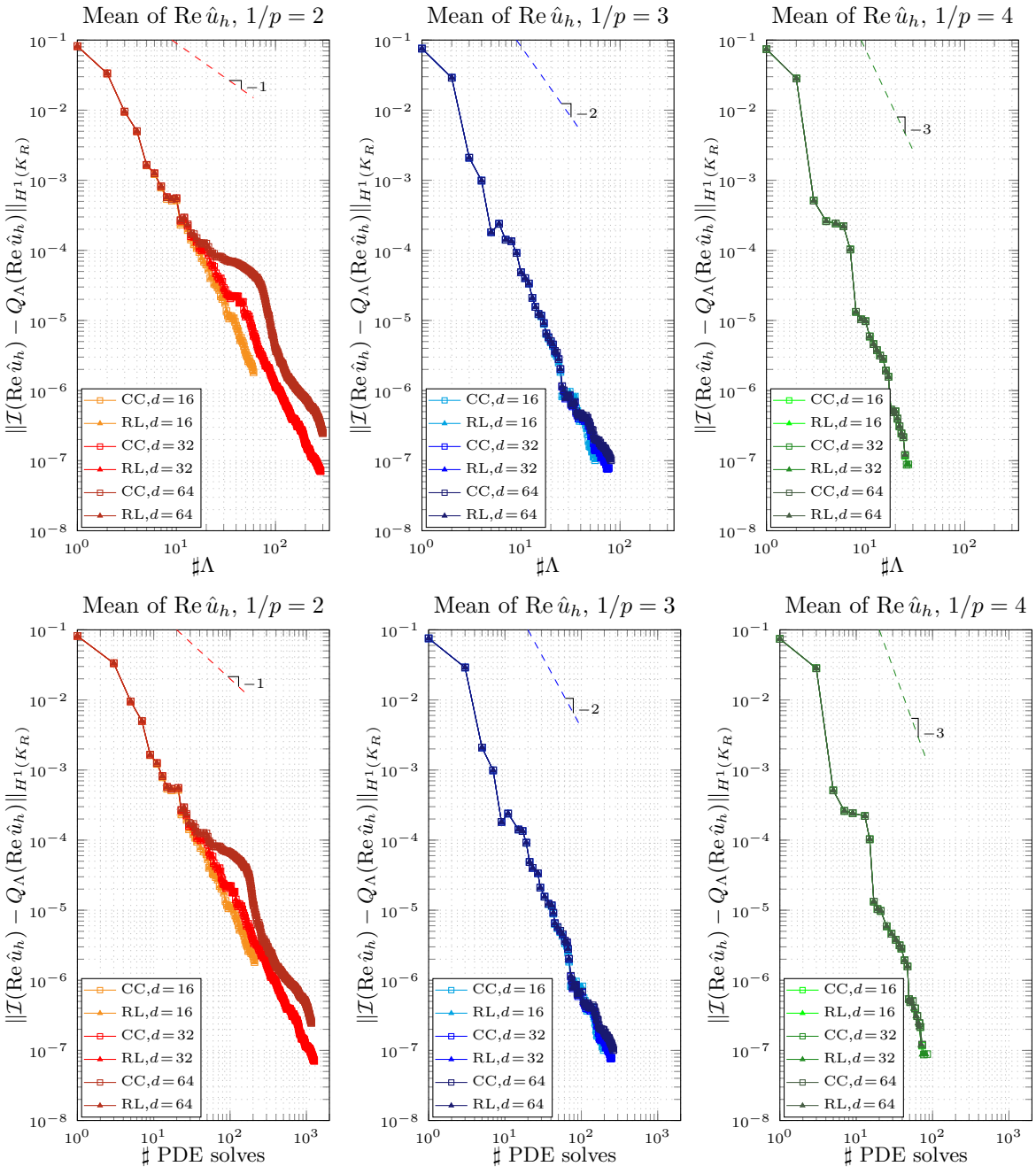

Figure 7.1.15: Comparison of the errors for the quadrature of the real part of the solution with respect to the cardinality of the index set Λ (top) and to the number of PDE solves (bottom), using Clenshaw-Curtis and $\mathfrak{R}$-Leja points, for variations of the sparsity parameter $\frac{1}{p} = 2$ (left), 3 (middle) and 4 (right). Maximal shape variations with respect to r_0 of about 22% for $\frac{1}{p} = 2$, 17% for $\frac{1}{p} = 3$ and 15% for $\frac{1}{p} = 4$. Domain mapping (3.1.2) with mollifier (3.1.3).

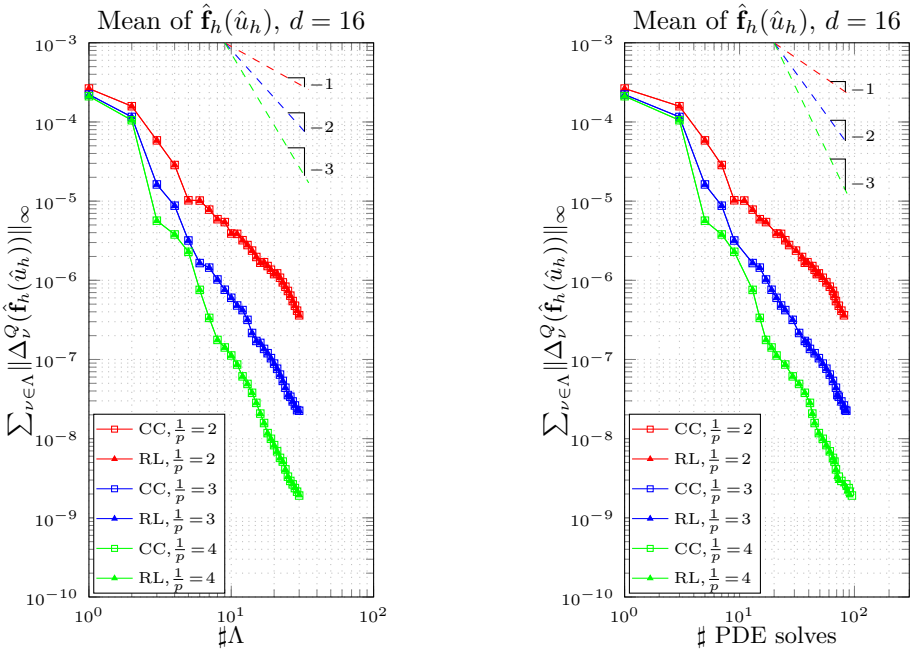

Figure 7.1.16: Comparison of the *estimated errors* for the quadrature of the far field Fourier coefficients with respect to the cardinality of the index set Λ (left) and the number of PDE solves (right), using Clenshaw-Curtis and $\mathfrak{R}$-Leja points, for 16 dimensions. The three dashed lines on the top of each plot correspond to the convergence rates of 1 (red), 2 (blue) and 3 (green). Maximal shape variations with respect to r_0 of 22% for $\frac{1}{p} = 2$, 17% for $\frac{1}{p} = 3$ and 15% for $\frac{1}{p} = 4$. Domain mapping (7.1.1).

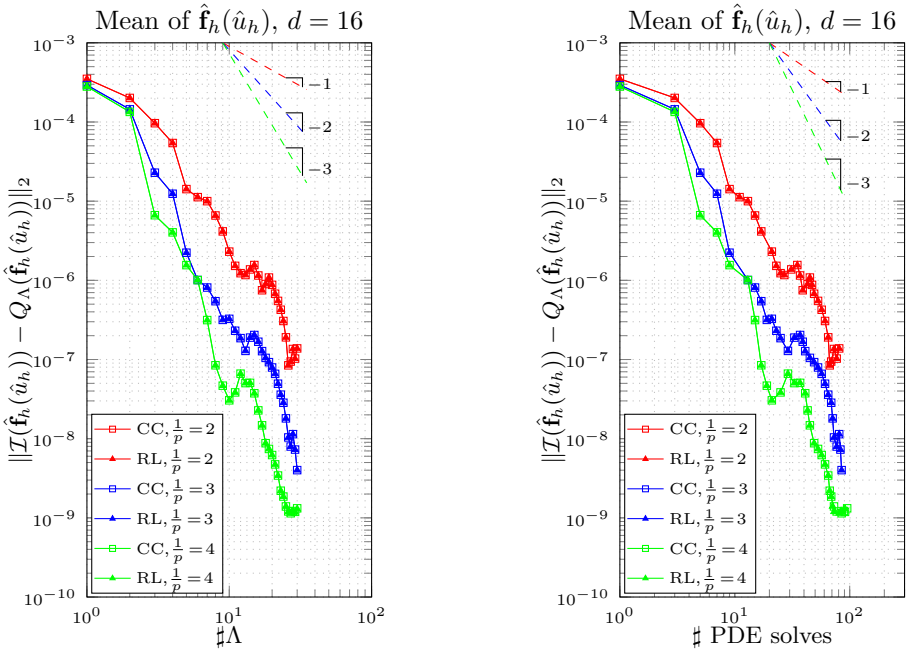

Figure 7.1.17: Comparison of the errors for the quadrature of the far field Fourier coefficients with respect to the cardinality of the index set Λ (left) and the number of PDE solves (right), using Clenshaw-Curtis and $\mathfrak{R}$-Leja points, for 16 dimensions. Maximal shape variations with respect to r_0 of 22% for $\frac{1}{p} = 2$, 17% for $\frac{1}{p} = 3$ and 15% for $\frac{1}{p} = 4$. Domain mapping (7.1.1).

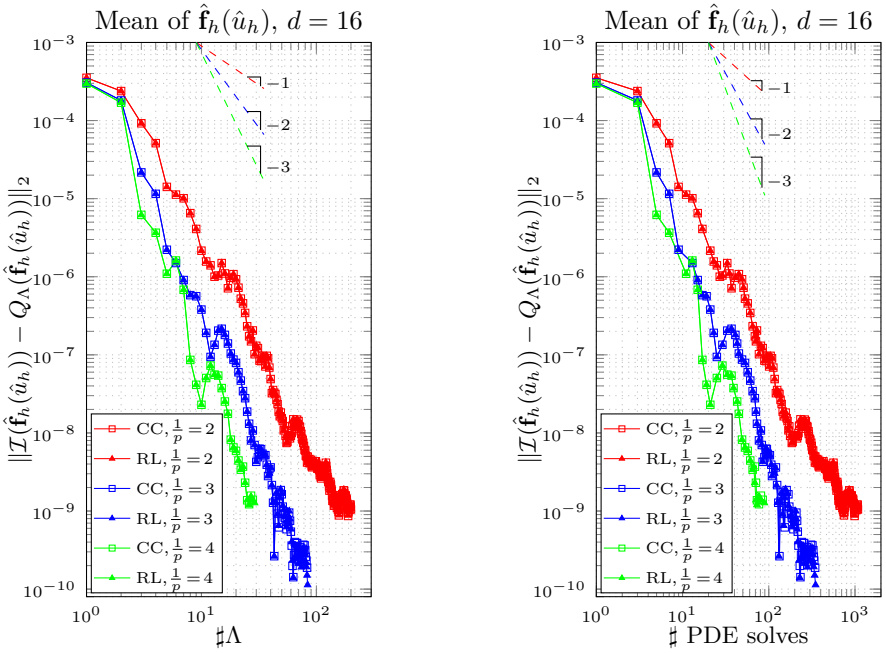

Figure 7.1.18: Comparison of the errors for the quadrature of the far field Fourier coefficients with respect to the cardinality of the index set Λ (left) and the number of PDE solves (right), using Clenshaw-Curtis and $\mathfrak{R}$-Leja points, for 16 dimensions. Maximal shape variations with respect to r_0 of 22% for $\frac{1}{p} = 2$, 17% for $\frac{1}{p} = 3$ and 15% for $\frac{1}{p} = 4$. Domain mapping (3.1.2) with mollifier (3.1.3).

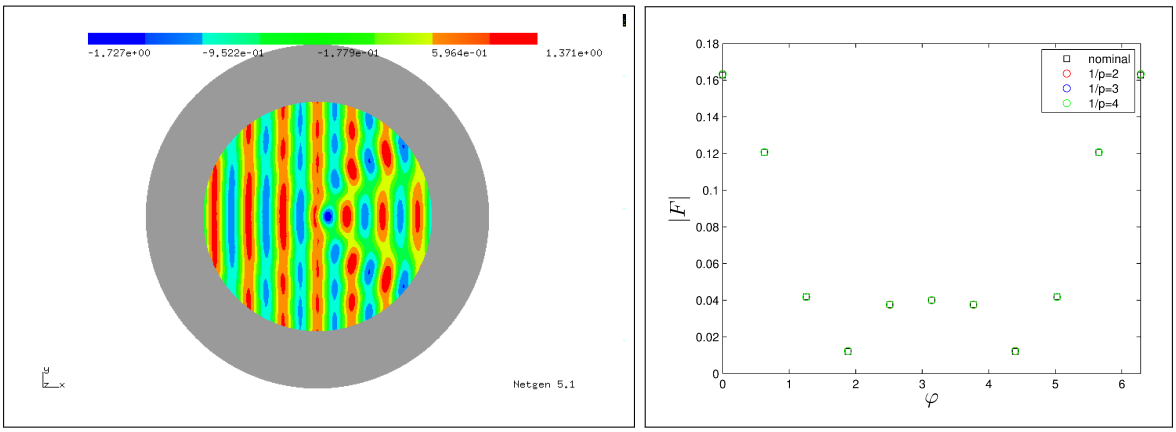

Figure 7.1.19: Particle in free space, 16 dimensions, Clenshaw-Curtis points: estimated mean of the real part of the solution when $\frac{1}{p} = 3$ (left) and of the far field modulus for $\frac{1}{p} = 2, 3, 4$ (right). Maximal shape variations with respect to r_0: 1.7% for the solution (left), $15 - 22\%$ for the far field (right). Domain mapping (7.1.1).

7.2. Particle on substrate

The incident wave u_i has frequency $f = 10^4$THz and is coming from the left with an incidence angle of $\frac{\pi}{4}$ with respect to the substrate surface ($\boldsymbol{d} = (\frac{\sqrt{2}}{2}, \frac{\sqrt{2}}{2})$). The scatterer is a dielectric with relative permittivity $\varepsilon_2 = 2$. The substrate, considered to be of infinite extension, is a dielectric with relative permittivity $\varepsilon_{sub} = 3$, and the medium above it is air ($\varepsilon_1 = 1$). Thus, to be precise, the coefficient κ^2 in (1.0.2) is equal to κ_0^2 in air, $\kappa_0^2\varepsilon_2$ inside the scatterer and $\kappa_0^2\varepsilon_{sub}$ in the substrate. In all experiments, the PML starts at $R = 100$nm and ends at $R' = 150$nm, with absorption coefficient $\alpha = 0.5$ [CM98]. In all cases, the domain mapping (7.1.1) is used, with $r_0(\varphi)$ replaced by $\tilde{r}(\boldsymbol{y}, \varphi)$ as defined in (3.1.5).

All the convergence plots reported in this section show the error *estimated* by the algorithm, due to the unavailability, for each case considered, of a reference solution.

Interpolation of the real part of the solution on the nominal configuration

For the expansion of the stochastic radius (3.1.6), we consider again the three different values $\frac{1}{p} = 2, 3, 4$ for the sparsity parameter, and dimension 16, 32 and 64 of the parameter space. In particular, the coefficients are given by $s_j = \frac{0.1 r_0}{j^{\frac{1}{p}}}$, $j \geq 1$, and $\alpha_1 = \alpha_2 = \frac{1}{4}$ for the displacement of the two endpoints A and B (see (3.1.4)). These parameters lead to a maximal shape variation of 41%, 37% and 36% with respect to r_0 for $\frac{1}{p} = 2, 3, 4$, respectively (for all the three dimensions of the parameter space considered).

For each PDE solve, a finite element space of globally continuous, piecewise 2nd-order ansatz functions on an unstructured triangular mesh has been used, together with a 2nd-order boundary approximation. The total number of degrees of freedom is 41877, of which 35694 excluding the PML region. Again, as Q.o.I. we consider only the part of the solution that is not contained in the PML.

Figure 7.2.1 shows the *estimated* interpolation error $\max_{\nu \in \mathcal{N}(\Lambda)} \|\Delta_\nu^I(\hat{\boldsymbol{\mu}}_h)\|$ for each of the dimensions of the parameter space. Figure 7.2.2 shows, for each value of the sparsity parameter, the comparison of the *estimated error* curves for different dimensions of the parameter space. The increments $\|\Delta_\nu^I(\hat{\boldsymbol{\mu}}_h)\|$, $\nu \in \Lambda$, are the relative increments with respect to $\|\Delta_0^I(\hat{\boldsymbol{\mu}}_h)\|_\infty = \|\hat{\boldsymbol{\mu}}_h(\boldsymbol{y} = \boldsymbol{0})\|_\infty$.

Interpolation of the modulus of the far field pattern

In the presence of a substrate of infinite extension, it is shown in [HS] that, to compute the far field pattern, we can proceed in the same way as we did in the free space case, using formula (7.1.4) for $\hat{\boldsymbol{\xi}} \in [0, \pi]$ (with $\hat{\boldsymbol{\xi}}$ the angle with respect to the substrate surface, starting from the right). The Green's function for the far field is given, in this case, by

$$G(\hat{\boldsymbol{\xi}}, \boldsymbol{x}) = \begin{cases} e^{-i(\kappa_{1,x_1} x_1 + \kappa_{1,x_2} x_2)} + \mathrm{R}\, e^{-i(\kappa_{1,x_1} x_1 - \kappa_{1,x_2} x_2)} & \text{if } \boldsymbol{x} = (x_1, x_2) \text{ is in the upper half plane (air),} \\ \mathrm{T} e^{-i(\kappa_{sub,x_1} x_1 + \kappa_{sub,x_2} x_2)} & \text{if } \boldsymbol{x} = (x_1, x_2) \text{ is in the lower half plane (substrate),} \end{cases} \tag{7.2.1}$$

with κ_{1,x_1}, κ_{1,x_2} the two components of the wavevector $\boldsymbol{\kappa}_1 = \kappa_1 \boldsymbol{d}$ (and similarly for $\boldsymbol{\kappa}_{sub}$), $\mathrm{R} = \frac{\kappa_{1,x_2} - \kappa_{sub,x_2}}{\kappa_{1,x_2} + \kappa_{sub,x_2}}$ the reflection coefficient and $\mathrm{T} = 1 - \mathrm{R}$ the transmission coefficient; being

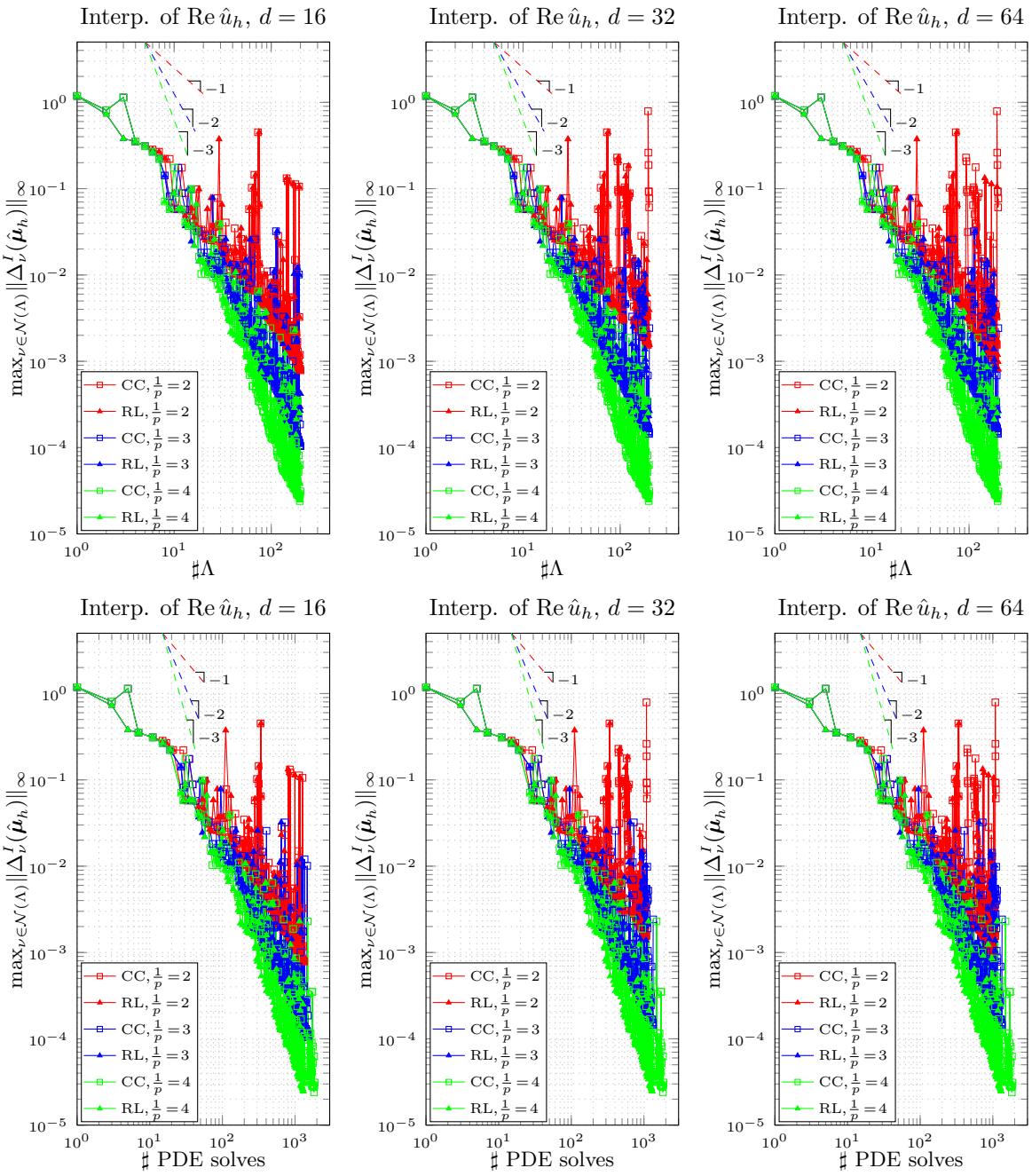

Figure 7.2.1: Comparison of the *estimated errors* for the interpolated solution with respect to the cardinality of the index set Λ (top) and to the number of PDE solves (bottom), using Clenshaw-Curtis and $\mathfrak{R}$-Leja points, for 16 (left), 32 (middle) and 64 (right) dimensions. The three dashed lines on the top of each plot correspond to the convergence rates of 1 (red), 2 (blue) and 3 (green). Maximal shape variations with respect to r_0 of 41% for $\frac{1}{p} = 2$, 37% for $\frac{1}{p} = 3$ and 36% for $\frac{1}{p} = 4$. Domain mapping (7.1.1) with r_0 replaced by $\tilde{r}$.

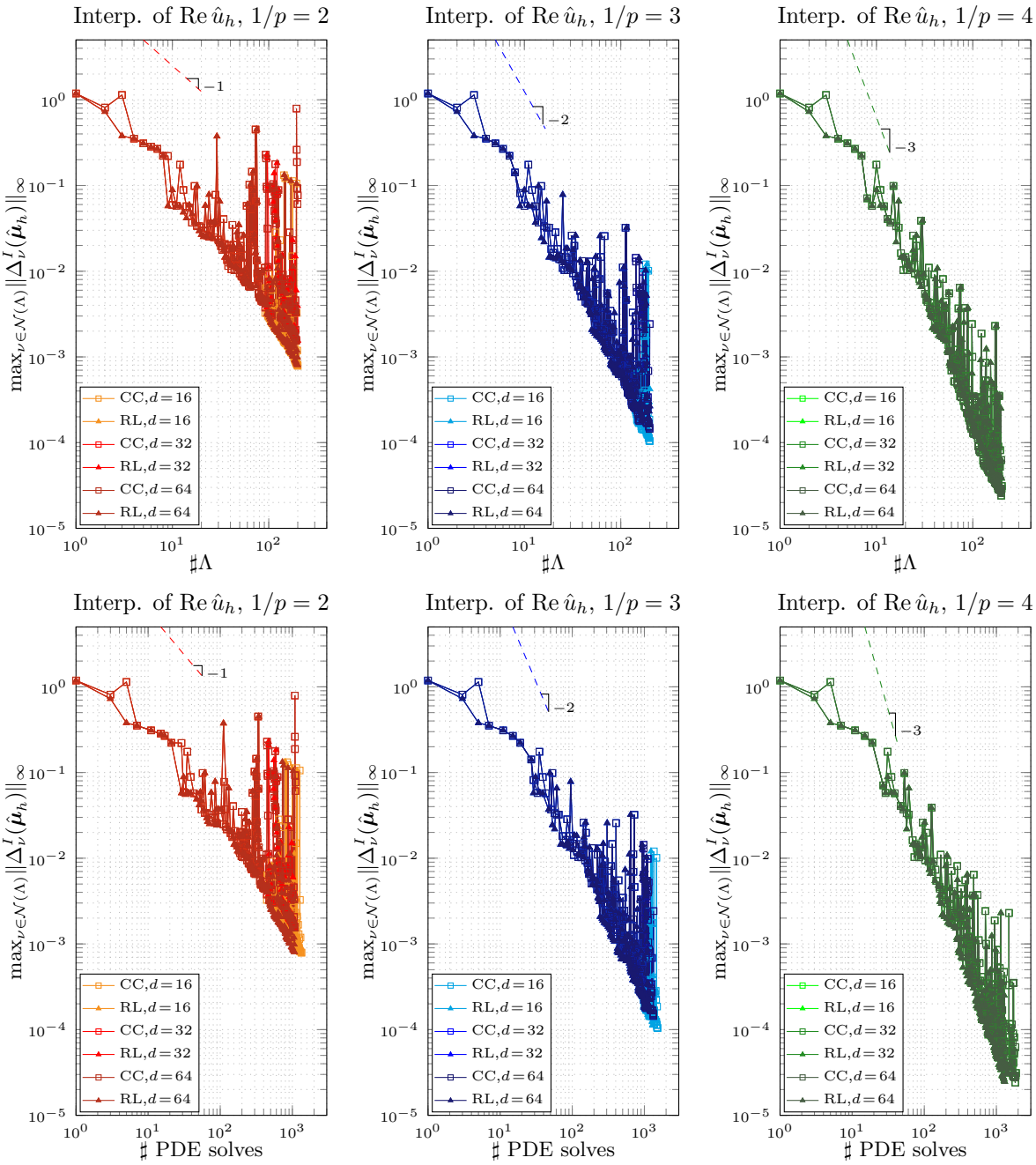

Figure 7.2.2: Comparison of the *estimated errors* for the interpolated solution with respect to the cardinality of the index set Λ (top) and to the number of PDE solves (bottom), using Clenshaw-Curtis and $\mathfrak{R}$-Leja points, for variations of the sparsity parameter $\frac{1}{p} = 2$ (left), 3 (middle) and 4 (right). Maximal shape variations with respect to r_0 of 41% for $\frac{1}{p} = 2$, 37% for $\frac{1}{p} = 3$ and 36% for $\frac{1}{p} = 4$. Domain mapping (7.1.1) with r_0 replaced by $\tilde{r}$.

in the TE case, we have $\kappa_{sub,x_1} = \kappa_{1,x_1}$. We use the same normalizing constant C_F as in the free space case, and the volume-based formula (7.1.5) on the nominal configuration.

As quantity to interpolate, we consider 12 equispaced points between $[0, \pi]$, i.e. $\hat{\boldsymbol{\xi}}_j = j\frac{\pi}{11}$ for $j = 0, \dots, 11$.

The scaling of the coefficients in the stochastic radius expansion is the same that we have used for the interpolation of the solution ($s_j = \frac{0.1 r_0}{j^{\frac{1}{p}}}$, $j \geq 1$, $\alpha_1 = \alpha_2 = \frac{1}{4}$). When using the same finite element space as the one used for the interpolation of the solution, though, we could observe very poor convergence. Thus, we have used a finer mesh and again 2nd-order finite elements with 2nd-order boundary approximation. The total number of degrees of freedom is 199325, of which 112391 in the integration region $\hat{A}$, which has inner radius 20nm and outer radius 80nm.

The results for the error *estimated* by the algorithm are shown in Figure 7.2.3 (with $\hat{\mathbf{f}}_h(\hat{u}_h)$ the vector of the approximated values of the far field modulus computed at the 12 sampling angles). The increments $\|\Delta^I_\nu(\hat{\mathbf{f}}_h(\hat{u}_h))\|_\infty$, $\nu \in \Lambda$, are relative to the initial increment $\|\Delta^I_0(\hat{\mathbf{f}}_h(\hat{u}_h))\|_\infty = \|\hat{\mathbf{f}}_h(\hat{u}_h)(\boldsymbol{y} = \mathbf{0})\|_\infty$. Due to the highly oscillatory behavior of the estimated error, we present two separate plots for the Clenshaw-Curtis and the $\mathfrak{R}$-Leja points.

Quadrature of the real part of the solution on the nominal configuration

We consider the quadrature of the solution in nominal coordinates, as in the free space case. The setting (scaling of the coefficients and finite element space) is the same as for the interpolation case, except that here the increments for the error estimation are the absolute error increments. Figure 7.2.4 shows the behavior of the *estimated* error comparing the different coefficient decays for each dimension of the parameter space. Figure 7.2.5 compares, for each variation of the sparsity parameter, the performance of the algorithm for dimension 16, 32 and 64 of the parameter space.

As an example, the left plot in Figure 7.2.7 shows the estimated mean for the real part of the total field for $\frac{1}{p} = 3$, dimension 16 of the parameter space and Clenshaw-Curtis points.

Quadrature of the modulus of the far field pattern

We have seen that for the interpolation of the far field pattern we had to consider a finer finite element space than the one used for the interpolation (and quadrature) of the solution. For the quadrature of the far field pattern, instead, the finite element space used for the interpolation of the solution was sufficient. The integration region $\hat{A}$ has inner radius 20nm and outer radius 80nm, and it carries 20401 degrees of freedom.

The Q.o.I. is the same as in the interpolation case, that is 12 point evaluations on the unit circle, and we consider again $\frac{1}{p} = 2, 3, 4$ and 16 dimensions in the parameter space.

The results with the *estimated* error are shown in Figure 7.2.6. The increments $\|\Delta^Q_\nu(\hat{\mathbf{f}}_h(\hat{u}_h))\|_\infty$ are the absolute error increments.

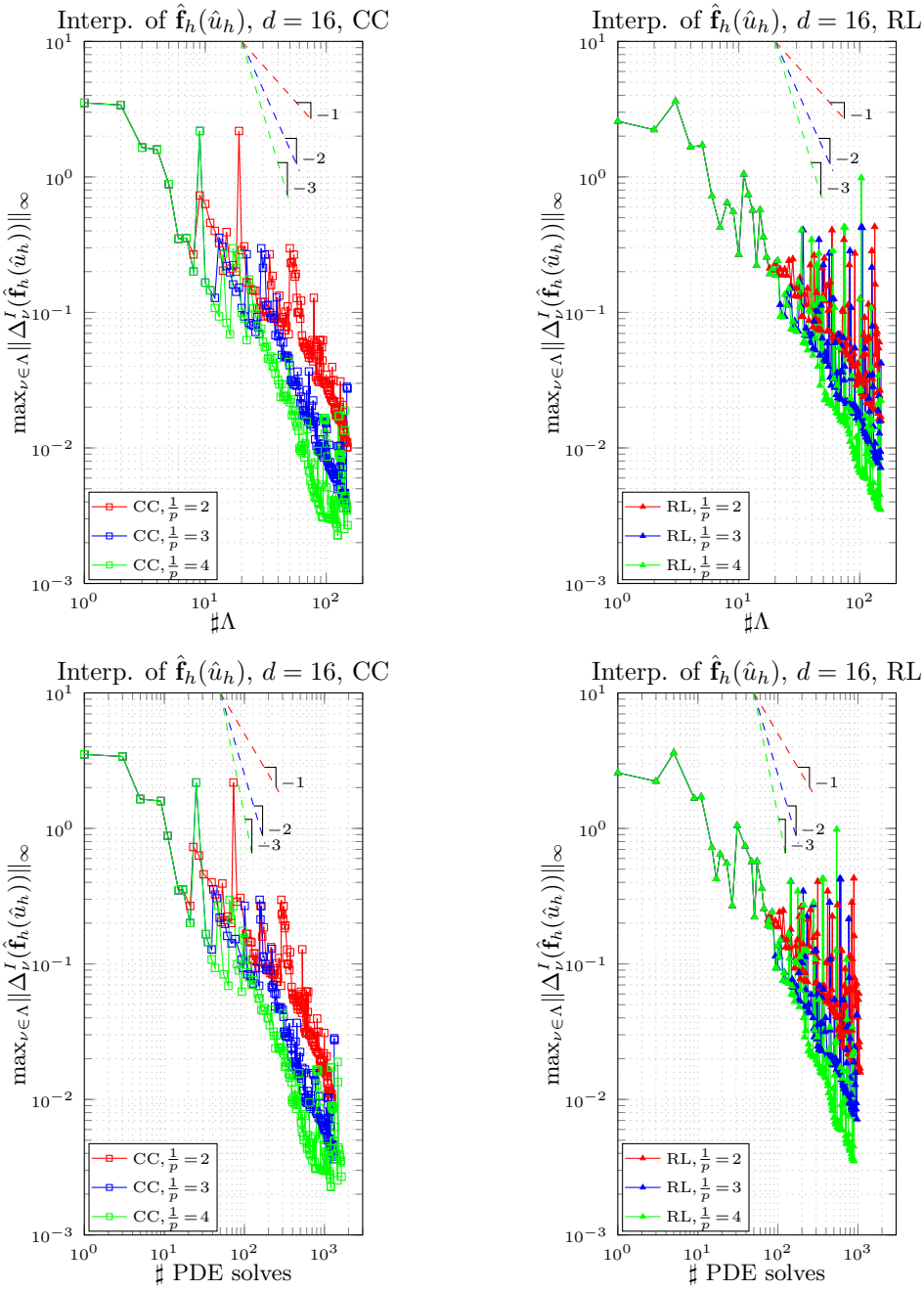

Figure 7.2.3: Comparison of the *estimated errors* for the interpolation of the values of the far field modulus with respect to the cardinality of the index set Λ (top) and the number of PDE solves (bottom), using Clenshaw-Curtis (left) and $\mathfrak{R}$-Leja points (right), for 16 dimensions. The three dashed lines on the top of each plot correspond to the convergence rates of 1 (red), 2 (blue) and 3 (green). Maximal shape variations with respect to r_0 of 41% for $\frac{1}{p} = 2$, 37% for $\frac{1}{p} = 3$ and 36% for $\frac{1}{p} = 4$. Domain mapping (7.1.1) with r_0 replaced by $\tilde{r}$.

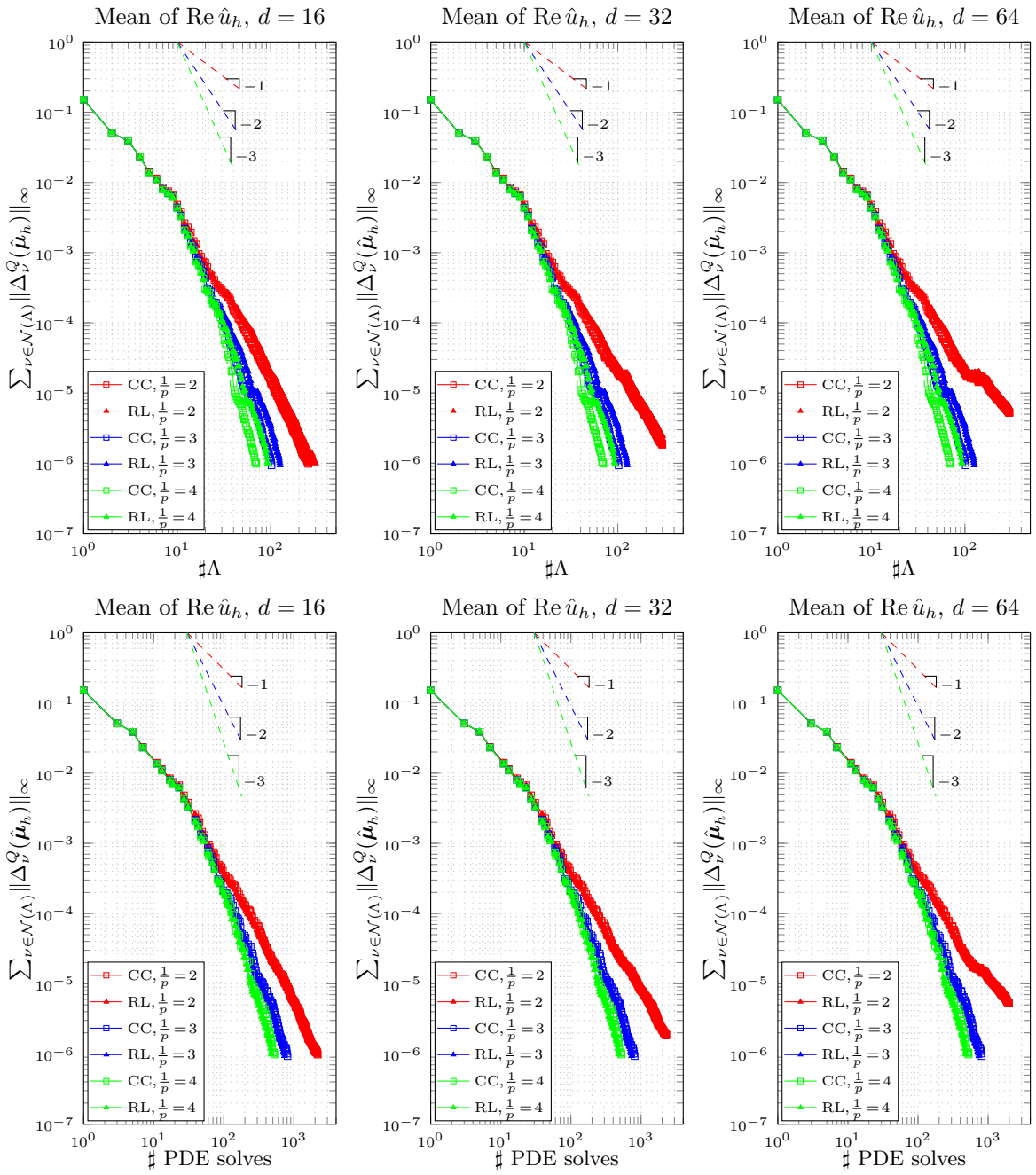

Figure 7.2.4: Comparison of the *estimated errors* for the quadrature of the solution with respect to the cardinality of the index set Λ (top) and to the number of PDE solves (bottom), using Clenshaw-Curtis and $\mathfrak{R}$-Leja points, for 16 (left), 32 (middle) and 64 (right) dimensions. The three dashed lines on the top of each plot correspond to the convergence rates of 1 (red), 2 (blue) and 3 (green). Maximal shape variations with respect to r_0 of 41% for $\frac{1}{p} = 2$, 37% for $\frac{1}{p} = 3$ and 36% for $\frac{1}{p} = 4$. Domain mapping (7.1.1) with r_0 replaced by $\tilde{r}$.

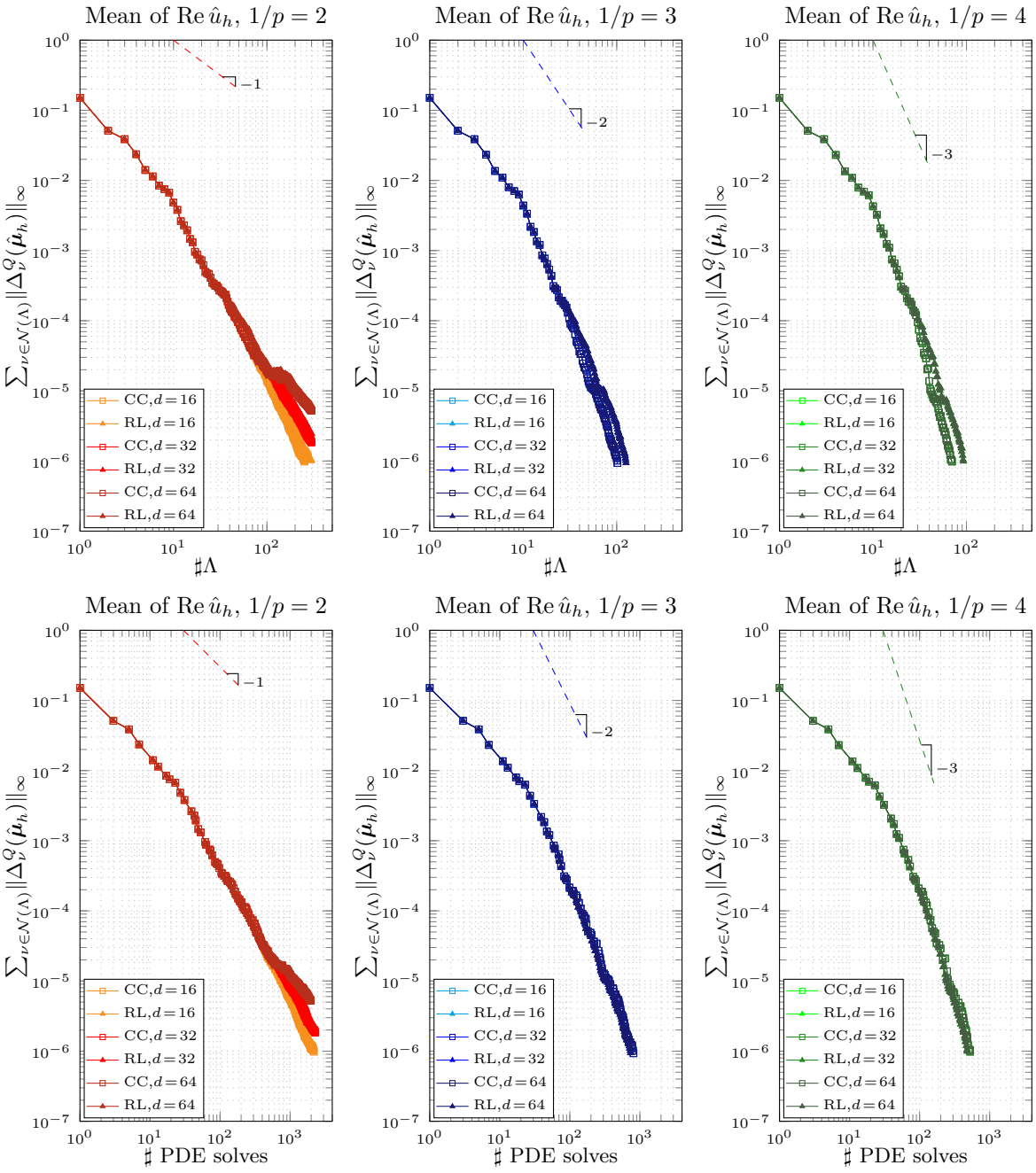

Figure 7.2.5: Comparison of the *estimated errors* for the quadrature of the solution with respect to the cardinality of the index set Λ (top) and to the number of PDE solves (bottom), using Clenshaw-Curtis and $\mathfrak{R}$-Leja points, for variations of the sparsity parameter $\frac{1}{p} = 2$ (left), 3 (middle) and 4 (right). Maximal shape variations with respect to r_0 of 41% for $\frac{1}{p} = 2$, 37% for $\frac{1}{p} = 3$ and 36% for $\frac{1}{p} = 4$. Domain mapping (7.1.1) with r_0 replaced by $\tilde{r}$.

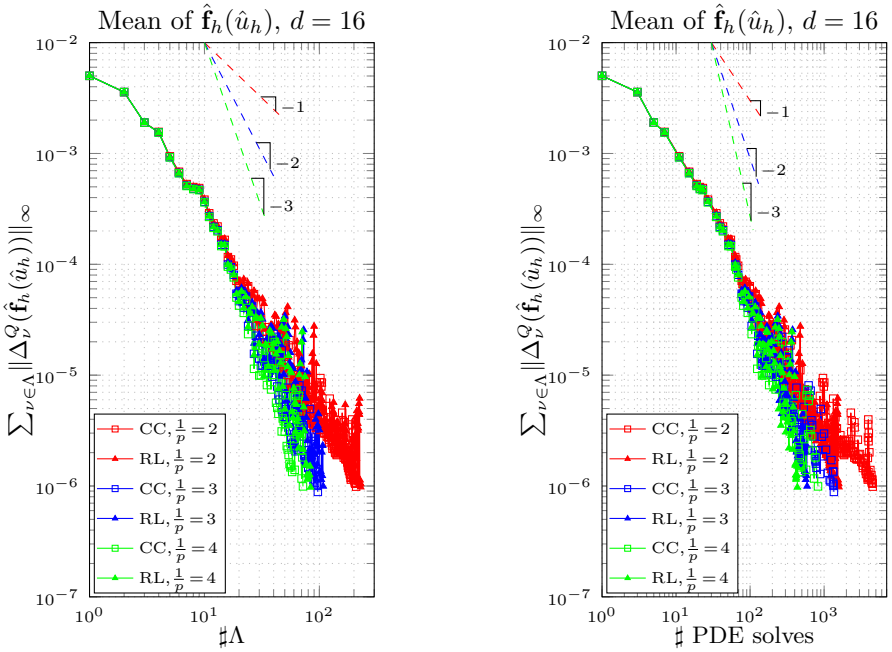

Figure 7.2.6: Comparison of the *estimated errors* for the quadrature of the values of the far field modulus with respect to the cardinality of the index set Λ (left) and the number of PDE solves (right), using Clenshaw-Curtis and $\mathfrak{R}$-Leja points, for 16 dimensions. The three dashed lines on the top of each plot correspond to the convergence rates of 1 (red), 2 (blue) and 3 (green). Maximal shape variations with respect to r_0 of 41% for $\frac{1}{p} = 2$, 37% for $\frac{1}{p} = 3$ and 36% for $\frac{1}{p} = 4$. Domain mapping (7.1.1) with r_0 replaced by $\tilde{r}$.

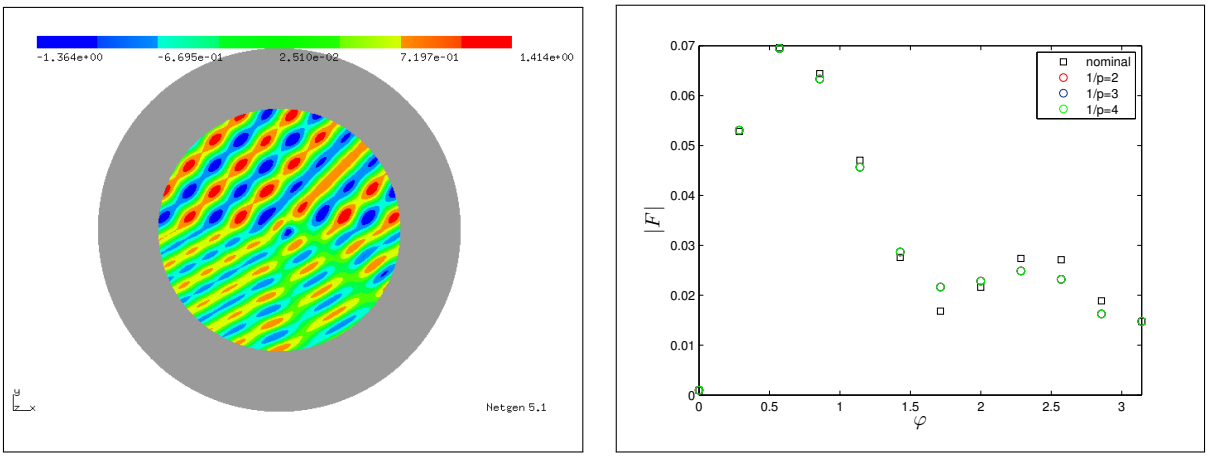

Figure 7.2.7: Particle on substrate, 16 dimensions, Clenshaw-Curtis points: estimated mean of the real part of the solution when $\frac{1}{p} = 3$ (left) and of the far field modulus for $\frac{1}{p} = 2, 3, 4$ (right). Maximal shape variations with respect to r_0: 37% for the solution (left), $36 - 41\%$ for the far field (right). Domain mapping (7.1.1) with r_0 replaced by $\tilde{r}$.

7.3. Comments on the results

From the results presented in the two previous sections we can deduce the following considerations:

- The convergence rates $\frac{1}{p} - 2$ expected from the theory (cf. Theorem 4.3.14) are achieved and surpassed. Actually, what we observe in all experiments is a higher convergence rate, close to $\frac{1}{p} - 1$. Similar observations were already made in [SS13]. This might mean that the theory is not sharp for at least a class of problems including those we have considered in this work. Since the observations in [SS13] were in the framework of Bayesian inversion for elliptic boundary value problems with unknown diffusion coefficient, it seems that what could be improved in the theory is not related to the fact of considering uncertain domains, but rather with some characteristics of the Karhunen-Loève-type expansion used to describe the uncertain quantity.

- All the experiments show dimension robustness of the algorithm with respect to the dimension of the parameter space. Of course when considering higher parameter dimensions the errors are larger, but Theorems 4.1.5 and 4.1.6 show that there is a dimension-independent upper bound on the constants multiplying the convergence rates.

- There is no case where we can observe a substantial difference of behavior between Clenshaw-Curtis and $\mathfrak{R}$-Leja points, also when considering the convergence with respect to the number of PDE solves. This might be due to the fact that, when the index set contains indices associated with low-order interpolation/quadrature operators, the number of PDE solves required by the two families of quadrature points do not differ significantly, although in the univariate case the number of Clenshaw-Curtis points increases exponentially with the order of the quadrature rule while the number of $\mathfrak{R}$-Leja points increases polynomially.

- The behavior of the error estimator for the interpolation case is highly oscillatory, especially if we look at the interpolation of the solution and of the farfield functional for the particle on substrate. If we consider the case of the interpolation of the solution in free space, the comparison between the error estimator $\max_{\nu\in\mathcal{N}(\Lambda)}\|\Delta_\nu^I(\hat{\boldsymbol{\mu}}_h)\|_\infty$ and the actual error $\sup_{\boldsymbol{y}\in\mathcal{P}_J}\|\mathrm{Re}\,\hat{u}_h(\boldsymbol{y}) - I_\Lambda(\mathrm{Re}\,\hat{u}_h)(\boldsymbol{y})\|_{H^1(K_R)}$ shows that the error estimator is effective but it overestimates the error. This is not surprising if we think that L^∞-estimates are sensitive to the choice of the set of points considered.

- The estimator for the quadrature error is instead not only effective but also fairly accurate. When considering the far field for the substrate case, the quadrature error estimator converges for a mesh where the interpolation error estimator fails to converge.

- In the free space case, where we have considered two different domain mappings (although for two different coefficient decay settings), we can see that, as expected from the theory, the convergence order of finite elements is not relevant. What is relevant is that the finite element error is not too large, making the algorithm fail. Of course, the order of convergence matters when we are interested in reducing the computational effort.

- In our experiments we have considered only the error associated with sparse interpolation/quadrature. In Lemma 5.2.1 we have stated that, for a fixed finite elements discretization, the discrete solution fulfills the $(\boldsymbol{b}, p, \varepsilon)^*$-assumption in the same domain of holomorphy as the continous solution. Thus, it is not clear why the Smolyak algorithm fails for finite element discretizations that are not accurate enough. A possible explanation could be that the theory guarantees that there exists a downward closed index set that gives the expected convergence rate for the sparse interpolant or the integral, but for finite element discretizations that are too coarse the error pollution in the difference operators does not allow the

error indicators of the algorithm to identify the most important indices; then the error indicator for interpolation, which is less accurate, would suffer more from this effect.

8. Nonsmooth dependence on parameters

In the previous chapters, we have considered interpolation and quadrature in the parameter space applied to the solution $\hat{u}$ *on the nominal configuration*. However, in applications, one is mostly interested in having information on the solution u on the *physical* space.

For interpolation, since the interpolated discrete solution $I_\Lambda \hat{u}_h = I_\Lambda \hat{u}_h(\boldsymbol{y}, \hat{\boldsymbol{x}})$ (or $I_\Lambda \hat{u}_{h,\Lambda} = I_\Lambda \hat{u}_{h,\Lambda}(\boldsymbol{y}, \hat{\boldsymbol{x}})$ for the parameter-adaptive case) still depends on $\boldsymbol{y} \in \mathcal{P}_J$, once we consider a particular realization $\boldsymbol{y} \in \mathcal{P}_J$ we also know the domain mapping $\Phi(\boldsymbol{y})$ and thus the solution on the physical configuration. However, one should be careful, because the sparse interpolation operator and the map Φ, in general, do not commute. Thus, the mapped interpolant $\Phi^{-*}(I_\Lambda \hat{u}_h)$ (where Φ^{-*} denotes the pullback with respect to Φ^{-1}) is still an approximation to the solution on the mapped domain but it is *not* its interpolant $I_\Lambda u_h$.

For quadrature, the result $Q_\Lambda \hat{u}_h$ does not depend on $\boldsymbol{y}$ anymore and thus the domain mapping is not available anyways. The first idea that would come to mind would be to consider a mesh in physical space, fixed for all realizations $\boldsymbol{y} \in \mathcal{P}_J$, and, for each realization $\boldsymbol{y}$ requested by the Smolyak algorithm, map the solution from the nominal coordinates to this grid using the mapping $\Phi(\boldsymbol{y})$; then, one could apply the Smolyak quadrature on the mapped solution. However, from Theorem (6.1.7), we can see that, for each $\boldsymbol{y} \in \mathcal{P}_J$, the solution $\hat{u}(\boldsymbol{y})$ is smooth in each subdomain but *not* across the interface $\hat{\Gamma}$. This destroys the analytic dependence of $u(\boldsymbol{y}, \boldsymbol{x}) = \hat{u}(\boldsymbol{y}, \Phi(\boldsymbol{y})\hat{\boldsymbol{x}})$ on $\boldsymbol{y}$, and we cannot expect convergence of the Smolyak algorithm.

To better understand this loss of analyticity, we consider the one-dimensional problem:

$$\begin{cases} -\big(\alpha(y,x)u'(y,x)\big)' = 0 \quad x \in (0,1), \\ u(0) = 1, \quad u(1) = 0, \\ \text{for every } y \in \left[\dfrac{1}{4}, \dfrac{3}{4}\right], \end{cases} \tag{8.0.1}$$

where $'$ denotes the derivative with respect to x, and, introducing $\alpha_l, \alpha_r \in \mathbb{R}_+$, $\alpha_l \neq \alpha_r$:

$$\alpha(y,x) = \begin{cases} \alpha_l & \text{if } x \in (0,y), \\ \alpha_r & \text{if } x \in (y,1). \end{cases}$$

The location $y \in \left[\frac{1}{4}, \frac{3}{4}\right]$ of the interface is the image of a uniformly distributed random variable $Y \sim \mathcal{U}\left([\frac{1}{4}, \frac{3}{4}]\right)$. The solution is given by

$$u(y,x) = \begin{cases} -\frac{\alpha_r}{\alpha_l(1-y)+\alpha_r y}x + 1 & \text{if } x \in [0,y), \\ \frac{\alpha_l}{\alpha_l(1-y)+\alpha_r y}(1-x) & \text{if } x \in [y,1], \end{cases}$$

and presents a kink at the interface y. Consequently, the evaluation of the solution at a fixed point x in physical space cannot be analytic as function of y if this point is crossed by the interface. This is evident from Figure 8.0.1, which shows, for three different points in the domain, the value of the solution to (8.0.1) as a function of y. In the left and center plots, since the points $x = 0.5$ and $x = 0.3$, respectively, are crossed by the interface, we can see that $u(y,x)$ is not analytic as a function of y and has a kink when $y = x$. The right plot correponds to the value of the solution

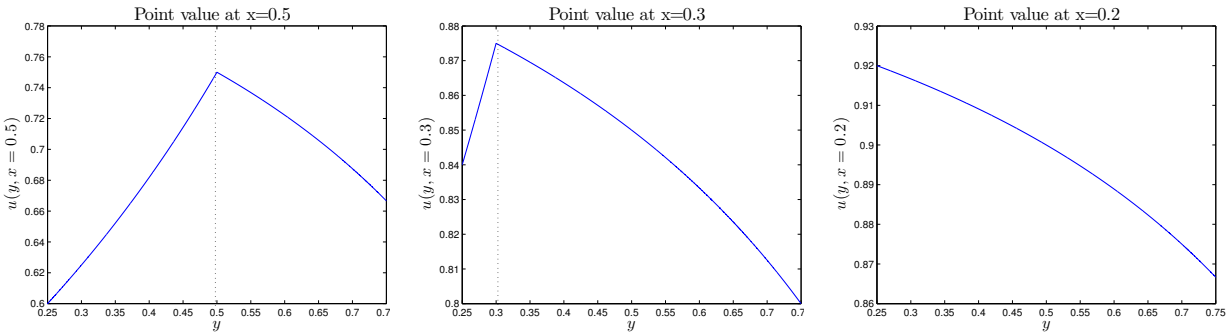

Figure 8.0.1: Point values of the solution to (8.0.1) for $\alpha_l = 3$ and $\alpha_r = 1$.

at the point $x = 0.2$, never crossed by the interface ($y \in \left[\frac{1}{4}, \frac{3}{4}\right]$), and thus $u(y, x)$ is analytic in y.

Still, if we consider a mapping from a nominal configuration where the preimage of the interface y corresponds to the point $\frac{1}{2}$, that is the domain mapping

$$x(y) = \Phi(y, \hat{x}) = \begin{cases} 2y\hat{x} & \text{if } \hat{x} \in \left[0, \frac{1}{2}\right), \\ 2(1-y)\hat{x} + (2y-1) & \text{if } \hat{x} \in \left[\frac{1}{2}, 1\right], \end{cases}$$

then, since in the nominal configuration the location of the interface is *fixed*, we can directly see (as we expect from the discussion of subsection 4.3) that the pulledback solution $\hat{u}(y, \hat{x}) := u(y, \Phi(y)(\hat{x}))$ is holomorphic in a complex discs of center $\frac{1}{2}$ and radius $\frac{1}{4} + \varepsilon$, $\varepsilon > 0$:

$$\hat{u}(y, \hat{x}) = \begin{cases} -\frac{2\alpha_r y}{\alpha_l(1-y)+\alpha_r y}\hat{x} + 1 & \text{if } x \in \left[0, \frac{1}{2}\right), \\ \frac{2\alpha_l(1-y)}{\alpha_l(1-y)+\alpha_r y}(1-\hat{x}) & \text{if } x \in \left[\frac{1}{2}, 1\right]. \end{cases} \tag{8.0.2}$$

We can conclude that the $(\boldsymbol{b}, p, \varepsilon)$-holomorphy assumption (subsection 4.1) is in general not fulfilled by the solution in physical space in the case of stochastic interface problems with discontinuous coefficients. Thus, the convergence of the sparse quadrature (and interpolation) operator is not ensured by Theorem 4.1.6 (resp. Theorem 4.1.5). This statement has also been confirmed by the numerical results that we present hereunder.

Consider, in the radius expansion, $s_j = c_j = \frac{0.2 r_0}{j^3}, j = 1, \ldots, 8$, corresponding to a 16-dimensional parameter space, and to a shape variation of 34% with respect to r_0. The domain mapping is (7.1.1), and all the other physical and discretization parameters are the same as in subsection 7.1.3. We have run the sparse quadrature algorithm with Clenshaw-Curtis abscissas for the evaluation of the real part of the solution in one point in *physical space*, corresponding, for each realization, to a different point in nominal space. Since we do not have a reference solution, we consider the error *estimated* by the algorithm at each iteration.

The left plot in Figure 8.0.2 shows the convergence plots considering the point evaluation at different points along the horizontal axis. We report the value of the numerical *error estimator* $\sum_{\nu \in \mathcal{N}(\Lambda)} |\Delta_\nu^I(\operatorname{Re} u_h(\boldsymbol{x}))|$, computed by the algorithm at each iteration. The first point is the center of the scatterer $\boldsymbol{x} = (0, 0)$, which is mapped back to itself by the domain mapping (7.1.1). Since this point is never crossed by the interface, this point evaluation is analytic and we observe convergence of the algorithm. For the same reason, the algorithm converges for the points $\boldsymbol{x} = (0.004, 0)$ and $\boldsymbol{x} = (0.04, 0)$, which are always inside the scatterer and in the far field region, respectively. The points $\boldsymbol{x} = (0.008, 0)$ and $\boldsymbol{x} = (0.012, 0)$ might be crossed by the interface, but we still observe convergence. This can be explained by the fact that these two points are crossed by the interface only for some realizations, but for most of the quadrature points selected

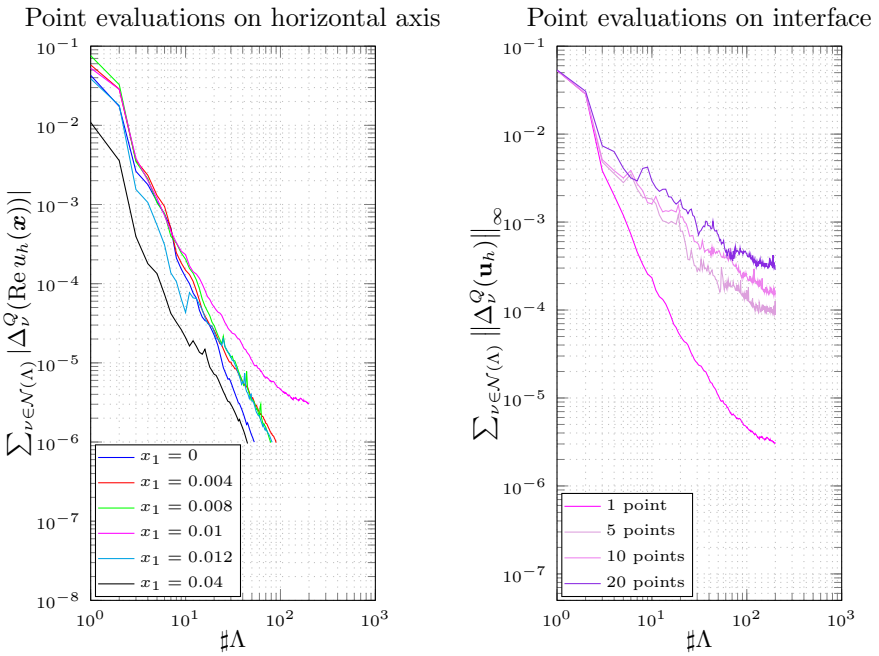

Figure 8.0.2: Convergence plots for the *estimated quadrature error* for the value of the real part of the solution when evaluated in a point in physical space, $d = 16$. Left: point evaluations at different points along the horizontal axis in physical space; right: convergence results considering respectively only 1, 5, 10 or 20 point evaluations at points that in *physical* space are on the circumference of radius r_0. Maximal shape variation of 34% with respect to r_0.

by the algorithm they remain either inside the scatterer (for $\boldsymbol{x} = (0.008, 0)$), either outside it (for $\boldsymbol{x} = (0.012, 0)$); thus, the algorithm still manages to converge in these cases. If we consider instead the point $\boldsymbol{x} = (0.01, 0)$, which is on the circumference of radius r_0 and thus it is crossed by the interface many times, we can see that the convergence curve saturates. However, the curve saturates after an error of 10^{-5}, which may still be acceptable. When we want to consider the entire solution in physical space, though, we might need more point evaluations simultaneously. For this reason, we have run a second experiment.

The right plot in Figure 8.0.2 shows the convergence curves for the sparse quadrature when considering as quantity of interest 1, 5, 10 or 20 point evaluations of $\mathrm{Re}\, u_h$ for equispaced points in physical space that are on the circumference of radius r_0. Again, we plot the value of the numerical error estimator $\sum_{\nu\in\mathcal{N}(\Lambda)} \left\|\Delta_\nu^I(\mathbf{u}_h)\right\|_\infty$ calculated by the algorithm at each iteration. Here, the quantity $\mathbf{u}_h$ represents an array with, respectively, 1, 5, 10 or 20 real-valued entries, and $\|\cdot\|_\infty$ the maximum norm. As we can observe, the higher is the number of point evaluations that we consider simultaneously, the sooner the error curve saturates; this is expected, because, the more point evaluations we address at the same time, the more are the surfaces of nonsmoothness in the parameter space, and the harder it gets for the algorithm to build a set of indices giving a good approximation to the mean for all the point evaluations.

9. Conclusions, remarks and outlook

In the framework of uncertainty quantification for solutions to PDEs on random domains, we have focused on the Helmholtz transmission problem with a stochastic interface, and presented a methodology to construct a surrogate model (interpolation) or estimate statistics (quadrature) for the solution or linear output functionals based on it. We have treated the low-frequency case, when the bilinear form associated with the Helmholtz equation is coercive, and the results and techniques presented in this work can be applied to any other equation posed on a stochastic domain, provided the associated bilinear form fulfills a uniform inf-sup condition and the bilinear and linear forms are continuous. As it is evident from our analysis, indeed, stability of the quantity of interest with respect to the forcing terms (as ensured, for instance, by the Lax-Milgram lemma) is a crucial property for the validity of the theory.

To model the random shape perturbations, we have introduced a high-dimensional parametrization for the stochastic interface, which can come from, but it is not necessarily, a Karhunen-Loève-type expansion. A mapping technique to a nominal configuration as introduced in [XT06, TX06] has enabled us to exploit the theoretical results for elliptic PDEs on fixed domains with random coefficients, and, from a computational point of view, to achieve an efficient implementation, being the nominal configuration the only domain to be meshed.

We have shown that the solution to the variational formulation posed on the nominal space and a class of linear output functionals satisfy the sufficient smoothness conditions with respect to the parameter to guarantee high-order convergence rates that are robust with respect to dimension of the parameter space [CCS14, SS13]. In the numerical experiments, we have employed the sparse adaptive Smolyak algorithm presented in [SS13], and observed dimension independence of the convergence rates. The rates measured in the experiments, though, are at least one order higher than the ones prescribed by the theory, confirming the behavior already observed in [SS13].

In a very general framework that goes beyond the application considered in this work, we have proved the convergence results for the full sparse tensor solution, that is for the case that sparse interpolation or quadrature are applied to a quantity of interest subject to some space discretization error. In the case of nested sequences of interpolation/quadrature points, we have obtained results that can be used as starting point to develop an adaptive strategy and reduce the computational cost.

When applying the aforementioned convergence results in the free space case, we have shown how the smoothness of the interface, expressed in terms of decay of the coefficients in its parametric representation, translates into smoothness of the solution to the PDE posed on the nominal configuration, with estimates which are uniform in the number of stochastic parameters.

With the analysis of a one-dimensional interface problem and some numerical experiments, we have highlighted that the holomorphy assumption breaks down and the algorithm may fail to converge for point evaluations on the physical space when the point might be crossed by the interface for some realizations.

9.1. Extensions

A few general considerations can be carried out from this work.

Relaxing the assumptions on the random variables

In Assumption 2.1.2 we have postulated the random variables $\{Y_l\}_{l=1}^{2J}$ to be independent, identically distributed as $\mathcal{U}([-1,1])$, for every $J \in \mathbb{N}$. It is clear that we can substitute the uniform distribution with any other distribution that has compact image. The hypothesis that the random variables are identically distributed can be easily relaxed, too. Indeed, if $\{Y_l\}_{l=1}^{2J}$, $J \in \mathbb{N}$, are still independent but not identically distributed as uniform random variables, the joint probability distribution μ can still be factorized as in (2.2.2). Then, denoting by $g = g(\boldsymbol{y})$, $\boldsymbol{y} \in \mathcal{P}_J$, the quantity of interest, if each univariate probability distribution has still compact image, one can apply the analysis and algorithms that we have presented to $g(\boldsymbol{y})\mu(\boldsymbol{y})$ in place of $g(\boldsymbol{y})$, $\boldsymbol{y} \in \mathcal{P}_J$.

The independence assumption is harder to drop, but it can be done, too. Namely, if the random variables are not independent, then the joint probability distribution μ cannot be expressed as product of the univariate distributions anymore. Its image space, though, is still $\mathcal{P}_J$, the tensor product of the univariate image spaces. For interpolation, denoting again the quantity of interest by $g(\boldsymbol{y})$, $\boldsymbol{y} \in \mathcal{P}_J$, one has to show that the quantity $g(\boldsymbol{y})\mu(\boldsymbol{y})$ admits a holomorphic extension to polyellipses in the complex plain. If this holds, then the theoretical analysis is still valid and the algorithms presented can still be applied to $g(\boldsymbol{y})\mu(\boldsymbol{y})$. For quadrature, we can proceed as described in [BNT10, Sect. 2]. Namely, we can introduce an auxiliary probability density function $\hat{\mu}(\boldsymbol{y}) : \mathcal{P}_J \to \mathbb{R}_+$ corresponding to the probability density function of $2J = \dim \mathcal{P}_J$ independent random variables, for instance the one used in this work, associated to $2J$ independent, uniformly distributed random variables. Then, after showing smoothness of the quantity $g(\boldsymbol{y})\frac{\mu(\boldsymbol{y})}{\hat{\mu}(\boldsymbol{y})}$ in the complex polyellipses, we can apply the theory and algorithms to the quantity $\mathbb{E}_{\hat{\mu}}\left[g(\boldsymbol{y})\frac{\mu(\boldsymbol{y})}{\hat{\mu}(\boldsymbol{y})}\right] = \int_{\mathcal{P}_J} g(\boldsymbol{y})\frac{\mu(\boldsymbol{y})}{\hat{\mu}(\boldsymbol{y})}\hat{\mu}(\boldsymbol{y})\,\mathrm{d}\boldsymbol{y}$, with weights computed as in [BNT10, Formula (2.3)].

Probabilistic interpretation of the coefficient decay

In Lemma 2.1.6 we have interpreted the decay of the coefficient sequences $\mathcal{C}$ and $\mathcal{S}$ in terms of space regularity, and then used this result in Chapter 6 to prove the associated smoothness of the solution. However, one can also give a probabilistic interpretation of the decay of these sequences. Namely, considering the random variables $\tilde{Y}_l(\omega) = \beta_l Y_l(\omega)$, for $l = 1, \dots, 2J$ and $\omega \in \Omega$, with $\beta_l = c_{\frac{l+1}{2}}$ for l odd and $\beta_l = s_{\frac{l}{2}}$ for l even, these variables describe the probabilistic law of the Fourier coefficients. Denoting $\Delta r(\omega,\varphi) := r(\omega,\varphi) - r_0(\varphi) = \sum_{l\geq 1}\tilde{Y}_l\psi_l(\varphi)$, where $\psi_l(\varphi) = \cos\left(\frac{l+1}{2}\varphi\right)$ for l odd and $\psi_l(\varphi) = \sin\left(\frac{l}{2}\varphi\right)$ for l even, the Parseval identity gives

$$\|\Delta r(\omega,\cdot)\|^2_{L^2_{per}([0,2\pi))} = \sum_{l\geq 1}|\tilde{Y}_l(\omega)|^2, \quad \text{for every } \omega \in \Omega.$$

This equation tells us that the random variable $\sum_{l\geq 1}|\tilde{Y}_l(\omega)|^2$ describes the probabilistic law with which the quantity $|\Delta r(\omega,\cdot)|^2$ oscillates around the value 0, in mean square sense over $\varphi \in [0, 2\pi)$.

To investigate the effect of the decay of the coefficients, we consider the two plots in Figure 9.1.1. On the left, we can see the approximate probability density function (pdf) for $\|\Delta r(\omega,\cdot)\|^2_{L^2_{per}([0,2\pi))}$, in the case that the coefficient sequences $\mathcal{C}$ and $\mathcal{S}$ are in $\ell^p(\mathbb{N})$ for $p = \frac{1}{2}, \frac{1}{3}, \frac{1}{4}$. On the right, we

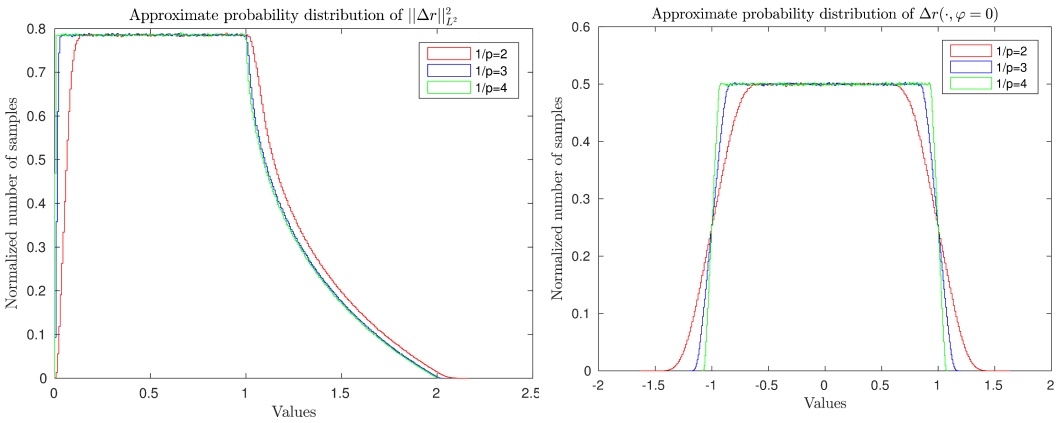

Figure 9.1.1: Probabilistic interpretation of coefficient decay: approximate pdfs for different coefficient decays.

can observe the approximate pdf for $\Delta r(\omega, 0) = \sum_{l \in \mathbb{N}, l \text{ odd}} \tilde{Y}_l$. In both cases, the plots have been produced drawing independent samples of the random variable and collecting them in a histogram.

We can deduce that the faster the decay, the more localized is the displacement of the points and the sharper is the pdf. It is clear from the right plot that, the faster the coefficients decay, the closer is the distribution of $\Delta r(\omega, 0)$ to the uniform distribution, that is, to the distribution of $\beta_1 \tilde{Y}_1(\omega)$. Concerning the distribution of $\|\Delta r(\omega, \cdot)\|^2_{L^2_{per}([0,2\pi))}$, we observe that around the value 0 there is a very thin layer where the probability density sharply decreases coming from the right. This is due to the fact that the events $\sum_{l \geq 1} \tilde{Y}_l^2 \leq \varepsilon$ have very low probability for $\varepsilon > 0$ small.

Different interface parametrizations

In Chapter 2, we have mentioned that other functions could be used in place of the Fourier harmonics to parametrize the stochastic radius. We will return on this topic in the first paragraph of Section 9.2. For a general treatment of domain transformations, we refer to [CSZ].

High-order quasi-Monte Carlo integration

The smoothness properties of the solution on the nominal domain and of linear output functionals of the form (6.3.1) with respect to the high-dimensional parameter guarantee that also high-order quasi-Monte Carlo methods based on interlaced polynomial lattice rules as described in [DKLG$^+$14] would allow to achieve high-order convergence rates without suffering from the curse of dimensionality. This is the reason why, in the numerical experiments, in order to compute an independent reference solution, we have used a high-order quasi-Monte Carlo integration code [Gan16, GS16].

9.2. Outlook

Many aspects of what we have presented need further investigation. In the following, we list those that turned out to be relevant throughout the development of our work.

Modeling shape variations and constructing mappings

The modeling of the variations in the shape and the construction of the domain mapping are closely related. In Chapter 2, we have presented a parametrization that is available only for star-shaped scatterers. For nominal geometries that are polygons, one might use an expansion in terms of only sinusoids (not cosinusoids) along the normal direction of each edge, and add a two-dimensional random variable (or three-dimensional for 3d geometries) for the movement of each corner. However, such approach to modeling the interface is not easy to extend to complicated geometries. Also, when the nominal geometry has corners, it is very important that the interface model is able to reproduce properly the corner rounding.

During discussions with Dr. Peng Chen (currently at U.T. Austin), it turned out that an effective way to model shape variations for a wide class of nominal geometries would be to use isogeometric elements, directly perturbing the control points for the NURBS with some random variables.

A similar, still general approach, would be to use discrete diffeomorphisms given as vector fields, as the one described in [HP15], based on B-splines.

Alternatively, one could model the interface through a level-set method [OF01, AJT02]. Denoting by Ψ a level-set function on a domain Q which includes all possible shapes, and assuming normal perturbations, Ψ fulfills the following transport equation:

$$\frac{\partial \Psi}{\partial t} + v|\nabla \Psi| = 0 \quad \text{in } Q \times [0, T].$$

The interface is given by the zero level-set of Ψ at a fixed final time T, and the term v is the speed of the transport along the normal direction to the interface. In order to express random shape variations we can model v as

$$v(\omega, \boldsymbol{x}) = \sum_{l \geq 0} \beta_l Y_l(\omega) \psi_l(\boldsymbol{x}), \quad \boldsymbol{x} \in \Gamma(\omega),\, \omega \in \Omega, \tag{9.2.1}$$

with some real coefficients $\{\beta_l\}_{l \geq 0}$, some real-valued random variables $\{Y_l(\omega)\}_{l \geq 0}$, and some linearly independent functions $\{\psi_l\}_{l \geq 0}$. The initial condition $\Phi(0, \boldsymbol{x})$ can be taken to be the nominal configuration. The level-set method casted in this way has the advantage that, by knowing Ψ, we know the displacement in the whole domain. However, the random field v is not directly associated with a physical quantity that can be measured, and this would represent a prominent disadvantage when trying to estimate the terms in (9.2.1) from laboratory measurements. We refer to [NSM07, NCSM08], already mentioned in the introduction, as an alternative version of the level-set method.

Finally, given instead the case that the interface model is already given and we need to propagate the interface displacements to the whole domain, more general methods than the analytic mappings described in subsection 3.1.2 need to be examined. As already mentioned in that section, a possibility is to use an harmonic extension [LTZ01]. In any case, it is important that the domain displacement is localized around the interface, in order to contain the propagation of possible interface singularities like corners; if this is the case, one could adopt an *hp*-finite element method to handle singularities, using h refinement only in small regions around them.

Constructing an interface model from measurements

An important aspect when dealing with perturbed geometries, which has not been treated in this work, is the inverse problem of extracting a model for the shape perturbations given a set of measurements. In this light, it is convenient that the quantity describing the shape variations has

a physical meaning so that it can be measured, directly or indirectly. This shows the advantage of modeling directly the interface boundary as we did in our work.

The construction of a model from experimental data has been addressed in the last ten-fifteen years, mostly from an engineering point of view. Consider that we want to reconstruct the radius expansion used in Chapter 2, written in the general form

$$r(\omega,\varphi) = r_0(\varphi) + \sum_{l=1}^{L} \beta_l Y_l(\omega)\psi_l(\varphi), \quad \varphi \in [0,2\pi), L \in \mathbb{N}, \omega \in \Omega. \tag{2.1.4}$$

This means estimating r_0, the truncation $L \in \mathbb{N}$, $\{\beta_l\}_{l=1}^L$, $\{\psi_l\}_{l=1}^L$, and $\{Y_l\}_{l=1}^L$. The probability distribution of the random variables $\{Y_l\}_{l=1}^L$ cannot be fixed a priori and needs to be estimated from the measurements; the reason is clarified in Section B of the Appendix. We consider $\{\psi_l\}_{l=1}^L$ to be elements of an orthonormal basis of the Hilbert space H where r takes values. In our case, $H = L^2_{per}([0,2\pi)$.

To estimate the model parameters we have at our disposal, for instance, noisy realizations of r

$$r_{ij} := r(\omega_i,\varphi_j) + \varepsilon_{ij}, \quad \omega_i \in \Omega, i = 1,\dots,N_i, j = 1,\dots,N_j, \varphi_j \in [0,2\pi), \tag{9.2.2}$$

where we assume the measurement noises $\{\varepsilon_{ij}\}_{\substack{1\le i\le N_i,\\ 1\le j\le N_j}}$ to be independent, identically distributed.

For sake of simplicity, let us assume that $r_0 \equiv 0$. In the general case, one can estimate r_0 by averaging over the samples and then apply the procedure described below to the quantity $r - r_0$.

The first step is to identify the coefficients $\{\beta_l\}_{l=1}^L$ and the functions $\{\psi_l\}_{l=1}^L$. As suggested in [DGS06], if the covariance function can be estimated directly from measurements, or indirectly with an inverse problem, then we can estimate its eigenvalues λ_l and associated eigenfunctions w_l, $l = 1,\dots,L$, and set $\beta_l = \sqrt{\lambda_l}$, $\psi_l = w_l$, $l = 1\dots,L$. If instead the covariance operator is not available, then one can use an eigenvalue problem associated with the physical problem at hand to construct an Hilbertian basis $\{\psi_l\}_{l=1}^L$ [DGS06]. In both cases, the truncation parameter L can be selected using some cross validation strategy [RS05, Sect. 5.4.2].

Once $\{\beta_l\}_{l=1}^L$ and $\{\psi_l\}_{l=1}^L$ are available, we have to estimate the distribution of the multivariate random variable $\boldsymbol{Y} = \{Y_l\}_{l=1}^L$. Realizations of $\{Y_l\}_{l=1}^L$ can be obtained through the formula $Y_l = \frac{1}{\beta_l} < r, \psi_l >_H$, where $< \cdot,\cdot >_H$ denotes the scalar product in H.

The introduction in [PSDF12] presents a good survey about the possible methods. The approach that has received more attention in the last years is the polynomial chaos expansion (PCE) method. This is one of the so-called indirect methods, where the key idea is to *assume* the existence of a transformation $\boldsymbol{t}$ such that

$$\boldsymbol{Y} = \boldsymbol{t}(\boldsymbol{\xi}),$$

where $\boldsymbol{\xi} = (\xi_1,\dots,\xi_{N_g})$, $N_g \in \mathbb{N}$, is a vector of known random variables, and the objective is to construct $\boldsymbol{t}$. In the polynomial chaos expansion method, $\boldsymbol{t}$ is the projection of $\boldsymbol{Y}$ on the space spanned by the polynomial chaos basis $\{\phi_{\boldsymbol{\alpha}}\}_{\boldsymbol{\alpha}\in\mathbb{N}^{N_g}}$ whose elements are orthogonal with respect to the probability measure of $\boldsymbol{\xi}$. For instance, if the distribution of $\boldsymbol{\xi}$ is Gaussian, then $\boldsymbol{Y}$ is projected on the Hermite chaos basis. Projecting $\boldsymbol{Y}$ means that we can express it as

$$\boldsymbol{Y}(\omega) = \sum_{\boldsymbol{\alpha}\in\mathbb{N}^{N_g}} \boldsymbol{\gamma}^{(\boldsymbol{\alpha})}\phi_{\boldsymbol{\alpha}}(\boldsymbol{\xi}(\omega)), \quad \omega \in \Omega. \tag{9.2.3}$$

Constructing the transformation $\boldsymbol{t}$ means identifying the projection vectors $\left\{\boldsymbol{\gamma}^{(\boldsymbol{\alpha})}\right\}_{\boldsymbol{\alpha}\in\mathbb{N}^{N_g}}$. For this, different approaches can be used. In [DGS06] and [GD06], these coefficients are estimated

using the maximum likelihood principle, while in [GD06] they are approximated using Bayesian inference. The work presented in [GD06] contains also an analysis of the influence of the choice of the truncation parameters N_g (the dimension of $\boldsymbol{\xi}$), of p (the maximum polynomial degree of chaos basis elements), and in general of the parameters that have to chosen when applying the algorithm, on the bias of the resulting estimator.

The methodology presented in [Soi10, Soi11] combines the techniques used in the polynomial chaos expansion method with the approach used in prior algebraic stochastic modeling (PASM) methods. The idea is to introduce a family of prior models for the quantity to be estimated, avoiding the estimation of the covariance operator, and use the maximum entropy principle in [Soi10] and Bayesian estimation in [Soi11] to build a posterior model. The techniques of the PCE method are used in the sense that both the prior and posterior models are constructed assuming a Karhunen-Loève-type expansion and estimating the projection vectors $\left\{\boldsymbol{\gamma}^{(\boldsymbol{\alpha})}\right\}_{\boldsymbol{\alpha}\in\mathbb{N}^{N_g}}$.

We refer to [SNC09] for the identification of polynomial chaos expansions for the level-set method [NSM07, NCSM08]. There, both the cases of uncorrelated random variables and mutually independent random variables in the expansion are addressed.

The techniques presented in the aforementioned papers have proven to be effective and very powerful, but what seems to be still missing is a rigorous mathematical analysis of them.

Improving the computational efficiency

We have mentioned in Chapter 5 that the result of Theorem 5.4.1 can be used as starting point for a parameter-adaptive choice of the finite element resolution. This could be combined with a multilevel Stochastic Collocation (MLSC) technique [TJWG15] to further speed up the computations.

Alternatively, it would be interesting to improve the computational efficiency combining the collocation algorithm with a reduced basis approach [RHP08], as it has been done in [CS15] in the framework of Bayesian inversion.

Handling the nonsmooth case

Chapter 8 clearly shows that the smoothness assumption with respect to the high-dimensional parameter does not hold for point values of the solution on the physical domain $u = u(\boldsymbol{y}, \boldsymbol{x})$, $\boldsymbol{y} \in \mathcal{P}_J$, $\boldsymbol{x} \in K_R$, in the case that the point $\boldsymbol{x}$ is crossed by the interface for some parameter realizations. Finding a solution to this issue is ongoing work.

A possible remedy could be to trace the hyperplane

$$\mathcal{P}_{\boldsymbol{x},\Gamma} := \{\boldsymbol{y} \in \mathcal{P}_J : \boldsymbol{x} \in \Gamma(\boldsymbol{y})\}, \tag{9.2.4}$$

which has codimension 1, and apply sparse quadrature separately on the two sides of the hyperplane. However, this approach has two major disadvantages that make it unpractical: first, it is not easy to find the hyperplane, second, if we consider more than one point evaluation, one would have to trace an hyperplane for each of the evaluation points that are crossed by the interface.

Instead, a Monte Carlo approach would work, because it only requires square integrability of the quantity of interest. The price to pay is a much lower convergence rate. In order to make the computational load feasible, the idea is to use *multilevel* Monte Carlo (MLMC).

The MLMC method is based on saving computational effort through a balance of the space discretization error and the Monte Carlo sampling error [BSZ11, Gil15]. In order to fully exploit

this load saving strategy, it is important to determine correctly the convergence rate of the space discretization for each $\boldsymbol{y} \in \mathcal{P}_J$. Let us focus on the convergence rate for a linear finite element discretization.

If we consider point evaluation as the Dirac delta output functional $\delta_{\boldsymbol{x}}(u(\boldsymbol{y})) := u(\boldsymbol{y}, \boldsymbol{x})$, then $\delta_{\boldsymbol{x}} \in H^{-1-\varepsilon}(K_R)$ for every $\varepsilon > 0$, and we could deduce a convergence rate of $h^{1-\varepsilon}$, $\varepsilon > 0$, where h denotes the meshwidth. However, this convergence rate is not optimal.

The first observation is that what needs to be established in MLMC is the convergence rate not exactly for *all* $\boldsymbol{y} \in \mathcal{P}_J$, but for all $\boldsymbol{y} \in \mathcal{P}_J \setminus \mathcal{N}_\Gamma$, where $\mathcal{N}_\Gamma$ is a zero measure subset of $\mathcal{P}_J$, see proof to Lemma 4.4 in [BSZ11]. This means that we do not need to determine the convergence rate of $u(\boldsymbol{y}, \boldsymbol{x})$ in the case that $\boldsymbol{x} \in \Gamma_{\Gamma(\omega)}$, because the hyperplane $\mathcal{P}_{\boldsymbol{x},\Gamma}$ as defined in (9.2.4) has measure zero for every $\boldsymbol{x} \in K_R$.

The second observation is that L^∞-error estimates [Nit76, Sch98] for linear finite elements guarantee that, for a solution w of an elliptic boundary value problem on a domain D,

$$\|w - w_h\|_{L^\infty(D)} \leq Ch^2 |\log h| \|w\|_{W^{2,\infty}(D)}, \tag{9.2.5}$$

where w_h denotes the linear finite element solution, $C > 0$ is a constant independent of h and w, and $D \in \mathbb{R}^2$.

For the Helmholtz transmission problem (1.0.1) in free space, we can conjecture that if $u(\boldsymbol{y}) \in W^{2,\infty}(D_2) \cup W^{2,\infty}(K_R \cap D_1)$ for every $\boldsymbol{y} \in \mathcal{P}_J \setminus \mathcal{P}_{\boldsymbol{x},\Gamma}$, then $u(\boldsymbol{y}, \boldsymbol{x})$ will converge with rate $h^2 |\log h|$, for every $\boldsymbol{y} \in \mathcal{P}_J \setminus \mathcal{P}_{\boldsymbol{x},\Gamma}$.

As we have done in Chapter 6, our intention is to prove the regularity of the point evaluation on the *nominal* configuration. The correct functional setting to prove classical smoothness of solutions to elliptic boundary value problems are the Hölder spaces $C^{2,\alpha}$ for $\alpha \in (0, 1)$. Indeed, we cannot consider C^2-regularity because there are cases when the right-hand side is continuous but the solution is not in C^2 (see Problem 4.9 in [GT01]). Then, we need to prove the following:

Proposition 9.2.1. *If the coefficients in* (3.2.4) *are such that* $\hat{\alpha} \in C^{1,\alpha}(K_R \cap \hat{D}_1) \cup C^{1,\alpha}(\hat{D}_2)$ *and* $\hat{\kappa^2} \in C^{0,\alpha}(K_R \cap \hat{D}_1) \cup C^{0,\alpha}(\hat{D}_2)$ *for every* $J \in \mathbb{N}$ *and every* $\boldsymbol{y} \in \mathcal{P}_J$*, with* J*- and* $\boldsymbol{y}$*-independent norm bounds, then* $\hat{u} \in C^{2,\alpha}(K_R \cap \hat{D}_1) \cup C^{2,\alpha}(\hat{D}_2)$ *for every* $J \in \mathbb{N}$ *and every* $\boldsymbol{y} \in \mathcal{P}_J$*, with a* J*- and* $\boldsymbol{y}$*-independent norm bound.*

This result can be proved using either Green's representation formula for the solution $\hat{u}$ (see Chapter 6 in [GT01]), or local integral estimates and equivalence between Campanato and Hölder norms (see Chapter 6 in [WYW06]).

A criticism that could be raised is that Hölder spaces are not separable, and one should distinguish between weak and strong measurability. However, one could either use the fact that $\|w\|_{C^k(D)} \leq \|w\|_{C^{k,\alpha}(D)}$ for every $w \in C^{k,\alpha}(D)$ and $\|w\|_{C^{k,\alpha}(D)} \leq \|w\|_{C^{k+1}(D)}$ for every $w \in C^{k+1}(D)$, or assume that, for every $J \in \mathbb{N}$ and every $\boldsymbol{y} \in \mathcal{P}_J$, $\hat{u}$ belongs to a separable subset of $C^{2,\alpha}(K_R \cap \hat{D}_1) \cup C^{2,\alpha}(\hat{D}_2)$.

If we further show that the constant C in (9.2.5) can be bounded independently of $J \in \mathbb{N}$ and $\boldsymbol{y} \in \mathcal{P}_J$, then we obtain that the point evaluation functional $u(\boldsymbol{y}, \boldsymbol{x})$ converges with rate $h^2 |\log h|$ for every $J \in \mathbb{N}$ and every $\boldsymbol{y} \in \mathcal{P}_J \setminus \mathcal{P}_{\boldsymbol{x},\Gamma}$, and we can use this rate to determine the distribution of samples among the MLMC levels.

As remarked in Chapter 8, the solution of an interface problem is in general only continuous across the interface, which translates in C^0-smoothness with respect to the high-dimensional parameter. However, when introducing the model problems in Chapter 1, we have mentioned that, in the TE

mode, the highest-order coefficient α is continuous in the whole domain. Using Proposition 9.2.1 and the transmission conditions at the interface, a simple application of the triangle inequality shows that in this case the solution $\hat{u}$ would have global regularity $C^{1,\alpha}$, $\alpha \in (0,1)$. In this situation, it would be interesting to analyze the performance of a quasi-Monte Carlo method [KSS12, DKS13] and compare it to the Monte Carlo approach.

A. Banach space-valued random variables

A.1. Lebesgue-Bochner spaces

Let $(\Omega, \mathcal{A}, \mu)$ be a measure space, where $\mathcal{A}$ denotes a σ-algebra on Ω and $\mu : \mathcal{A} \to \mathbb{R}_+$ is a measure.

Definition A.1.1. A measure μ on a measurable space $(\Omega, \mathcal{A})$ is *finite* if $\mu(\Omega) < \infty$, and it is *σ-finite* if Ω is the union of a sequence $A_1, A_2, \ldots$ of sets that belong to $\mathcal{A}$ and satisfy $\mu(A_i) < \infty$ for every i.

Definition A.1.2. A measure μ is called *complete* if the conditions $A \in \mathcal{A}$, $A' \subset A$ and $\mu(A) = 0$ imply that $A' \in \mathcal{A}$.

In this section we assume the measure μ to be complete.

Consider a Banach space $(B, \|\cdot\|_B)$ and a function $s : \Omega \to B$ such that

$$s = \sum_{k=1}^{n} a_k \mathbb{1}_{A_k}, \tag{A.1.1}$$

for some $n \in \mathbb{N}$, where $a_k \in B$, $\mathbb{1}_A$ denotes the indicator function of A and $A_k \in \mathcal{A}$, $A_j \cap A_k = \emptyset$ for $1 \leq k, j \leq n$, with $k \neq j$. Then s is called a *simple function*.

Contrarily to real-valued functions, for Banach-space valued functions there are different definitions of measurability. We present them as in [Rya02, Sect. 2.3].

Definition A.1.3. A function $f : \Omega \to B$ is *μ-measurable* if there exists a sequence of simple functions $(s_n)_{n\geq 1}$ such that $s_n(\omega) \to f(\omega)$ as $n \to \infty$ for μ-a.e. $\omega \in \Omega$.

In the following definition, we denote by B^* the dual space of B.

Definition A.1.4. A function $f : \Omega \to B$ is *weakly μ-measurable* if, for every $b^* \in B^*$, the scalar-valued function $b^*(f)$ is μ-measurable.

Definition A.1.5. A function $f : \Omega \to B$ is *Borel μ-measurable* if, for every open subset $\mathcal{O}$ of B, $f^{-1}(\mathcal{O})$ is a measurable set.

These three definitions are connected by the concept of separability. From [Rya02, Sect. 2.3], we have the following definition:

Definition A.1.6. A function $f : \Omega \to B$ is *μ-essentially separably valued* if there exists a measurable subset A of Ω, whose complement has μ-measure zero, such that $f(A)$ is contained in a separable subspace of B.

Then it holds:

Theorem A.1.7 (Pettis measurability theorem)**.** *Let $(\Omega, \mathcal{A}, \mu)$ be a σ-finite measure space and $f : \Omega \to B$ a function. The following statements are equivalent:*

(i) f *is* μ*-measurable;*

(ii) f *is weakly* μ*-measurable and* μ*-essentially separably valued;*

(iii) f *is Borel* μ*-measurable and* μ*-essentially separably valued.*

Proof. See [Rya02, Prop. 2.15]. □

In particular, the above theorem tells us that the notions of μ-measurability, weak μ-measurability and Borel μ-measurability do coincide if the Banach space B is separable.

The Bochner integral of a μ-measurable function $f : \Omega \to B$ is defined in an analogous way to the Lebesgue integral for real-valued functions. For any simple function s as in (A.1.1), we define its integral over Ω with respect to μ as

$$\int_\Omega s \, \mathrm{d}\mu := \sum_{k=1}^{n} a_k \mu(A_k).$$

We say that s is *integrable* if $\mu(A_k)$ is finite whenever $a_k \neq 0$, $1 \leq k \leq n$.

Definition A.1.8. A μ-measurable function $f : \Omega \to B$ is *Bochner integrable* if there exists a sequence $(s_n)_{n\geq 1}$ of μ-measurable simple functions converging μ-almost everywhere to f and satisfying

$$\lim_{n\to\infty} \int_\Omega \|f - s_n\|_B \, \mathrm{d}\mu = 0.$$

The Bochner integral of f over Ω with respect to μ is defined as

$$\int_\Omega f \, \mathrm{d}\mu := \lim_{n\to\infty} \int_\Omega s_n \, \mathrm{d}\mu.$$

Theorem A.1.9 (Bochner's theorem)**.** *If* $f : \Omega \to B$ *is a* μ*-measurable function, then* f *is Bochner integrable if and only if the scalar function* $\|f\|_B$ *is integrable, and*

$$\Big\| \int_\Omega f \, \mathrm{d}\mu \Big\|_B \leq \int_\Omega \|f\|_B \, \mathrm{d}\mu.$$

Proof. See [Rya02, Prop. 2.16 and Cor. 2.17]. □

Definition A.1.10. For $0 < p \leq \infty$, define

$$\mathcal{L}^p(\Omega, B) := \left\{ f : \Omega \to B, f \text{ strongly measurable and } \|f\|_{\mathcal{L}^p(\Omega,B)} < \infty \right\},$$

where

$$\|f\|_{\mathcal{L}^p(\Omega,B)} := \begin{cases} \left(\int_\Omega \|f\|_B^p \, \mathrm{d}\mu\right)^{\frac{1}{p}} & \text{if } 0 < p < \infty, \\ \operatorname{esssup}_\Omega \|f\|_B & \text{if } p = \infty. \end{cases}$$

Define also $\mathcal{N}^p := \{f \in \mathcal{L}^p, f = 0 \ \mu\text{-a.e.}\}$. Then $L^p(\Omega, B) := \mathcal{L}^p(\Omega, B)/\mathcal{N}^p$ is called *Lebesgue-Bochner* space. It is equipped with the norm $\|[f]\|_{L^p(\Omega,B)} := \|f\|_{\mathcal{L}^p(\Omega,B)}$, where $[f]$ denotes the equivalence class of f.

For ease of notation, we simply write $\|f\|_{L^p(\Omega,B)}$, omitting the symbol $[\cdot]$.

For $p \geq 1$, $(L^p(\Omega, B), \|\cdot\|_{L^p(\Omega,B)})$ is a complete normed space, that is, a Banach space.

A.2. Tensor product of measures

We first address the tensor product of two measures. Then, we extend the definitions to the tensor product of any finite number of measures and finally to the tensor product of a countable number of measures.

Definition A.2.1. Let $(\Omega_1, \mathcal{A}_1)$, $(\Omega_2, \mathcal{A}_2)$ be two measurable spaces. The smallest σ-algebra over $\Omega_1 \otimes \Omega_2$ generated by sets of the form $A_1 \times A_2$, where $A_1 \in \mathcal{A}_1$ and $A_2 \in \mathcal{A}_2$, is called the *product σ-algebra* of $\mathcal{A}_1$ and $\mathcal{A}_2$, and is denoted by $\mathcal{A}_1 \otimes \mathcal{A}_2$.

The following theorem ensures that, if two measure spaces are σ-finite, then we can uniquely define the so-called product measure on $(\Omega_1 \otimes \Omega_2, \mathcal{A}_1 \otimes \mathcal{A}_2)$.

Theorem A.2.2. *Let $(\Omega_1, \mathcal{A}_1, \mu_1)$ and $(\Omega_2, \mathcal{A}_2, \mu_2)$ be σ-finite measure spaces. For A in $\mathcal{A}_1 \otimes \mathcal{A}_2$, denote $A^{\omega_1} := \{\omega_2 \in \Omega_2 : (\omega_1, \omega_2) \in A\}$ and $A^{\omega_2} := \{\omega_1 \in \Omega_1 : (\omega_1, \omega_2) \in A\}$.*

The set function $\mu_1 \otimes \mu_2$, defined for every set $A \in \mathcal{A}_1 \otimes \mathcal{A}_2$ by

$$(\mu_1 \otimes \mu_2)(A) := \int_{\Omega_1} \mu_2(A^{\omega_1}) \, \mathrm{d}\mu_1(\omega_1) = \int_{\Omega_2} \mu_1(A^{\omega_2}) \, \mathrm{d}\mu_2(\omega_2),$$

is a σ-finite measure with the property that, for every set of the form $A_1 \times A_2$ with $A_1 \in \mathcal{A}_2$ and $A_2 \in \mathcal{A}_2$,

$$(\mu_1 \otimes \mu_2)(A_1 \times A_2) = \mu_1(A_1)\mu_2(A_2). \tag{A.2.1}$$

The measure $\mu_1 \otimes \mu_2$ is called *product measure* of μ_1 and μ_2.

Proof. See [Hal13, Thm. A and B in § 35]. □

If two measures are σ-finite, then Fubini's theorem holds, cf. [Hal13, § 36].

Proceeding by mathematical induction, it is trivial to extend the previous concepts to the tensor product of any finite number n of σ-finite measure spaces $(\Omega_i, \mathcal{A}_i, \mu_i)$, $i = 1, \ldots, n$ [Hal13, § 37]. Namely, there exists a unique measure $\mu_1 \otimes \ldots \otimes \mu_n$ on $\mathcal{A}_1 \otimes \ldots \otimes \mathcal{A}_n$, $n \in \mathbb{N}$, such that

$$(\mu_1 \otimes \ldots \otimes \mu_n)(A_1 \times \ldots \times A_n) = \prod_{i=1}^{n} \mu_i(A_i), \quad \text{for every } A_1 \in \mathcal{A}_1, \ldots, A_n \in \mathcal{A}_n. \tag{A.2.2}$$

To define the product measure on a sequence $(\Omega_i, \mathcal{A}_i, \mu_i)_{i \geq 1}$ of measure spaces, we need to strengthen the constraints on the measures μ_i, $i \geq 1$. Namely, we need to ask that all of them (or at least all but a finite number of them) are finite measures. In the following let us denote $\Omega^{(n)} := \bigotimes_{i \geq n+1} \Omega_i$ for some $n \in \mathbb{N}$. We have:

Theorem A.2.3. *Given a sequence $(\Omega_i, \mathcal{A}_i, \mu_i)_{i \geq 1}$ of measure spaces with $\mu_i(\Omega_i) = 1$ for every $i \geq 1$, there exists a unique measure μ on the product σ-algebra $\mathcal{A} := \bigotimes_{i \geq 1} \mathcal{A}_i$ such that, for every measurable set of the form $A \times \Omega^{(n)}$,*

$$\mu(A \times \Omega^{(n)}) = (\mu_1 \otimes \ldots \otimes \mu_n)(A). \tag{A.2.3}$$

Proof. See [Hal13, § 38]. □

Since every finite measure can be rescaled so that the measure of the entire space is 1, the previous theorem can be applied to any countable product of finite measures.

B. Hilbert space-valued random variables: the covariance operator

For a survey on random variables and their main properties, we refer to [Hal13]. Herein, we focus on the definition and properties of the covariance operator for random variables taking values on a separable Hilbert space H with scalar product $\langle \cdot, \cdot \rangle_H$. We denote by $(\Omega, \mathcal{A}, \mathbb{P})$ a probability space, and by $\mathbb{E}(X) := \int_\Omega X(\omega)\, \mathrm{d}\mathbb{P}(\omega)$ the mean of a random variable $X \in L^1(\Omega, H)$.

We use the symbol $H \otimes H$ for the tensor product space consisting of elements $\varphi \otimes \psi$ such that $\varphi, \psi \in H$. We endow the space $H \otimes H$ with the inner product $\langle u, v \rangle_{H\otimes H} := \sum_{i,j} \langle \varphi_i, \varphi_j' \rangle_H \langle \psi_i, \psi_j' \rangle_H$ for every $u = \sum_{i=1}^n \varphi_i \otimes \psi_i$, $v = \sum_{j=1}^m \varphi_j' \otimes \psi_j'$, where $\varphi_i, \psi_i, \varphi_j', \psi_j' \in H$ for $i = 1 \dots, n$ and $j = 1, \dots, m$ [CL85, p. 20]. The norm induced by this inner product is $\|u\|_{H\otimes H} := \sqrt{\langle u, u \rangle_{H\otimes H}}$. The completion of $H \otimes H$ with respect to this norm is a Hilbert space [CL85, p. 22].

Definition B.0.1. For $X \in L^2(\Omega, H)$, the *covariance* $\mathrm{Cov}(X)$ of X is the element of $H \otimes H$ defined as

$$\mathrm{Cov}(X) := \mathbb{E}\left((X - \mathbb{E}(X)) \otimes (X - \mathbb{E}(X))\right). \tag{B.0.1}$$

The *variance* of X is defined as

$$\mathrm{Var}(X) := \mathbb{E}\left(\|\mathrm{Cov}(X)\|_{H\otimes H}\right) = \mathbb{E}\left(\|X - \mathbb{E}(X)\|_H^2\right) = \|X - \mathbb{E}(X)\|_{L^2(\Omega,H)}^2.$$

The covariance can also be seen as a nonnegative, symmetric operator $Q : H \to H$ of trace class, called *covariance operator*, with

$$\langle \mathrm{Cov}(X), \varphi \otimes \psi \rangle_{H\otimes H} = \langle Q\varphi, \psi \rangle_H, \quad \text{for every } \varphi, \psi \in H$$

[DPZ14, p. 26].

If $H = L^2(D)$ for $D \subseteq \mathbb{R}^n$, $n \geq 0$, then the covariance operator has a representation as integral operator:

Theorem B.0.2 (Mercer's theorem)**.** *For $\varphi \in H = L^2(D)$, the covariance operator $Q : H \to H$ of a random variable $X \in L^2(\Omega, H)$ is given by*

$$Q\varphi(\boldsymbol{x}) = \int_D \mathrm{cov}_X(\boldsymbol{x}, \boldsymbol{z})\varphi(\boldsymbol{z})\, \mathrm{d}\boldsymbol{z}, \quad \textit{for all } \boldsymbol{x} \in D. \tag{B.0.2}$$

The function $\mathrm{cov}_X : D \times D \to \mathbb{R}$ is called covariance kernel *of X. Given the eigenvalues $(\lambda_i)_{i\geq 1}$ and an eigenbasis $(e_i)_{i\geq 1}$ of Q, the covariance kernel can be represented as*

$$\mathrm{cov}_X(\boldsymbol{x}, \boldsymbol{z}) = \sum_{i=1}^{\infty} \lambda_i e_i(\boldsymbol{x}) e_i(\boldsymbol{z}). \tag{B.0.3}$$

Proof. We refer to [Lax02, Thm. 11 in Ch. 30]. Here we just mention that the fact that Q has a spectral decomposition comes from the fact that it is of trace class, and thus compact. Moreover, since Q is nonnegative, all its eigenvalues $(\lambda_i)_{i\geq 1}$ are nonnegative. □

Any random variable with finite second moments has the remarkable property of having a Fourier-like expansion, which allows to express Hilbert space-valued random variables in terms of real-valued random variables:

Theorem B.0.3 (Karhunen-Loève expansion)**.** *Let $X \in L^2(\Omega, H)$ be a random variable with mean $m \in H$ and covariance operator Q (nonnegative, symmetric and of trace class). Let $(\lambda_i)_{i\geq 1}$ be the sequence of eigenvalues of Q, numbered in decreasing order, and $(e_i)_{i\geq 1}$ the sequence of the corresponding normalized eigenvectors. Then*

$$X = m + \sum_{i=1}^{\infty} \sqrt{\lambda_i}\beta_i e_i, \tag{B.0.4}$$

where $(\beta_i)_{i\geq 1}$ is a sequence of real-valued random variables such that (denoting by $\delta_{j,k}$ the Kronecker delta)

$$\mathbb{E}[\beta_j] = 0, \quad \mathbb{E}[\beta_j \beta_k] = \delta_{jk},$$

for all $j, k \in \mathbb{N}$ such that $\lambda_j, \lambda_k > 0$.

The convergence of the series (B.0.4) *is understood in the $L^2(\Omega, H)$ sense.*

Proof. See [Loè63, Thm. B in 34.5]. □

If X has normal distribution, then the random variables $(\beta_i)_{i\geq 1}$ associated with nonzero eigenvalues are mutually independent and normally distributed as $\mathcal{N}(0, 1)$. In the other case that X is not normally distributed, the distribution of the random variables $(\beta_i)_{i\geq 1}$ is not known a priori and they are uncorrelated but not necessarily mutually independent.

For Gaussian random variables, then, it is sufficient to estimate the eigenvalues and eigenvectors of the covariance operator to obtain the expansion (B.0.4). For non-Gaussian fields, however, if we *assume* that X admits an expansion as (B.0.4) and fix *a priori* the distribution of the random variables $(\beta_i)_{i\geq 1}$, then we can still use the properties of the covariance operator to estimate the terms in (B.0.4). We remark that, having fixed a priori the distribution of the random variables, the resulting expansion will not be exactly the Karhunen-Loève expansion of X.

Proposition B.0.4. *Let $X \in L^2(\Omega, H)$ be a random variable with mean $m \in H$ and covariance operator Q (nonnegative, symmetric and of trace class). Consider the random variable $Y \in L^2(\Omega, H)$ given by*

$$Y = m + \sum_{i=1}^{\infty} \psi_i(\boldsymbol{x})\beta_i, \tag{B.0.5}$$

where $(\beta_i)_{i\geq 1}$ is a sequence of independent, identically distributed real-valued random variables with zero mean and variance $\sigma^2 \in \mathbb{R}_+$, and $(\psi_i)_{i\geq 1}$ is a sequence of elements of H.

If we choose $\psi_i = \frac{\sqrt{\lambda_i}}{\sigma} e_i$, $i \in \mathbb{N}$, where $(\lambda_i)_{i\geq 1}$ and $(e_i)_{i\geq 1}$ are the sequences of eigenvalues and associated normalized eigenvectors of Q, respectively, then Y has the same mean and same covariance as X.

Proof. That $\mathbb{E}[Y] = \mathbb{E}[X]$ is trivial. For the covariance, using the assumptions on $(\beta_i)_{i\geq 1}$ and $\psi_i = \frac{\sqrt{\lambda_i}}{\sigma} e_i$, $i \in \mathbb{N}$:

$$\mathrm{Cov}(Y) = \sum_{j,k=1}^{\infty} \psi_j \otimes \psi_k \mathbb{E}[\beta_j \beta_k] = \sum_{k=1}^{\infty} \sigma^2 \psi_k \otimes \psi_k = \sum_{k=1}^{\infty} \sigma^2 \frac{\lambda_k}{\sigma^2} e_k \otimes e_k = \sum_{k=1}^{\infty} \lambda_k e_k \otimes e_k = \mathrm{Cov}(X).$$

□

Given a set of measurements of X, we might want to estimate the covariance of X from them, and then obtain a Karhunen-Loève-type expression for X. Actually, as we know from probability theory, if X is not normally distributed, then Proposition B.0.4 does not guarantee that X and Y have the same distribution. Fixing a priori the distribution of the random variables $(\beta_i)_{i\geq 1}$ is a very strong modeling assumption: if we think of H as a function space, e.g. $H = L^2(D)$, then this means fixing a priori with which probability law the value of X at a point $\boldsymbol{x}$ oscillates around its mean value $m(\boldsymbol{x})$.

Thus, if, given some measurements of X, we want to estimate a Karhunen-Loève-type expansion for X, we also need to estimate the distribution law of the random variables $(\beta_i)_{i\geq 1}$, as discussed in Section 9.2.

C. Fourier series

The content of this section is mostly based on [Gra04].

We consider the real interval $[0, 2\pi]$ where the points $\varphi = 0$ and $\varphi = 2\pi$ are identified. We denote the Lebesgue integrable functions on the resulting torus as $L^1_{per}([0, 2\pi))$. Analogous notation is used for other spaces defined on the torus, e.g. $L^p_{per}([0, 2\pi))$, $p \in \mathbb{N}$, $C^0_{per}([0, 2\pi))$.

Definition C.0.1. For a real-valued function $f \in L^1_{per}([0, 2\pi))$ and $j \in \mathbb{N}_0$, we define

$$\hat{f}_j = \frac{1}{2\pi} \int_0^{2\pi} f(\varphi)\psi_j(\varphi)\,\mathrm{d}\varphi,$$

where

$$\psi_0 = 1, \quad \psi_j(\varphi) = \cos(j\varphi) \text{ if } j \text{ is even}, \quad \psi_j(\varphi) = \sin(j\varphi) \text{ if } j \text{ is odd}. \tag{C.0.1}$$

We call $\hat{f}_j$ the (real) jth *Fourier coefficient* of f.

The (real) *Fourier series* of f at $\varphi \in [0, 2\pi)$ is

$$\hat{f}_0 + \sum_{j \geq 1} \hat{f}_{2j-1} \cos(j\varphi) + \hat{f}_{2j} \sin(j\varphi). \tag{C.0.2}$$

We have to define in which sense the series (C.0.2) converges. The most general result is the following:

Proposition C.0.2 (Fourier inversion)**.** *Assume that $f \in L^1_{per}([0, 2\pi))$ and that*

$$\sum_{l \geq 0} |\hat{f}_l| < \infty.$$

Then

$$f(\varphi) = \hat{f}_0 + \sum_{j \geq 1} \hat{f}_{2j-1} \cos(j\varphi) + \hat{f}_{2j} \sin(j\varphi) \quad \text{a.e. in } [0, 2\pi),$$

and thus f is almost everywhere equal to a continuous function.

Proof. See [Gra04, Prop. 3.1.14]. □

Moreover, we may ask which functions we can approximate using trigonometric polynomials and 'how good' the approximation can be. For this, we have the following results:

Proposition C.0.3. *It holds:*

(a) The set of trigonometric polynomials $\{\psi_l\}_{l \geq 0}$ defined in (C.0.1) *is dense in $L^p_{per}([0, 2\pi))$ for $1 \leq p < \infty$.*

(b) (Bessel theorem) *In particular, $\{\psi_l\}_{l \geq 0}$ in* (C.0.1) *is a complete orthonormal system for the Hilbert space $L^2_{per}([0, 2\pi))$.*

(c) (Weierstrass approximation theorem for trigonometric polynomials) *Every function in $C^0_{per}([0, 2\pi))$ is a uniform limit of trigonometric polynomials.*

Proof. See [Gra04], Prop. 3.1.10, Cor. 3.1.11 and Prop. 3.1.15 - Prop. 3.1.16. □

There is a strict connection between the decay properties of Fourier coefficients and smoothness of a function. This is presented in the remainder of this section.

First, we need the following technical lemma, whose proof is postponed to the end of this section.

Lemma C.0.4. *Let $\boldsymbol{q} = (q_j)_{j\geq 1}$ be a real, monotonically decreasing sequence belonging to $\ell^p(\mathbb{N})$, $0 < p < \infty$.*

Then there exists a real constant $C_{\boldsymbol{q}} > 0$ (depending on the sequence $\boldsymbol{q}$) and $J \in \mathbb{N}$ such that

$$|q_j| \leq C_{\boldsymbol{q}} \frac{1}{j^{\frac{1}{p}}}, \quad \text{for every } j > J. \tag{C.0.3}$$

Thanks to the latter result, we can prove the following:

Lemma C.0.5. *If the sequences of Fourier coefficients $(\hat{f}_{2j-1})_{j\geq 1}$ and $(\hat{f}_{2j})_{j\geq 1}$ of a function $f \in C^0_{per}([0, 2\pi))$ have each a monotonic majorant in $\ell^p(\mathbb{N})$ for $0 < p < 1$, then*

$$\|f\|_{C^k_{per}([0,2\pi))} \leq C,$$

with

$$k = \begin{cases} \left\lfloor \frac{1}{p} - 1 \right\rfloor & \text{if } \frac{1}{p} - 1 \text{ is not an integer,} \\ \frac{1}{p} - 2 & \text{otherwise.} \end{cases} \tag{C.0.4}$$

The constant C may depend on the sequence $(\hat{f}_l)_{l\geq 1}$.

Proof. From (C.0.2), computing the kth derivative and considering that $\sup_{\varphi\in[0,2\pi)} |\sin(l\varphi)| = \sup_{\varphi\in[0,2\pi)} |\cos(l\varphi)| = 1$, $l \in \mathbb{N}$, we obtain an upper bound for the $C^k_{per}([0, 2\pi))$-seminorm of f:

$$|f|_{C^k_{per}([0,2\pi))} = \sup_{\varphi\in[0,2\pi)} \left| \frac{d^k f(\varphi)}{d\varphi^k} \right| \leq \sum_{j\geq 1} j^k (|\hat{f}_{2j-1}| + |\hat{f}_{2j}|). \tag{C.0.5}$$

If $(\hat{f}_{2j-1})_{j\geq 1}$ has a monotonic majorant in $\ell^p(\mathbb{N})$, then, according to Lemma C.0.4, there exists $J \in \mathbb{N}$ such that

$$|\hat{f}_{2j-1}| \lesssim \frac{1}{j^{\frac{1}{p}}} \quad \text{and thus} \quad j^k |\hat{f}_{2j-1}| \lesssim \frac{1}{j^{\frac{1}{p}-k}}, \quad \text{for all } j > J$$

(where $\lesssim$ denotes inequality up to a constant that may depend on the sequence). The analogous holds for the sequence $(\hat{f}_{2j})_{j\geq 1}$.

Then, the sum in (C.0.5) converges for every k such that

$$\frac{1}{p} - k > 1,$$

that is if we choose k as in (C.0.4). □

Conversely:

Lemma C.0.6. *If $f \in C^k_{per}([0,2\pi))$ for an integer $k \geq 0$, then*

$$|\hat{f}_{2j-1}|, |\hat{f}_{2j}| \leq C(k,f)\frac{1}{(1+j)^k}, \quad j \geq 1, \tag{C.0.6}$$

for a positive constant $C(k,f)$ dependent on k and f but independent of $j \in \mathbb{N}$.

In particular, the sequences $(\hat{f}_{2j-1})_{j\geq 1}$ and $(\hat{f}_{2j})_{j\geq 1}$ have a monotonically decreasing majorant belonging to $\ell^p(\mathbb{N})$ for every $p > \frac{1}{k}$.

Proof. If $f = f(\varphi) \in C^k_{per}([0,2\pi))$, then Corollary 3.2.10 in [Gra04] implies that

$$|\hat{f}_{2j-1}|, |\hat{f}_{2j}| \leq \lambda(k)\frac{\max\left(\|f\|_{L^1_{per}([0,2\pi))}, \left\|\frac{d^k f}{d\varphi^k}\right\|_{C^0_{per}([0,2\pi))}\right)}{(1+j)^k}, \quad j \in \mathbb{N},$$

with $\lambda = \lambda(k)$ a constant depending only on k but not on j and f. We obtain (C.0.6) simply taking $C(k,f) = \lambda(k)\max\left(\|f\|_{L^1_{per}([0,2\pi))}, \left\|\frac{d^k f}{d\varphi^k}\right\|_{C^0_{per}([0,2\pi))}\right)$.

Since the constant $C(k,f)$ is independent of $j \in \mathbb{N}$, the coefficients sequences $(\hat{f}_{2j-1})_{j\geq 1}$ and $(\hat{f}_{2j})_{j\geq 1}$ have a monotonically decreasing majorant in $\ell^p(\mathbb{N})$ for every p such that $kp > 1$, i.e. $p > \frac{1}{k}$. □

From the previous lemmas, we may expect that, for $0 < p < \frac{1}{2}$, the decay of the Fourier coefficients $(\hat{f}_l)_{l\geq 1}$ of a function f determines the decay of the Fourier coefficients of its derivative $\frac{df(\varphi)}{d\varphi}$. From (C.0.2), the decay properties of the latter are the same as the ones of the sequence $(l\hat{f}_l)_{l\geq 1}$. If we use Lemma C.0.4, we obtain that, if $(\hat{f}_l)_{l\geq 1} \in \ell^p(\mathbb{N})$ for $0 < p < \frac{1}{2}$, then $(l\hat{f}_l)_{l\geq 1} \in \ell^r(\mathbb{N})$ with $r = \frac{p}{1-p} + \varepsilon$, for every $\varepsilon > 0$. Using instead Lemma C.0.5 applied to f and then C.0.6 applied to the derivative of f, we would obtain, for the sequence $(l\hat{f}_l)_{l\geq 1}$, a summability exponent $r = \frac{p}{1-2p} + \varepsilon$, for every $\varepsilon > 0$. The following lemma shows instead that, with a slightly stronger assumption on the decay of the sequence $(\hat{f}_l)_{l\geq 1} \in \ell^p(\mathbb{N})$, we can conclude that $(l\hat{f}_l)_{l\geq 1} \in \ell^r(\mathbb{N})$ with $r = \frac{p}{1-p}$.

Lemma C.0.7. *Let $\boldsymbol{q} = (q_j)_{j\geq 1}$ be a sequence belonging to $\ell^p(\mathbb{N})$, $0 < p < \frac{1}{2}$, and let the sequence $(j|q_j|^p)_{j\geq 1}$ be monotonically decreasing.*

Then the sequence $(jq_j)_{j\geq 1}$ belongs to $\ell^r(\mathbb{N})$ with $r = \frac{p}{1-p}$, $0 < r < 1$.

Proof. We prove the result by contradiction: we show that, if the sequence $(jq_j)_{j\geq 1}$ does not belong to $\ell^r(\mathbb{N})$ with $r = \frac{p}{1-p}$, then the sequence $\boldsymbol{q}$ does not belong to $\ell^p(\mathbb{N})$.

If $(jq_j)_{j\geq 1} \notin \ell^r(\mathbb{N})$, then there exists $J \in \mathbb{N}$ such that

$$|jq_j|^{\frac{p}{1-p}} \geq \frac{C}{jd_j}, \quad \text{for all } j \geq J, \tag{C.0.7}$$

where $C > 0$ is a constant independent of j, and $(d_j)_{j\geq 1}$ is a sequence such that $d_j > 0$ for every $j \geq 1$ and $\sum_{j\geq 1}\frac{1}{jd_j} = +\infty$.

For every $j \geq J$, we have:

$$|jq_j|^{\frac{p}{1-p}} \geq \frac{C}{jd_j} \Leftrightarrow |q_j|^{\frac{p}{1-p}} \geq \frac{C}{j^{\frac{1}{1-p}}d_j} \Leftrightarrow |q_j|^p \geq \frac{C'}{jd_j^{1-p}}, \tag{C.0.8}$$

with $C' := C^{1-p}$. Thanks to the assumption that the sequence $(j|q_j|^p)_{j\geq 1}$ is monotonically decreasing, we can choose the sequence $(d_j)_{j\geq 1}$ to be monotonically increasing.

We now distinguish two cases.

If $d_j < 1$ for every $j \in \mathbb{N}$, then $\frac{C'}{jd_j^{1-p}} > \frac{C'}{j}$ for every $j \geq J$, and, according to (C.0.8), the sequence $(|q_j|^p)_{j\geq 1}$ diverges.

Otherwise, if there exists $J' \in \mathbb{N}$ such that $d_{J'} \geq 1$, then, for every $j \geq J'$, $d_j \geq 1$, and thus $d_j^{1-p} \leq d_j$. The latter estimate combined with (C.0.8) implies that $|q_j|^p \geq \frac{C'}{jd_j}$ for every $j \geq \max\{J, J'\}$, meaning that the sequence $(|q_j|^p)_{j\geq 1}$ diverges. □

Proof of Lemma C.0.4

We can reformulate the statement in the following way:

Lemma C.0.8. *Let $\boldsymbol{q} = (q_j)_{j\geq 1}$ be a real, monotonically decreasing sequence belonging to $\ell^1(\mathbb{N})$. Then, there exists a real constant $C_{\boldsymbol{q}} > 0$ (depending on the sequence $\boldsymbol{q}$) and an integer $J \in \mathbb{N}$ such that*

$$|q_j| \leq C_{\boldsymbol{q}} \frac{1}{j}, \quad \text{for every } j > J. \tag{C.0.9}$$

Proof. We prove this result by contradiction. If the statement were not true, then, for all $C > 0$ and all $J_n \in \mathbb{N}$, $n \in \mathbb{N}$, we could find an index $j_n > J_n$ such that $j_n|q_{j_n}| > C$. Let us choose $C = 1$.

We construct, by induction, a subsequence of $\boldsymbol{q}$. For $n = 1$, let $J_1 := 1$; then there exists $j_1 > J_1$ such that $j_1|q_{j_1}| > 1$. For $n = 2$, we can select $J_2 := 2j_1$, and by assumption we can find $j_2 > J_2$ such that $j_2|q_{j_2}| > 1$. In general, for any $n \in \mathbb{N}$, given j_{n-1} such that $j_{n-1}|q_{j_{n-1}}| > 1$, we define $J_n := 2j_{n-1}$, and we can find $j_n > J_n$ for which $j_n|q_{j_n}| > 1$. In this way, we have constructed a subsequence $(q_{j_n})_{n\geq 1}$ of $(q_j)_{j\geq 1}$.

Being the sequence $(q_j)_{j\geq 1}$ monotonically decreasing, it holds that

$$\sum_{j=1}^{\infty} |q_j| \geq \sum_{n=1}^{\infty} (j_n - j_{n-1}) \frac{1}{j_n},$$

with the convention that $j_0 = 0$. Since we have $j_n > J_n = 2j_{n-1}$ for every $n \in \mathbb{N}$, then

$$\sum_{j=1}^{\infty} |q_j| \geq \sum_{n=1}^{\infty} \left(1 - \frac{j_{n-1}}{j_n}\right) > \sum_{n=1}^{\infty} \left(1 - \frac{1}{2}\right) = \sum_{n=1}^{\infty} \frac{1}{2} = +\infty,$$

which contradicts the hypothesis that the sequence belongs to $\ell^1(\mathbb{N})$. □

Lemma C.0.4 is an immediate consequence of the above result.

D. Analyticity of Banach space-valued functions of several complex variables

Here we briefly present how the concept of holomorphy of a function $f : \mathbb{C} \to \mathbb{C}$ extends to maps $f : \mathbb{C}^N \to B$, where $N \in \mathbb{N}$ and B is a Banach space over $\mathbb{C}$.

We denote by $\mathcal{B}_{\boldsymbol{\rho}}(\boldsymbol{z}^0)$ the polydisc of polyradius $\boldsymbol{\rho} \in \mathbb{R}^N_+$ centered in $\boldsymbol{z}^0 \in \mathbb{C}^N$, i.e. $\mathcal{B}_{\boldsymbol{\rho}}(\boldsymbol{z}^0) := \Big\{\boldsymbol{z} \in \mathbb{C}^N : |z_j - z_j^0| < \rho_j \text{ for every } j = 1, \dots, N\Big\}$, and by $\{\boldsymbol{e}_j\}_{j=1}^N$ the canonical basis in $\mathbb{C}^N$.

Definition D.0.1. [Her06, III.1.2] Consider a map $f : \mathcal{O} \subseteq \mathbb{C}^N \to B$, where $\mathcal{O}$ is an open set.

- f is *analytic* in $\mathcal{O}$ if, for every $\boldsymbol{z}^0 \in \mathcal{O}$, there exists a polydisc $\mathcal{B}_{\boldsymbol{\rho}}(\boldsymbol{z}^0) \subseteq \mathcal{O}$ such that, for every $\boldsymbol{z} \in \mathcal{B}_{\boldsymbol{\rho}}(\boldsymbol{z}^0)$, $f(\boldsymbol{z})$ can be written as a convergent power series

$$f(\boldsymbol{z}) = \sum_{\boldsymbol{k} \in \mathbb{N}_0^N} c_{\boldsymbol{k}} (z_1 - z_1^0)^{k_1} \dots (z_N - z_N^0)^{k_N}, \tag{D.0.1}$$

  with coefficients $c_{\boldsymbol{k}}$ in B.

- f is *holomorphic* in $\mathcal{O}$ if it is holomorphic in each variable separately, that is, if at each point $\boldsymbol{z} \in \mathcal{O}$, the first-order partial derivatives $\partial_{z_j} f := \lim_{|t| \to 0} \frac{f(\boldsymbol{z} + t\boldsymbol{e}_j) - f(\boldsymbol{z})}{t}$, $t \in \mathbb{C} \setminus \{\boldsymbol{0}\}$, $j = 1, \dots, N$, exist;

- f is *scalarly analytic* or *holomorphic* if, for every element in the dual of B, that is for every $b^* \in B^*$, the function $b^* \circ f : \mathcal{O} \to \mathbb{C}$ is analytic or holomorphic.

Theorem D.0.2. [Her06, Thm 1 in III.1.2] *For maps $f : \mathbb{C}^N \to B$ where B is a Banach space, analyticity, holomorphy and scalar analyticity are equivalent properties.*

Proof. See [Her06, III.1.2], in particular proofs to Prop. 2c and Thm. 1. □

The previous theorem tells us that, for functions of several complex variables, separate holomorphy and holomorphy are equivalent. This result, known as *Hartog's theorem* (see e.g. Thm. 1.2.5 in [Kra82] for $B = \mathbb{C}$) is peculiar to $\mathbb{C}^N$ and it does not hold in $\mathbb{R}^N$. In $\mathbb{R}^N$, indeed, there are functions that are C^∞ in each variable separately but are not C^∞ when considered as maps on $\mathbb{R}^N$. A typical example is $f : \mathbb{R}^2 \to \mathbb{R}$ defined as $f(\boldsymbol{x}) = \frac{x_1 x_2}{x_1^2 + x_2^2}$ for $\boldsymbol{x} \neq (0, 0)$ and $f(0, 0) = 0$.

As for functions of one complex variable, we have the two following results:

Theorem D.0.3. *If $f : \mathcal{B}_{\boldsymbol{\rho}}(\boldsymbol{z}^0) \subseteq \mathbb{C}^N \to B$ is holomorphic, then it has partial derivatives of all orders $\partial_{\boldsymbol{z}}^{|\boldsymbol{k}|} f$, $\boldsymbol{k} = (k_1, k_2, \dots, k_N) \in \mathbb{N}^N$, which are holomorphic in $\mathcal{B}_{\boldsymbol{\rho}}(\boldsymbol{z}^0)$.*

The coefficients $c_{\boldsymbol{k}}$ in (D.0.1) *are given by*

$$c_{\boldsymbol{k}} = \frac{1}{k_1! \dots k_N!} \partial_{\boldsymbol{z}}^{|\boldsymbol{k}|} f(\boldsymbol{z}^0),$$

for every $\boldsymbol{k} \in \mathbb{N}_0^N$.

Proof. See Corollaries 2 and 3a in [Her06, III.1.2]. □

Theorem D.0.4 (Cauchy's integral formula)**.** *If $f : \mathcal{O} \subseteq \mathbb{C}^N \to B$ is holomorphic, then the formula*

$$\partial_{\boldsymbol{z}}^{|\boldsymbol{k}|} f(\boldsymbol{z}) = \frac{k_1! \dots k_N!}{(2\pi i)^N} \int_{|\zeta_N - z_N^0| = \rho_N} \dots \int_{|\zeta_1 - z_1^0| = \rho_1} \frac{f(\boldsymbol{\zeta})}{(\zeta_1 - z_1)^{k_1+1} \dots (\zeta_N - z_N)^{k_N+1}} \, \mathrm{d}\zeta_1 \dots \mathrm{d}\zeta_N, \tag{D.0.2}$$

holds for every $\boldsymbol{z} \in \mathcal{B}_{\boldsymbol{\rho}}(\boldsymbol{z}^0) \subseteq \mathcal{O}$ and every $\boldsymbol{k} \in \mathbb{N}_0^N$ (with the convention that $0! = 1$).

Proof. See Corollary 3b in [Her06, III.1.2]. □

E. Proof of Lemma 3.1.4 (regularity of the domain mapping for the particle in free space)

Fulfillment of Assumption 3.1.2(i)

We have to prove that $\Phi(\boldsymbol{y})$ is a C^k-orientation preserving diffeomorphism in each subdomain, with k the smoothness of the stochastic radius r and a J- and $\boldsymbol{y}$-independent norm bound.

In the regions where $\chi = 0$, the mapping Φ given by (3.1.2) corresponds to the identity, and thus it is bijective. Where not zero, χ is strictly monotonic in each subdomain, and thus Φ is bijective everywhere in K_R.

We present here the computations for the smoothness of Φ in $\hat{D}_2$, the argument for the smoothness in $K_R \cap \hat{D}_1$ being analogous. More precisely, we consider the mapping in the region $\hat{D}_{2,\chi} := \left\{\hat{\boldsymbol{x}} \in \hat{D}_2 : \frac{r_0^-}{4} \leq \|\hat{\boldsymbol{x}}\| \leq r_0(\hat{\varphi}_{\hat{\boldsymbol{x}}})\right\}$. Indeed, Assumption 3.1.2(i) is trivially satisfied for $\|\hat{\boldsymbol{x}}\| \leq \frac{r_0^-}{4}$, and the smoothness assumption on χ guarantees that the mapping is smooth across the circle of radius $\frac{r_0^-}{4}$. For the continuity of the inverse and its derivatives across the circle of radius $\frac{r_0^-}{4}$, let us consider an annulus together with its boundary, enclosing the circle of radius $\frac{r_0^-}{4}$ in its interior. Since the map Φ and, as we will show, its derivatives, are continous in the annulus with boundary, which is a compact subset of $\mathbb{R}^2$, then also Φ^{-1} and its derivatives are.

For the continuity of Φ and its inverse, using Assumption 2.1.3, we have the J- and $\boldsymbol{y}$-independent bounds:

$$\begin{aligned}
\|\Phi(\boldsymbol{y})\|_{C^0(\hat{D}_{2,\chi})} &\leq \max_{\hat{\boldsymbol{x}}\in\hat{D}_{2,\chi}} \|\hat{\boldsymbol{x}}\| + \max_{\hat{\boldsymbol{x}}\in\hat{D}_{2,\chi}} \|\chi(\hat{\boldsymbol{x}})\| \max_{\hat{\boldsymbol{x}}\in\hat{D}_{2,\chi}} |r(\boldsymbol{y},\hat{\varphi}_{\hat{\boldsymbol{x}}}) - r_0(\hat{\varphi\boldsymbol{x}})| = r_0^+ + \frac{r_0^-}{2}, \\
\|\Phi^{-1}(\boldsymbol{y})\|_{C^0(D_{2,\chi}(\boldsymbol{y}))} &= \max_{\boldsymbol{x}\in D_{2,\chi}(\boldsymbol{y})} \|\Phi^{-1}(\boldsymbol{y},\boldsymbol{x})\| = \max_{\hat{\boldsymbol{x}}\in\hat{D}_{2,\chi}} \|\Phi^{-1}\left(\boldsymbol{y},\Phi(\boldsymbol{y},\hat{\boldsymbol{x}})\right)\| = \max_{\hat{\boldsymbol{x}}\in\hat{D}_{2,\chi}} \|\hat{\boldsymbol{x}}\| = r_0^+,
\end{aligned}$$

where we have denoted $D_{2,\chi}(\boldsymbol{y}) := \Phi(\boldsymbol{y})(\hat{D}_{2,\chi})$ and $r_0^+ := \sup_{\varphi\in[0,2\pi)} r_0(\varphi)$.

For ease of computations of the derivatives, since the mapping from cartesian to polar coordinates is a C^∞-diffeomorphism away from the origin, we work with the mapping Φ in polar coordinates. Namely, we consider:

$$\tilde{\Phi}(\boldsymbol{y})(\hat{\rho},\hat{\varphi}) = \begin{pmatrix}\rho\\ \varphi\end{pmatrix} = \begin{pmatrix}\hat{\rho} + \tilde{\chi}(\hat{\rho},\hat{\varphi})(r(\boldsymbol{y},\hat{\varphi}) - r_0(\hat{\varphi}))\\ \hat{\varphi}\end{pmatrix}, \quad \text{for } \frac{r_0^-}{4} \leq \hat{\rho} \leq r_0(\hat{\varphi}) \text{ and } \hat{\varphi} \in [0,2\pi), \tag{E.0.1}$$

where, denoting by Φ_p the mapping from cartesian to polar coordinates, $(\hat{\rho},\hat{\varphi}) = \Phi_p(\hat{\boldsymbol{x}})$, $(\rho,\varphi) = \Phi_p(\boldsymbol{x})$ and $\tilde{\chi} := \chi \circ \Phi_p^{-1}$.

The Jacobian matrices of $\tilde{\Phi}$ and $\tilde{\Phi}^{-1}$ are given by:

$$D\tilde{\Phi}(\boldsymbol{y}) = \begin{pmatrix} 1 + \dfrac{\partial\tilde{\chi}}{\partial\hat{\rho}}(r(\boldsymbol{y},\hat{\varphi}) - r_0(\hat{\varphi})) & \dfrac{\partial\tilde{\chi}}{\partial\hat{\varphi}}(r(\boldsymbol{y},\hat{\varphi}) - r_0(\hat{\varphi})) + \tilde{\chi}\dfrac{\partial}{\partial\hat{\varphi}}(r(\boldsymbol{y},\hat{\varphi}) - r_0(\hat{\varphi})) \\ 0 & 1 \end{pmatrix},$$

$$\begin{aligned} D\tilde{\Phi}^{-1}(\boldsymbol{y}) &= (D\tilde{\Phi})^{-1} \circ \tilde{\Phi}^{-1}(\boldsymbol{y}) \\ &= \frac{1}{\det D\tilde{\Phi}(\boldsymbol{y})} \begin{pmatrix} 1 & -\dfrac{\partial\tilde{\chi}}{\partial\hat{\varphi}}(r(\boldsymbol{y},\hat{\varphi}) - r_0(\hat{\varphi})) - \tilde{\chi}\dfrac{\partial}{\partial\hat{\varphi}}(r(\boldsymbol{y},\hat{\varphi}) - r_0(\hat{\varphi})) \\ 0 & 1 + \dfrac{\partial\tilde{\chi}}{\partial\hat{\rho}}(r(\boldsymbol{y},\hat{\varphi}) - r_0(\hat{\varphi})). \end{pmatrix}. \end{aligned} \tag{E.0.2}$$

Exploiting Assumption 3.1.3 on χ and Assumption 2.1.3 on the coefficients on the radius expansion, we can bound each entry of $D\tilde{\Phi}(\boldsymbol{y})$:

$$\begin{aligned} \left|1 + \frac{\partial\tilde{\chi}}{\partial\hat{\rho}}(r(\boldsymbol{y},\hat{\varphi}) - r_0(\hat{\varphi}))\right| &\leq 1 + \left|\frac{\partial\tilde{\chi}}{\partial\hat{\rho}}\right| \frac{r_0^-}{2} \leq 1 + \sqrt{2}\|\chi\|_{C^1(\hat{D}_{2,\chi})}\frac{r_0^-}{2} \leq 2, \\ \left|\frac{\partial\tilde{\chi}}{\partial\hat{\varphi}}(r(\boldsymbol{y},\hat{\varphi}) - r_0(\hat{\varphi})) + \tilde{\chi}\frac{\partial}{\partial\hat{\varphi}}(r(\boldsymbol{y},\hat{\varphi}) - r_0(\hat{\varphi}))\right| &\leq \left|\frac{\partial\tilde{\chi}}{\partial\hat{\varphi}}\right| |r(\boldsymbol{y},\hat{\varphi}) - r_0(\hat{\varphi})| + |\chi| \sum_{j=1}^{\infty} j\,(|c_j| + |s_j|) \\ &\leq \|\chi\|_{C^1(\hat{D}_{2,\chi})} \left(\sqrt{2}r_0^+\frac{r_0^-}{2} + C_r\right), \end{aligned}$$

with $C_r := \sum_{j=1}^{\infty} j\,(|c_j| + |s_j|) < \infty$.

The above estimates show that we have a J- and $\boldsymbol{y}$-independent bound on the C^1-norm of Φ.

It is clear from the expression of $D\tilde{\Phi}^{-1}$ that, if we provide also a J- and $\boldsymbol{y}$-independent (positive) lower bound on $\det D\tilde{\Phi}(\boldsymbol{y})$, then we also have a J- and $\boldsymbol{y}$-independent upper bound on the C^1-norm of Φ^{-1}. It holds:

$$\det D\tilde{\Phi}(\boldsymbol{y}) \geq 1 - |r(\boldsymbol{y},\hat{\varphi}) - r_0(\hat{\varphi})| \left|\frac{\partial\tilde{\chi}}{\partial\hat{\rho}}\right| \geq 1 - \frac{r_0^-}{2}\sqrt{2}\|\chi\|_{C^1(\hat{D}_{2,\chi})} \geq 1 - \frac{r_0^-}{2}\sqrt{2}C_\chi > 0, \tag{E.0.3}$$

where we have used the bound on $\|\chi\|_{C^1(\hat{D}_{2,\chi})}$ provided by Assumption 3.1.3.

For the higher-order derivatives of Φ, it is clear from (3.1.2) that this map is as many times differentiable as $\chi(\cdot)$, $r(\boldsymbol{y},\cdot)$ and $r_0(\cdot)$ are. The mollifier χ and the nominal radius r_0 are assumed to be smooth and they do not depend on $J \in \mathbb{N}$ and on $\boldsymbol{y} \in \mathcal{P}_J$. Thus, the J- and $\boldsymbol{y}$-uniform bound on the $C^0(\hat{D}_{2,\chi})$-norm of the derivatives is ensured by the J- and $\boldsymbol{y}$-uniform bound on $\|r(\boldsymbol{y},\cdot)\|_{C^k_{per}([0,2\pi))}$, with k the highest differentiability order of the radius.

Concerning the higher-order derivatives of Φ^{-1}, they are obtained from chain rule on the entries of $D\Phi^{-1} = (D\Phi)^{-1}\circ\Phi^{-1}$. More precisely, a derivative of order m is given by the sum and product of powers of entries of $(D\Phi(\boldsymbol{y}))^{-1}$ with the product of derivatives of $\Phi(\boldsymbol{y})$ up to the mth order. Since we have already stated the J- and $\boldsymbol{y}$- uniform upper bounds on the norms of the derivatives of $\Phi(\boldsymbol{y})$ and of the entries of $(D\Phi(\boldsymbol{y}))^{-1}$, then we can conclude that Φ is a C^k-diffeomorphism, with k the smoothness of the radius $r(\boldsymbol{y},\cdot)$ and J- and $\boldsymbol{y}$-independent norm bounds.

Fulfillment of Assumption 3.1.2(ii)

It is clear from (3.1.2) that this assumption is satisfied.

Fulfillment of Assumption 3.1.2(iii)

Also in this case, we restrict our computations to the domain $\hat{D}_{2,\chi}$, being the case trivial for $\|\hat{\boldsymbol{x}}\| \leq \frac{r_0^-}{4}$ and analogous for $\|\hat{\boldsymbol{x}}\| \geq r_0(\hat{\varphi}_{\hat{\boldsymbol{x}}})$.

Again, it is convenient to work in polar coordinates. We use the notation $\tilde{\sigma}_1$ and $\tilde{\sigma}_2$ for minimum and maximum singular values of $D\tilde{\Phi}$, respectively.

It holds that $\tilde{\sigma}_2(\boldsymbol{y}) = \|D\tilde{\Phi}(\boldsymbol{y})\|_2 \leq \|D\tilde{\Phi}(\boldsymbol{y})\|_F$, where $\|\cdot\|_F$ denotes the Frobenius norm. Since from the previous computations we have a J- and $\boldsymbol{y}$-uniform upper bound on the $C^0(\hat{D}_{2,\chi})$-norm of each entry of $D\tilde{\Phi}$, then there exists a J- and $\boldsymbol{y}$-uniform upper bound on the $C^0(\hat{D}_{2,\chi})$-norm of $\tilde{\sigma}_2$, too.

Furthermore,

$$\tilde{\sigma}_1(\boldsymbol{y}) = \frac{\det(D\tilde{\Phi}^\top(\boldsymbol{y})D\tilde{\Phi}(\boldsymbol{y}))}{\tilde{\sigma}_2(\boldsymbol{y})} = \frac{\left(\det D\tilde{\Phi}(\boldsymbol{y})\right)^2}{\tilde{\sigma}_2(\boldsymbol{y})}.$$

Coupling the J- and $\boldsymbol{y}$-uniform upper bound on $\tilde{\sigma}_2$ with the J- and $\boldsymbol{y}$-uniform lower bound (E.0.3) on $\det D\tilde{\Phi}(\boldsymbol{y})$, we obtain a J- and $\boldsymbol{y}$-uniform positive lower bound on the $C^0(\hat{D}_{2,\chi})$-norm of $\tilde{\sigma}_1$.

Finally, since the mapping from cartesian to polar coordinates is a C^∞-diffeomorphism away from the origin, we can state that there exist J- and $\boldsymbol{y}$-uniform, upper and lower, positive bounds on the $C^0(\hat{D}_{2,\chi})$-norm of the singular values of $D\Phi$ and $D\Phi^{-1}$.

References

[AJT02] Grégoire Allaire, François Jouve, and Anca-Maria Toader. A level-set method for shape optimization. *Comptes Rendus Mathematique*, 334(12):1125–1130, 2002.

[Ber94] Jean-Pierre Berenger. A perfectly matched layer for the absorption of electromagnetic waves. *Journal of Computational Physics*, 114(2):185–200, 1994.

[BNT10] Ivo Babuška, Fabio Nobile, and Raul Tempone. A stochastic collocation method for elliptic partial differential equations with random input data. *SIAM review*, 52(2):317–355, 2010.

[BS08] Susanne C Brenner and Ridgway Scott. *The mathematical theory of finite element methods*, volume 15. Springer Science & Business Media, 2008.

[BSZ11] Andrea Barth, Christoph Schwab, and Nathaniel Zollinger. Multi-level Monte Carlo finite element method for elliptic PDEs with stochastic coefficients. *Numerische Mathematik*, 119(1):123–161, 2011.

[CCNT16] Julio E Castrillon-Candas, Fabio Nobile, and Raul F Tempone. Analytic regularity and collocation approximation for PDEs with random domain deformations. *Comput. Math. Appl.*, 71(6):1173–1197, 2016.

[CCS14] Abdellah Chkifa, Albert Cohen, and Christoph Schwab. High-dimensional adaptive sparse polynomial interpolation and applications to parametric PDEs. *Foundations of Computational Mathematics*, 14(4):601–633, 2014.

[CCS15] Abdellah Chkifa, Albert Cohen, and Christoph Schwab. Breaking the curse of dimensionality in sparse polynomial approximation of parametric PDEs. *Journal de Mathématiques Pures et Appliquées*, 103(2):400–428, 2015.

[CDS10] Albert Cohen, Ronald DeVore, and Christoph Schwab. Convergence rates of best N-term Galerkin approximations for a class of elliptic sPDEs. *Foundations of Computational Mathematics*, 10(6):615–646, 2010.

[CDS11] Albert Cohen, Ronald DeVore, and Christoph Schwab. Analytic regularity and polynomial approximation of parametric and stochastic elliptic PDEs. *Analysis and Applications*, 9(01):11–47, 2011.

[Chk13] Moulay Abdellah Chkifa. On the Lebesgue constant of Leja sequences for the complex unit disk and of their real projection. *Journal of Approximation Theory*, 166:176–200, 2013.

[CK07] Claudio Canuto and Tomas Kozubek. A fictitious domain approach to the numerical solution of PDEs in stochastic domains. *Numerische mathematik*, 107(2):257–293, 2007.

[CK12] David Colton and Rainer Kress. *Inverse acoustic and electromagnetic scattering theory*, volume 93. Springer Science & Business Media, 2012.

[CL85] Elliot W Cheney and William A Light. Approximation theory in tensor product spaces. *Lecture Notes in Math*, 1169, 1985.

[CM98] Francis Collino and Peter Monk. The perfectly matched layer in curvilinear coordinates. *SIAM Journal on Scientific Computing*, 19(6):2061–2090, 1998.

[CM12] Jean-Paul Calvi and Phung Manh. Lagrange interpolation at real projections of Leja sequences for the unit disk. *Proceedings of the American Mathematical Society*, 140(12):4271–4284, 2012.

[CS13] Alexey Chernov and Christoph Schwab. First order k-th moment finite element analysis of nonlinear operator equations with stochastic data. *Mathematics of Computation*, 82(284):1859–1888, 2013.

[CS15] Peng Chen and Christoph Schwab. Sparse-grid, reduced-basis Bayesian inversion. *Computer Methods in Applied Mechanics and Engineering*, 297:84–115, 2015.

[CSZ] Albert Cohen, Christoph Schwab, and Jakob Zech. Shape Holomorphy of the stationary Navier-Stokes Equations. *In preparation.*

[DGS06] Christophe Desceliers, Roger Ghanem, and Christian Soize. Maximum likelihood estimation of stochastic chaos representations from experimental data. *International Journal for Numerical Methods in Engineering*, 66(6):978–1001, 2006.

[DKLG+14] Josef Dick, Frances Y Kuo, Quoc T Le Gia, Dirk Nuyens, and Christoph Schwab. Higher Order QMC Petrov–Galerkin Discretization for Affine Parametric Operator Equations with Random Field Inputs. *SIAM Journal on Numerical Analysis*, 52(6):2676–2702, 2014.

[DKS13] Josef Dick, Frances Y Kuo, and Ian H Sloan. High-dimensional integration: the quasi-Monte Carlo way. *Acta Numerica*, 22:133–288, 2013.

[DPZ14] Giuseppe Da Prato and Jerzy Zabczyk. *Stochastic equations in infinite dimensions*, volume 152. Cambridge university press, 2014.

[DZ11] Michel C Delfour and J-P Zolésio. *Shapes and geometries: metrics, analysis, differential calculus, and optimization*, volume 22. Siam, 2011.

[Gan16] Robert N. Gantner. A Generic C++ Library for Multilevel Quasi-Monte Carlo. In *Proceedings of the Platform for Advanced Scientific Computing Conference*, PASC '16, pages 11:1–11:12, New York, NY, USA, 2016. ACM.

[GD06] Roger G Ghanem and Alireza Doostan. On the construction and analysis of stochastic models: Characterization and propagation of the errors associated with limited data. *Journal of Computational Physics*, 217(1):63–81, 2006.

[GG03] Thomas Gerstner and Michael Griebel. Dimension–adaptive tensor–product quadrature. *Computing*, 71(1):65–87, 2003.

[Gil15] Michael B Giles. Multilevel Monte Carlo methods. *Acta Numerica*, 24:259, 2015.

[Gra04] Loukas Grafakos. Classical and modern Fourier analysis. *AMC*, 10, 2004.

[GS03] Roger G Ghanem and Pol D Spanos. *Stochastic finite elements: a spectral approach*. Courier Corporation, 2003.

[GS16] Robert N. Gantner and Christoph Schwab. *Computational Higher Order Quasi-Monte Carlo Integration*, pages 271–288. Springer International Publishing, Cham, 2016.

[GT01] David Gilbarg and Neil S Trudinger. *Elliptic partial differential equations of second order*, volume 224. Springer Science & Business Media, 2001.

[Hal13] Paul R Halmos. *Measure theory*, volume 18. Springer, 2013.

[Har10] Helmut Harbrecht. On output functionals of boundary value problems on stochastic domains. *Mathematical Methods in the Applied Sciences*, 33(1):91–102, 2010.

[Her06] Michel Hervé. *Analytic and Plurisubharmonic Functions: In Finite and Infinite Dimensional Spaces. Course Given at the University of Maryland, Spring 1970*, volume 198. Springer, 2006.

[HL13] Helmut Harbrecht and Jingzhi Li. First order second moment analysis for stochastic interface problems based on low-rank approximation. *ESAIM: Mathematical Modelling and Numerical Analysis*, 47(05):1533–1552, 2013.

[Hon05] Riki Honda. Stochastic BEM with spectral approach in elastostatic and elastodynamic problems with geometrical uncertainty. *Engineering analysis with boundary elements*, 29(5):415–427, 2005.

[HP15] Ralf Hiptmair and Alberto Paganini. Shape optimization by pursuing diffeomorphisms. *Computational Methods in Applied Mathematics*, 15(3):291–305, 2015.

[HPS16] Helmut Harbrecht, Michel Peters, and Markus Siebenmorgen. Analysis of the domain mapping method for elliptic diffusion problems on random domains. *Numerische Mathematik*, pages 1–34, 2016.

[HS] Ralf Hiptmair and Sahar Sargheini. Scatterers on the substrate: Far field formulas. *Report 2015-02, Seminar for Applied Mathematics, ETH Zürich, Switzerland.*

[HSS08] Helmut Harbrecht, Reinhold Schneider, and Christoph Schwab. Sparse second moment analysis for elliptic problems in stochastic domains. *Numerische Mathematik*, 109(3):385–414, 2008.

[HSSS] Ralf Hiptmair, Laura Scarabosio, Claudia Schillings, and Christoph Schwab. Large deformation shape uncertainty quantification in acoustic scattering. *Report 2015-31, Seminar for Applied Mathematics, ETH Zürich, Switzerland.*

[JHN12] Carlos Jerez-Hanckes and Jean-Claude Nédélec. Asymptotics for Helmholtz and Maxwell solutions in 3-D open waveguides. *Commun. Comput. Phys*, 11(2):629–646, 2012.

[Kra82] Steven George Krantz. *Function theory of several complex variables.* Wiley New York, 1982.

[KSS12] Frances Y Kuo, Christoph Schwab, and Ian H Sloan. Quasi-Monte Carlo finite element methods for a class of elliptic partial differential equations with random coefficients. *SIAM Journal on Numerical Analysis*, 50(6):3351–3374, 2012.

[Lax02] Peter D Lax. *Functional Analysis (Pure and Applied Mathematics: A Wiley-Interscience Series of Texts, Monographs and Tracts).* New York: Wiley-Interscience, 2002.

[LMWZ10] Jingzhi Li, Jens Markus Melenk, Barbara Wohlmuth, and Jun Zou. Optimal a priori estimates for higher order finite elements for elliptic interface problems. *Applied numerical mathematics*, 60(1):19–37, 2010.

[Loè63] Michel Loève. *Probability theory.* Van Nostrand, Princeton, NJ, 1963.

[LS98] Matti Lassas and Erkki Somersalo. On the existence and convergence of the solution of PML equations. *Computing*, 60(3):229–241, 1998.

[LTZ01] Ruo Li, Tao Tang, and Pingwen Zhang. Moving Mesh Methods in Multiple Dimensions Based on Harmonic Maps. *Journal of Computational Physics*, 170(2):562–588, 2001.

[Mai07] Stefan Alexander Maier. *Plasmonics: fundamentals and applications*. Springer Science & Business Media, 2007.

[McL00] William Charles Hector McLean. *Strongly elliptic systems and boundary integral equations*. Cambridge university press, 2000.

[MCM11a] DH Mac, S Clenet, and JC Mipo. Calculation of field distribution in electromagnetic problems with random domains. In *Computation in Electromagnetics (CEM 2011), IET 8th International Conference on*, pages 1–2. IET, 2011.

[MCM11b] Duy Hung Mac, Stéphane Clenet, and Jean-Claude Mipo. Transformation methods for static field problems with random domains. *Magnetics, IEEE Transactions on*, 47(5):1446–1449, 2011.

[MCMM10] D Hung Mac, Stéphane Clenet, Jean-Claude Mipo, and Olivier Moreau. Solution of static field problems with random domains. *Magnetics, IEEE Transactions on*, 46(8):3385–3388, 2010.

[MNK11] P Surya Mohan, Prasanth B Nair, and Andy J Keane. Stochastic projection schemes for deterministic linear elliptic partial differential equations on random domains. *International journal for numerical methods in engineering*, 85(7):874–895, 2011.

[MNT13] Mohammad Motamed, Fabio Nobile, and Raúl Tempone. A stochastic collocation method for the second order wave equation with a discontinuous random speed. *Numerische Mathematik*, 123(3):493–536, 2013.

[MS98] Peter Monk and Endre Süli. The adaptive computation of far-field patterns by a posteriori error estimation of linear functionals. *SIAM Journal on Numerical Analysis*, 36(1):251–274, 1998.

[NCSM08] Anthony Nouy, Alexandre Clement, Franck Schoefs, and N Moës. An extended stochastic finite element method for solving stochastic partial differential equations on random domains. *Computer Methods in Applied Mechanics and Engineering*, 197(51):4663–4682, 2008.

[Néd01] Jean-Claude Nédélec. *Acoustic and electromagnetic equations: integral representations for harmonic problems*, volume 144. Springer Science & Business Media, 2001.

[Nit76] Joachim Nitsche. Über L^∞-Abschätzungen von Projektionen auf finite Elemente. *Finite Elemente (Tagung, Inst. Angew. Math., Univ. Bonn, Bonn, 1975). Bonn. Math. Schrift*, 89:13–30, 1976.

[NSM07] Anthony Nouy, Franck Schoefs, and Nicolas Moës. X-SFEM, a computational technique based on X-FEM to deal with random shapes. *European Journal of Computational Mechanics/Revue Européenne de Mécanique Numérique*, 16(2):277–293, 2007.

[OF01] Stanley Osher and Ronald P. Fedkiw. Level Set Methods: An Overview and Some Recent Results. *Journal of Computational Physics*, 169(2):463 – 502, 2001.

[PSDF12] Guillaume Perrin, Christian Soize, Denis Duhamel, and C Funfschilling. Identification of polynomial chaos representations in high dimension from a set of realizations. *SIAM Journal on Scientific Computing*, 34(6):A2917–A2945, 2012.

[RHP08] Gianluigi Rozza, Dinh Bao Phuong Huynh, and Anthony T Patera. Reduced basis approximation and a posteriori error estimation for affinely parametrized elliptic coercive partial differential equations. *Archives of Computational Methods in Engineering*, 15(3):229–275, 2008.

[RS05] Jim O. Ramsay and Bernard W. Silverman. *Functional data analysis, Second Edition*. Springer, 2005.

[Rya02] Raymond A Ryan. *Introduction to Tensor Products of Banach Spaces*. Springer Science & Business Media, 2002.

[Sch98] Alfred Schatz. Pointwise error estimates and asymptotic error expansion inequalities for the finite element method on irregular grids: Part I. Global estimates. *Mathematics of Computation of the American Mathematical Society*, 67(223):877–899, 1998.

[SG11] Christoph Schwab and Claude Jeffrey Gittelson. Sparse tensor discretizations of high-dimensional parametric and stochastic PDEs. *Acta Numerica*, 20:291–467, 2011.

[SNC09] G. Stefanou, Anthony Nouy, and Alexandre Clement. Identification of random shapes from images through polynomial chaos expansion of random level set functions. *International Journal for Numerical Methods in Engineering*, 79(2):127–155, 2009.

[Soi10] Christian Soize. Identification of high-dimension polynomial chaos expansions with random coefficients for non-Gaussian tensor-valued random fields using partial and limited experimental data. *Computer methods in applied mechanics and engineering*, 199(33):2150–2164, 2010.

[Soi11] Christian Soize. A computational inverse method for identification of non-Gaussian random fields using the Bayesian approach in very high dimension. *Computer Methods in Applied Mechanics and Engineering*, 200(45):3083–3099, 2011.

[SS13] Claudia Schillings and Christoph Schwab. Sparse, adaptive Smolyak quadratures for Bayesian inverse problems. *Inverse Problems*, 29(6):065011, 2013.

[SS14] Claudia Schillings and Christoph Schwab. Sparsity in Bayesian inversion of parametric operator equations. *Inverse Problems*, 30(6):065007, 2014.

[TJWG15] Aretha L Teckentrup, Peter Jantsch, Clayton G Webster, and Max Gunzburger. A multilevel stochastic collocation method for partial differential equations with random input data. *SIAM/ASA Journal on Uncertainty Quantification*, 3(1):1046–1074, 2015.

[TX06] Daniel M Tartakovsky and Dongbin Xiu. Stochastic analysis of transport in tubes with rough walls. *Journal of Computational Physics*, 217(1):248–259, 2006.

[Wie38] Norbert Wiener. The homogeneous chaos. *American Journal of Mathematics*, pages 897–936, 1938.

[WYW06] Zhuoqun Wu, Jingxue Yin, and Chunpeng Wang. *Elliptic & parabolic equations*. World Scientific, 2006.

[XH05] Dongbin Xiu and Jan S Hesthaven. High-order collocation methods for differential equations with random inputs. *SIAM Journal on Scientific Computing*, 27(3):1118–1139, 2005.

[XT06] Dongbin Xiu and Daniel M Tartakovsky. Numerical methods for differential equations in random domains. *SIAM Journal on Scientific Computing*, 28(3):1167–1185, 2006.